

Studies on Noricumazole A derivatives and their HCV p7 inhibitory activity

Von der Naturwissenschaftlichen Fakultät der
Gottfried Wilhelm Leibniz Universität Hannover

zur Erlangung des Grades
Doktorin der Naturwissenschaften (Dr. rer. nat.)

genehmigte Dissertation
von
Dobromira Nedeva Lekova,
Magistar (University of Chemical Technology and Metallurgy)

2022

Referent: Prof. Dr. rer. nat. Andreas Kirschning
Korreferent: Prof. Dr. rer. nat. Markus Kalesse
Tag der Promotion: 24.03.2022

Zusammenfassung

Studies on Noricumazole A derivatives and their HCV p7 inhibitory activity

Noricumazol A ist ein Naturstoff der zum ersten Mal aus dem Myxobakterium *Sorangium cellulosum*, So ce399 isoliert wurde. Es konnte gezeigt werden, dass Noricumazol A Hepatitis C-spezifische antivirale Aktivität aufweist, welche den Viruslebenszyklus direkt beeinflusst und eine geringe Zytotoxizität gegenüber der Wirtszelle aufweist ($[IC_{50}] = 8.6 \text{ nM}$, $[CC_{50}] = 12.8 \text{ nM}$). Darüber hinaus zeigt es eine überdurchschnittliche Inhibierung des spannungsabhängigen Natriumionenkanals NaV1.7 sowie eine stabilisierende und inhibierende Wirkung gegenüber dem pH- und spannungsabhängigen Kaliumkanal KcsA.

In dieser Arbeit wurden verschiedene Synthesestrategien zur Darstellung von neuen Noricumazol A-Derivaten untersucht.

Zunächst wurde eine konvergente Synthese von Derivaten, welche alle aktivitätsrelevanten strukturellen Elemente enthält, verfolgt. Die angestrebte Struktur sollte einen Thiazol-Ring, welcher eine Reduktion der Zytotoxizität zeigte sowie acylierte Hydroxyfunktionen an C3 und C11, welche eine überdurchschnittliche Aktivitätssteigerung zeigten, enthalten. Der Schlüsselschritt zur Kupplung der finalen Fragmente blieb hierbei erfolglos aufgrund der initialen Oxidation des Westfragments, die zuerst zu einer Reihe nicht reproduzierbarer Ergebnisse führte.

Eine weitere konvergente Synthesestrategie zur Darstellung eines Noricumazol A-Derivats ohne Hydroxyfunktion an C13 wurde ebenfalls verfolgt. Hierbei wurde die abschließende Kupplung von zwei Schlüsselfragmenten über eine *o*-Lithiierung untersucht.

Des Weiteren wurde zur Untersuchung der Wirkung von Noricumazol A-Derivaten an Viroporin HCV p7 ein optischer Transporttest entwickelt. Hierfür wurde der Fluoreszenzfarbstoff PBFI als optischer Kaliumsensor zwecks Nachweises der HCV p7 vermittelten Transportaktivität von Kaliumionen in die Liposomen genutzt. Dadurch war es möglich, die Transportaktivität des Viroporins HCV p7 als Funktion der Zeit zu beobachten. Eine Zunahme der Fluoreszenzintensität wird dabei als Transportaktivität interpretiert und über eine Injektion einer konzentrierten Kaliumchlorid-Lösung in die laufende Kinetik herbeigeführt. Die Abwesenheit von HCV p7 bei den Kontroll-Liposomen Resonanz auf die Kaliumchlorid-Injektion, während durch die Präsenz von HCV p7 eine starke Zunahme des Fluoreszenzsignals zu beobachten war. In Gegenwart von Noricumazol A wird die Transportaktivität konzentrationsabhängig herabgesetzt mit einer Dosis-Wirkungsabhängigkeit von einem IC_{50} von $4 \mu\text{M}$.

Abstract

Studies on Noricumazole A derivatives and their HCV p7 inhibitory activity

Noricumazoles A is a natural product isolated for the first time from myxobacterium *Sorangium cellouloum*, So ce399. Noricumazole A has been found to have hepatitis C specific antiviral activity by directly effecting the virus life-cycle while maintaining low cytotoxicity towards the host cell ($[IC_{50}] = 8.6 \text{ nM}$, $[CC_{50}] = 12.8 \text{ nM}$). Furthermore, Noricumazole A has shown above average inhibitory activity of the voltage-sensitive sodium channel NaV1.7 as well as stabilizing and inhibitory effect on the pH and voltage-dependent potassium ion channel KcsA. In this work, different strategies towards new Noricumazole A derivatives have been investigated. Initially a convergent approach to synthesize a derivative that constitutes of all activity relevant structural elements has been followed. The envisioned structure contained a thiazole ring that has been observed to decrease cytotoxicity as well as the acylated hydroxyl groups at C3 and C11 that have shown to inhibit above average increase of activity. The key coupling step between the two final fragments has been unsuccessful due to the initial oxidation step of the western fragment that has given none-reproducible results.

A different strategy towards structurally different Noricumazole derivative has also been pursued – a derivative lacking the hydroxilic group at C13. The convergent synthesis was directed towards two key fragments that would be brought together in an *o*-lithiation end-game reaction.

Furthermore, an optical transport test was developed to study the effect of Noricumazole A derivatives on the viroporin HCV p7. For this purpose, the fluorescent dye PBFI was used as an optical potassium sensor of detecting the HCV p7 mediated potassium transport activity of potassium ions into the liposomes. The transport capacity was reconstituted with PBFI and purified HCV p7 ion channel in liposomes. This made it possible to observe the transport activity of HCV p7 as a function of time. The change in the fluorescence intensity is interpreted as transport activity and is generated by injecting a concentrated potassium chloride solution into the current kinetics. The absence of HCV p7 ion channels in the control liposomes generates little response to the potassium chloride injection, while the presence of HCV p7 shows a drastic increase in the fluorescence signal. In the presence of Noricumazole A, the transport activity is reduced depending on the concentration and results in a dose-response dependence of an IC_{50} of $4 \mu\text{M}$.

Key words: Noricumazole, HCV p7, ion channel

Table of Contents

I. Zusammenfassung	I
II. Abstract	II
1. List of abbreviations	1
2. Introduction	3
2.1 Hepatitis C	3
2.2 Noricumazole	7
2.3 Isolation and structure elucidation	9
2.4 Biosynthesis	10
2.5 Antiviral activity	11
2.6 Influence on ion channels	12
2.7 Structure-activity relationship analysis in Noricumazole A	17
3. Purpose of the project	19
4. Discussion and results	20
4.1 Retrosynthesis	20
4.1.1 Retrosynthesis of the eastern fragment	20
4.1.2 Retrosynthesis of the western fragment	21
4.2 Synthesis	22
4.2.1 Synthesis of the eastern fragment	22
4.2.2 Synthesis of the western fragment	24
4.2.3 Coupling reaction	25
4.2.4 Towards optimization of the oxidation reaction	33
4.3 Test derivative. Retrosynthesis	35
4.3.1 Synthesis of eastern fragment 112 and test fragment 114	39
4.3.2 End game – <i>ortho</i> -lithiation	44
5. Monitoring the HCV p7 activity by optical transport assays	47
5.1 Optimization of the p7 assay on microarray	57
5.2 Pull-down assays	61
6. Summary and outlook	63
6.1 Conclusions and summary	63
6.2 Outlook of the project	68
7. Experimental part	70
7.1 Materials and methods	70
7.2 Synthesis of eastern fragment 25	72

7.3 Synthesis of western fragment 24	88
7.4 Chiral ligands	97
7.5 Test substrates	104
8. Liposome assays	128
8.1 Synthesis of the pGST-P/ fusion protein	128
8.2 Isolation of the fusion protein GST-P7	128
8.3 Preparation of unilamellar liposomes.....	129
8.4 HTPS trials.....	130
8.5 PBFI trials	132
9. References	142
10. Appendix.....	148

1. List of abbreviations

Ac	acetyl
aq	aqueous solution
eq.	equivalents
Ar	aryl
Bn	benzene
Boc	<i>t</i> -Butyloxycarbonyl
br	broad
<i>n</i> -Bu	<i>n</i> -Butyl
<i>t</i> -Bu	<i>t</i> -Butyl
ca.	circa
Cp	cyclopentadienyl
δ	chemical shift
DAA	direct acting antivirals
d	days
d	doublet
dppf	1,1'-bis(diphenylphosphino)ferrocene
DMAP	4-(dimethylamino)-pyridine
DME	ethylenglycoldimethylether
TMEDA	<i>N,N'</i> -dimethylethylendiamin
DMF	<i>N,N</i> -dimethylformamid
DMSO	dimethylsulfoxid
ESI	edectrosprayionisation
Et	ethyl
GT	geno type
g	gram
GC-MS	Gaschromatographie mit Massenspektrometrie-Kopplung
h	hours
HCV	hepatitis C virus
HPLC	high-pressure liquid chromatography
Hz	hertz
<i>J</i>	coupling constant
LC-MS	liquid chromatography–mass spectrometry
LDA	lithiumdiisopropylamide
m	multiplet
M	molar
[M+]	molecular peak
Me	methyl
Mes	mesitylene
mg	milligram
MHz	megahertz
min	minuten
mL	milliliter
mmol	millimol
MS	mass spectrometry
<i>m/z</i>	mass / charge
NPHV	nonprimate hepavirus
NMR	nuclear magnetic resonance
PE	petroleum ether (40-60 °C)

Ph	phenyl
ppm	<i>parts per million</i>
Py	pyridin
q	quartet
quant.	Quantitative
RNA	ribonucleic acid
rpm	rounds per minute
RT	room temperature
s	singulet
<i>T</i>	temperature
t	triplet
TEM	Transmission electron microscopy
Tf	trifluoromethanesulfonate
Tr	triphenylmethyl
TBAF	tetrabutylammoniumfluorid
TFA	trifluoro acetic acid
THF	tetrahydrofuran
TMEDA	<i>N,N,N',N'</i> -tetramethylethylenediamine
TMS	trimethylsilyl

2. Introduction

2.1 Hepatitis C

Hepatitis C virus (HCV) infection is a global health problem affecting approximately 71 million people worldwide. The virus causes acute and chronic hepatitis, which if untreated can progress to liver cirrhosis, hepatic failure or hepatocellular carcinoma.¹ Although antiviral chemotherapy exists, HCV infection is still one of the most common causes of liver transplantation.^{2, 3, 4}

HCV is a prototype member of the *Hepacivirus* genus within the *Flaviviridae* family. Its genome is made up of an enveloped, 9.6-kb positive-sense single-stranded RNA. Translation of the viral RNA yields a polyprotein that contains about 3000 amino acids. After cleavage by both cellular and viral proteases 10 mature virus gene products are generated: the structural proteins nucleocapsid C and envelope E1 and E2; the p7 ion channel; and the non-structural proteins which replicate the viral genome and regulate the host cell metabolism: NS2, NS3, NS4A, NS4B, NS5A and NS5B.^{3,4}

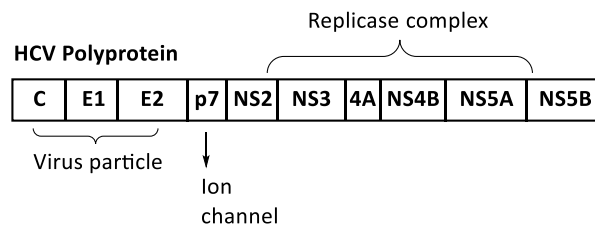


Figure 1 Functionality of the different proteins of the genome sequence of HCV.⁴

After initial infection, HCV virions are transported to the liver by the blood stream. There they attach to the surface of hepatocytes and a receptor-mediated cell entry takes place (endocytosis). When the HCV particle is released into the cytoplasm an uncoating of the virion occurs and the viral RNA is released. Cellular factors then aid the initiation of RNA translation. After translation, the HCV proteins are associated with intracellular membranes derived from the endoplasmic reticulum where replication takes place. Those membranes are deformed into uniquely shaped structures termed 'membranous webs'.

Afterwards, the NS proteins replicate the positive sense RNA genome. A negative strand intermediate is first produced by the viral RNA-dependent RNA polymerase NS5B. The negative strand RNA then serves as a template for the production of new positive strand viral genomes.

Nascent genomes can then be further assembled together and packaged within new virus particles. The new virus particles are thought to bud into the secretory pathway and are released at the cell surface. The release usually leads to cell-death of the hepatocyte. The high mutation rate of the virus reproduction in just one host cell leads to complications in therapy development.^{5,6}

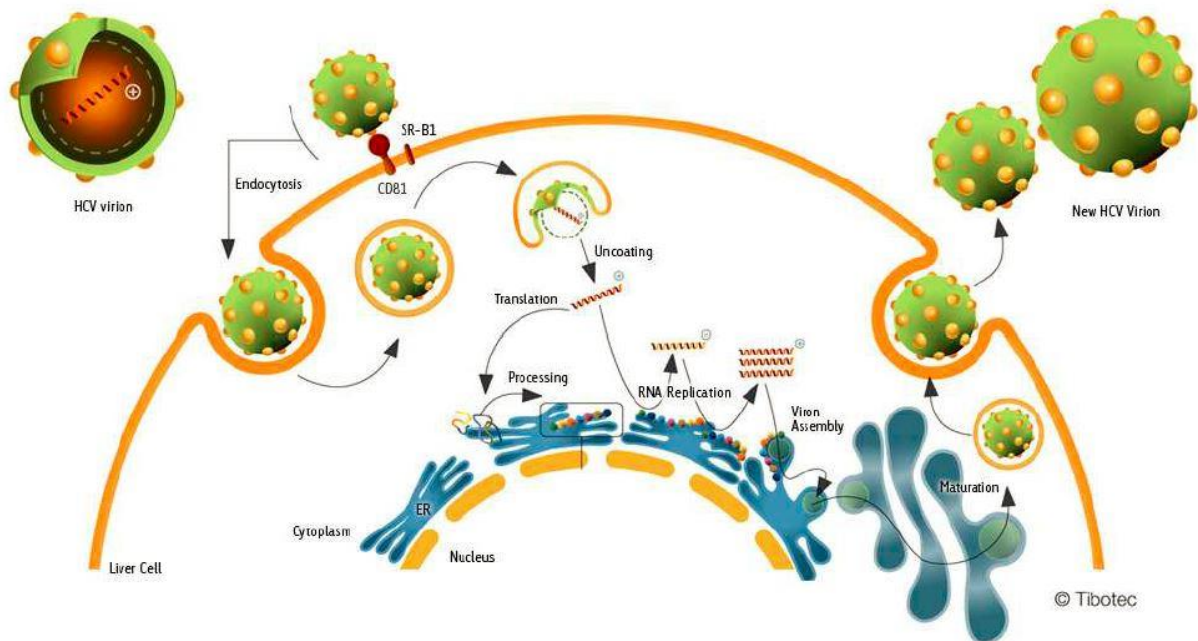


Figure 2 Life-cycle of Hepatitis C in a liver cell.⁷

HCV has six well defined genotypes identified worldwide as GTs 1 – 6. These genotypes may further vary in subtypes as is demonstrated in HCV GT 1a and GT 1b. The difference between the nucleotide sequences can be more than 50%. Genotypes are of clinical importance as a factor in response to HCV treatment.

In the past, the treatment for HCV has been dual therapy with pegylated Interferon alpha **1** and ribavirin **2**.^{8,9}

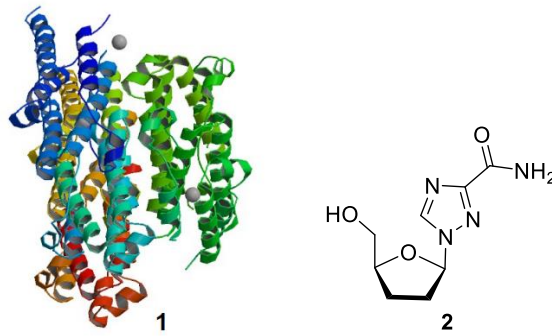


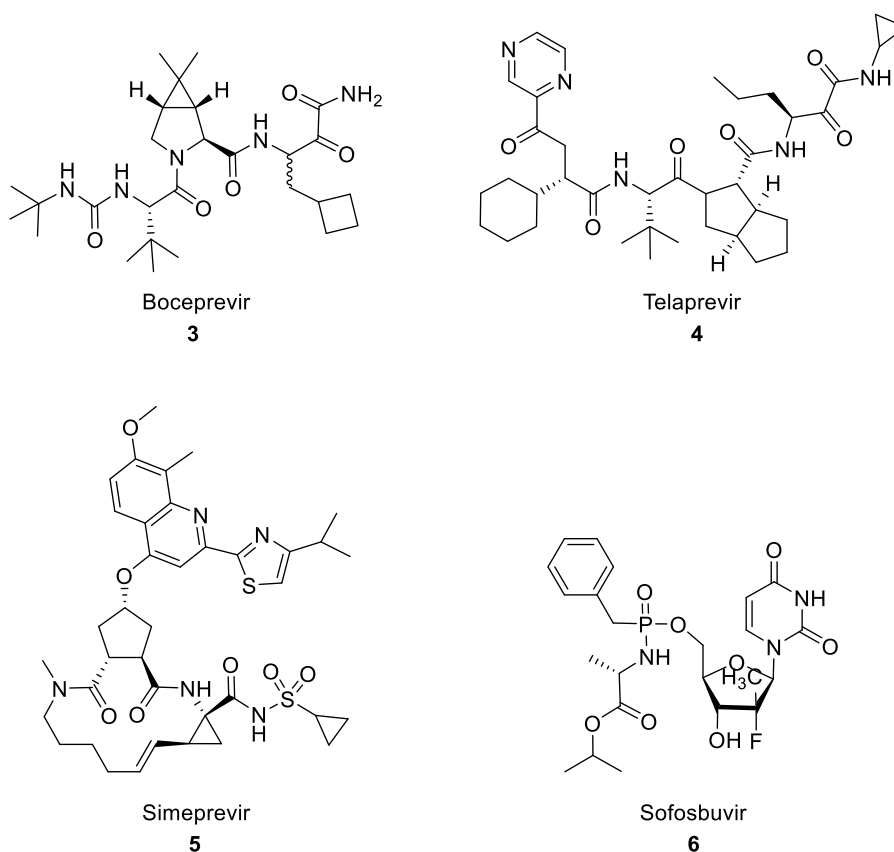
Figure 3 Standard dual HCV therapy.¹⁰

Interferon alpha is a cytokine – a signaling protein that can trigger the body’s immune response to viruses and other pathogens. Furthermore, it can activate interferon-stimulated genes, which encode proteins that inhibit various stages of viral replication. Ribavirin is a synthetic antiviral nucleoside analogue that has no impact on HCV on its own, but in combination it induces the inhibition of the viral growth and replication. This treatment has had low rates of success and significant adverse effects.¹¹

A better understanding of the HCV genome and proteins has enabled the development of a treatment that has greater efficacy and tolerability as well as high cure rates. Particularly, this has been the breakthrough of direct-acting antivirals (DAAs).

The treatment development has first been established with the approval in 2011 of the two oral DAAs Boceprevir and Telaprevir. These drugs have been used in combination with PEG-IFN and RBV for GT 1 that have brought the sustained virological response (SVR) rates up to 70%, however these agents have sustained broad adverse effect profiles.^{12, 13}

In 2013 a new standard was established with the approval of Simeprevir and Sofosbuvir as the first oral once-daily treatments that have had no adverse effects and have produced SVR rates higher than 90% either together, in combination or with PEG-IFN plus RBV in selected genotypes.¹⁴



Scheme 1 Important DAA drugs in the development for HCV treatment

Since then many DAA medications have been approved - treatments that do not use IFN are available for all HCV genotypes. Those are generally well-tolerated, all-oral regimens for various HCV genotypes and stages of liver disease.

The newer DAA medications act to target specific points of the HCV viral life cycle. These drugs target specific nonstructural proteins of the virus that results in disruption of viral replication and infection. DAAs are classified according to their mechanism of action and therapeutic target.

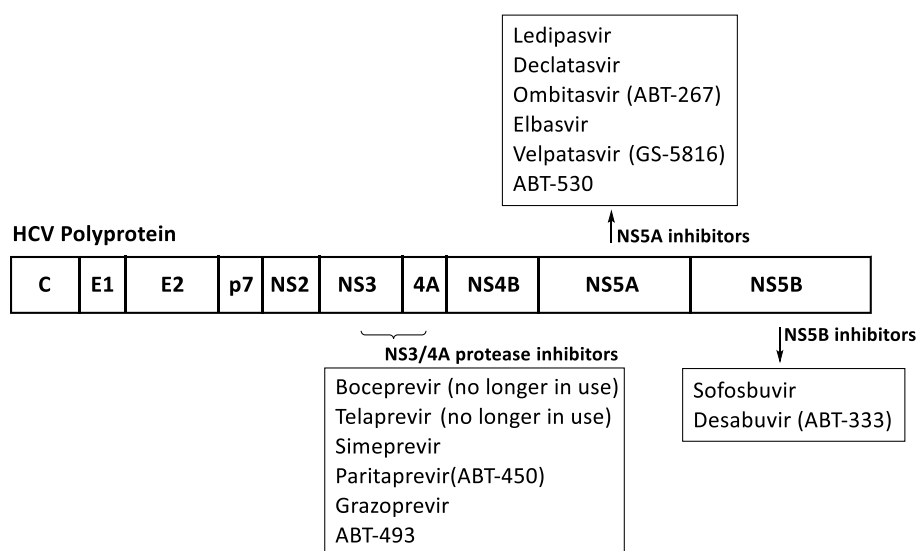


Figure 4 Molecular targets for HCV direct acting anti viral therapy.

The main targets are nonstructural proteins 3/4A (NS3/4A) protease inhibitors (PIs), NS5B nucleoside polymerase inhibitors (NPIs), NS5B non-nucleoside polymerase inhibitors (NNPIs), and NS5A inhibitors. Medications that target the NS3/4A protease contain the suffix “-previr,” medications that inhibit the NS5B polymerase have the suffix “-buvir,” and NS5A inhibitors end in “-asvir”.^{15, 16}

2.2 Noricumazole

For many years natural products have played a major role in modern drug discovery programs. About 42% of all small-molecule drugs approved worldwide in the period 1981-2014 were natural products or their close semi-synthetic derivatives.

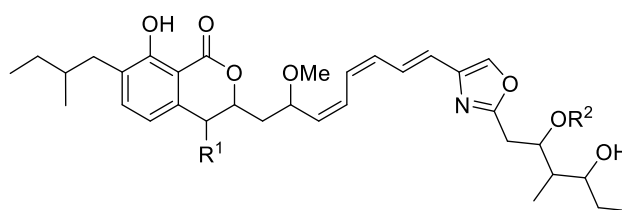
Myxobacteria are known to produce some 5% of known bacterial natural products. Myxobacteria are rod-shaped Gram-negative, soil-dwelling bacteria, recognized for their complex social behavior and life cycle. They are found worldwide in all climate zones and vegetation belts, preferentially wherever there is a rich microbial flora.^{17, 18}

Myxobacteria come in two basically different cell shapes, representing two suborders. Species of the suborder *Cystobacterineae* have long, slender, highly flexible cells with tapering ends, usually boat to needle shaped. In the suborder *Sorangineae*, the cells are cylindrical with rounded ends, often shorter and stouter than the former (Figure 5).^{19, 20}

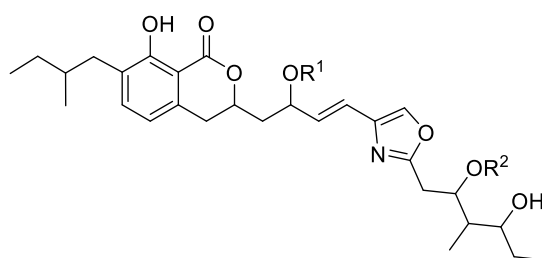
antibiotic Sorangicin A **9** acts by inhibiting the RNA synthesis within bacteria cells. Carolacton **10** inhibits the bacterial pathogens *Streptococcus mutans* and *Streptococcus pneumonia* responsible for dental caries and pneumococcal infections by interfering with serine/ threonine protein kinase PknB-mediated signaling in growing cells.^{23, 24, 25, 26}

2.3 Isolation and structure elucidation

Icumazoles A, B1 and B2 were isolated for the first time from an antifungal extract of myxobacterium *Sorangium cellulosum*, So ce701 as part of a biological activity screening trial at the Helmholtz Center of Infectious Diseases (HZI Braunschweig). Possessing similar structural elements, Noricumazoles A, B and C were later isolated from the fermentation extract of *Sorangium cellouloum*, So ce399 and their exact structure were elucidated. Furthermore, the evaluation of their biological activity led to interesting findings.



Icumazole A (**11**) $R^1 = R^2 = H$
 Icumazole B1 (**12**) $R^1 = H$; $R^2 = \text{pentofuranosyl}$
 Icumazole B2 (**13**) $R^1 = \text{pentofuranosyl}$; $R^2 = H$



Noricumazole A (**14**) $R^1 = R^2 = H$
 Noricumazole B (**15**) $R^1 = H$; $R^2 = \text{pentofuranosyl}$
 Noricumazole C (**16**) $R^1 = \beta\text{-D-glucopyranosyl}$; $R^2 = H$

Scheme 3 Structures of Icumazole A (**11**), B1 (**12**), B2 (**13**) and Noricumazole A (**14**), B (**15**) and C (**16**).

After series of spectrometric and spectroscopic methods the final structures of Icumazole and Noricumazole were determined by Jansen *et al.* First the elemental compositions were resolved by high resolution ESIMS. Further, the composition of bond sequence were confirmed by NMR analysis including ^1H , ^{13}C , ^1H - ^1H -COSY, NOESY, TOCSY, HMQC, HMBC methods.

The absolute configuration of all stereogenic centers was established by a chemical approach based on Noricumazole A. The Rychnovski's acetonide method was used to determine the relative configuration of the 1, 3 – diol moieties. One diastereomer was then synthesized as well as its epi-diastereomer and were compared with the authentic samples from biosynthesis to confirm the absolute stereochemistry of all stereogenic centers.

The final structure elucidation of the Noricumazole A structure was greatly supported by the total synthesis of the molecule as well as further synthesis of diastereomeric derivatives reported by the Kirschning group.^{27, 28}

2.4 Biosynthesis

The biosynthesis of Noricumazole from *Sorangium cellulosum*, So ce399 has not yet been elucidated. Further research is necessary to identify the gene clusters and relevant biosynthesis proteins. Due to the typical polyketide structure of the molecule, it could be speculated that the biosynthesis of Noricumazole A is based on a hybrid, non-ribosomal polyketidesynthase (NR-PKS), type 1.

The postulated biosynthesis of Noricumazole as depicted in Figure 6 begins with loading propionyl coenzyme A at the starting domain, which processes it as activated thioester.

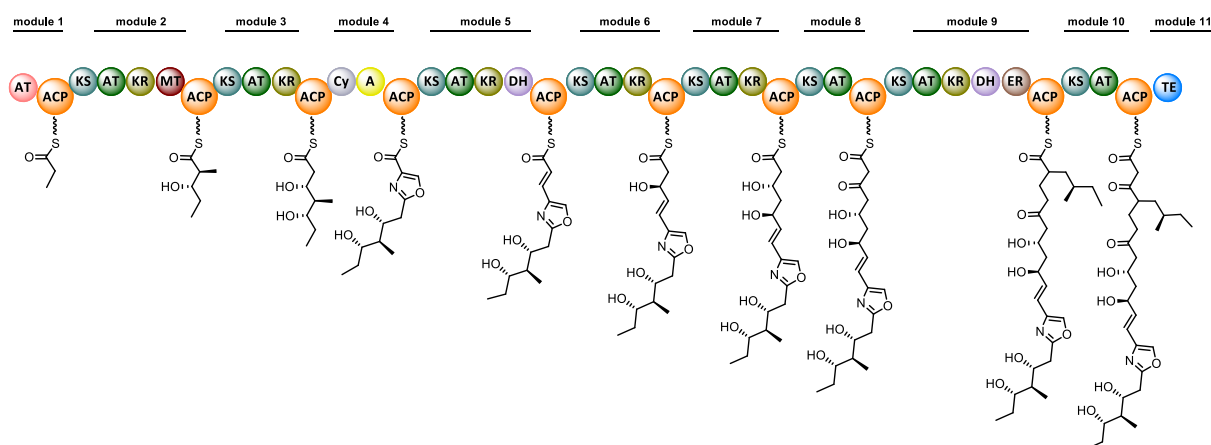


Figure 6 Postulated biosynthesis of Noricumazole A.

Two malonyl coenzyme A elongation units follow that build the carbon chain from C21 to C16. The methyl groups at C22 and C23 could be introduced either from a methylation domain in module 2 or directly from loading methylmalonyl coenzyme A as elongation unit.

The oxazole ring formation could be achieved with an amino acid building unit such as serine coenzyme A by amide formation and subsequent cyclase catalyzed cyclization.

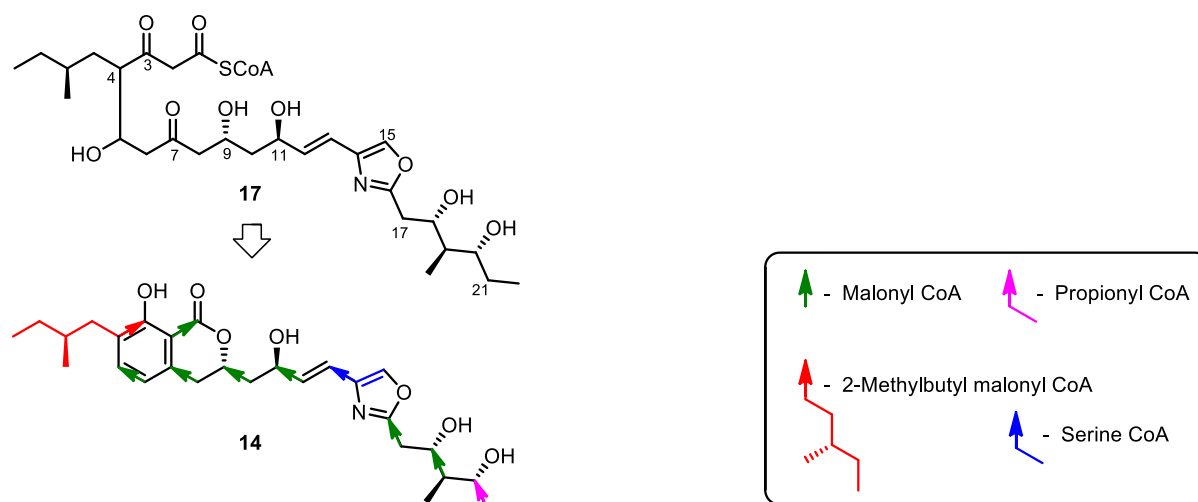


Figure 7 Postulated biosynthetic cyclization of Noricumazole A

Further four malonyl coenzyme A elongations would follow to build the main carbon chain from C5 to C21. At this point the aliphatic side chain could be introduced by loading 2-methylbutyl malonyl CoA as an elongation unit. An additional malonyl CoA unit would give the open-chain polyketide **17** that would be cleaved off by the PKS and cyclized to yield the Noricumazole A molecule **14**.

Further studies are necessary to evaluate and confirm the exact mechanism of the Noricumazole biosynthesis.

2.5 Antiviral activity

Noricumazole A was found to have hepatitis C specific antiviral activity by directly effecting the virus life-cycle while maintaining low cytotoxicity towards the host cell ($[IC_{50}] = 8.6 \text{ nM}$, $[CC_{50}] = 12.8 \text{ nM}$). In the course of a series of studies from Pietschmann *et al.* that have been based on human liver carcinoma cells, a comprehensive description of the virus life-cycle was achieved and Noricumazole A was identified as a substance that inhibits the replication of the hepatitis C virus by 90%.^{29, 30, 31}

2.5.1 Influence on ion channels.

Ion channels are essential for the normal function of important biological processes such as cardiac, skeletal and smooth muscle contraction, T-cell activation, nerve-impulse generation, pancreatic beta-cell insulin release and many more. They are proteins that regulate the selective

passage of ions through cellular membranes. Due to their vital role in steering biological functions, ion channels are often suitable drug targets in the research and development of new drugs.

A wide range of viruses also encode ion channel proteins called viroporins for the purpose of modifying host-cell ion homeostasis to aid viral infection. Viroporins are small hydrophobic proteins comprised of not more than 120 amino acids and encode at least one transmembrane passage. Viroporins make up a large family of multifunctional proteins from diverse virus families mainly concentrated in RNA viruses. A number of pathogenic human viruses, such as hepatitis C virus (HCV), influenza A virus (IAV), human immunodeficiency virus 1 (HIV-1), several picornaviruses, respiratory syncytial virus (RSV), and coronaviruses (CoVs) encode at least one viroporin. These transmembrane proteins support important phases of the viral life cycle through various mechanisms. In general viroporins are not essential for RNA replication of the virus but they promote the virus assembly/release and, in the case of the M2 protein, also virus entry.

Viroporins oligomerize in cell membranes to form ion conductive channels. Typically viroporins do not show preference for particular ionic species as they display mild ion selectivity. Ion channel activity is relevant for virus propagation and could have a big impact on host-cell ionic physiology. Ion channel activity ranges from almost essential, to highly or moderately necessary for viruses to yield properly. Taking this into consideration ion conductivity and its pathological stimulated pathways can represent targets for combined therapeutic interventions.^{32, 33, 34}

Noricumazole A has shown above average inhibitory activity of the voltage-sensitive sodium channel Nav1.7. In comparison with the reference substance that have been used in these electrophysiological tests – Phenytoin – Noricumazole A has shown 2.3 to 2.5 higher activity. Phenytoin is a well-known drug used as anticonvulsive agent for treatment of epilepsy seizures as well as antiarrhythmic substance for treatment of abnormal heart rhythm.

The biological influence of Noricumazole A on ion channels was further studied with regards to the pH and voltage-dependent potassium ion channel KcsA.³⁵

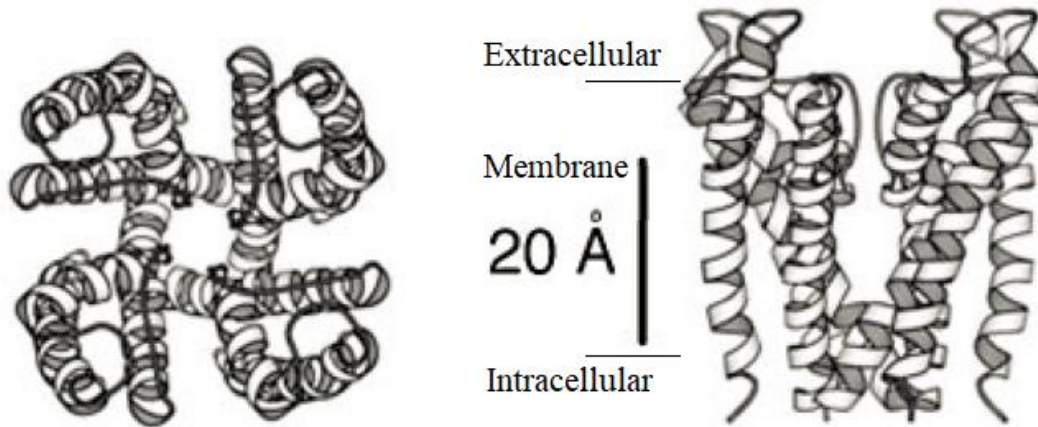


Figure 8 Top (left) and side (right) view of the structure of the KcsA ion channel.³⁶

The bacterial KcsA ion channel enables the selective transportation of potassium ions through the cellular membrane. The structure of the channel was established to consist of four identical subunits each containing two alpha-helices connected together to form a pore loop on the inside that is a suitable size for potassium ions but not for sodium ions (Figure 8).

The opening of the channel can be activated by low pH values.³⁷

Noricumazole A has been reported to be the first natural product that induces temperature-dependent stabilization of the tetrameric architecture of the KcsA ion channel. The tetrameric KcsA ion channels have shown to half dissociate into monomers at 82 °C. In the presence of Noricumazole A the KcsA tetramers have been observed to remain stable up to 90 °C. Only sodium chloride has been known to have a similar effect as well as potassium chloride specifically for KcsA ion channel.

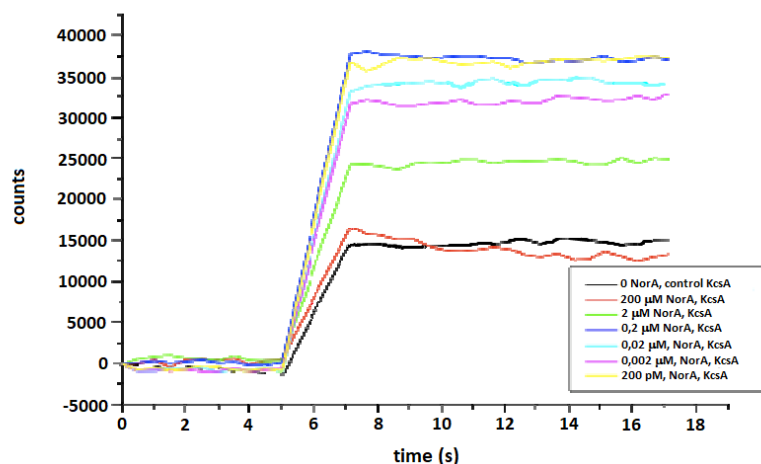


Figure 9 Inhibitory effect of different concentrations of Noricumazole A on the ion channel KcsA.

To further explore the influence of Noricumazole A on the biological function of the ion channel KcsA, a fluorescence liposome assay was conducted by the Kirschning group. The potassium sensitive dye PBFI was used to detect potassium transport in reconstituted liposome systems. Liposomes were charged with PBFI and purified KcsA ion channel. Afterwards potassium chloride solution was injected and potassium ions were transported inside the liposomes and the fluorescence signal was monitored. In the absence of KcsA, the control liposomes only showed weak response to the potassium chloride injection (Figure 9). Addition of Noricumazole A caused reduction of the fluorescence signal in a dose-dependent manner which confirmed a concentration-dependent inhibitory effect of the molecule.^{28, 38, 39, 40, 41, 42}

2.6 The viroporin p7 from hepatitis C virus

Most recent studies identify virus infections similar to hepatitis C in animals – dogs, horses, rodents, bats, nonhuman primates and cattle. Strikingly, the nonprimate hepacivirus (NPHV) described to infect dogs and horses is the closest homolog of HCV. Both viruses encode the same viral proteins and thus represent a model to study genome differences. Furthermore, targeted genome comparison of animal hepaciviruses might help elucidating the evolution of the ancestral virus lineages out of which HCV developed

Both HCV and NPHV encode the small membrane protein p7.⁴³ It consists of 63 amino acids and contains two trans-membrane alpha helices separated by a conserved basic loop. It is classified as a viroporin due to its small size and its ability to form oligomeric, hydrophobic ion channels in the endoplasmic reticulum membrane.

In lipid bilayer membranes p7 channel has shown to be permeable to potassium and sodium ions but has limited permeability to calcium ions.

Initial studies using transmission EM (TEM) and computer-based image analysis have suggested that in biological membranes p7 might exist as a mixture of oligomers with variable size.^{44, 45}

Further TEM study combined with single particle reconstruction of chemically synthesized full-length p7 of Gt2a, solubilized in short chain DHPC (1, 2-diheptanoyl-snglycero-3-phosphocholine) detergent micelles at pH 7.0, has produced the first 3D structure of hexameric p7 channels at 16 Å resolution. It was found that the p7 channel exists as a flower-shaped complex with 6 petals emerging from a conical base (Fig. 10).

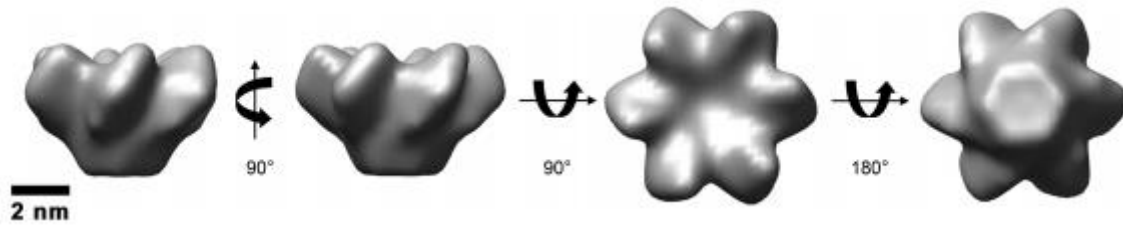


Figure 10 The 3D structure of a hexameric HCV p7 ion channel. The cone shaped structure is 8.1 nm in diameter at the widest point and 4.8 nm in height.⁴⁶

The generation of the first EM density map from this study has allowed modeling of simulated p7 monomers into the hexameric volume with a high fitting value (97.3%) as well as to predict interactions between them at the lower part of the channel (Fig. 11).⁴⁶

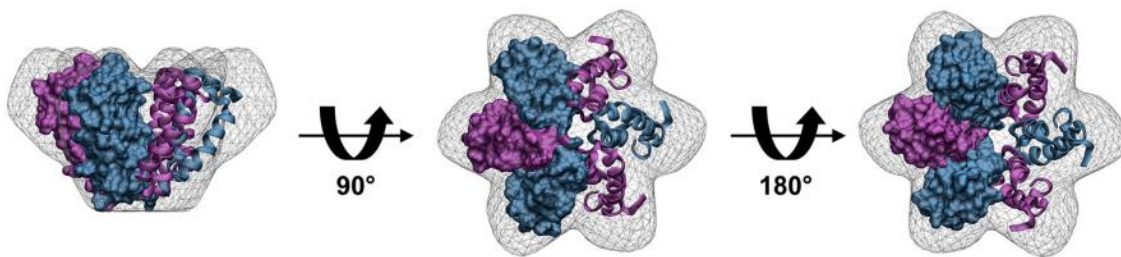


Figure 11 Atomistic models of p7 monomers fitted into the hexameric volume with their C and N termini oriented toward the petal tips. For illustration purposes, alternating colors of the monomers (blue and purple) are shown. In each model, 3 neighbouring monomers are surface represented; for the other 3 the peptide backbones are shown.⁴⁶

Clarke *et al.* reported genotype specific heptameric p7 complexes in low-resolution TEM images (Fig. 12).⁴⁷ A similar heptameric model has also been reported by Chandler *et al.*⁴⁸

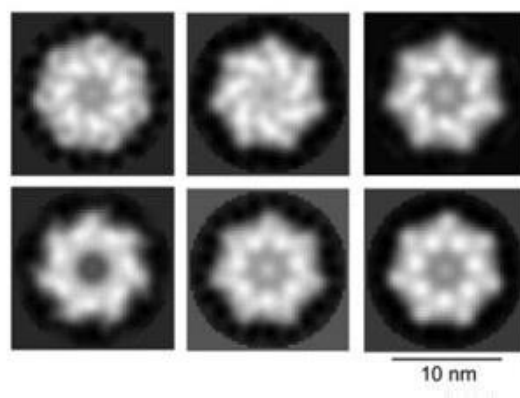
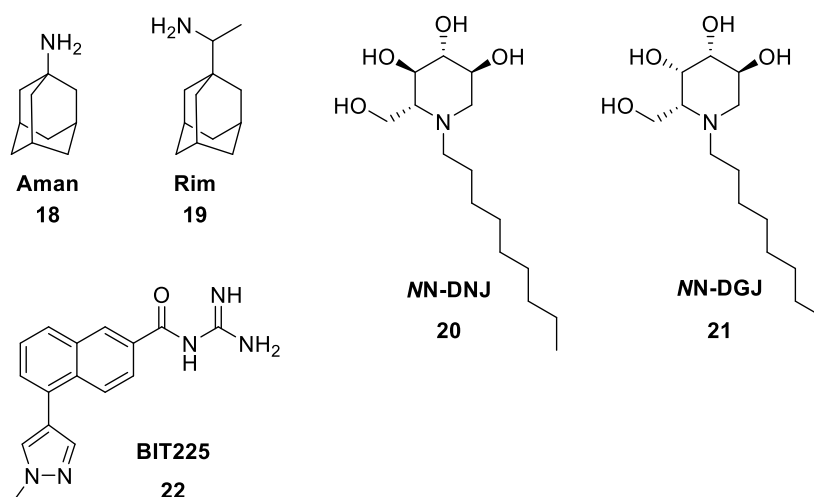


Figure 12 Heptameric stoichiometry of p7. These rotationally filtered images depict different conformations of the protein complex that may indicate a switch between different states or a tolerance for flexibility within the heptameric assembly.⁴⁷

In vitro studies revealed that p7 is essential for HCV assembly and release, whereas it is not essential for viral replication.⁴⁹

Although NPHV p7 shares comparable structural features with its human homolog and has an ion channel activity, the protein cannot fully replace HCV p7 during virus assembly. Studies where NPHV/HCV p7 chimeric viruses have been constructed have shown that the N terminus and transmembrane domains are nonexchangeable whereas the basic loop and the C terminus are exchangeable and lead to production of infectious viral particles, thus defining virus species-specific and interchangeable subdomains within p7.⁴³

A number of small molecules that inhibit production of HCV particles, presumably via interference with p7 function, were reported.⁵⁰ Amantadine **18** has been demonstrated to be a potential p7 inhibitor. Expression of p7 in mammalian cells could substitute for the channel activity of the influenza virus M2 protein and maintain virus infectivity. That activity could further be blocked by amantadine **18**.⁵¹ Furthermore, fluorescence-based liposome assays were established to observe the p7 ion-channel activity and its potential as therapeutic target. Employment of such assays using p7 from genotype 1b has shown a dose-dependent release of fluorescent indicator when mixed with liposomes. The drugs amantadine **18**, rimantadine **19** and several related compounds have shown to block the release activity of the ion channel.^{52, 53} BIT225 **22** has been the first acylguanidine in clinical trials against HCV and has also shown to inhibit p7 ion-channel activity in lipid membranes.⁵⁴



Scheme 4 Structures of biologically active compounds that have shown inhibitory activity towards p7

Extensive studies by Griffin *et al.* were conducted to differentiate the genotype- and subtype-dependent sensitivity of p7 to multiple inhibitors. It was found that p7 from genotype 1a isolate

is not blocked by amantadine, whereas amantadine successfully inhibited genotype 1b and 3a isolates. Rimantadine has been found to inhibit both genotypes 1a and 1b channel activity and virus production. Additionally, the long alkyl chain iminosugar derivatives N-nonyl deoxygalactonojirimycin (NN-DGJ) **21** and N-nonyl deoxynojirimycin (NN-DNJ) **20** have been reported to reduce infectious virus production for genotype 2a and 1b in a dose-dependent manner with no observable cellular cytotoxicity (Griffin et al., 2008).⁵⁵

Differing results have been obtained with various inhibitors in the context of different genotypes. These contrasting results suggest that p7 inhibitors may need to be developed in a genotype-specific manner.⁵⁶

Screening such compounds could aid the better understanding of p7 function and support further clinical development to optimize HCV-specific antiviral treatments.

2.7 Structure-activity relationship in Noricumazole A

Initial structure-activity analysis could be conducted based on the synthesis of more than 20 derivatives of Noricumazole by the Kirschning group.^{27, 28}

It was shown that some structural elements are essential for the biological activity and some small structural modifications could decrease the cytotoxicity.

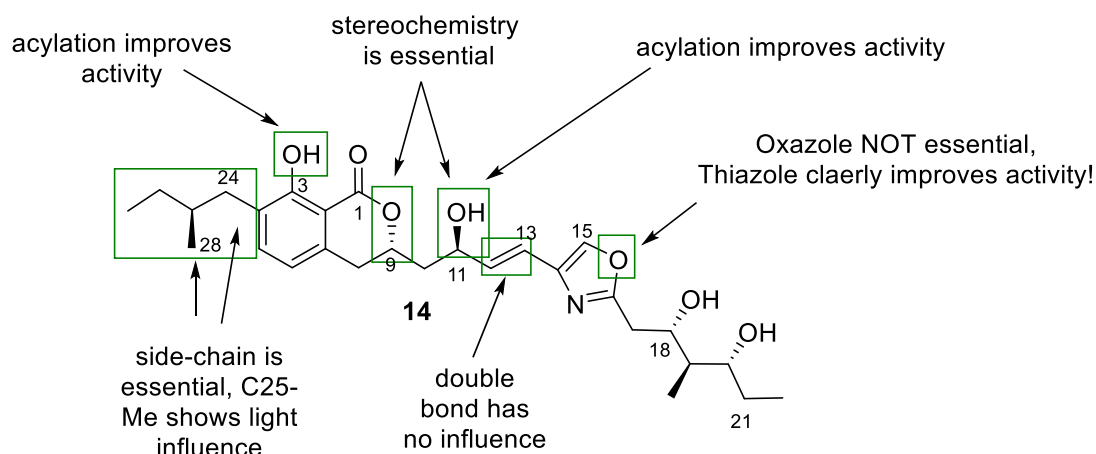


Figure 13 The importance of certain structural elements of Noricumazole A.

The SAR picture (Figure 13) displays that absence of the aliphatic side-chain at C4 reduces antiviral activity and that stereochemical information at C9 and C11 is important for the biological activity. Furthermore, the oxazole ring and unsaturated unit at C12 and C13 have

been proven not to be essential for antiviral activity. In contrast, a thiazole ring results in more potent activity (it is not clear whether a five-membered ring is essential for activity). The hydroxyl groups at C3 and C11 have shown to inhibit above average increase of activity after being acylated.

Further derivatization of the molecule with regards to the hydroxyl groups at C11 and C3 as well as the oxazole ring would help to better understand the importance of those structural elements for the biological activity as well as would help confirm the initial SAR-trends that have been identified.

3 Purpose of the project

Continuing the work of Barbier et. al., the purpose of this project is to synthesize Noricumazole A derivatives, compare their HCV biological activity and expand the initial SAR map.^{27, 28}

The initial target would be a derivative **23** that constitutes all the biological activity relevant structural features described in the initial SAR analysis.

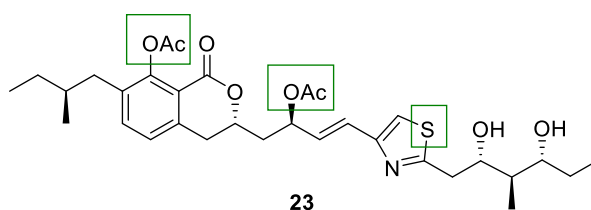


Figure 14 Envisioned derivative of Noricumazole A.

The total synthesis of the derivatives would follow a convergent synthetic pathway based on the first reported total synthesis of Noricumazole A.

Furthermore, additional investigations are to be conducted in order to get further insights into the mechanism of action of the Noricumazole A derivatives towards the HCV ion channel p7. Important conclusions are to be made regarding the ion channel's potential role as a drug target. For these purposes, a development and implementation of biophysical assays are to be conducted. Their set up would resemble the liposome-based fluorescent dye release assay reported by Griffin and it would investigate the p7 ion-channel activity and its drug inhibition ability towards various active molecules.

4 Discussion and results

4.1 Retrosynthesis

In order to select a suitable analogue of Noricumazole as synthetic target (Figure 15), the structure-activity findings discussed in chapter 2.7 and previous work were taken into consideration.^{27, 28} The aim was the synthesis of an analogue containing the key structural elements important for the biological activity, i.e. acylation of the hydroxyl groups at C3 and C11, the presence of stereochemistry at C9 and C11 as well as the thiazole ring.

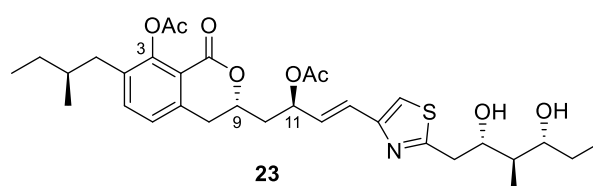
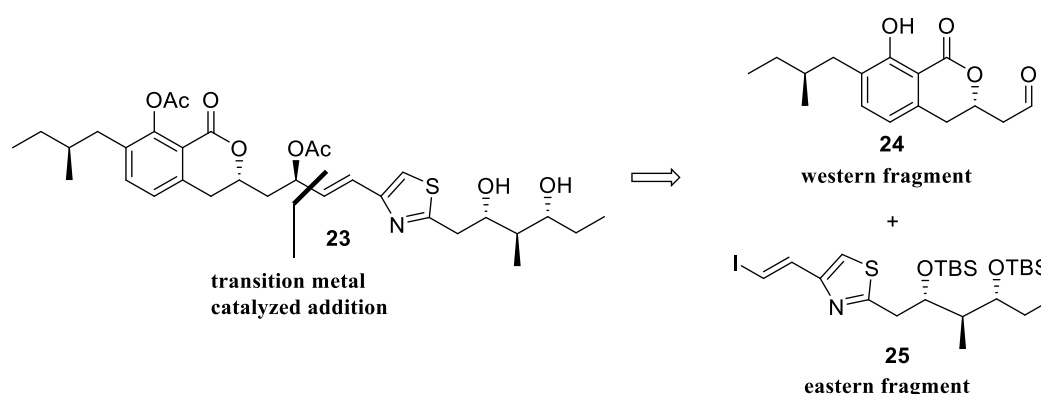


Figure 15: 3,11 – Ac Noricumazole S.

The planned strategy for the synthesis of the new derivative followed a convergent approach identical to the original total synthesis of Noricumazole A, i.e. the molecule would be split in two key fragments named eastern and western (Scheme 5).²⁷ Those would then be connected by a transition metal catalysed addition.



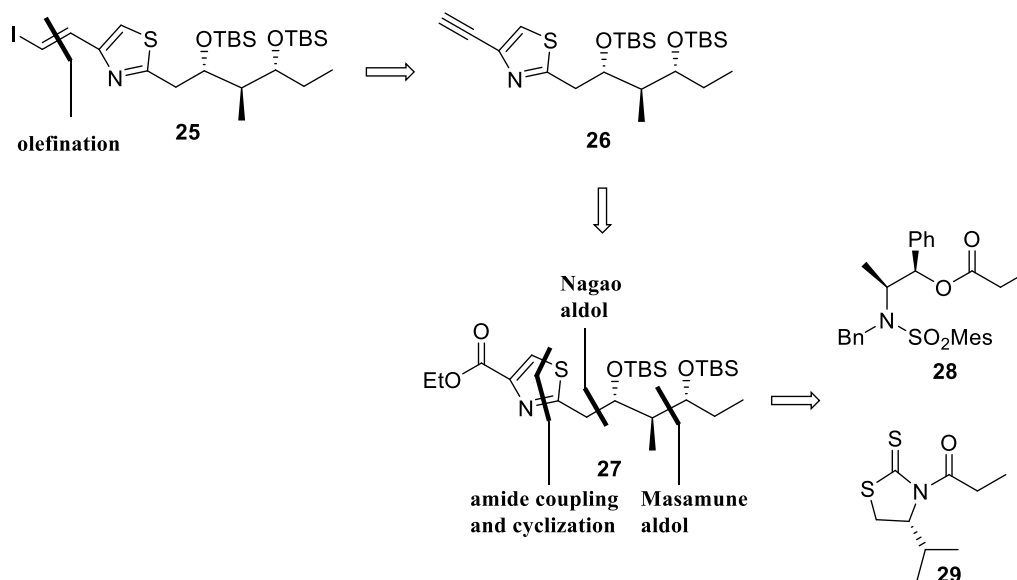
Scheme 5: Key retrosynthetic step for merging the western and the eastern fragments.

4.1.1. Retrosynthesis of the Eastern fragment

The typical polyketide structure of the Eastern fragment **25** was planned to be achieved by a classical aldol approach, employing the MASAMUNE *anti*-selective aldol and NAGAO aldol reactions to set the three stereocenters (Scheme 6).^{57, 58} Next, an amide coupling and cyclization would furnish precursor **27**. Alkyne **26** would be formed after reduction of ester **27** to an aldehyde and a SEYFERTH-GILBERT homologation to the desired precursor **26**.⁵⁹ The vinyl

iodide **25** was expected to be synthesized through a sequential *syn*-hydrozirconation and iodination of terminal alkyne **26**.

NAGAO **29** and MASAMUNE **28** chiral auxiliaries would be key starting building elements for this synthetic pathway.^{57, 58}

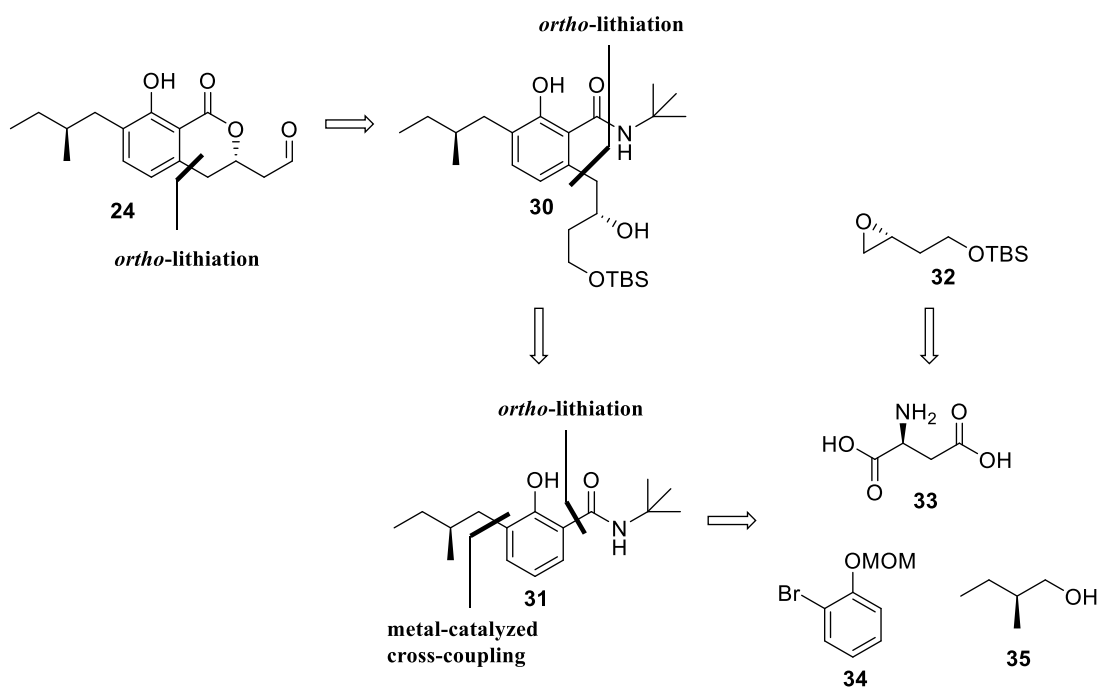


Scheme 6: Retrosynthesis of the Eastern fragment.

4.1.2 Retrosynthesis of the Western fragment

The synthetic strategy towards the western fragment was planned to involve the construction of the tetra – substituted phenolic precursor **30** that would be formed as a result of three sequential organometallic reactions (Scheme 7). The constitution of the lactone ring would be established after the synthesis of the key precursor **30**. This precursor was planned to be obtained from amide **31** through *ortho*-lithiation employing chiral epoxide opening similar to conditions initially described by KWON.⁶⁰ The chiral oxirane **32** would serve as a key starting material that provides the necessary stereochemistry at the lactone ring in the final structure. The literature known synthesis starts from commercially available L-aspartic acid **33** and follows a four step sequence.^{61, 62}

Amide **31** was expected to be established after *ortho*-lithiation followed by a metal-catalyzed coupling of the alkyl side-chain to the MOM-protected bromophenol precursor **34**. The necessary alkyl halide was planned to be synthesized from alcohol **35**.⁶³

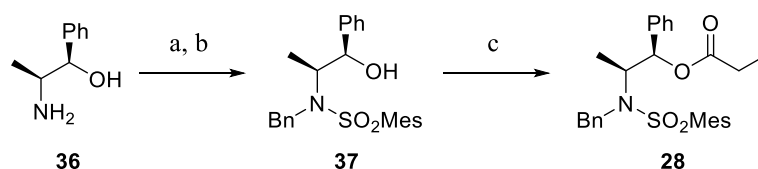


Scheme 7: Retrosynthesis of the western fragment.

4.2 Synthesis

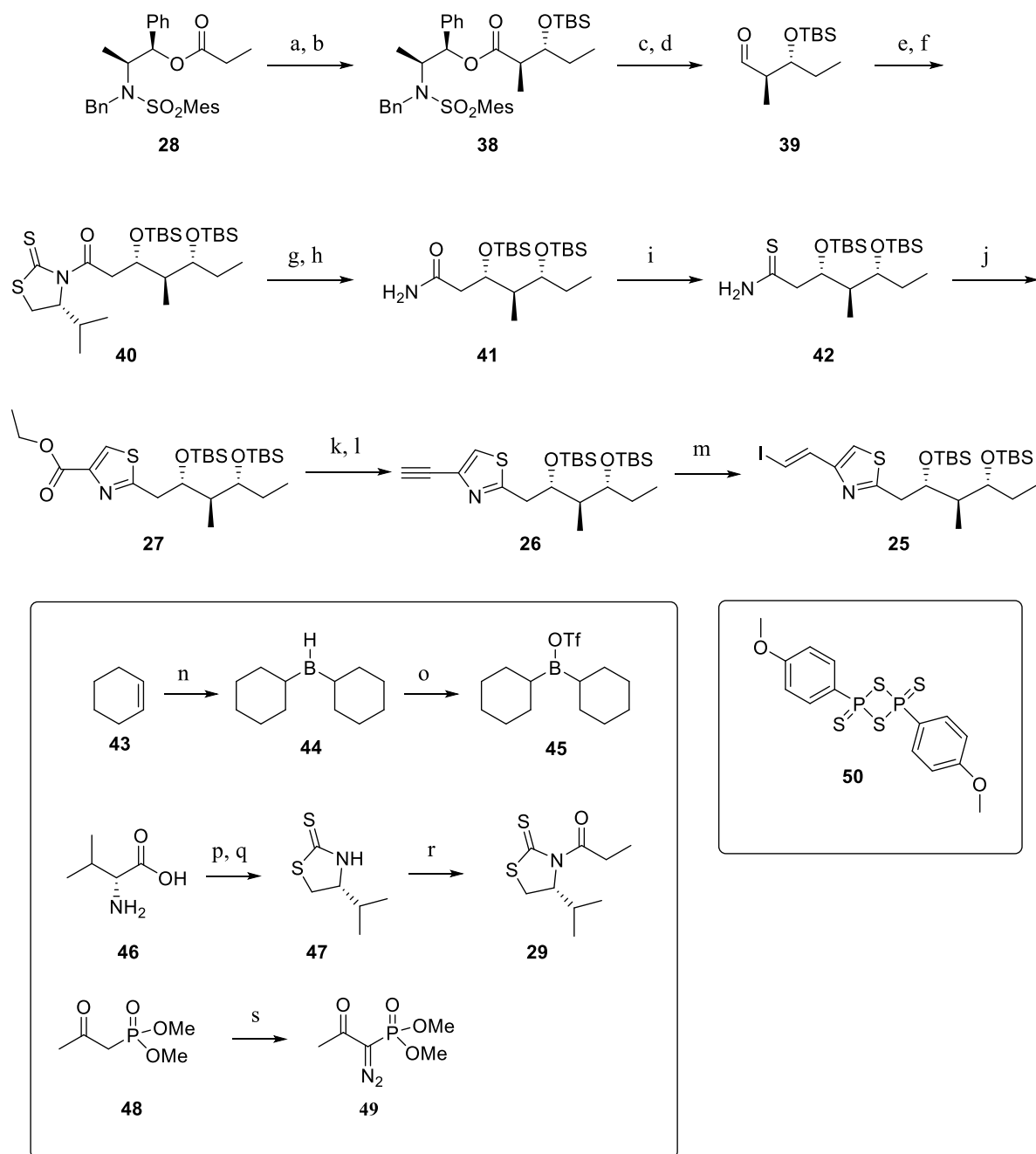
4.2.1 Synthesis of the eastern fragment

The synthesis of the eastern fragment started from the MASAMUNE chiral auxiliary **28** that was freshly prepared following the three-step procedure described originally (Scheme 8).⁵⁷



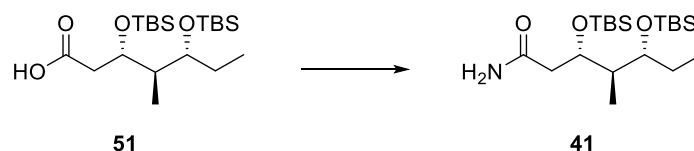
Scheme 8: Synthesis of MASAMUNE chiral auxiliary **xx**. Reaction conditions: a) MesSO₂Cl, NEt₃, THF, 0°C, 2 h; b) BnBr, KO^tBu, DMF, RT, 3h, 98%; c) propanoyl chloride, pyridine, CH₂Cl₂, RT, 16 h, 98 %.

The chiral MASAMUNE ester **28** then underwent a boron-mediated *anti*-aldol reaction with propionaldehyde (Scheme 9). The resultant alcohol was immediately TBS-protected (**38**) and the ester was further reduced to the corresponding alcohol using DIBAL-H. DESS-MARTIN oxidation and NAGAO aldol reaction with chiral auxiliary **29** followed. Another immediate TBS-protection took place that provided the desired precursor **40**, in which three stereocenters are established. Hydrolytic removal of the chiral auxiliary gave the free acid that was further transformed to the amide intermediate **41**.



Scheme 9: Synthesis of eastern fragment **25**. Reaction conditions: **a)** (c-Hex)₂BOTf **46**, NEt₃, CH₂Cl₂, -78 °C, 2h; propionaldehyde, -78 °C, 1h; 0 °C, 1h; RT, o/n, 95%; **b)** 2, 6 – lutidine, TBSOTf, CH₂Cl₂, -78 °C to 0 °C, 1,5 h, 98 %; **c)** DIBAL-H, CH₂Cl₂, -78 °C, 3h; RT, o/n, 68%; **d)** DMP, NaHCO₃, CH₂Cl₂, RT, 1,5 h; **e)** TiCl₄, DIPEA, CH₂Cl₂, -50 °C to -40 °C, 2h; **29**, -78 °C, 1,5h; **f)** 2,6 – lutidine, TBSOTf, CH₂Cl₂, -78 °C to RT, 1h, 36% over 2 steps; **g)** 30% H₂O₂, 1M LiOH, THF/H₂O, 0 °C to RT, o/n, 50%; **h)** ; **i)** Lawesson's reagent **50**, THF, RT, 4h, ; **j)** ethyl bromopyruvate, Me₂CO, -10 °C, 2h; TFAA, pyridine, CH₂Cl₂, -30 °C to RT, o/n, 88%; **k)** DIBAL-H, CH₂Cl₂, -78 °C, 2h, quant.; **l)** K₂CO₃, OHIRA-BESTMANN reagent **49**, MeOH, 0 °C, 14h, 96%; **m)** ZrCp₂(H)Cl, THF, 0 °C; NIS, -78 °C, 20 min, 89%; **n)** BH₃·Me₂S, Et₂O, 0 °C, 3 h, -20 °C, 24 h; **o)** TfOH, Hexan, RT, 1,5 h, -78 °C, 24 h, 98 %; **p)** NaBH₄, I₂, THF, 0 °C to reflux, 24h; **q)** CS₂, KOH, EtOH/H₂O, reflux, 48h, 53%; **r)** NEt₃, CH₃CH₂COCl, CH₂Cl₂, 0 °C to RT, 24h, 90%; **s)** NaH, TosN₃, benzene/THF, 0 °C to RT, 2h, 89%.

This transformation needed to be optimized since the conditions used in previous studies did not lead to the desired product but only led to the deprotection of one of the alcohol groups (Table 1 Entry 1). Typical peptide coupling conditions successfully gave the desired product in moderate yield.⁶⁴



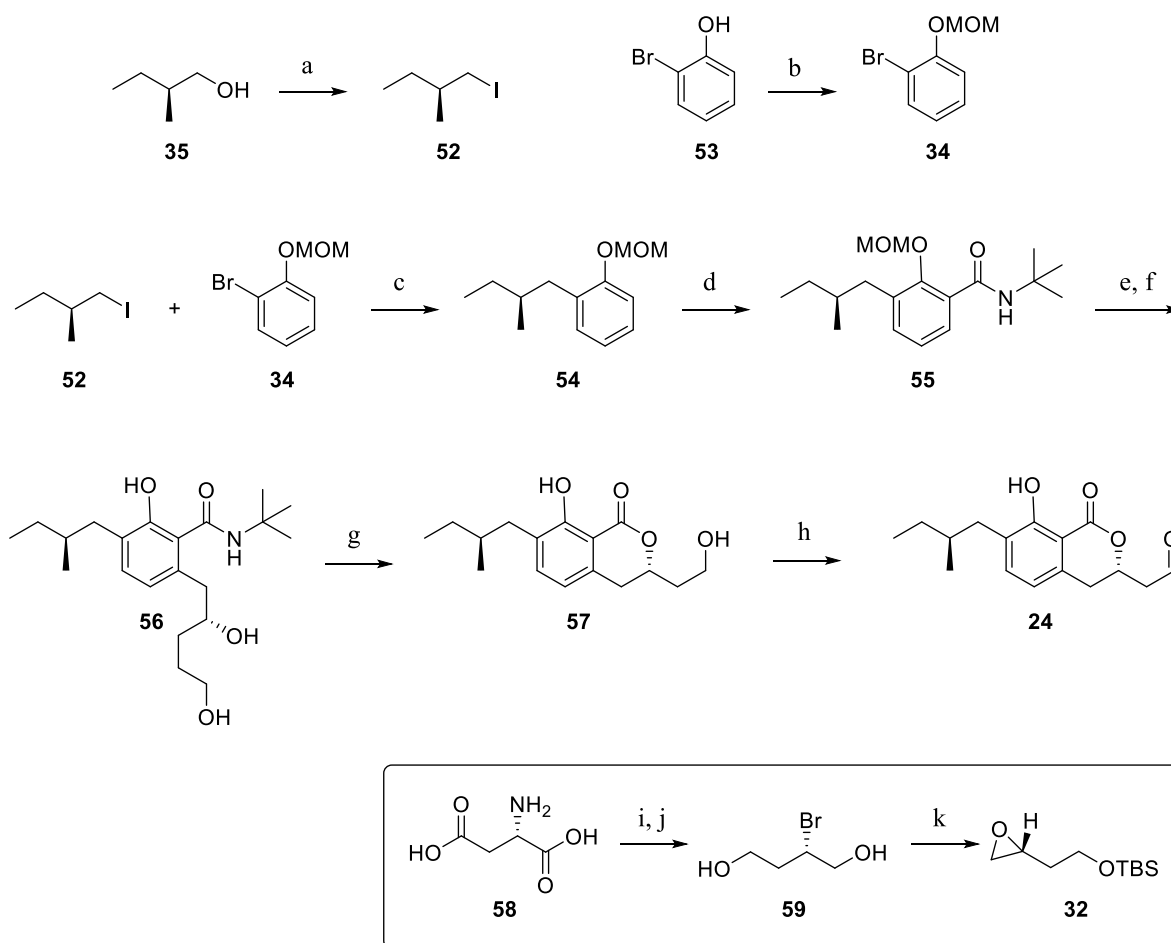
Entry	Reaction conditions	Results
1	i. (COCl) ₂ , Et ₂ O, 0°C to RT, 1 h; ii. NH ₃ , MeOH, 0°C to RT, 1 h.	No product. Mono-deprotection of 51 .
2	i. EDC, HOBT, NH ₃ , ii. CH ₂ Cl ₂ , 0°C to RT, 1 h.	Traces of product.
3	i. EDC, HOBT, NH ₃ , DIPEA ii. CH ₂ Cl ₂ , 0°C to RT, 1 h to 24 h.	52%

Table 1 Optimization of amide **20** formation.

Thionation of the amide with Lawesson's reagent **50** was followed by the coupling with bromide-ethyl ester and subsequent cyclization that furnished the thiazole ethyl ester **27** (Scheme 9). DIBAL-H reduction to the aldehyde and a SEYFERTH-GILBERT homologation utilizing the OHIRA-BESTMANN reagent **49** yielded the terminal alkyne **26**. Treatment with SCHWARZ reagent and *N*-Iodosuccinimide gave the vinyl iodide **25**. The hydrozirconation proceeded through *syn*-hydrometalation to furnish *trans* vinyl iodide in good yield. The reagent that were commercially not available were synthesized according to literature procedures (Scheme 5).^{59, 65, 66, 67}

4.2.2 Synthesis of the western fragment

The starting building units for the Western fragment were prepared by iodination of (*S*)-(-)-2 - methylbutanol and MOM-protection of 2-bromophenol respectively (Scheme 10). **52** and **34** were then coupled in an iron-catalyzed Kumada cross-coupling reaction to precursor **53**.⁶⁸



Scheme 10: Synthesis of western fragment **24**. Reaction conditions: **a)** I₂, PPh₃, imidazole, CH₂Cl₂, RT, 2h, 83%; **b)** MOMCl, K₂CO₃, DMF, 0 °C to RT, 2h, 99%; **c)** **xx**, Mg, THF, reflux, 2h; **xx**, Fe(acac)₃, TMEDA, HMTA, THF, 0 °C, 1,5 h, 63%; **d)** *n*BuLi, TMEDA, Et₂O, -30 °C, 2h; -5 °C, 3h; *t*BuNCO, RT, o/n; 71 %; **e)** *n*BuLi, TMEDA, Et₂O, -78 °C to -40 °C, 2h; **32**, -78 °C to -40 °C, o/n, 37%; **f)** half conc. HCl, EtOH, 50 °C, 1h, 53%; **g)** PTSA, toluene, reflux, 50 min, 62 %; **h)** **i)** KBr, H₂SO₄, NaNO₂, H₂O, 0 °C, 2h, ; **j)** BH₃·SMe₂, THF, RT, o/n, ; **k)** NaH, TBSCl, TBAI, THF, -10 °C to RT, 1,5 h.

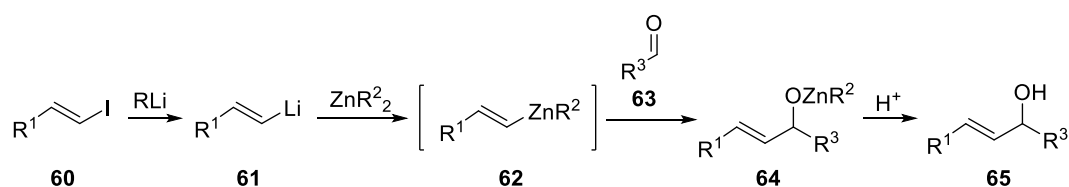
The *ortho* lithiation of **54** with *n*-BuLi was followed by treatment with tert-butyl isocyanate. The resulting amide **55** then undergoes a second *ortho*-lithiation step with a subsequent alkylation employing freshly prepared TBS-protected chiral oxirane **32**. The deprotection of the hydroxyl groups followed by lactonization furnished precursor **57**. Finally, Dess-Martin oxidation led to the desired aldehyde fragment **24**.⁶⁹

4.3 Coupling reaction

The final step in the synthesis of the Noricumazole derivative **23** was the stereoselective coupling of fragments **24** and **25**. Initially it was tried to utilize previously reported conditions

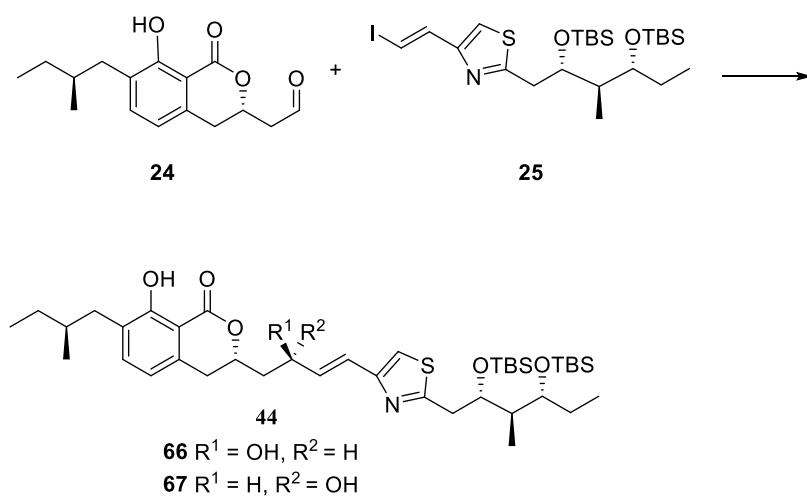
that involved substrate controlled nucleophilic addition of aldehyde **24** to vinyl iodide **25**.^{70, 71}

First, the vinyl iodide was transformed into vinyl lithium (**61**) (Scheme 11). This underwent transmetalation with dimethyl or diethyl zinc to form the key vinyl zinc species **62**. Aldehyde **63** was then added and after aqueous work-up the final alcohol **65** was collected.



Scheme 11 Mechanism of the zinc-catalyzed coupling of vinyl iodide **60** and an aldehyde **63**.

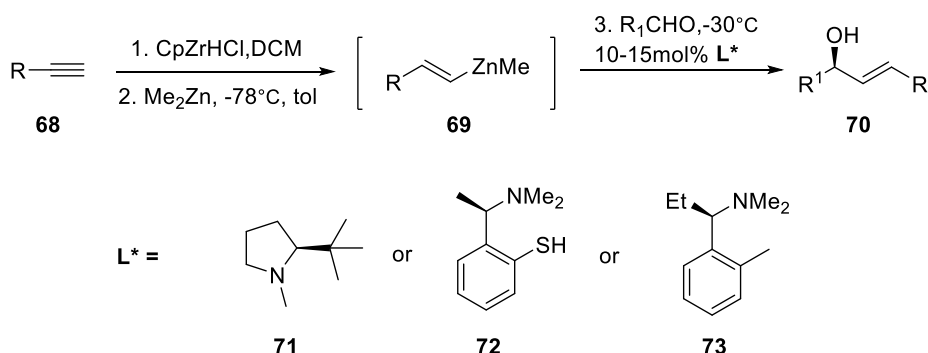
However, following this established strategy only poor yields were achieved and reproducibility was low. Optimization in terms of temperature and reaction time did not enhance the efficacy of the C-C coupling step (Table 2).



Entry	Reaction conditions	Results
1	i. <i>t</i> -BuLi (2 eq), 25 (1 eq.); ii. Me ₂ Zn; iii. 24 (1 eq.), 24 h	No product
2	i. <i>t</i> -BuLi (4 eq), 25 (2 eq.); ii. Me ₂ Zn; iii. 24 (1 eq.), 2 h	Traces of product
3	i. <i>t</i> -BuLi (4 eq), 25 (2 eq.); ii. Me ₂ Zn; iii. 24 (1 eq.), 24 h	34% xx + xx
4	i. <i>t</i> -BuLi (2 eq), 25 (1 eq.); ii. 24 (1 eq.), 24 h	No product

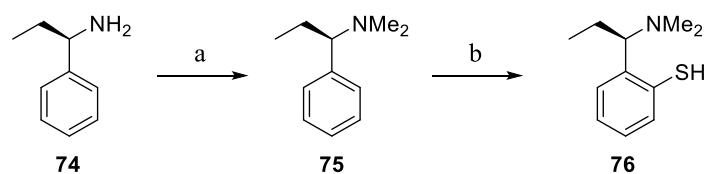
Table 2 Eastern **25** and western **24** fragments coupling conditions.

In search for an alternative approach for this coupling key step the established WIPF protocol for *in situ* transmetallation of alkenylzirconocenes to the alkylzinc species **69** and their subsequent catalytic asymmetric addition to aldehydes that employs a chiral ligand seemed to be suitable (Scheme 12).⁷³ This would allow the direct coupling of terminal alkyne **26** with aldehyde **25** and the use of chiral ligands, such as **71** and **72** especially, and this step was reported to give excellent stereoselectivity.⁷⁴



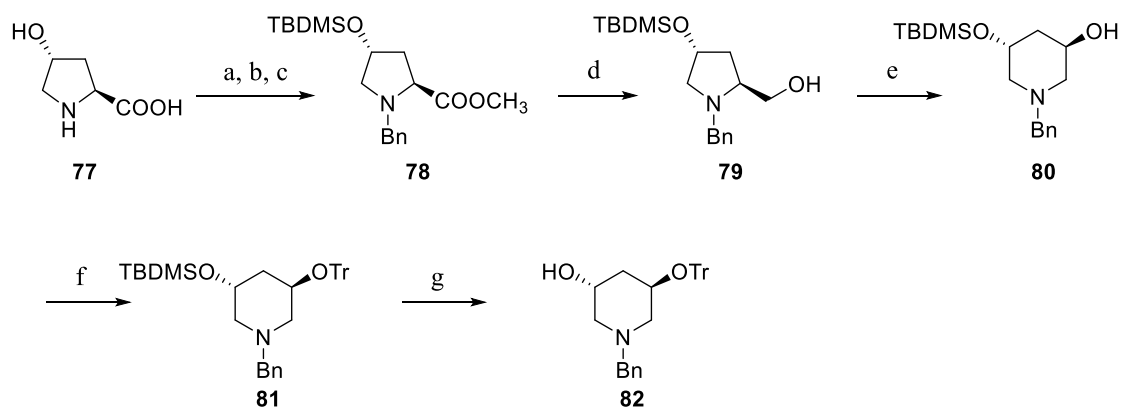
Scheme 12 Enantioselective vinylation of aldehydes with Wipf's method.

The synthesis of thiol amine **72** started with ESCHWEILER-CLARK methylation of (*R*)-ethylbenzylamine **74**, followed by *ortho* lithiation and conversion with elemental sulphur that yielded the desired ligand **72**.⁷⁵



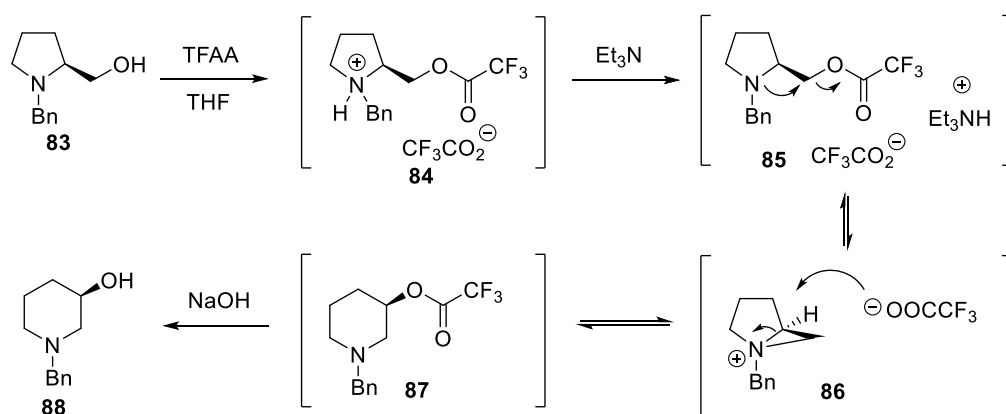
Scheme 13 Synthesis of Wipf chiral ligand. Reaction conditions: a) CH₂O, HCOOH, EtOH, reflux, 24 h, 87%; b) i. *t*-BuLi, RT, 24 h; ii. S₈, THF, -50 °C, 16 h; iii. H₂O.

A series of piperidine β-amino alcohol ligands reported by COSSY et al. for the enantioselective diethylzinc addition to aromatic and aliphatic aldehydes were also synthesized (Scheme 14).⁷⁶ Ligands **80** and **82** were prepared from the corresponding proline precursors **79** a, b by utilizing a ring expansion reaction. The proline precursors **79** were synthesized from commercially available *trans*-4-hydroxy-L-proline **77**.



Scheme 14 Synthesis of COSSY chiral ligands. Reaction conditions: **a)** SOCl₂, MeOH, 0°C to RT, 4 h; **b)** BnBr, Et₃N, CH₂Cl₂, RT to reflux, 5 h; **c)** DMAP, RCl, RT, 12 h, 43% over 3 steps; **d)** LiAlH₄, THF, 0°C to reflux, 2 h; **e)** **i.** (CF₃CO)₂O, THF, 0°C, 1 h, **ii.** Et₃N, 0°C to RT, 24 h reflux, 24 h, **iii.** NaOH (2.5 M), RT, 2 h, 70% over 3 steps; **f)** TrCl, Et₃N, CH₂Cl₂, RT, 48 h, 83%; **g)** *n*-Bu₄NF, RT, 72 h, 60%.

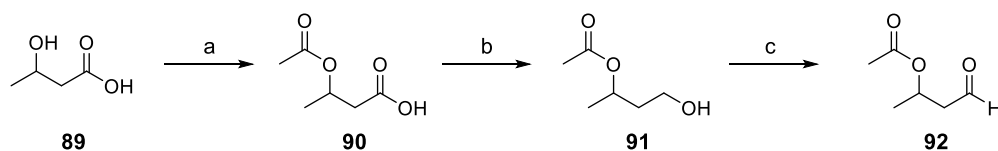
Mechanistic studies were conducted in the COSSY group to establish details of the ring expansion reaction.⁷⁷



Scheme 15 Mechanism for the rearrangement of prolinols to 3-hydroxypiperidines.

The first step towards the formation of 3-hydroxypiperidine is the esterification of the hydroxyl group with trifluoroacetic anhydride and formation of ammonium salt **84** (Scheme 15). Addition of Et₃N is essential for the rearrangement as it produces intermediate **85** which undergoes a S_Ni process to give key aziridinium intermediate **86**. The trifluoroacetate anion then attacks from the back side to generate the stable ester **87**. Finally, saponification of ester **87** yields the desired product **88**.^{78, 79}

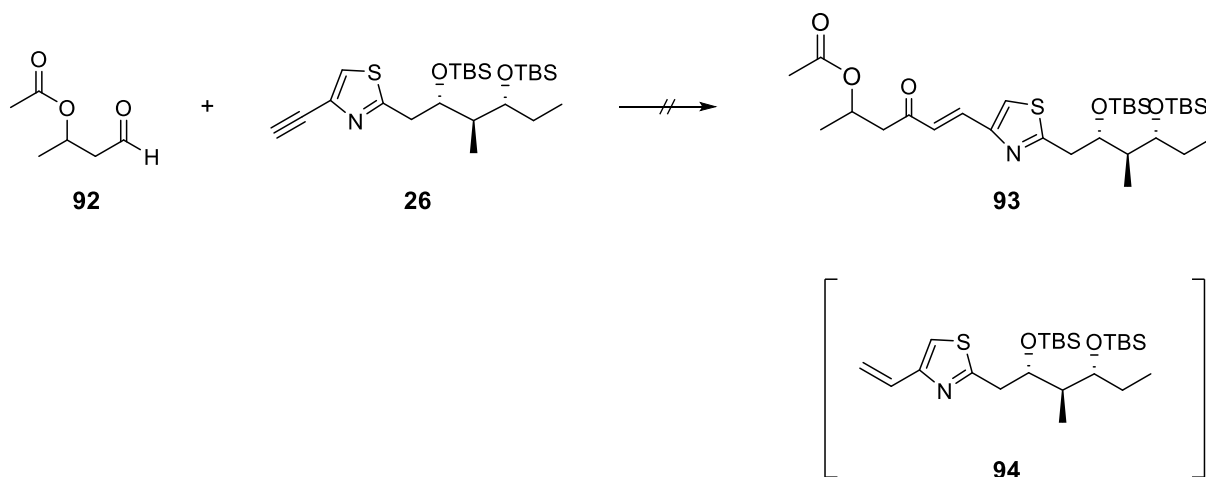
Due to the time consuming and challenging synthesis of the western fragment a model compound was tested first. For that purpose a suitable structural model to substitute the Western fragment in the test reactions was synthesized (Scheme 16).



Scheme 16 Synthesis of eastern fragment test analogue **92**. Reaction conditions: **a)** AcCl, 50°C, 5h, ; **b)** BH₃·THF, THF, 0°C to RT, 12 h, ; **c)** DMP, NaHCO₃, CH₂Cl₂, 0°C to RT, 1h .

3-Hydroxybutyric acid **89** was treated with acetyl chloride to yield the acetylated precursor **90**. After treatment with the borane tetrahydrofuran complex the carboxylic group was successfully reduced to the primary alcohol **91** as was described for similar structures.⁸⁰ The free alcohol was directly subjected to Dess-Martin oxidation conditions to yield the desired aldehyde product **92**.

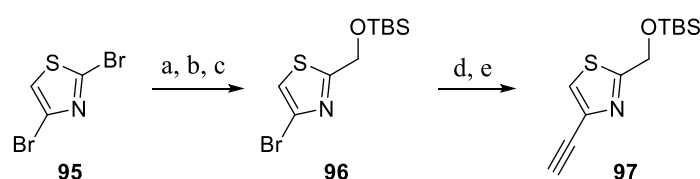
Test reactions were conducted with freshly prepared **92**, since it proved to be very unstable even at -40°C under an inert atmosphere. Test conditions followed well-described hydrozirconation-transmetalation strategies utilized in natural product syntheses.⁸¹ However, using 1.05 eq of the Schwarz reagent and 1.1 eq of Et₂Zn (entries 1 and 2) did not furnish the desired product even after 48 h of stirring at RT (Table 3). The reduced alkene **94** was the only new product that could be isolated.



Entry	Reaction conditions	Results
1	i. 26 , Schwarz reagent (1.05 eq), RT, 5 min; ii. 92 , 0°C to RT, 12 h	94
2	i. 26 , Schwarz reagent (1.05 eq), RT, 5 min; ii. 92 , 0°C to RT to 35 °C, 12 h	Decomposition
3	i. 26 , Schwarz reagent (1.05 eq), RT, 30 min; ii. Et ₂ Zn (1.1 eq.), 92 , -78°C to 0°C to RT, 48 h	94
4	i. 26 , Schwarz reagent (1.05 eq), 0°C to RT, 1 h; ii. Et ₂ Zn (1.5 eq.), 92 , -65°C to 0°C, 5 h	Traces of product
5	i. 26 , Schwarz reagent (1.05 eq), 0°C to RT, 1 h; ii. Et ₂ Zn (1.5 eq.), 92 , -65°C to 0°C to RT, 12 h	Traces of product

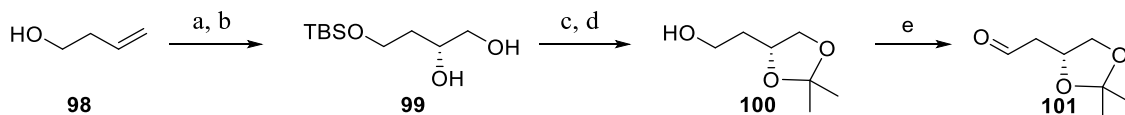
Table 3 Optimization of the coupling reaction employing test molecule **92**.

Another model system was also tested, where the aldehyde **101**, containing a dioxolane ring, was more stable upon synthesis and a simple thiazole alkyne analogue **97** was synthesized over five steps from commercially available 2,4 -dibromo-thiazole **95** (Scheme 17). It was transformed to the intermediate aldehyde in a two-step process involving lithiation and subsequent reaction with DMF as reported previously by NICOLAOU et al.^{82, 83} The aldehyde was reduced to the alcohol that was further TBS-protected to yield **96**. The 4-bromo group was retained throughout this point and could be used for the Sonogashira-Hagihara reaction to afford the terminal alkyne **97** after TBS deprotection.⁸⁴



Scheme 17 Synthesis of test analogue **97**. Reaction conditions: **a**) i. *n*BuLi, Et₂O, -78°C, 0,5 h; ii. DMF, -78°C to RT, 2 h; **b**) NaBH₄, MeOH, RT, 0,5 h; **c**) TBSCl, Imidazole, CH₂Cl₂, RT, 0,5 h; **d**) ethynyltrimethylsilane, PdCl₂(PPh₃)₂, CuI, DIPA-H, 60 °C, 12 h; **e**) K₂CO₃, MeOH, 0 °C to RT, 1h.

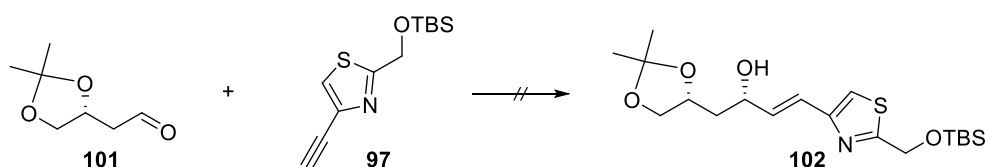
Aldehyde **101** was obtained after silyl protection of alcohol **100** and a subsequent asymmetric Sharpless dihydroxylation to yield diol **99** (Scheme 18). Acetal protection, deprotection of the primary alcohol and its subsequent oxidation yielded the desired aldehyde **101**.^{85, 86}



Scheme 18 Synthesis of test analogue **101**. Reaction conditions: **a)** TBSCl, imidazole, DMAP, CH₂Cl₂, RT, 1 h; **b)** AD-mix-β, *t*-BuOH/H₂O, 0 °C, 12 h; **c)** 2,2-DMP, PTSA, CH₂Cl₂, 0 °C to RT, 1 d; **d)** TBAF, THF, 0 °C, 2 h; **e)** PCC, CH₂Cl₂, 0 °C to RT, 1h.

Alkenylzirconocene chlorides that can be prepared through hydrozirconation of an alkyne are reportedly rather poor nucleophiles in carbon-carbon bond forming reactions. There are several different methods known to solve this problem. The most convenient approach is an organometallic transmetalation that was tested initially. Another approach, however, is activation of the organozirconium compound using a Lewis acid by generating a highly electrophilic cationic zirconocene species or by activating the organic electrophilic carbonyl substrate. In some cases, the reaction proceeds successfully due to the dual activating effect of the Lewis acid on both the organozirconium species and the substrates.⁸⁷

Conditions that were tested in the model system were reported by SUZUKI where a catalytic amount of silver perchlorate was applied to generate a cationic species that serve as carbonyl activator (Table 3, Entry 1-5).⁸⁸ Different catalytic amounts and reaction times were tested, but no conversion was observed. Afterwards the property of organoboron compounds to undergo transmetalation to the corresponding organozinc species by employing freshly prepared dicyclohexylborane **44** was consequentially explored (Table 3, Entry 8-9).⁸⁹ The classical hydrozirconation-transmetalation strategy was also tested with a fresh sample of Me₂Zn (Table 3, Entry 11-12). The latter gave some promising results as traces of the desired product were detected by means of LC-MS measurements. However, the product was never isolated and structurally clarified by means of NMR analysis.

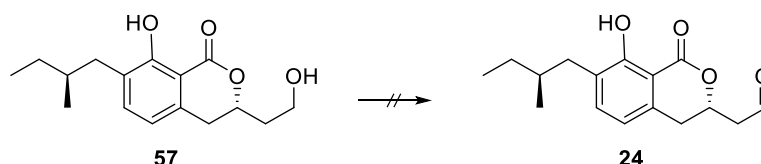


Entry	Reaction conditions	Results
1	i. 97 , Schwarz reagent (1.2 eq), RT, 30 min;	No product
	ii. AgClO ₄ (1 mol %), 101 , 0°C to RT, 15 min.	
2	i. 97 , Schwarz reagent (1.2 eq), RT, 30 min;	No product
	ii. AgClO ₄ (5 mol %), 101 , 0°C to RT, 15 min.	
3	i. 97 , Schwarz reagent (1.2 eq), RT, 30 min;	No product
	ii. AgClO ₄ (10 mol %), 101 , 0°C to RT, 10 min.	
4	i. 97 , Schwarz reagent (1.2 eq), RT, 30 min;	No product
	ii. AgClO ₄ (1 mol %), 101 , 0°C to RT, 12 h.	
5	i. 97 , Schwarz reagent (1.2 eq), RT, 30 min;	No product
	ii. AgClO ₄ (5 mol %), 101 , 0°C to RT, 12 h.	
6	i. 97 , Cy ₂ BH (2 eq), 0°C, 1 h;	No product
	ii. Ti(O <i>i</i> Pr) ₄ (3 eq.), 101 , reflux, 3 h.	
7	i. 97 , Cy ₂ BH (1.5 eq), 0°C to RT, 30 min;	No product
	ii. Ti(O <i>i</i> Pr) ₄ (3 eq.), 101 , reflux, 1 h	
8	i. 97 , Cy ₂ BH (1.1 eq), 0°C to RT, 30 min;	No product
	ii. Me ₂ Zn (1.2 eq.), 101 , -78 °C to 0 °C to RT, 2 h	
9	i. 97 , Cy ₂ BH (1.2 eq), 0°C to RT, 30 min;	No product
	ii. Et ₂ Zn (1.2 eq.), 101 , -65 °C to 0°C, 5 h	
10	i. 97 , Schwarz reagent (1.05 eq), 0°C to RT, 1 h;	No product
	ii. Et ₂ Zn (1.5 eq.), 101 , -65 °C to 0°C, 5 h	
11	i. 97 , Schwarz reagent (1.05 eq), 0°C to RT, 1 h;	Traces of product
	ii. Me ₂ Zn (1.2 eq.), 101 , -78 °C to 0°C, 5 h	
12	i. 97 , Schwarz reagent (1.05 eq), 0°C to RT, 1 h;	Traces of product
	ii. Me ₂ Zn (1.5 eq.), 101 , -78 °C to 0°C, 14 h	

Table 4 Optimizatoion of coupling reaction between test precursors **101** and **97**.

4.3.1 Towards optimization of the oxidation reaction

The coupling conditions had to be consequentially tested with the originally envisioned aldehyde. For this purpose sufficient amount of the aldehyde **2** had to be prepared. The previously used oxidation reaction turned out to be unsuccessful in this instance, which lead to the necessity of optimization of the oxidation conditions (Table 5).



Entry	Reaction conditions	Results
1 ^{a,b,c}	DMPI, NaHCO ₃ , RT	No product
2 ^b	DMSO, COCl ₂ , Et ₃ N, CH ₂ Cl ₂ , -78 °C to -40 °C to RT	No product
3	Et ₃ N, SO ₃ · Pyridine, CH ₂ Cl ₂ /DMSO, 0 °C to RT, 20 min	Decomposition
4	TEMPO, NaOCl, KBr, H ₂ O, CH ₂ Cl ₂ , 0 °C, 15 min	Decomposition
5 ^b	TPAP, NMO, 4 Å MS, CH ₂ Cl ₂ , RT	No product
6 ^{a,b}	PCC, CH ₂ Cl ₂ , RT	Decomposition at purification
7 ^{a,b}	PCC polymer, CH ₂ Cl ₂ , RT	No product
8	PDC, 4 Å MS, CH ₂ Cl ₂ , RT, 1h	Product observed on TLC

^a More equivalents of the oxidizing agent were consequentially added.

^b Different reaction times were tested.

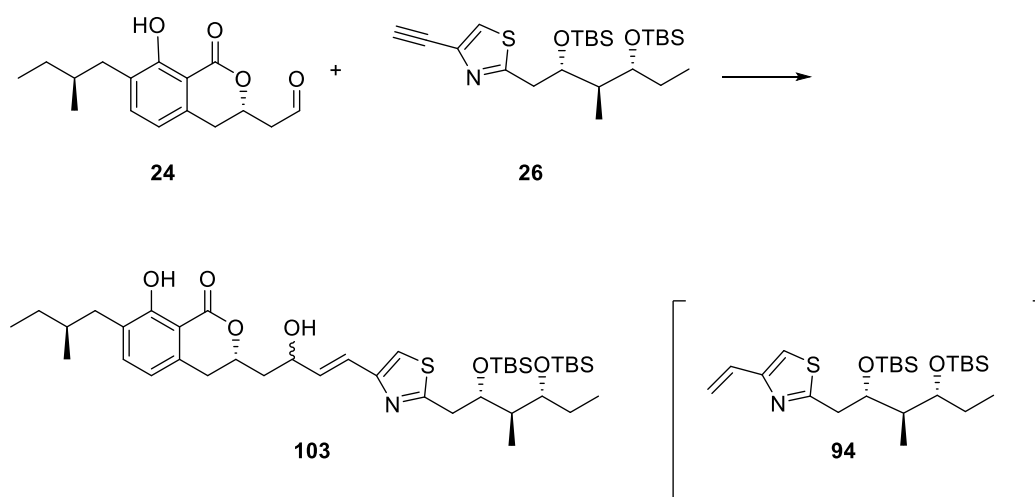
^c Higher reaction temperature was tested as well.

Table 5 Optimization of oxidation of precursor **57**.

Firstly, the same oxidation conditions as for the oxidation of the test molecule **100** were tried (Table 5, Entry 1). Different equivalents, reaction times as well as higher temperature did not lead to the formation of the desired aldehyde.

SWERN oxidation was consequentially tested and the reaction time was gradually extended to 48 h, however, also this effort did not yield any product (Table 5, Entry 2). Classical PARIKH-DOERING oxidation conditions employing DMSO and sulphur trioxide pyridine complex led to

decomposition of the substrate (Table 5, Entry 3).^{90, 91} TEMPO - mediated oxidation was also accompanied by decomposition after only a very short reaction time (Table 5, Entry 4).⁹² LEY-GRIFFIT conditions were insufficient even at extended reaction times (Table 5, Entry 5).⁹³ Using PCC as an oxidant gave promising results as conversion was observed as judged by thin-layer chromatography (TLC) after having optimized the reaction time and equivalents of the oxidant.⁹⁴ After purification, however, TLC analysis showed decomposition. In order to improve the purification step commercially available polymer bound PCC reagent was exploited.⁹⁵ Despite extended reaction times and using a large excess of the oxidizing reagent conversion could not be achieved (Table 5, Entry 6-7). Employing PDC oxidant also led to a conversion as judged by TLC and after a silica-gel filtration step the product was collected in dichloromethane solution. This was used directly in the next coupling step. Due to the unsuccessful test trials of the coupling and the little available amounts of the final fragments only a few coupling conditions could be tested.



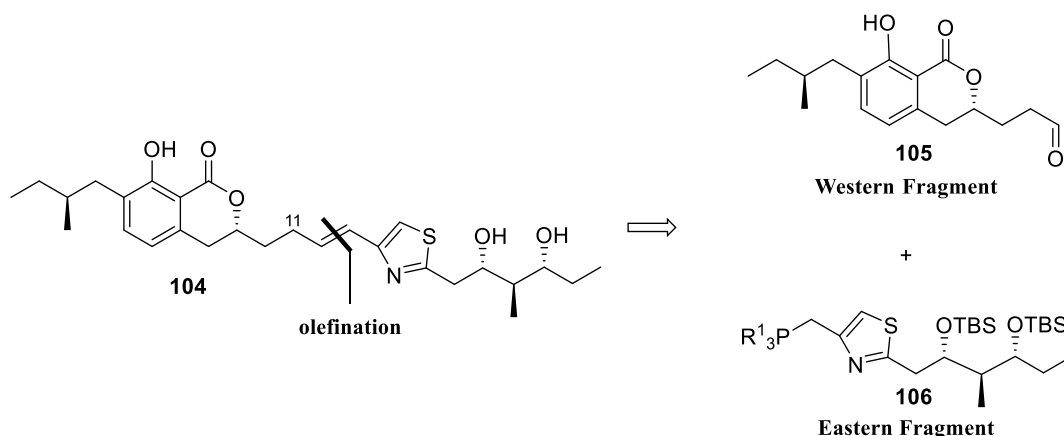
Entry	Reaction conditions	Results
1	i. 26 , Schwarz reagent (1,05 eq), RT, 30 min; ii. Et ₂ Zn (1,5 eq.), 24 , -78 °C to 0 °C, 2 h	94
4	i. 26 , Schwarz reagent (1,05 eq), 0 °C to RT, 1 h; ii. Me ₂ Zn (1,2 eq.), 24 , -78 °C to 0 °C, 14 h	Traces of product
5	i. 26 , Schwarz reagent (1,05 eq), 0 °C to RT, 1 h; ii. Me ₂ Zn (1,5 eq.), 24 , -60 °C to 0 °C to RT, 14 h	Traces of product

Table 6 Optimization of conditions for coupling of fragments **24** and **26**.

Terminal alkyne **26** was treated with Schwarz reagent and followed by transmetalation using Et_2Zn . A crude solution of freshly prepared aldehyde **24** was then added and the reaction monitored after 2 hours. Unfortunately only the reduced eastern fragment **94** could be isolated. In another entry, the transmetalation was explored *via* a fresh sample of Me_2Zn in different equivalent ratios. Though traces of the desired product were detected by LC-MS measurements of the crude reaction mixture, no pure product was isolated even after extended reaction times. As a result of the unsuccessful coupling trials a new synthetic approach towards Noricumazole derivatives was devised.

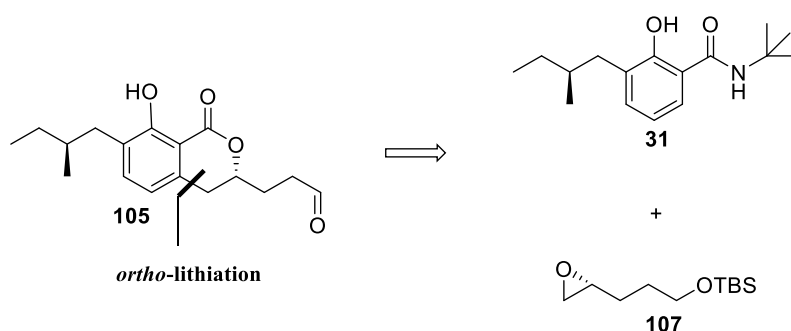
4.3.2 Test derivative. Retrosynthesis

Due to the findings in the optical assays (Chapter 5.) that revealed that the stereochemistry at **C11** is crucial for the ion-channel activity of the molecule, the total synthesis of another derivative that lacks a functional group at this position was considered. Such a derivative would be an interesting matrix to confirm the biological assay's results. Furthermore, an asymmetric allylic oxidation at **C11** as a final step was considered to achieve the initially desired derivative.



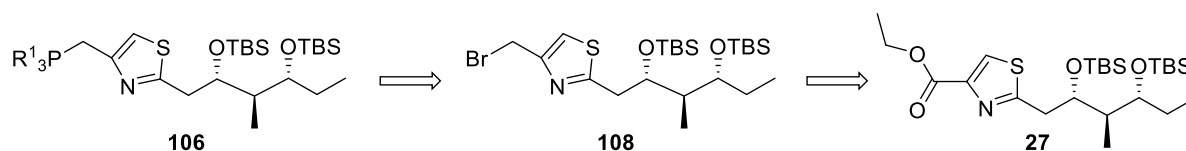
Scheme 19 Retrosynthetic approach towards derivative **104**.

The retrosynthesis strategy for the western fragment follows the pathway discussed for derivative **23**. The difference with that previous approach was the need for a new chiral oxirane **107** with a backbone elongation by one carbon atom.



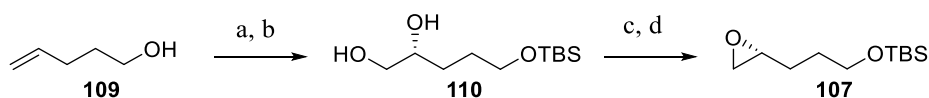
Scheme 20 Retrosynthesis of western fragment **105**.

Retrosynthesis of the eastern fragment would utilize a bromo-precursor **108** which would be obtained from intermediate **27** after reduction of the ester functionality (Scheme 21).



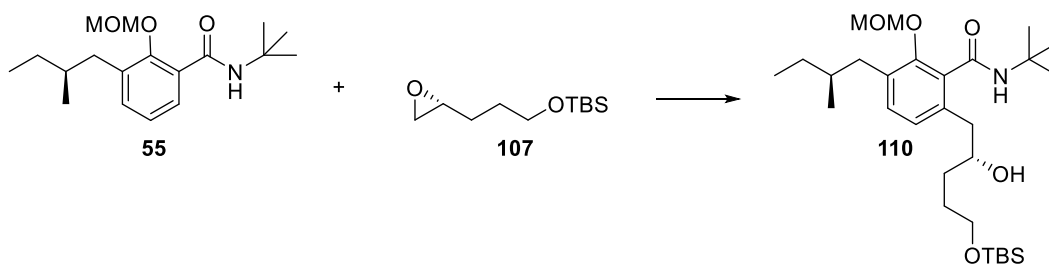
Scheme 21 Retrosynthesis of eastern fragment **106**.

The synthesis of chiral epoxide **107** started from commercially available 2-allylethanol **109**. It was protected and dihydroxylated to the enantiomerically pure precursor **110**. The primary alcohol was selectively transformed in the next step using *p*-toluenesulfonyl chloride that underwent an intramolecular S_N2-reaction under basic conditions to yield the desired epoxide **107**.



Scheme 22 Synthesis of precursor **107**. Reaction conditions: **a)** TBSCl, Imidazole, CH₂Cl₂, RT, 1h; **b)** AD-mix- β , *t*-BuOH/H₂O, 0°C, 12 h, **c)** Bu₂SnO, Et₃N, TsCl, CH₂Cl₂, 0°C to RT, 3 h, 96%; **d)** K₂CO₃, MeOH, RT, 2 h, 65%.

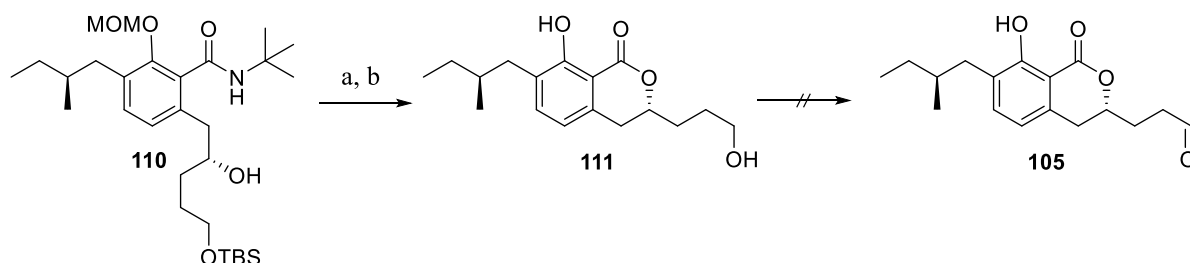
Conditions established for the *ortho*-lithiation step in the previous strategy were not successful in this case (Table 7, Entry 1). Using *sec*-BuLi did not yield any product (Table 7, Entry 2). Increasing the equivalent of TMEDA and the reaction time for the *ortho*-lithiation step gave promising results (Table 7, Entry 3). Increasing also the reaction temperature led to slight increase of the yield (Table 7, Entry 4). The obtained material was sufficient to test the following steps of the synthesis.



Entry	Reaction conditions	Results
1	i. 55 , <i>n</i> BuLi (3 eq), TMEDA (2 eq.) , -78 °C to -40 °C, 2 h	No product
	ii. 107 , -78 °C to -40 °C, 12 h	
2	i. 55 , <i>sec</i> BuLi (3 eq), TMEDA (2 eq.) , -78 °C to -40 °C, 2 h	No product
	ii. 107 , -78 °C to -40 °C, 12 h	
3	i. 55 , <i>n</i> BuLi (3 eq), TMEDA (3 eq.) , -78 °C to -40 °C, 3 h	33% + 14% 55
	ii. 107 , -78 °C to -40 °C, 12 h	
4	i. 55 , <i>n</i> BuLi (3 eq), TMEDA (3 eq.) , -78 °C to -30 °C, 3 h	38% + 15% 55
	ii. 107 , -78 °C to -30 °C, 12 h	

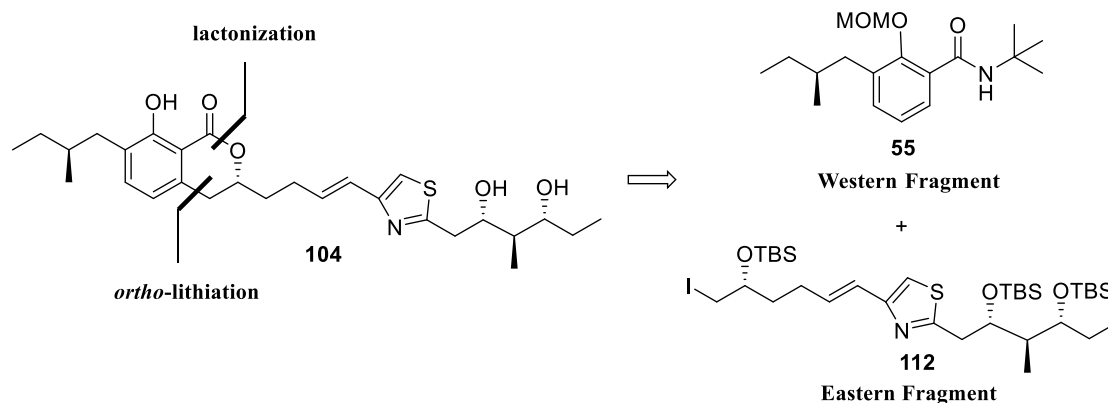
Table 7 Optimization of conditions for the *ortho* lithiation of intermediate **55**.

Cleavage of the two protecting groups with half-concentrated hydrochloric acid and consequential lactonization through treatment with PTSA successfully yielded key alcohol precursor **111**. The following oxidation step, however, proved to be challenging. Various oxidation conditions that were explored in previous attempts to optimize this last oxidation step were not successful.



Scheme 23 Synthesis of precursor **110**. Reaction conditions: **a)** HCl_{semi conc.}, EtOH, 50 °C, 1h, %; **b)** PTSA, toluene, reflux, 1 h, 70 %.

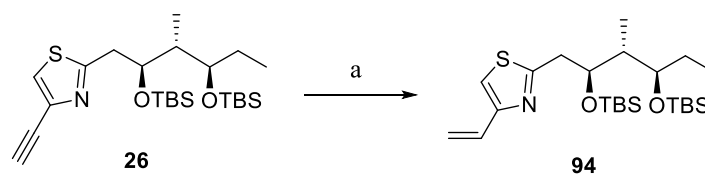
Due to the challenging oxidation of the eastern fragment a different approach towards new Noricumazole derivatives was further explored. A second retrosynthetic strategy was envisioned (Scheme 24).



Scheme 24 Retrosynthetic approach towards derivative **104**.

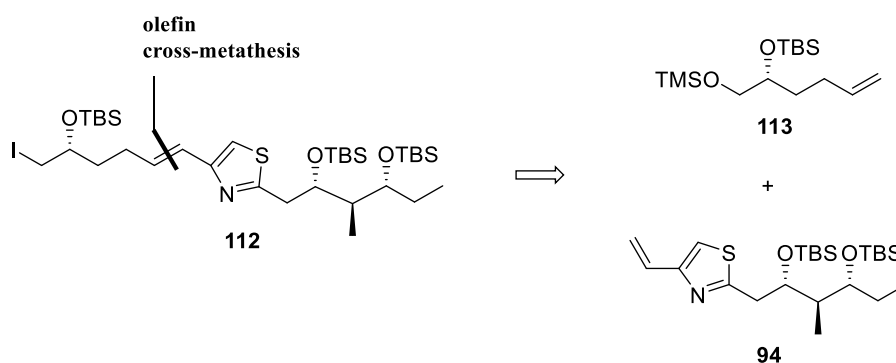
This retrosynthesis again is based on two main fragments: the western fragment **55** and eastern part **112** are connected by means of an *ortho*-functionalization of the trisubstituted phenolic precursor **55** (Scheme 24).

The western fragment **55** is a precursor that was synthesized in accordance with the previously developed strategy (Scheme 10, **55**). The eastern fragment **112** could be achieved from precursor **113** and **94** respectively (Scheme 26). Conveniently, the latter was a major side-product in the first synthetic strategy (Table 3, **94**). However, it could also be synthesized by the simple reduction of the terminal alkyne **26** using the Schwarz reagent (Scheme 25).



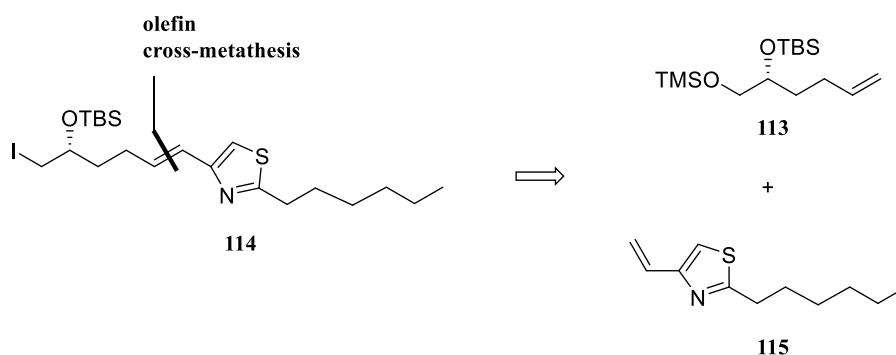
Scheme 25 Synthesis of precursor **94**. Reaction conditions: **a**) Schwarz reagent, CH_2Cl_2 , RT, 1h, 70%.

The two precursors could be connected by means of an olefin cross-metathesis (**Scheme 26**).



Scheme 26 Retrosynthesis of eastern fragment **112**.

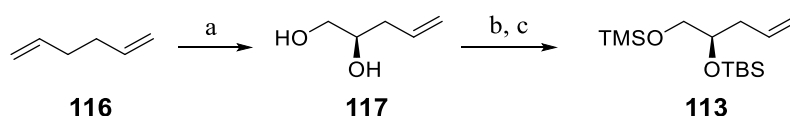
In order to test the olefin cross-metathesis reaction, an analogue test molecule **114** was also envisioned to be synthesized (Scheme 27), one without the polyketide functional groups that carry the stereochemistry. Such a test molecule would also give a suitable derivative of noricumazole that would provide more details about the structure-activity relationship (SAR) with respect to the stereochemistry and functionality of the polyketide backbone in the eastern fragment.



Scheme 27 Retrosynthesis of test fragment **114**.

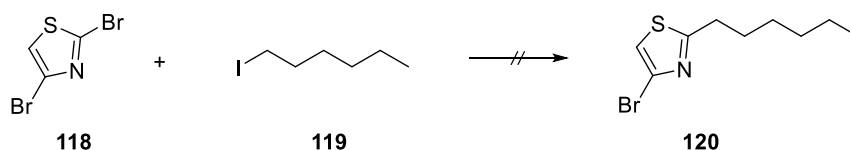
4.3.3 Synthesis of eastern fragment **112** and test fragment **114**.

The synthesis of Eastern fragment **91** started with the synthesis of precursor **90** (Scheme 28). Commercially available 1,5-hexadiene underwent an asymmetric Sharpless dihydroxylation under previously reported conditions.⁸⁶ The resultant diol **117** was selectively protected to give precursor **113**.



Scheme 28 Synthesis of precursor **113**. Reaction conditions: **a)** AD-mix- β , *t*-BuOH/H₂O, 0 °C, 12 h ; **b)** TMSCl, pyridine, CH₂Cl₂, 0 °C, 30 min, 73% **c)** TBSCl, imidazole, CH₂Cl₂, RT, 1h, 95%.

The initial strategy for the synthesis of precursor **116** at first was to directly functionalize 2, 5-dibromo thiazole **118** to the desired 2-alkyl-5-bromo product **120**.

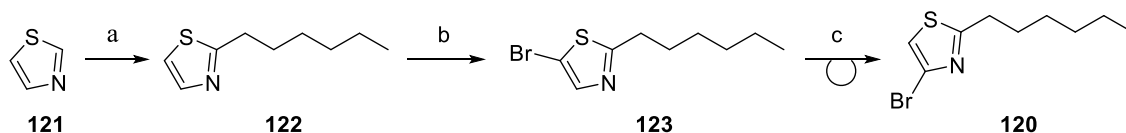


Entry	Reaction conditions	Results
1	i. 118 , <i>t</i> BuLi (1.1 eq), ZnCl ₂ (1.1 eq), -78 °C, 1 h; ii. 119 (1.1 eq), Pd ₂ (dba) ₃ , dppf, RT, 12 h;	No product
2	i. 118 , <i>t</i> BuLi (5 eq), ZnCl ₂ (3 eq), -78 °C, 1 h; ii. 119 (2.5 eq), Pd ₂ (dba) ₃ , dppf, RT, 12 h;	No product
3	i. 118 , <i>n</i> BuLi (1.2), -78 °C, 30 min; ii. 119 , -78 °C, 12 h;	No product
4	i. 118 , <i>t</i> BuLi (1.1), -78 °C, 30 min; ii. 119 , -78 °C to RT, 12 h;	No product
5	i. 118 , <i>i</i> PrMgCl (2 eq), 0 °C, 30 min; ii. 119 (1 eq), -50 °C to RT, 14 h;	No product
6	i. 118 , <i>i</i> PrMgCl (2 eq), 0 °C, 30 min; ii. 119 (1 eq), Fe(acac) ₃ , TMEDA, HMTA, -78 °C to RT, 14 h;	No product
7	i. 118 , <i>i</i> PrMgCl·LiCl (1.2 eq), -78 °C, 20 min; ii. 119 (1 eq), -78 °C to 0 °C, 2 h;	No product
8	i. 118 , <i>i</i> PrMgCl·LiCl (2 eq), -78 °C, 20 min; ii. 119 (1 eq), -78 °C to 0 °C, 12 h;	No product

Table 8 Optimization of the coupling reaction for the synthesis of precursor **120**.

Direct lithium halogen exchange (Table 7, Entry 3-4), as well as the transmetalation approach with zinc and palladium for initial cross coupling reactions were tested (Table 7, Entry 1-2).^{96, 97} Halogen-magnesium exchange was also tested by means of Grignard and turbo Grignard concepts.^{98, 99} None of the tested strategies led to a successful transformation.

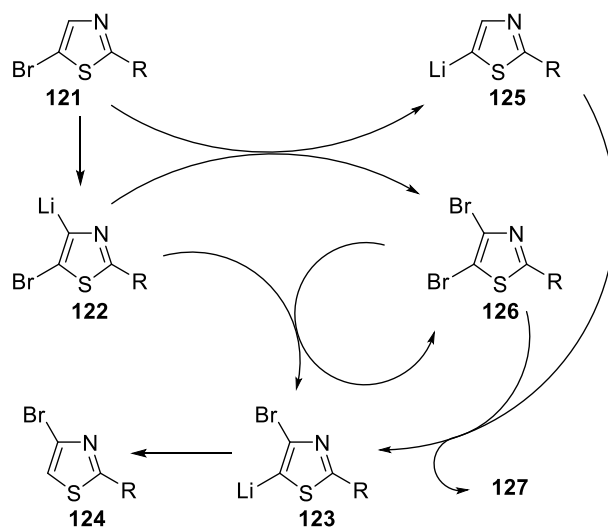
Another approach that was explored started from thiazole **121** that was lithiated and treated with 1-iodohexane (Scheme 29). The resultant 2-alkyl thiazole **122** was further brominated at position 4 according to a procedure described in literature.¹⁰⁰ A typical halogen-dance reaction followed that yielded the desired substrate suitable for the following coupling reaction.¹⁰¹



Scheme 29 Synthesis of precursor **120**. Reaction conditions: **a)** *n*BuLi, 1-iodohexane, -78 °C to RT, 2h, 56%; **b)** *n*BuLi, Br₂, THF, -78 °C to RT, 1h, 85%; **c)** LDA, THF, -78 °C, 1h, 53%.

Thiazole “dance” reaction

The “halogen dance” reaction can occur on a thiazole ring due to the difference in the acidities of the various positions. This leads to differences in stability of the different lithiated species. In this particular reaction, the 5-position is more acidic than the 4-position, thus favouring species at position 5 relative to position 4.¹⁰²

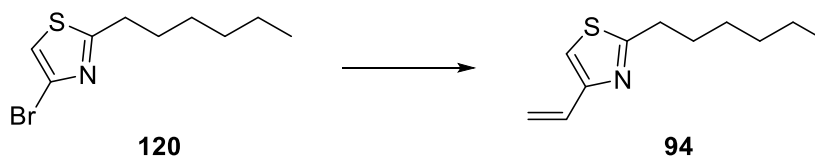


Scheme 30 Mechanism of the “thiazole dance” reaction.

The first step in the reaction sequence is the deprotonation of substrate **121** to yield the lithiated species **122**. In contrast to BuLi, intermediate **122** is capable of undergoing metal-halogen exchange reaction with the available substrate **121** to form two additional intermediate species **125** and **126**. This triggers a cascade reaction where lithiated intermediates **122** and **125** undergo a reaction with the dibromo species **126** until the more stable 4-bromo intermediate **123** is formed. After hydrolysis with water the desired 2-alkyl-4-bromothiazole **124** is obtained.¹⁰³

Stille and Suzuki coupling conditions were tested for the synthesis of the disubstituted thiazole precursor **92** (

Table 9). The Stille conditions that utilize PdCl₂(PPh₃)₂ as catalyst (Entry 3), gave the highest yield.^{104, 105, 106}



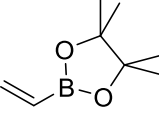
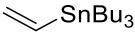
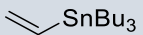
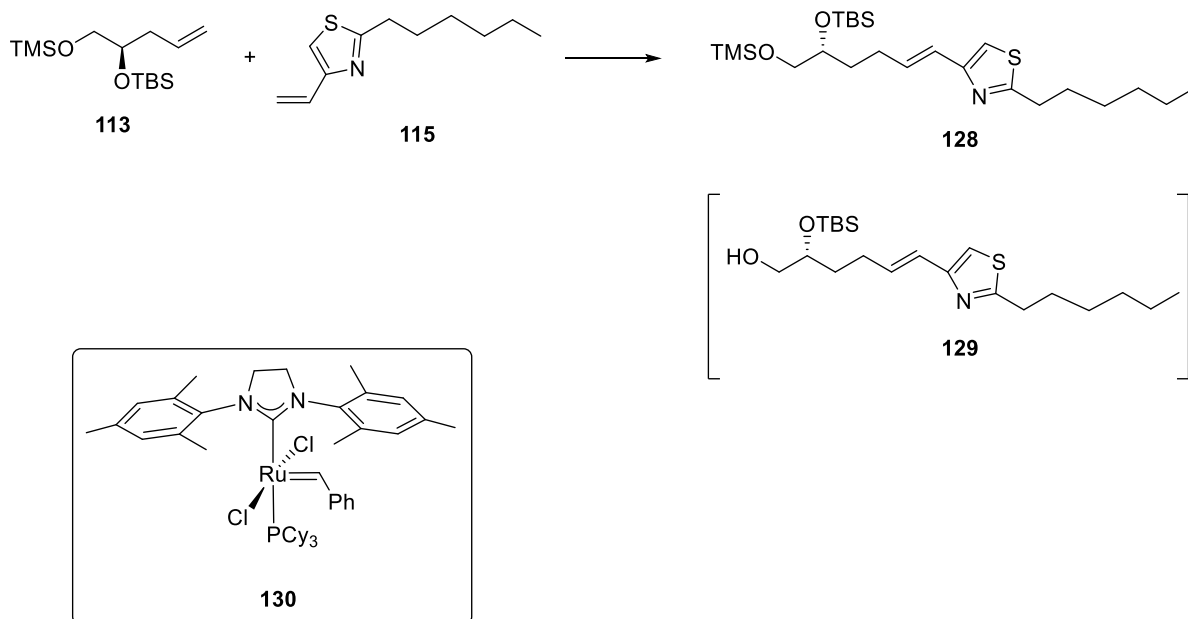
Entry	Reaction conditions	Yield
1	 Pd(dppf)Cl ₂ , Na ₂ CO ₃ , dioxane/water, 80°C, 14 h	57 %
2	 CuI, PEPPSI, CsF, THF, RT, 1h	Traces of product
3	 PdCl ₂ (PPh ₃) ₂ , dioxane, 100°C, 14 h	95%

Table 9 Coupling conditions for the synthesis of **92**.

The next step in the synthesis of eastern fragments **112** and **114** was the olefin cross-metathesis reaction between **113** and **94** or **115** respectively. Using Grubbs 2nd generation catalyst was sufficient after optimization of the reaction conditions in terms of reaction time and substrate amounts (Table 10). Using substrate **113** in excess gave best results as it avoids possible homodimerization of either of the olefins.¹⁰⁷

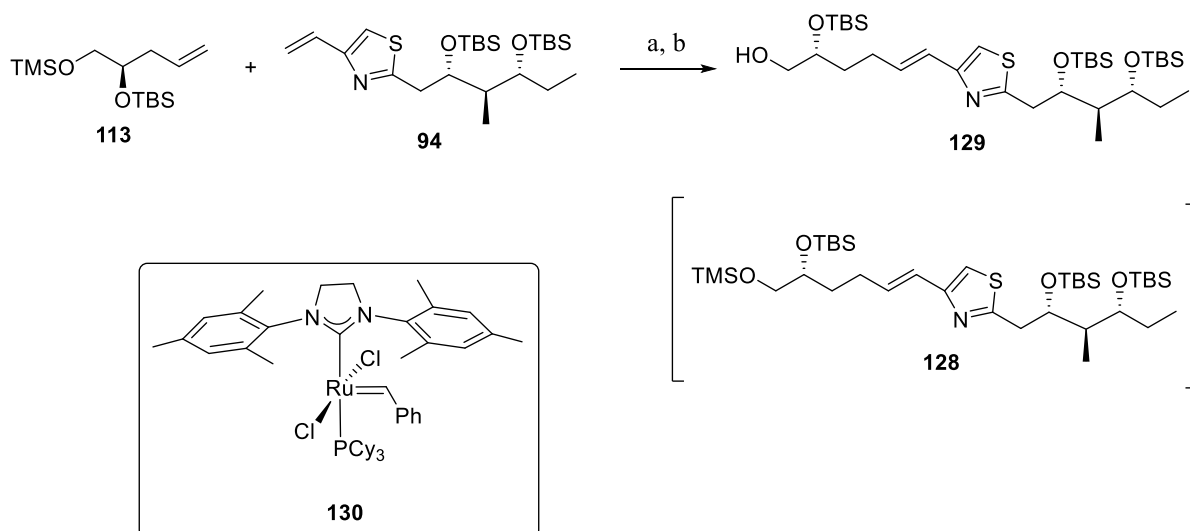


Entry	Catalyst	130 [mol %]	90 [eq.]	92 [eq.]	Time [h]	Results
1	Grubbs 2 nd (130)	3	1	2	48	No product
2	Grubbs 2 nd (130)	3	2	1	48	Traces of product
3	Grubbs 2 nd (130)	10	2	1	48	Traces of product
4	Grubbs 2 nd (130)	7	1,5	1	24	78 % product
5	Grubbs 2 nd (130)	7	1,8	1	24	84 % product

*All reactions were conducted at 40 °C in CH₂Cl₂

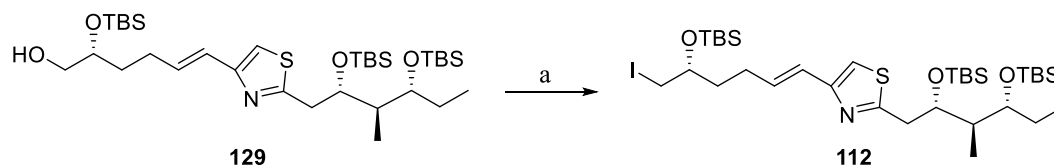
Table 10 Optimization of olefin cross-metathesis for test precursor **128**.

The olefin cross-metathesis reaction was conducted for precursor **109** using the optimized conditions collected from the optimized test reactions (Table 10, Entry 5). These proved to be successful for precursor **130** too (Scheme 31). Minor optimization during work-up of the reaction increased the yield for the desired deprotected primary alcohol. The crude mixture was stirred in silica gel in CH₂Cl₂ for an hour before purification by column chromatography.



Scheme 31 Olefin cross-metathesis reaction for substrate **109**. Reaction conditions: **a**) Grubbs 2nd (**130**), CH₂Cl₂, 40 °C, 24 h; **b**) silica gel, CH₂Cl₂, RT, 1h; 86% **129** over 2 steps.

The final step for the synthesis of the eastern fragment **112** was the conversion of the primary alcohol **129** into the desired alkyl iodide utilizing APPEL conditions (Scheme 32).¹⁰⁸

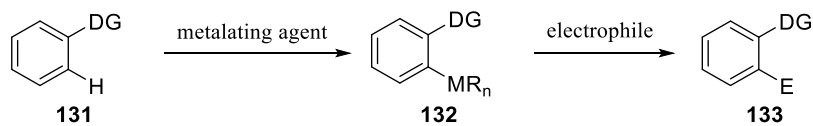


Scheme 32 Final step in the synthesis of eastern fragment **112**. Reaction conditions: **a**) PPh₃, imidazole, I₂, CH₂Cl₂, 0 °C, 45 min, 90%.

4.4 Endgame – *ortho* lithiation

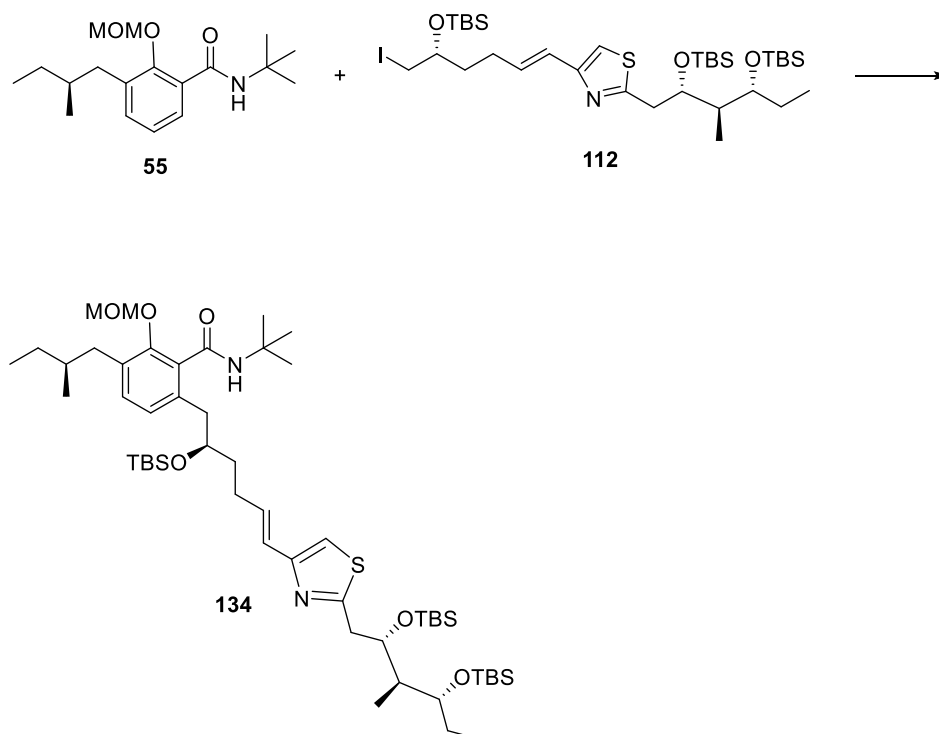
The last key step in the synthesis of derivative **104** was the merging of fragment **112** with **55** after *ortho*-lithiation of the arene. This procedure was successfully utilized in the previous strategy where a secondary amide served as the directing group.

The mechanism generally involves the regioselective C-H bond deprotonation of an arene that contains a directing group in the *ortho* position as in **128** using a mild base. This results in the metalation of the *ortho* carbon atom (Scheme 33). This is followed by the reaction of the intermediate arylmetal species with an electrophile. This generates the new C-C bond and yields the desired product **133**.



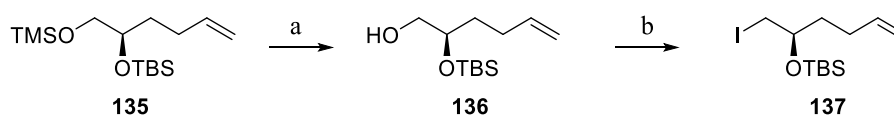
Scheme 33 General mechanism of an *ortho*-functionalization reaction of arenes.

The conducted test reaction gave promising results as traces of the desired product were detected by LC-MS.



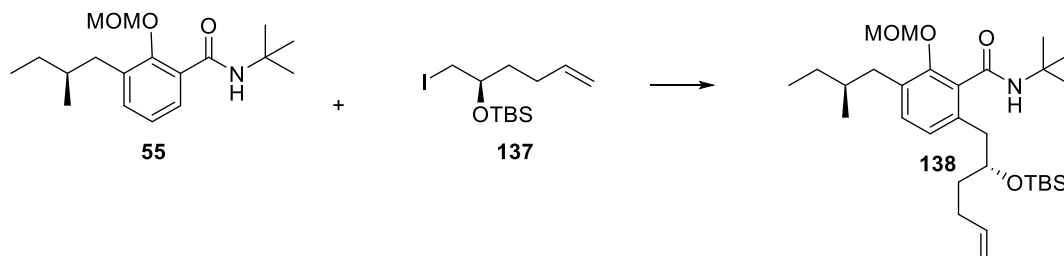
Scheme 34 Coupling of fragments **55** and **112**. Reaction conditions: i. **55**, *sec*-BuLi (2.5 eq.), TMEDA (2.5 eq.), -78 °C to -40 °C, 2h; ii. **112**, -78 °C to -40 °C, 12 h, Et₂O, traces of product **134** in LC-MS.

Due to the expensive and time-consuming synthesis of eastern fragment **112**, the optimization of the *ortho*-lithiation reaction was devised with a test system that utilizes fragment **137**. This fragment was obtained through a two-step transformation of precursor **135** where the unprotected primary alcohol **136** was halogenated to the corresponding alkyl-iodine precursor **137**.



Scheme 35 Synthesis of test analogue **137**. Reaction conditions: a) TBAF, THF, 30 min, 0 °C, 70%; b) PPh₃, Imidazole, I₂, toluene, 0 °C, 1h, 97 %.

Precursor **137** was then subjected to be tested in the *ortho*-functionalization reaction. Only a very few conditions were tested but they gave some promising results. Different lithiation agents were tested. For *sec*-BuLi and *tert*-BuLi traces of product could be detected by LC-MS of the crude mixture.



Entry	Reaction conditions	Results
1	i. 55 , <i>n</i> BuLi (3 eq), TMEDA (3 eq.) , -78 °C to -30 °C, 2 h	No product
	ii. 137 , -78 °C to -30 °C, 12 h	
2	i. 55 , <i>sec</i> BuLi (3 eq), TMEDA (3 eq.) , -78 °C to -30 °C, 2 h	Traces of product
	ii. 137 , -78 °C to -30 °C, 12 h	
3	i. 55 , <i>tert</i> BuLi (3 eq), TMEDA (3 eq.) , -78 °C to -40 °C, 3 h	Traces of product
	ii. 137 , -78 °C to -40 °C, 12 h	

Table 11 Optimization of *ortho* lithiation reaction.

Further optimization is necessary to conclude this desired synthetic step.

5. Monitoring the HCV p7 activity by optical transport assays

The viroporin HCV p7 was recombinantly synthesized in *E.coli* and affinity isolated using detergent to keep the protein soluble and reconstituted afterwards into dye charged liposomes. In order to investigate the potassium transport activity of a purified viroporin HCV p7 a fluorescent dye assay was developed. Furthermore, the assay aimed to identify inhibitory activity of synthesized new compounds and to allow an efficient selection from a small library of active molecules. Two miniaturised assay formats were used to monitor the p7 activity - the microplate and microarray format. Three different dyes (PBFI, APG2 and HPTS) have been improved for stability, bleaching or interaction reasons.

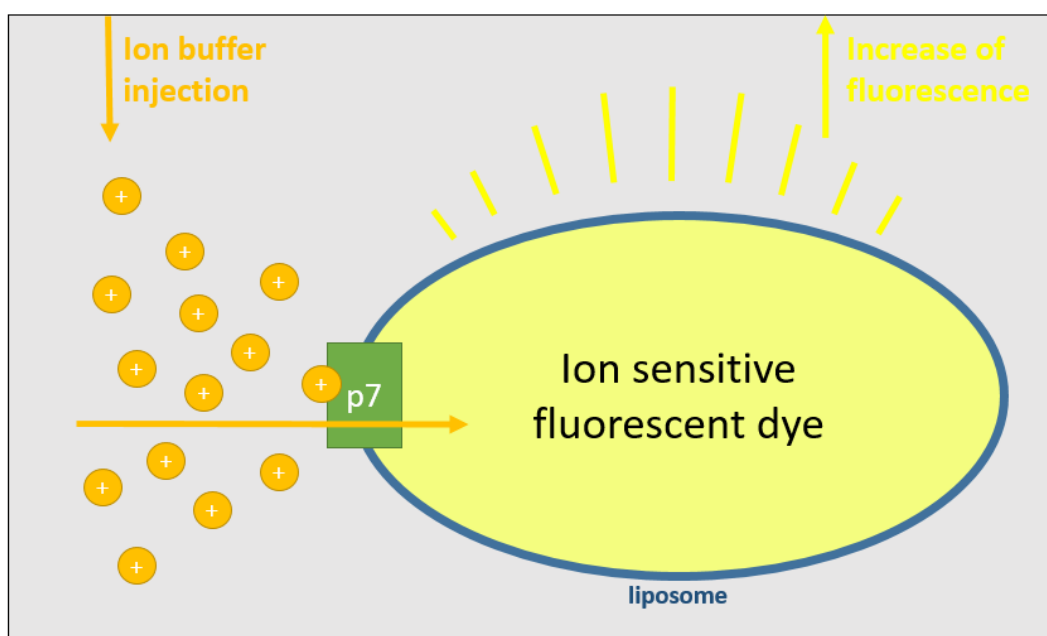


Figure 16 General principle of the fluorescent dye assay – liposomes, containing an ion sensitive fluorescent dye and loaded with the HCV p7 ion channel were prepared. On injection of an ion buffer an increase of the fluorescence could be measured, which was interpreted as ion channel activity. A sample of liposomes without the ion channel was always used as a control (base line). This setup of the assay could further be utilized to screen for HCV p7 inhibitory activity of a small library of active molecules.

First, the proton sensitive fluorescent dye HPTS (8-Hydroxypyrene-1,3,6-trisulfonic acid **139**) was used to sense shifts in the membrane potential when the buffer concentration changed. (Fig. 17).¹⁰⁹ The assay was conducted using a 96-well microplate format. The activity of an open ion channel is prone to a drastic change in the permeability and accompanied membrane potential. Therefore when a buffer containing such ions is injected, the HCV p7 reconstituted liposomes that are full of ion sensitive fluorescence indicator emit an enhanced fluorescence

signal that could be measured (Fig. 16). Liposomes that do not contain an ion channel would sustain a steady emission (base line).

HPTS has been widely emphasized in scientific, medicinal and commercial applications.^{110, 111, 112} It is highly water-soluble and also very cheap compared to other commercially available indicators. Excitation ratio imaging assay is possible as HPTS has absorbance maxima at 405 and 465 nm, respectively, that increase and decrease when the pH value is varied between 5 to 8.¹¹³ Furthermore, HPTS has been shown to lack cell permeability, an ability that is highly suitable for testing the activity of ion channels.¹¹⁴

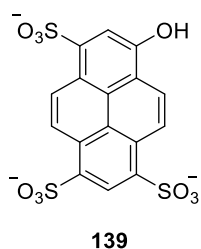


Figure 17 Structure of the pH-dependent fluorescent dye HPTS **139**.

Stable liposomes with low membrane permeability were prepared by sonication of the hydrated thin-film described before as the hydration method or Bangham procedure.^{115, 116} Basic optical microscope pictures show typical field of vesicles filtered through a 0.2 μm Unipore filter (Figure 18 a).

The ion-channel p7 activity of human (HCV) and horse (NHCV) was tested using HPTS (Figure 18 b). In figure 18 b is demonstrated that the preparations with viroporin (horse 1, human 2 and control 3) contain HPTS after preparation, reflecting a stable dye inclusion.

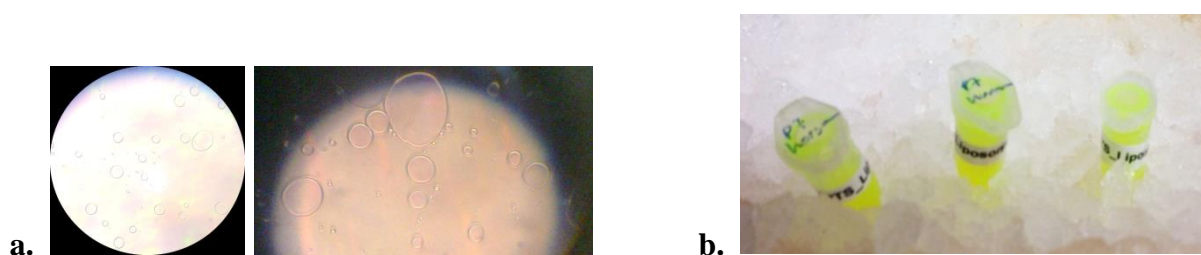


Figure 18 HPTS liposomes samples: a) microscope pictures; b) picture of the samples.

A promising result of the assay shows that after an injection of 20 mM KOH solution the fluorescence significantly increases that was interpreted as transport activity mediated by the viroporins from horse (NHCV) and human (HCV) (Figure 19). The results show that the NHCV p7 peptide exerted an ion channel activity higher than HCV p7 and both had higher

activity than the control sample. However, a background activity of around 20-30% of the total signal was detected with the control liposomes.

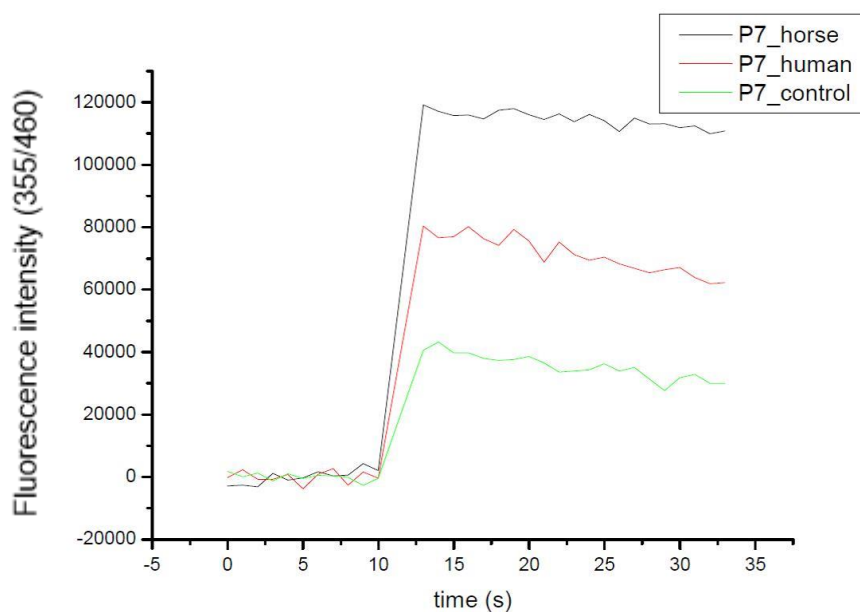


Figure 19 Potassium mediated transport activities of horse (NHCV) and human (HCV) p7. After 10 s a volume of 10 μ L containing 20 mM KOH was injected within 0.5 s into the running kinetic. The activity was analysed at an emission wavelength of 460 nm after an excitation at wavelength of 355 nm at an average time rate of 38 600 cps. Comparative fluorescence measurements of a control (no channel-green) sample and two different types of p7 ion channels (human-red and horse-black) samples.

As amantadine is a commercially available drug, reported to have ion-channel inhibition properties, it was used to analyse its blocking effect against the two types of p7 ion-channels.^{117, 118} In the presence of 1 mM amantadine the human HCV p7 showed inhibitory activity comparable by time rate and background intensity to the control, whereas the horse NHCV p7 was not inhibited by amantadine (Figure 20).

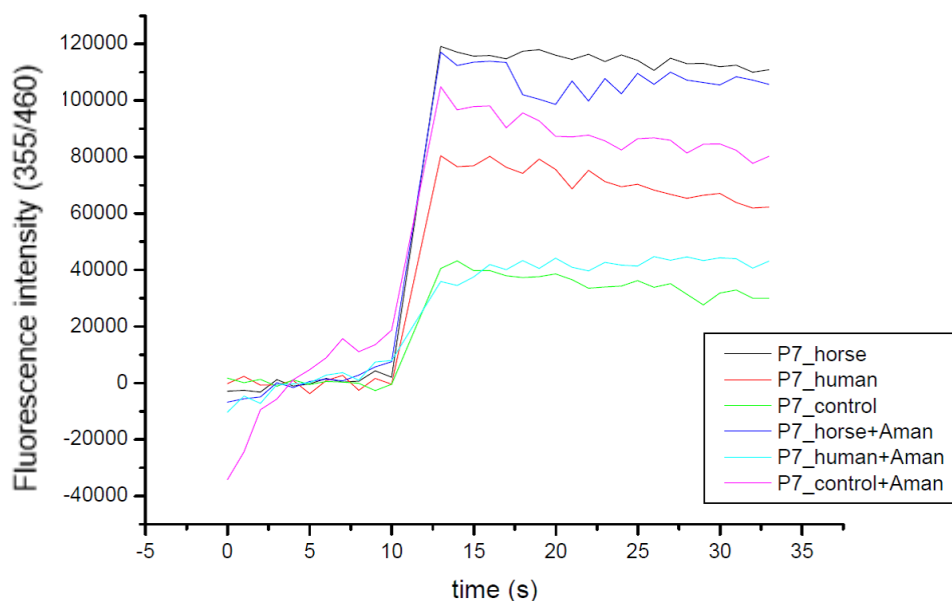
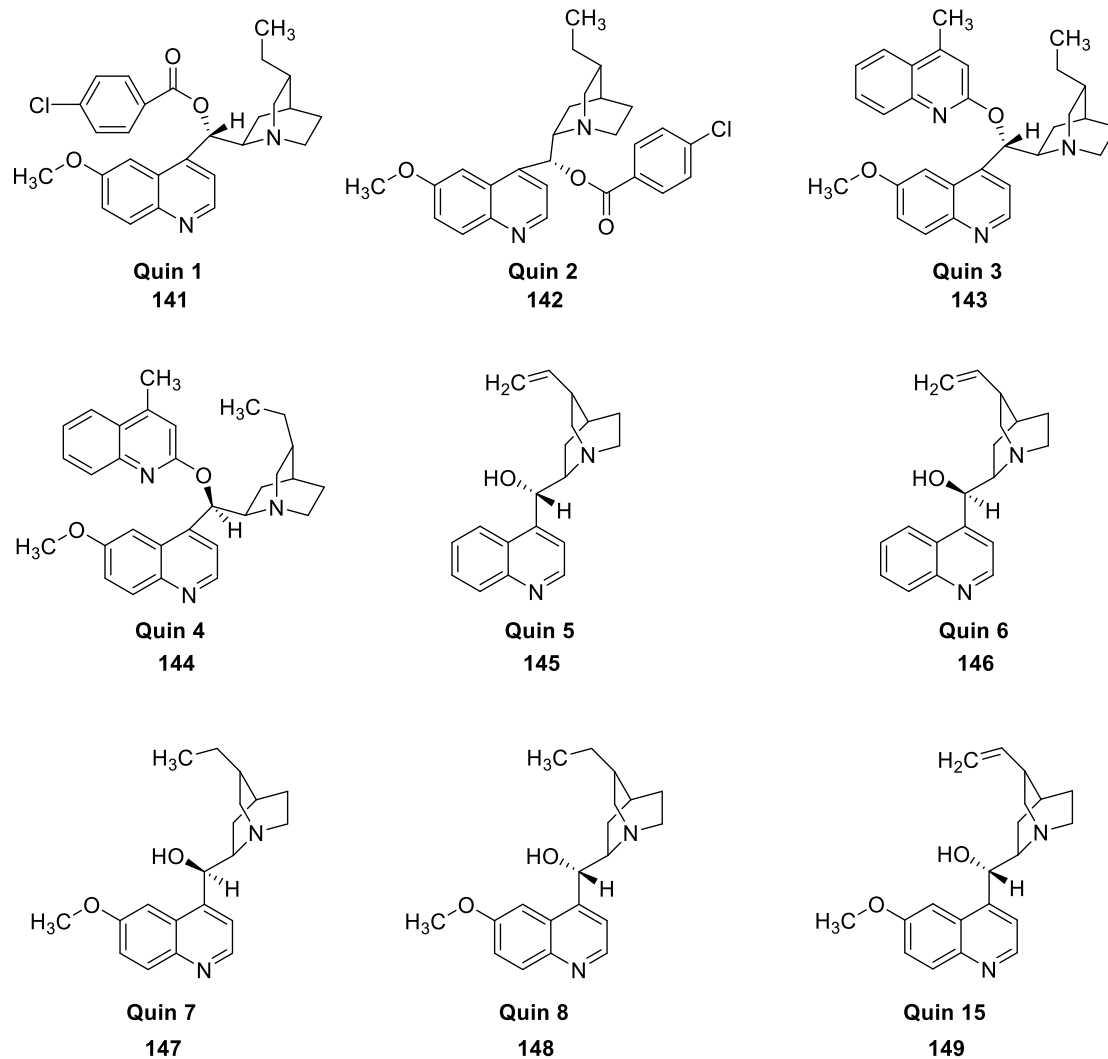


Figure 20 Activity of horse NHCV and human HCV p7 with and without 0,5 μ l 1 mM amantadine. After 10 s 10 μ L of 50 mM KOH were injected into the running kinetic. The activity was analysed at an emission wavelength of 460 nm after an excitation at wavelength of 355 nm at an average time rate of 26 600 cps.

In the course of the development it was found that the HPTS dye proved to be very sensitive to mildly acidic and mildly basic pH values that often lead to liposome leakage and in addition also high DMSO concentrations needed for the solubility of some compounds influenced the proton stability of the liposomes or some compounds itself tend to quench the dye directly. In order to improve the stability of the liposomes a different fluorescent indicator had to be selected.

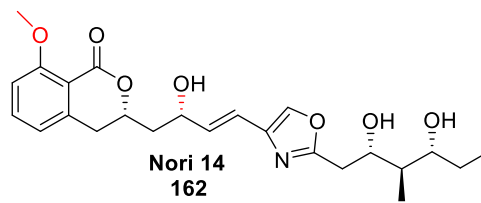
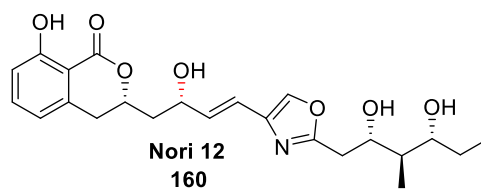
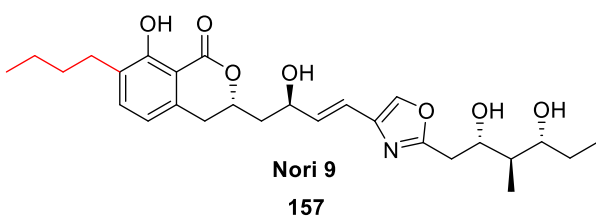
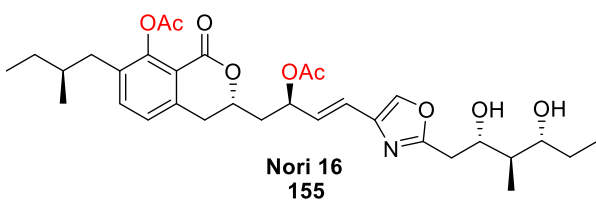
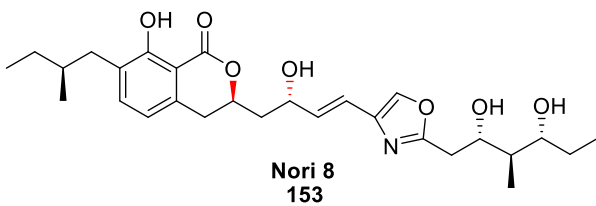
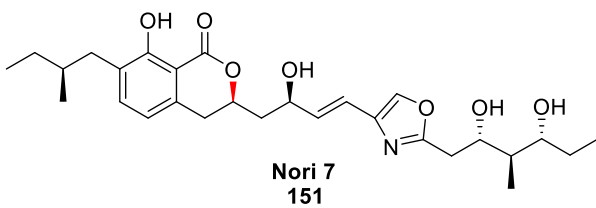
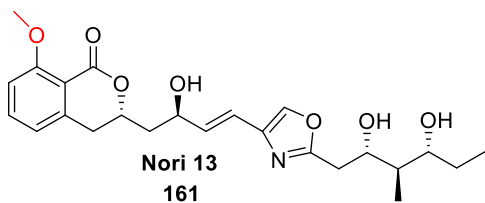
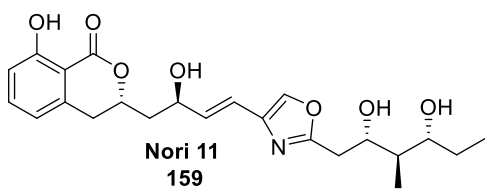
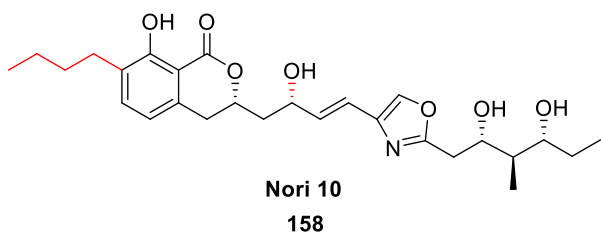
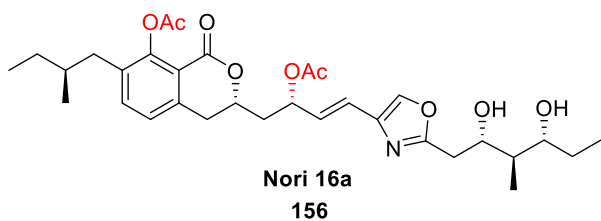
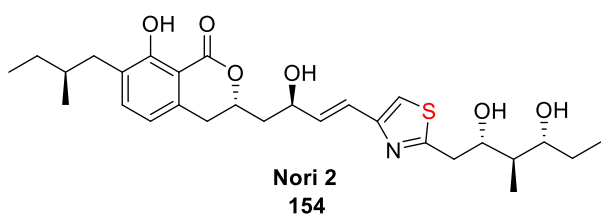
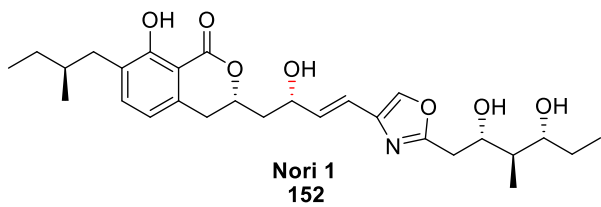
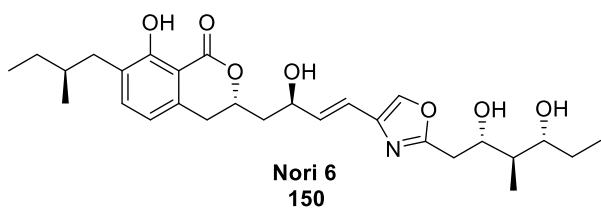
After a short screening of a set of fluorescent dyes, the potassium-sensitive PBF1 dye proved most suitable for the fluorometric measurements.

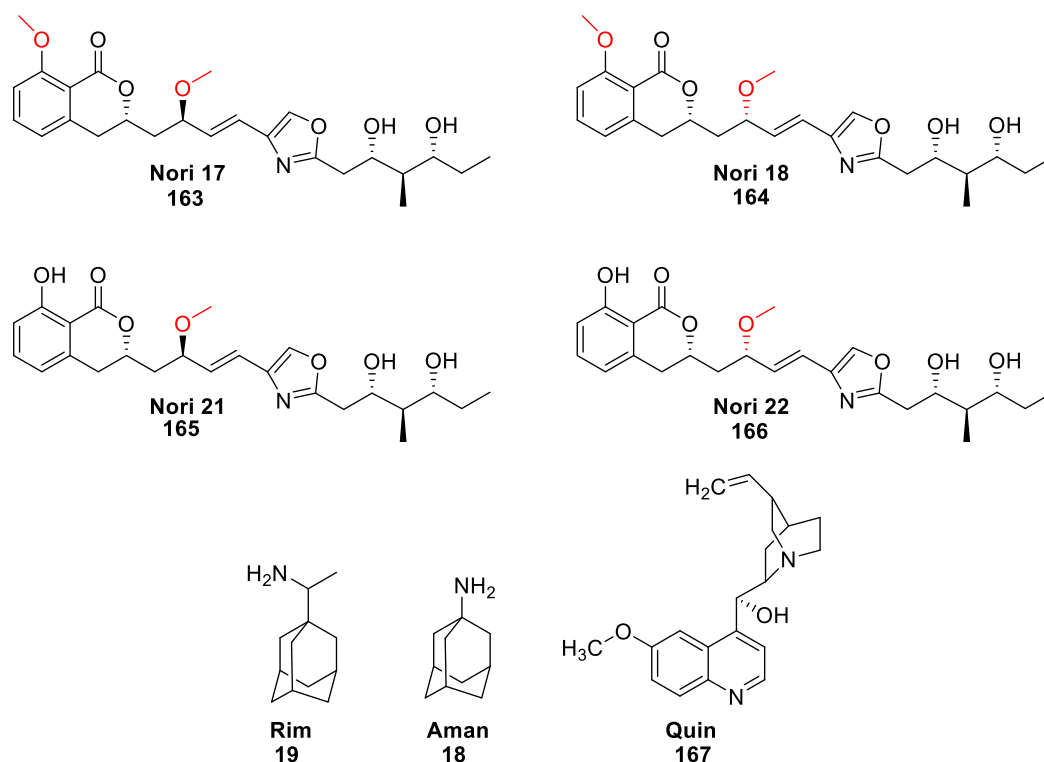
The benzofuran isophthalate derivative **140** consists of fluorophores linked to the nitrogen atoms of a crown ether chelator (Figure 21). The cavity size of the crown ether confers selectivity for K^+ versus Na^+ . The selectivity is reported to be sufficient for the detection of physiological concentrations of K^+ in the presence of other monovalent cations.¹¹⁹ When an ion binds to PBF1, the indicator's fluorescence quantum yield increases, inducing increase of fluorescence intensity.¹²⁰



Scheme 36 Quinidine derivatives tested in the p7 liposome assay.

In previous studies it was shown that noricumazole is also able to stabilize the tetrameric architecture of the potassium channel KcsA. This finding initiated the preparation of a small set of noricumazole derivatives **141-167** to be included into the inhibitory assays alongside rimantadine **19**, amantadine **18** and quinine **167** derivatives (Scheme 37).^{123, 124}

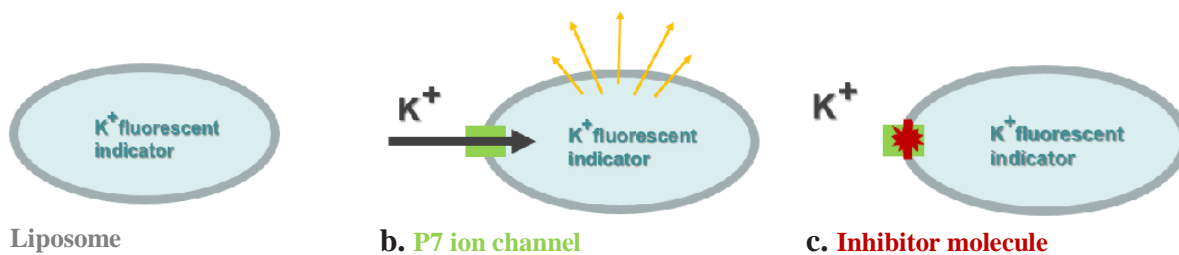




Scheme 37 Inhibitors tested in the p7 liposome assays.

The assays were conducted in a similar accordance to the procedure reported by Griffin et al that described the first assay for screening inhibitors of p7 ion channel function based on the release of fluorescent indicator from liposomes. Their study showed that a recombinant p7 from genotype 1b HCV caused a dose-dependent release of carboxyfluorescein (CF) fluorescent dye when mixed with liposomes and that this property was due to the formation of a size-selective pore rather than non-specific disruption of liposomes. Furthermore, the activity could be blocked by amantadine and several other compounds.⁵²

In our study, liposomes filled with the PBF1 indicator were prepared and loaded onto black-walled, flat-bottomed black-base 96-well microplate on ice (Scheme 38 a, b). In the next step of the process potassium ions were administered to the liposomes. An increase in membrane permeability was measured when HCV p7 reconstituted liposomes were present (Scheme 38 b). A rapid binding of potassium to PBF1 occurred that enhanced the fluorescent signal to be measured. When adding an inhibitor, the HCV p7-dependent permeabilization of the liposomes could be blocked and the decrease of the fluorescent signal was detected (Scheme 38 c).



Scheme 38 Graphic overview of the inhibitory screening assay.

Reactions for each condition were carried out in duplicate wells with two independent experimental repeats for statistical accuracy.

Five of the nine quinidine derivatives (Quin 1, Quin 4, Quin 5, Quin 6, Quin 7) induced more than 50% lower intensity of the fluorescent signal so that one can speculate that quinidine derivatives could be potential HCV inhibitors with a p7 specific mechanism of action (Figure 22).

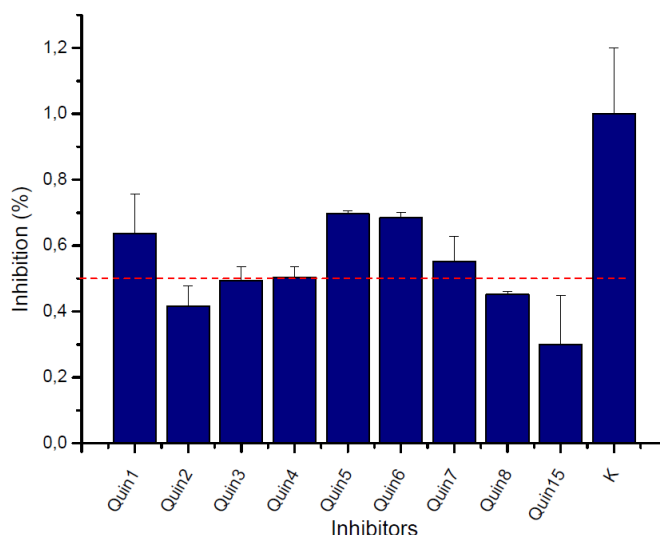
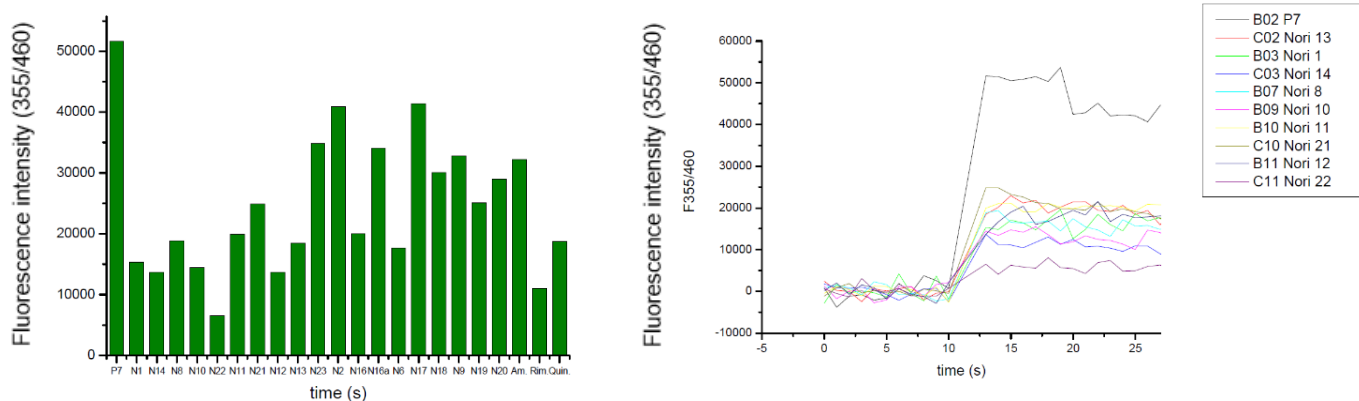


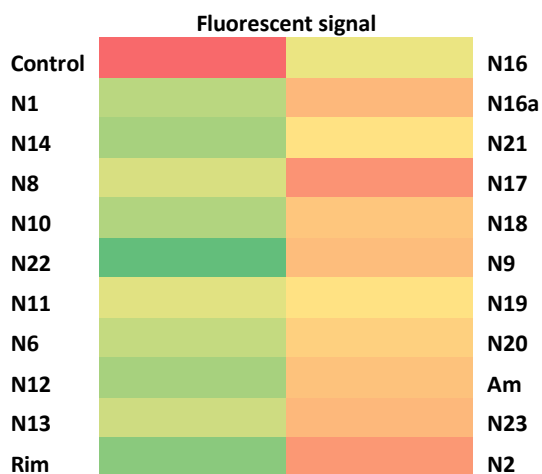
Figure 22 Quinidine derivatives inhibitor activity in the optical assay.

The screening of noricumazole derivatives proved successful too. Nine of the noricumazole derivatives showed potency as inhibitors as well as quinine and rimantadine (Figure 23). The latter exhibited strongest blocking character among the three commercial inhibitors



a.

b.



c.

Figure 23 Noricumazole inhibitory activity in the optical assay: a) Statistical overview; b) fluorescent measurement, c) heat map – green representing weak fluorescence (good inhibitory properties) and red/orange/yellow – strong fluorescence (bad inhibitory properties).

The compiled data of the noricumazole screening allows to draw a comparison between the most potent and least potent structures (Figure 23). The structure-activity relationship could be analyzed and the major similarities and differences in structure functionality that might have an influence on the ion-channel inhibition properties could be concluded.

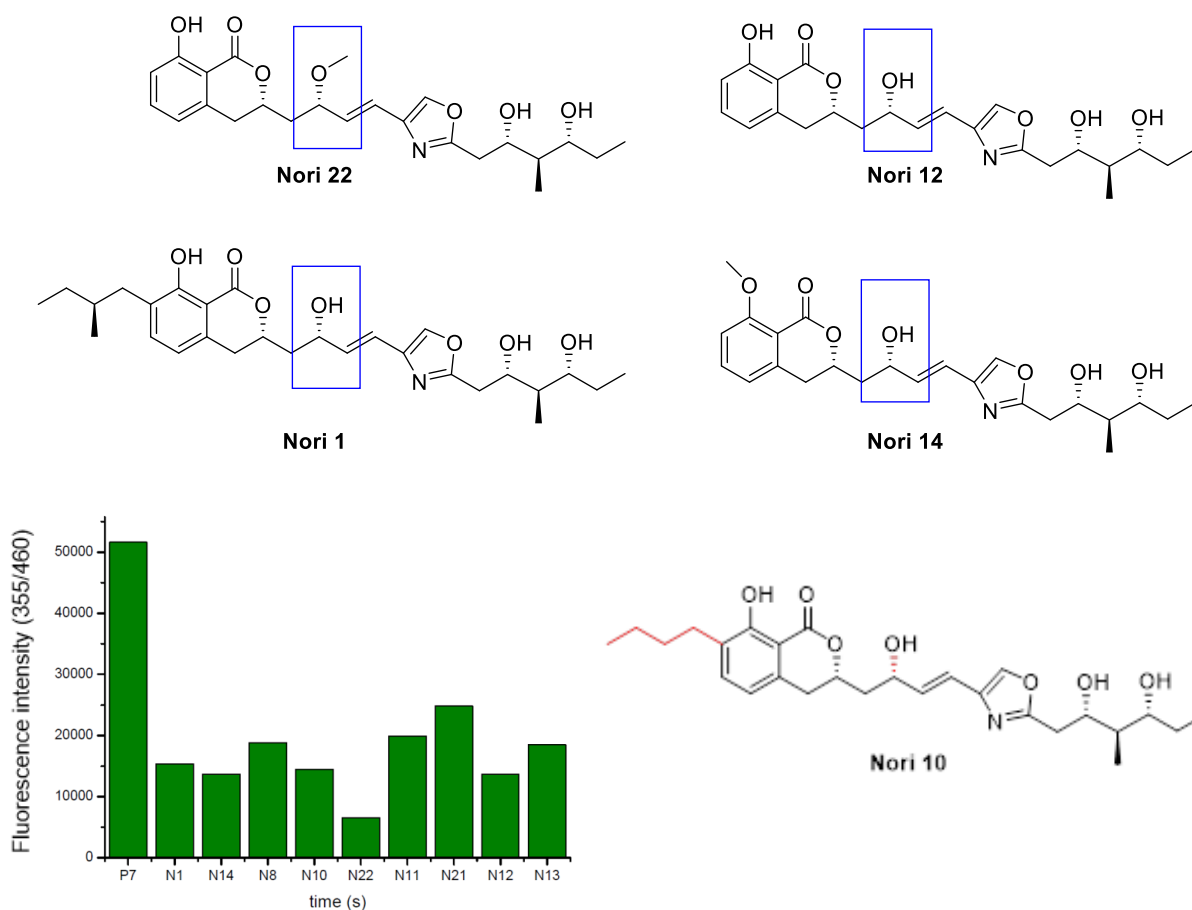


Figure 24 Structure-activity relationship analysis.

It seems the 11-epi stereoinformation is a characteristic feature among these most potent structures. This speculation could be confirmed if a derivative lacking functionality at this position would be at hand

5.1 Optimization of the p7 assay on microarray.

The principle of the liposome microplate assay was further developed into a microarray assay for p7 inhibitors screening by Albert et al.¹³¹ Microarray testing requires much less material and allows many simultaneous measurements. Since stronger fluorescent signals are necessary due to relatively higher background noise, the novel potassium sensitive dye Asante Potassium Green 2 (APG-2) was utilized for the tests.

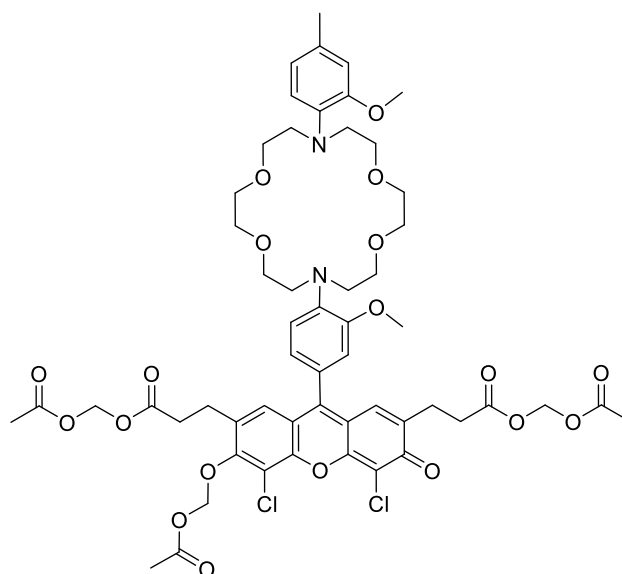


Figure 25 Structure of APG-2.

APG-2 has comparatively stronger fluorescence and dynamic range –excitation at 488-517 nm, emission at 540 nm - to the PBF1 dye that was originally used in the microplate assay.

Similar to the microplate assay, liposomes filled with APG-2 (20 μ M) were reconstituted with HCV p7. Liposomes without HCV p7 were used as negative control. Next, the liposomes were contactlessly spotted onto UniSart 3D Nitro Slides (Sartorius AG) with 16 pads. Spotting was done with a Nano-Plotter 2.1 (GeSiM mbH). Each spot contained 5 drops of 200 picolitre liposomes and each liposome type was spotted 10 times. This was followed by washing 3 times with 100 μ l Tris-HCL buffer (100 mM, 8 pH) to remove fluorescent dye outside the liposomes. The microarray was then dried under a mild stream of air and scanned via Axon Scanner Genepix 4000 B (Molecular Devices Inc.). Basic fluorescence line was established from this initial scanning that characterizes the liposomes filled with APG-2. The pads where inhibitors would be measured were loaded with 50 μ M inhibitor and 100 μ l Tris-HCl (100 mM, pH 8) for 30 min. A 5 min washing step with Tris-HCl (100 mM, pH 8) follows to remove unbound inhibitors. The activation of the dye was achieved by addition of 100 μ l 500 mM KCl and either 10 mM Citrat (pH 4,0) or 10 mM MES (pH 5,0). The potassium added in the later step is outside the liposomes and could only enter them through the p7 ion-channel. The amount of potassium that enters the liposomes is evaluated by its binding to the potassium fluorescence indicator APG-2 - a larger amount of potassium in the liposomes corresponds to stronger fluorescence. Liposomes with ion channels blocked by the inhibitory molecules exhibit reduced fluorescence. The chip was scanned a second time after activation. Subsequently, fluorescence values of different spots were compared after washing and after activation. The average of ten repetitions for each liposome was calculated and the background noise was subtracted (SM-BM). The

reliability was determined through signal to noise ratio (SNR). Microarray assay optimization was conducted through repetition of experiments, aiming for high signal differences between positive and negative controls with a high SNR. Additionally, negative effects of buffer solutions and inhibitors should be minimized in the negative control.

Trials to define the optimal temperature and APG-2 concentration for the assays were conducted. It was concluded that liposomes are most stable at the standard temperature of 4°C.

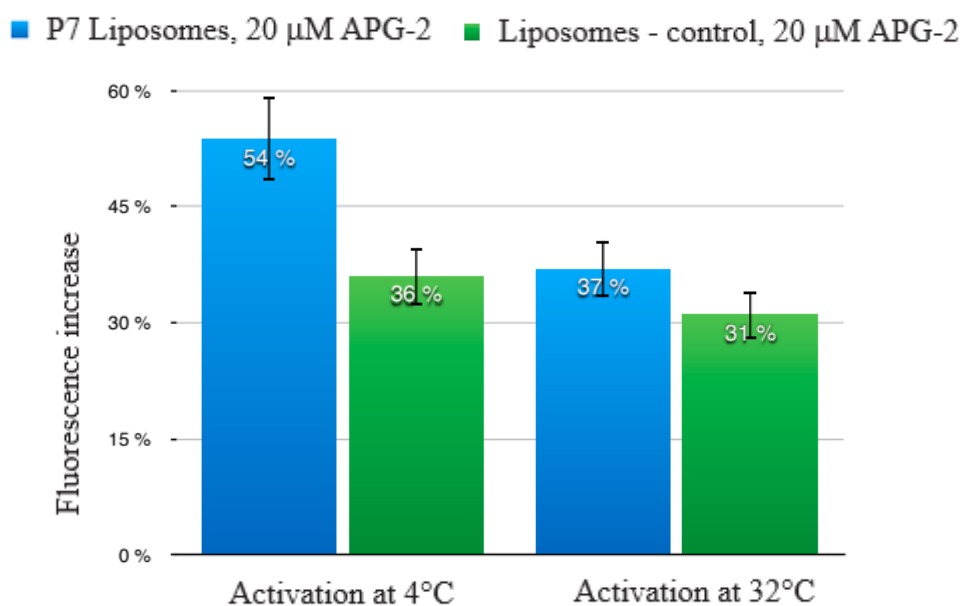


Figure 22 Mean percentage increase of fluorescence at different temperatures; control liposomes vs P7 liposomes. Activation with 500 mM KCl, 10 mM Mes pH 5.0.

Two different concentrations of the fluorescent indicator were tested. The lower concentration showed more stable results as higher concentrations increase the possibility of dye quenching and undesired interaction with the inhibitor molecules.

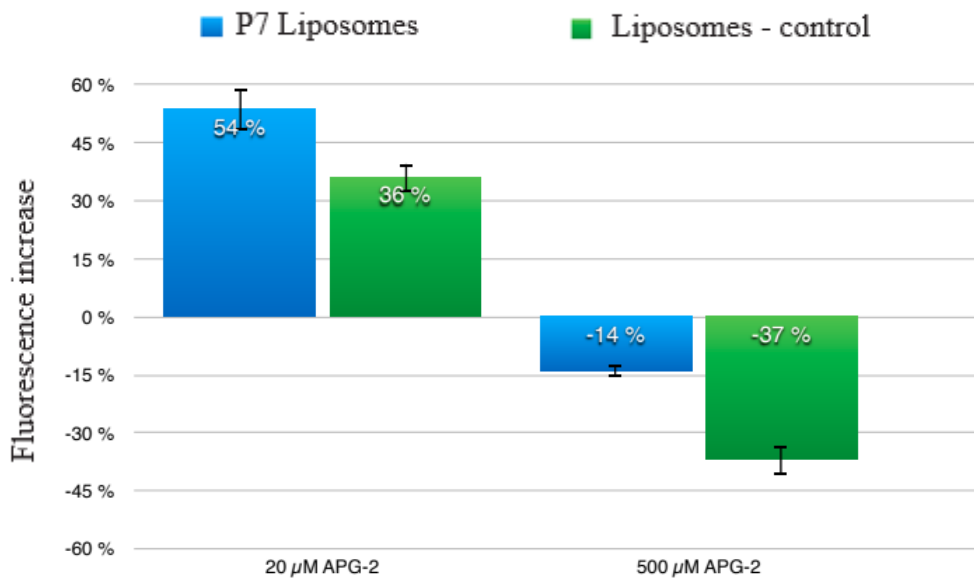


Figure 23 Mean percentage increase of fluorescence at different internal APG-2 concentrations; control liposomes vs P7 liposomes. Activation with 500 mM KCl, 10 mM Mes pH 5.0 at 4°C.

Since the pH influence the cell membrane charge it is an important factor for the ion-channel activity, the liposomes in the microarray we re scanned at five different pH values. It was observed that when the pH value is reduce the fluorescence values increased. Furthermore, a good differentiation could be made between the washing and activation step at pH 4 and 5. This effect appears to be strongest at pH 5 which was chosen as an optimal pH value for the assays.

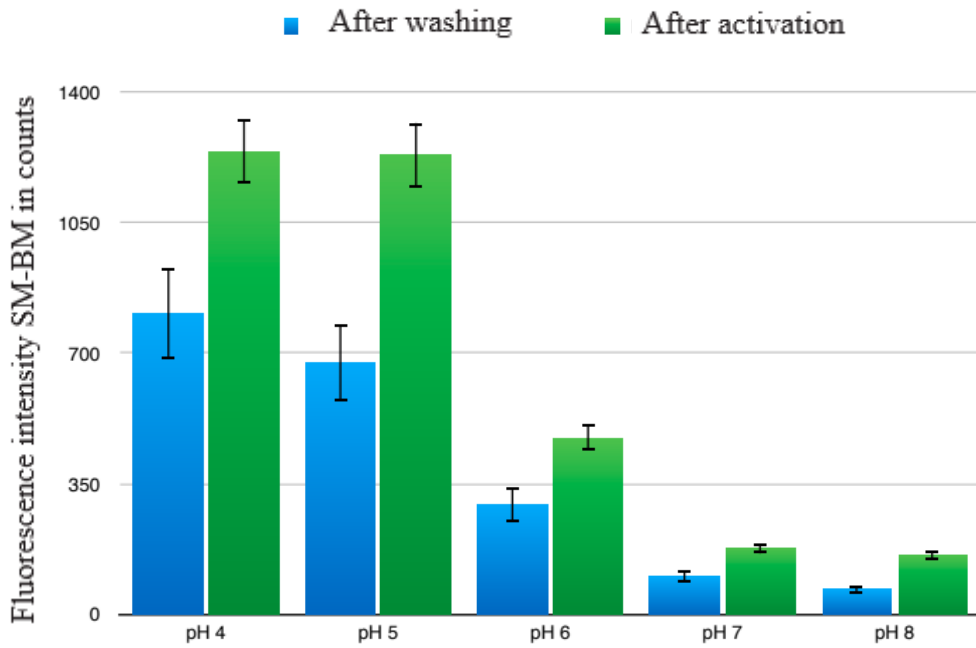


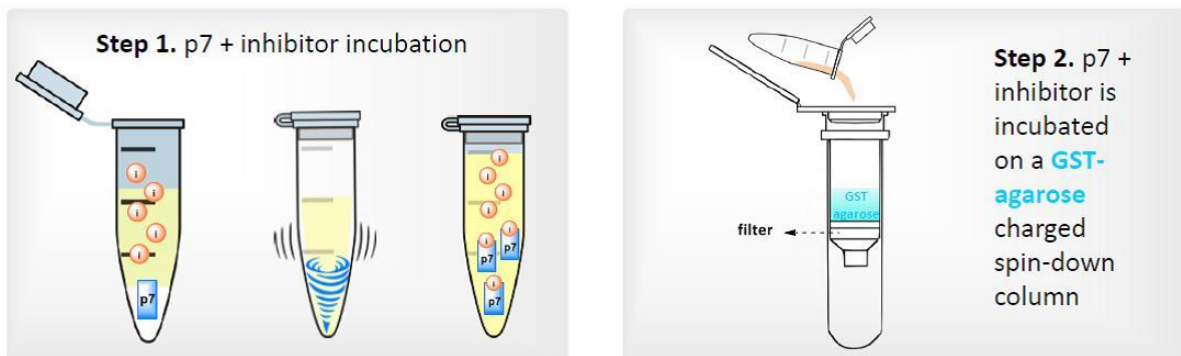
Figure 24 Absolute microarray SM-BM values, before and after activation at different pH values. Activation with 500 mM KCl, 10 mM of the following buffers: Citrate pH4, Mes pH 5.0, MES pH 6, Tris-HCl pH 7, Tris-HCl pH 8.

Even though the transfer of the liposome assay onto microarray is characterized by high loss of liposomes with each washing step, the low quantity of liposomes per spot (1 nl) enable the fast production of many results. Thus the microarray has the potential to be very cost-effective inhibitor screening technique.

5.2 Pull-down assays.

In order to explore the ion-channel inhibition mechanism an assay was developed that would allow to measure quantitatively the concentration of the active inhibitor molecule. The most potent Noricumazole derivative from the optical assays was chosen to be tested – Nori 22.

The experiment process started with incubating a defined amount of the inhibitor molecule with freshly prepared HCV p7 liposomes (Figure 25, step 1).



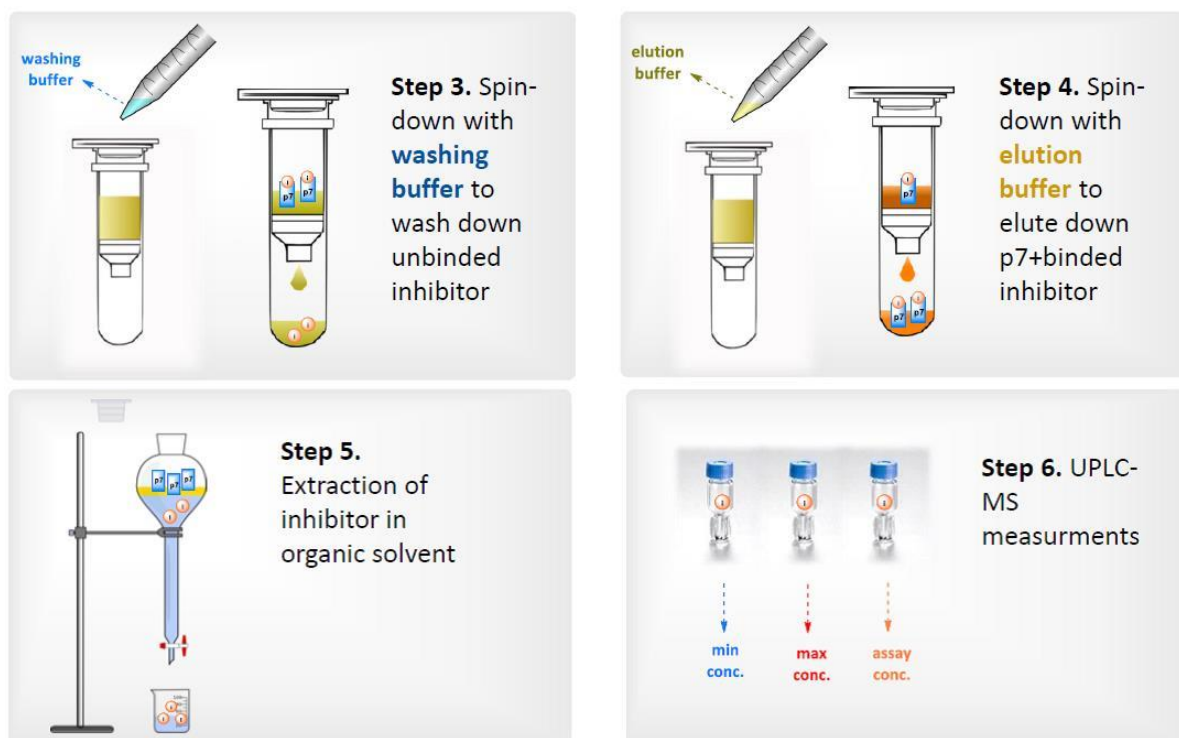


Figure 25 Graphic overview of the pull-down assay process.

After incubation, the remaining unbound inhibitor could be filtered through a GST-agarose spin-down column by a washing buffer (Figure 25, steps 2 and 3). Since the HCV p7 protein is GST-tagged it would be bound to the GST-agarose and it could be eluted after it is purified from the unbound inhibitor molecules (Figure 25 step 4). The inhibitor molecule could then be extracted from the elutant in an organic solvent, the solvent was evaporated and the residue was analysed by mass spectrometry (Figure 25, steps 5 and 6). For the UPLC-MS measurements, the assay sample was measured against two samples of the inhibitor molecule – one at minimum and one at maximum concentration.

The results were inconclusive, as the desired mass peak from the assay sample was of negligible concentration. An update of the assay process needs to be conducted to confirm those results. A sample of the washing eluant should be measured to confirm that the inhibitor was not bound to the p7 protein. Furthermore, longer incubation time might be necessary as conducted for some optical p7 assays before.¹²⁵

6. Summary and outlook

6.1 Conclusions and summary

A total synthesis approach towards new noricumazole A derivatives was investigated. The initial strategy was to synthesize a derivative that contains all activity relevant structural elements as known from previous work by Dr. Jenny Barbier. The envisioned structure contained a thiazole ring that leads to decreased cytotoxicity as well as the acylation of the hydroxyl groups at C3 and C11 that showed increased inhibition of activity.

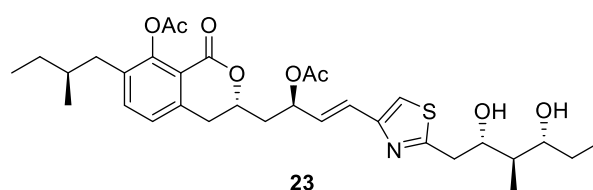
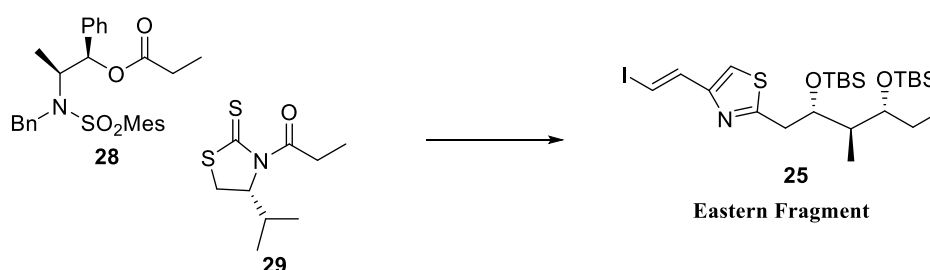


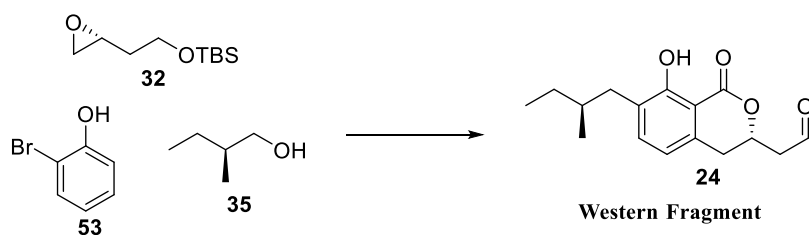
Figure 26 Initially envisioned noricumazole A derivative containing the main activity relevant features.

The total synthesis was based on the previous work and the design was highly convergent relying on two key fragments. The eastern fragment was prepared in 13 steps from Masamune ester, employing the Suzuki asymmetric aldol reaction, with an overall yield of 59 %.



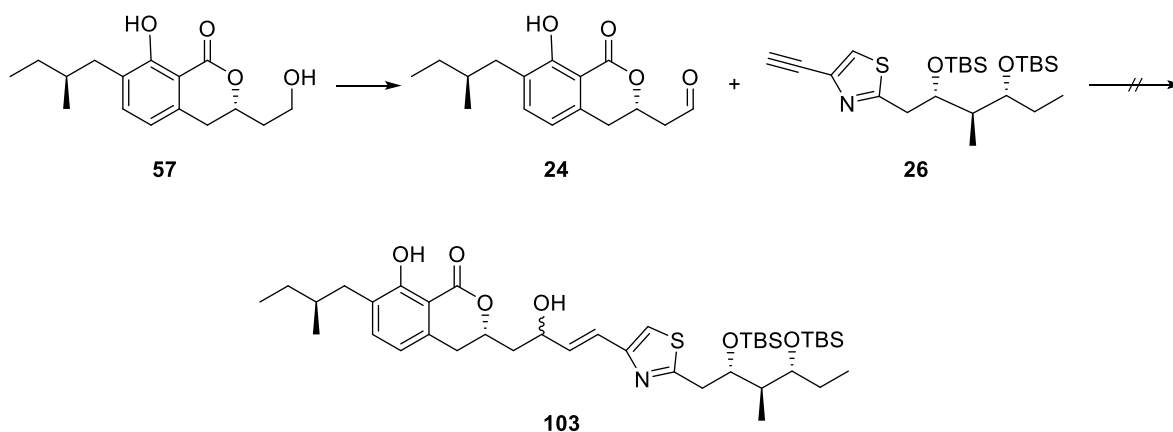
Scheme 39 Masamune ester **28** and Suzuki chiral auxiliary **29** – key building blocks in the synthesis of eastern fragment **25**.

The western fragment was achieved in 7 steps and the overall yield was 62%. The synthesis started from 1, 2-bromobenzene and involved three organometallic catalysed transformations.



Scheme 40 Key starting materials in the synthesis of western fragment **24**.

The key coupling step between the two final fragments had to be optimized, however the initial oxidation step of the western fragment gave none-reproducible results. Different conditions for the oxidation reaction as well as the following metal-catalysed addition were tried but without success. A small library of chiral ligands was synthesized for these trials of coupling.



Scheme 41 Key coupling reaction towards Noricumazole derivative **103**.

A different strategy towards structurally different noricumazole derivatives was also pursued. The derivative lacking the hydroxylic group at C13 would be a valuable contribution for SAR studies and would confirm the essential role of this group with regards to the inhibitory activity on HCV as well as p7 inhibition.

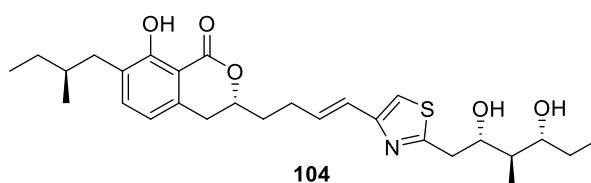
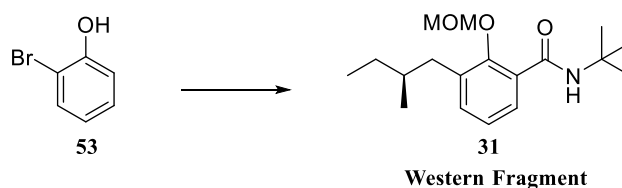


Figure 27 Noricumazole derivative **104**, lacking the hydroxylic group at C13.

The convergent synthesis was directed towards two key fragments that would be brought together in an *o*-lithiation end-game reaction. The western fragment was major intermediate in

the initial synthetic efforts towards derivative **104** and thus could be obtained from bromophenol in 3 steps and 78% yield.

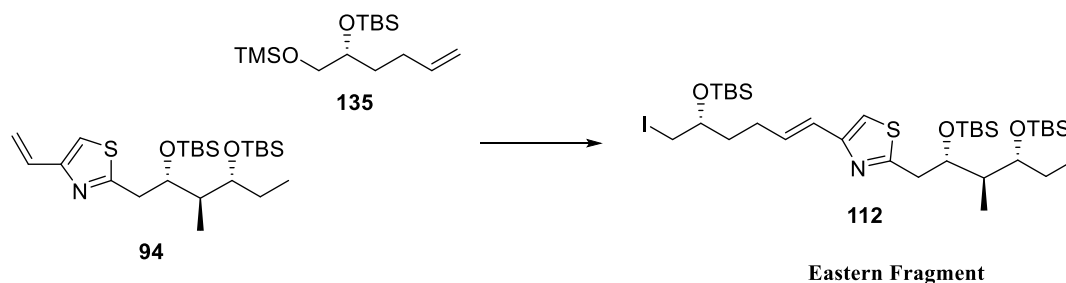


Scheme 42 Bromophenol **53** – key starting material for the synthesis of western fragment **31**.

The envisioned eastern fragment was achieved in a key cross-metathesis reaction between intermediates **94** and **135** in 40% yield.

The synthesis of intermediate **94** was based on our initial synthetic strategy and constituted of 13 steps, the final step being Schwarz reagent reduction of the terminal alkyne to intermediate **94** in 99% yield.

Intermediate **135** was achieved from 1,5-hexadiene that underwent asymmetric Sharpless dihydroxylation and two consequential selective silylations of the hydroxylic groups. **135** was afforded in 82% yield over 3 steps.



Scheme 43 Intermediates **94** and **135** – key substrates for the synthesis of eastern fragment **112**.

Additionally, to achieve an alternative of eastern fragment **112**, the structure analog **115** was also synthesized over 4 steps in 94% yield.

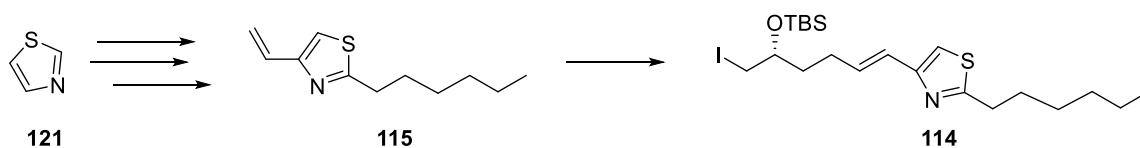
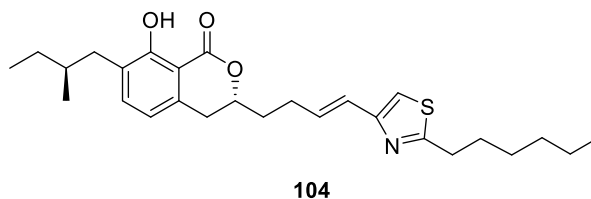


Figure 28 Key substrates in the synthesis of eastern fragment **114**.



Scheme 44 Noricumazole derivative **104**.

As easier achievable and cheaper intermediate **115** was designed to test the key *ortho*-lithiation step and also yield a valuable noricumazole derivative **104**.

The *ortho*-lithiation step was tested under conditions developed in our initial synthetic strategy towards derivative **23**. Traces of product were detected via LC-MS. Initial optimization of the reaction conditions was conducted on a test substrate. Further optimization is necessary to achieve reproducible yields.

Liposome assays

Liposome fluorescent assays were developed to investigate p7 ion-channel activity and its drug inhibition ability towards various active molecules.

An *in vitro* assay was initially conducted to compare the activity of human and horse HCV p7 viroporins. The findings showed that both the NHCV and HCV p7 peptide demonstrated an ion channel activity, whereas the human HCV p7 showed stable activity at low pH and further susceptibility to noricumazole and quinidine derivatives.

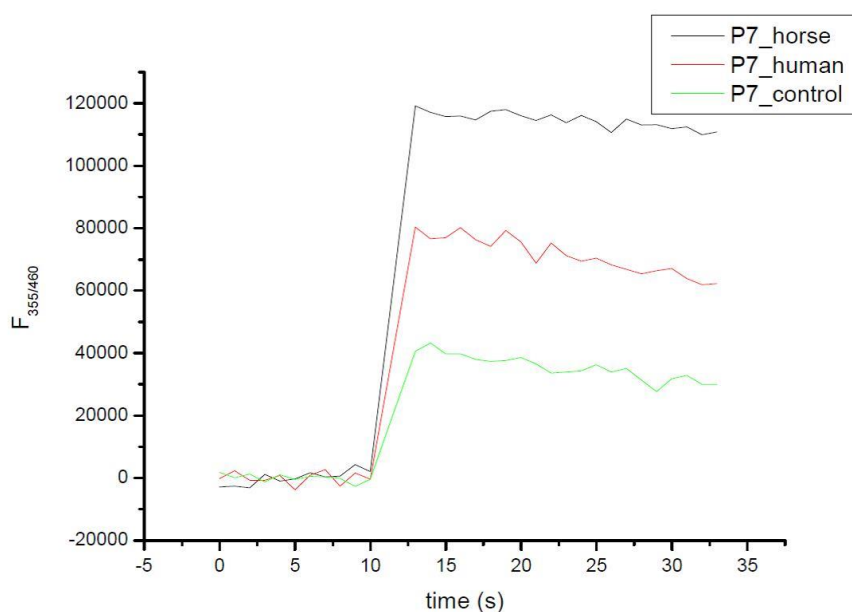


Figure 29 Comparative fluorescence measurement of a control sample (no ion channel) versus two types of p7 ion channel samples.

The inhibitory properties of a small set of noricumazole derivatives, previously synthesized in the Kirschning group, as well as rimantadine, amantadine and some quinine derivatives, was tested in a sequence of liposome fluorescent assays as well.

The assays gave promising results as five quinidine derivatives showed more than 50% lower intensity of the fluorescent signal, which shows a potential HCV inhibitory activity with p7 specific mechanism of action.

Nine of the noricumazole derivatives also showed potent inhibitory properties as quinine and rimantadine.

The data from the noricumazole screening allowed us to also draw some structure-activity relationship conclusions about the potential structural functionality that could have an influence on the ion-channel inhibition properties. The epimer stereochemistry of the hydroxilic group at C11 seems to be a common element among the structures with the most potent activity.

A microarray assay that would allow the simultaneous measurement of a big number of samples was also developed using the potassium sensitive fluorescent indicator APG-2. The optimal conditions in terms of temperature, fluorescent dye concentration and pH were established through a series of screening experiments.

Additionally, the liposome microplate assay principle was applied into a microarray assay setup for p7 inhibitors screening.¹³¹ This technique has the potential to be very cost-effective inhibitor screening method due to the low quantity of liposomes per spot (1 nl) that enable fast production of many results.

Furthermore, a specific assay that would allow the quantitative measurement of the concentration of a p7 inhibitor molecule was developed. It was conducted utilizing the most potent Noricumazole derivative from the optical assays. However, the final UPLC-MS measurements were inconclusive as the desired concentration was found in value too low than expected.

6.2 Outlook of the project

For future studies of the HCV activity of noricumazole, new derivatives need to be synthesized. The total synthesis of the two new derivatives **104** and **168** described in this thesis could be completed, confirming a new synthetic pathway towards further derivatization.

The reaction conditions of the key *ortho*-lithiation step need to be optimized in order to achieve reproducible yields. Other coupling conditions like different metal-catalyzed additions could be explored.

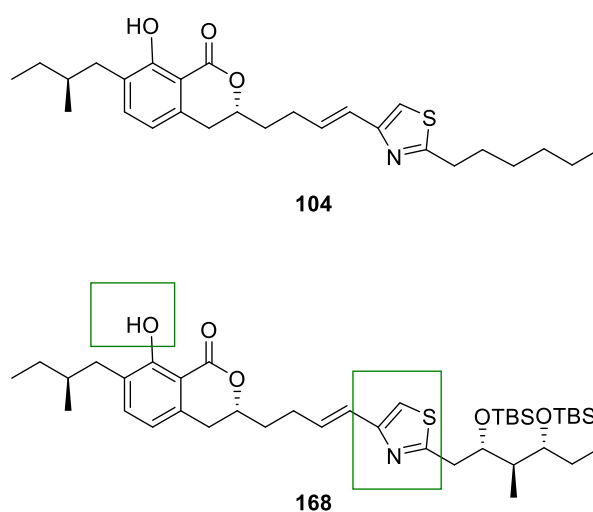


Figure 30 New Noricumazole derivatives.

The achievement of those two derivatives would confirm the importance of the hydroxylic group at C11 in the SAR map that was created after initial biological assays but it would also confirm the SAR conclusions drawn after the p7 liposome-fluorescent assays regarding the stereochemistry at this position.

Furthermore, the role of the stereo-triada at the thiasole side-chain regarding activity would be clarified.

Consequential derivatization of the hydroxylic group at C13 can also be explored as well as other ring-systems in place of the thiazole ring, in order to clarify the extend of influence of the cyclic system to the biological activity.

New noricumazole derivatives could be subjected to the liposome fluorescent assays to measure their inhibitory properties towards p7 ion channel. This would expand the relevant SAR analysis that can then be compared to the SAR map from the HCV inhibitory assays.

Further development of the liposome assay onto microarray has high potential to enable the fast inhibitor screening of many molecules.

The developed pull-down assays could also be optimized to achieve a reliable quantitative method for tracking the concentration of p7 inhibitors in the *in vitro* liposome assays.

7. Experimental part

7.1 Materials and methods

7.1.1 Reagents and solvents

Commercially available reagents (Acros Organics, Sigma Aldrich) and solvents were used as received or purified by conventional methods prior to use, described in the literature.

7.1.2 Thin-layer and column-chromatography

For TLC precoated silica gel 60 F254 plates (Merck, Darmstadt) were used and the spots were visualized with UV light at 254 nm or alternatively by staining with vaniline. Column chromatography was carried out using silica gel from Fluka (grain size 40-63 μm).

7.1.3 NMR spectroscopy

^1H spectra were recorded with 400 MHz with a Bruker Avance-400 and Bruker 200 MHz spectrometer. Chemical shifts are reported in δ (ppm) relative to TMS as the internal standard. Multiplicities are described with the following abbreviations: s - singlet, d - doublet, t - triplet, q - quartet, m - multiplet, b – broad. All coupling constants J are expressed in Hertz.

7.1.4 Mass spectroscopy

Mass spectra were recorded with a type LCT (ESI) equipped with a lockspray dual ion source in combination with a WATERS Alliance 2695 LC system, or with a type QTOF premier spectrometer (ESI mode) in combination with a Waters Acquity UPLC system equipped with a Waters Acquity UPLC BEH C18 1.7 μm column (solvent A: water + 0.1% (v/v) formic acid, solvent B: MeOH + 0.1% (v/v) formic acid; flow rate = 0.4 mL/min;

7.1.5 HPLC

High-performance liquid chromatography was performed using a VARIAN PROSTAR system (pump Prepstar Model 218, variable wavelength detector Prostar; preferred monitoring at $\lambda = 248$ nm) with the column TRENTEC Reprisil-Pur 120 C18 AQ (5 μm , 250 mm x 25 mm, with guard column 40 mm x 8 mm abbreviated C18-1) with parallel mass spectrometric detection (MICROMASS type ZMD ESI-Quad spectrometer). Semi-preparative high performance liquid chromatography was performed using a MERCK HITACHI Model 7000 system [pump L-7100, diode array detector L-7450 ($\lambda = 220$ -400 nm, preferred monitoring at $\lambda = 248$ nm)] with the column NUCLEODUR C18 ISIS (5 μm , 250 mm x 8 mm; abbreviated C18-2).

7.1.6 Melting points

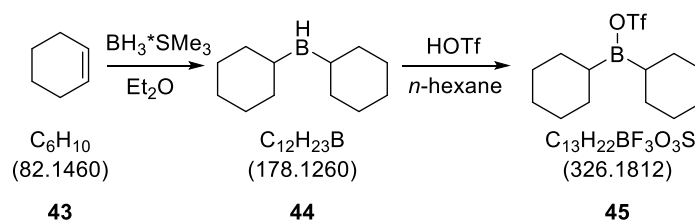
Melting points were determined on a SRS OptiMelt apparatus and are reported uncorrected.

7.1.7 Optical rotation

Specific optical rotation values $[\alpha]_D^t$ were measured on a polarimeter 341 (PERKIN ELMER) at a wavelength of 589 nm (D) and given temperature t .

7.2. Synthesis of Estern fragment [25]:

Dicyclohexylboron trifluoromethanesulfonate [45]:

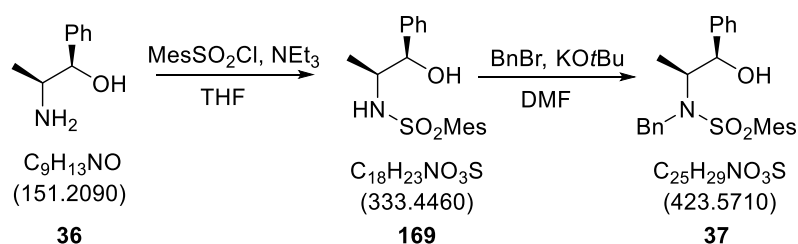


To a stirred solution of freshly distilled cyclohexene (9.86 mL, 97 mmol, 1.0 eq) in dry diethyl ether (20 mL) was added borane-dimethyl sulfide complex (4.62 mL, 49 mmol, 0.5 eq) dropwise (over 40 min) at 0 °C. The reaction mixture was stirred for 3 h at 0 °C and then the solid was allowed to settle for 24 h without stirring at -30 °C. The solvent was then removed via syringe and the residual solid was dried under Schlenk vacuum. The dicyclohexylborane thus obtained was immediately used without further purification.

The solid obtained in the previous step was suspended in dry hexane () and trifluoromethanesulfonic acid was added dropwise (over 30 min). Vigorous gas evolution occurred, the solid gradually dissolved and the solution developed a yellow-orange color. Stirring was continued for 1.5 h at room temperature and the reaction mixture was left for further 24 h without stirring at -30 °C. The solvent was removed via syringe and the colorless crystals were further dried under schlenk vacuum at 0 °C to yield dicyclohexylboron trifluoromethanesulfonate. The product was stored as 1M solution in hexane.

Synthesis of MASAMUNE auxilliary [28]:

N, N-Mesityl-benzyl-norephedrine [37]:



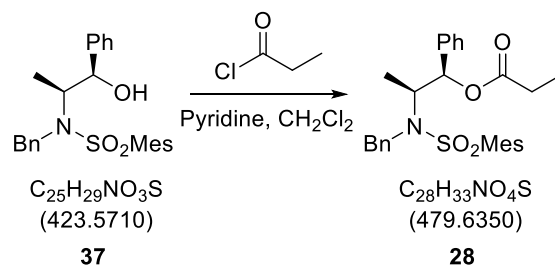
Freshly distilled triethylamine (11 mL, 79.4 mmol, 1.2 eq) was added dropwise to a solution of (-)-norephedrine (10 g, 66.2 mmol, 1 eq) in dry tetrahydrofuran (150 mL). The mixture was cooled to 0 °C and mesitylsulfonylchloride (14.5 g, 66.2 mmol, 1 eq) was added. The reaction mixture was then stirred for further 2 h at 0 °C. The organic phase was washed with water (100 mL), 1M HCl (80 mL), saturated sodium hydrogencarbonate solution (80 mL) and brine (80 mL), and dried with anhydrous sodium sulfate. The filtered organic solution was concentrated to yield the crude product which was used for the next step without further purification.

Mesityl-norephedrine (19.6g, 59 mmol, 1 eq) was solved in dry dichloromethane (200 mL) and potassium-*tert*-butoxide (6.61 g, 59 mmol, 1 eq) was added at 0 °C. Benzyl bromide (7 mL, 59 mmol, 1 eq) was added after 20 min and the mixture was stirred for 3 h at room temperature. Water (150 mL) was added and the aqueous phase was extracted with dichloromethane (120 mL). The combined organic layers were dried over anhydrous sodium sulfate, filtered and the solvent was evaporated. Recrystallization from petroleum ether yielded the pure product as colorless crystals (13.3 g, 31.4 mmol, 53%).

1H -NMR (200 MHz, $CDCl_3$): δ (ppm) = 7.36 – 7.19 (m, 8 H), 7.07 (d, 2 H), 6.93 (s, 2 H), 5.00 (s, 1 H), 4.78 (d, 1 H), 4.54 (d, 1 H), 3.82 (dq, 1 H), 2.65 (s, 6 H), 2.29 (s, 3 H), 2.12 (d, 1 H), 1.05 (d, 3 H).

The analytical data are consistent with those reported in the literature.⁵⁷

***N,N*-Mesityl-benzyl-*O*-propionyl-norephedrine [28]:**

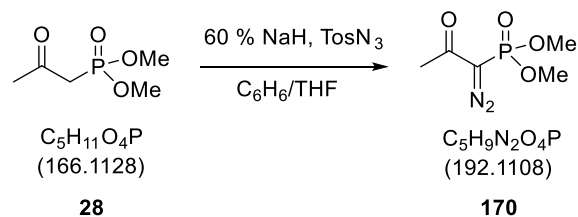


Pyridine (2.9 mL, 36 mmol, 1.2 eq) was added to a solution of *N,N*-mesityl-benzyl norephedrine (12.7 g, 30 mmol, 1 eq) in dichloromethane (150 mL). Propionylchloride (3.55 mL, 40 mmol, 1.35 mmol) was added at 0 °C and the mixture was stirred at room temperature for 16 h. Methyl-*tert*-butyl ether (120 mL) was added and the organic phase was washed with water (100 mL), saturated ammonium chloride solution (100 mL), water (100 mL), saturated sodium hydrogencarbonate solution (100 mL) and brine (100 mL). The combined organic phases were dried over anhydrous sodium sulfate, filtered and the solvent was evaporated to yield the pure product as a colorless crystalline solid (13.6 g, 28.3 mmol, 94%).

¹H-NMR (200 MHz, CDCl₃): δ (ppm) = 7.37–6.94 (m, 8 H), 6.99–6.93 (m, 4 H), 5.90 (d, 1 H), 4.72 (q, 2 H), 4.09 (qd, 1 H), 2.57 (s, 6 H), 2.33 (s, 3 H), 2.28–2.13 (m, 2 H), 1.17 (d, 3 H), 1.06 (t, 3 H).

The analytical data are consistent with those reported in the literature.⁵⁷

Synthesis of OHIRA-BESTMANN reagent [49]:

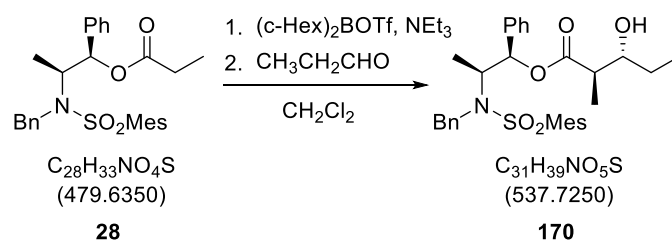


48 (0.4 mL, 3 mmol, 1 eq) solved in benzene (2.3 mL) was slowly added to NaH (0.11 g, 2.86 mmol, 0.95 eq) suspended in benzene/THF (11.4 mL/1.6 mL) at 0 °C. After stirring the mixture for 1 h, TosN₃ (5.7 mL, 2.86 mmol, 0.95 eq) solved in benzene (9 mL) was added slowly. The resultant suspension was then warmed up to RT, stirred for further 2 h, filtered through a plug of Celite and the solvent was evaporated and the crude was purified via column chromatography (EtOAc) to yield the product as pale yellow oil in 70 % (2.4 g, 1.2 mmol) yield.

¹H-NMR (200 MHz, CDCl₃): δ (ppm) = 3.82 (d, 6 H), 2.23 (s, 3 H).

The analytical data are consistent with those reported in the literature.⁶⁶

Masamune-Aldol product [170]:



Masamune ester (3.0 g, 6.25 mmol, 1 eq) was solved in dry dichloromethane (100 mL) and cooled down to $-78^{\circ}C$. Triethylamine (2.1 mL, 15 mmol, 2.4 eq) was added dropwise over 30 min and the mixture was stirred for 10 min. Dicyclohexylbortriflate acid (13.8 mL, 13.8 mmol, 2.2 eq) was then added dropwise at $-78^{\circ}C$ and constant stirring. The reaction mixture was stirred further 2 h at the same temperature. Freshly distilled propionaldehyde (1.8 mL, 25 mmol, 4 eq) was then slowly added and the mixture was stirred for 1h. The temperature was increased to $0^{\circ}C$ and the reaction was stirred for another hour. The reaction was hydrolyzed by adding pH buffer solution (25 mL), methanol (125 mL) and 30% H₂O₂ (12.5 mL). It was left to stir at room temperature overnight. The organic phase was separated and concentrated under vacuum. The crude product was precrystallized in chloroform and hexane and then purified by column chromatography (PE:EA = 9:1-6:1) to yield the desired product as colorless crystals (3 g, 5.6 mmol, 90%), $R_f = 0.35$ (PE:EE = 4:1).

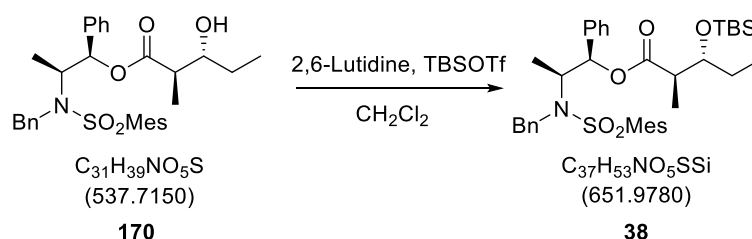
¹H-NMR (400 MHz, CDCl₃): δ 7.34 - 7.14 (m, 8H, Ar-H), 6.82-6.91 (m, 4H, Ar-H), 5.84 (d, 1H, $J = 4.4$ Hz, OCH), 4.77 (d, 1H, $J = 16.5$ Hz, NCH₂), 4.54 (d, 1H, $J = 16.5$ Hz, NCH₂), 4.07 (dq, 1H, $J = 7.1, 4.4$ Hz, NCH), 3.57 (m, 1H, CH(OTBS)), 2.49 (m, 7H, o-Mes-CH₃ and C(O)CHCH₃), 2.28 (s, 3H, p-Mes-CH₃), 1.55 (m, 1H, CH₂CH₃), 1.35 - 1.48 (m, 1H, CH₂CH₃), 1.18 (d, 3H, $J = 7.2$ Hz, NCHCH₃), 1.13 (d, 3H, $J = 7.4$ Hz, C(O)CHCH₃), 0.96 (t, 3H, $J = 7.5$ Hz, CH₂CH₃) ppm;

¹³C-NMR (400 MHz, CDCl₃, CDCl₃ = 77.0 ppm) δ 174.5, 142.2, 140.55, 139.5, 139.3, 132.3, 128.7, 128.6, 128.3, 127.4, 126.5, 78.4, 74.5, 57.4, 48.7, 45.8, 27.4, 23.2, 20.6, 14, 13.8, 9.8.

HRMS (ESI): m/z : calculated for C₃₁H₃₉NO₅Na: 560.2447 [M + Na]⁺: found: 560.2444 [M + Na]⁺.

The analytical data are consistent with those reported in the literature.^{27,28}

TBS-protected Masamune-Aldol product [38]:



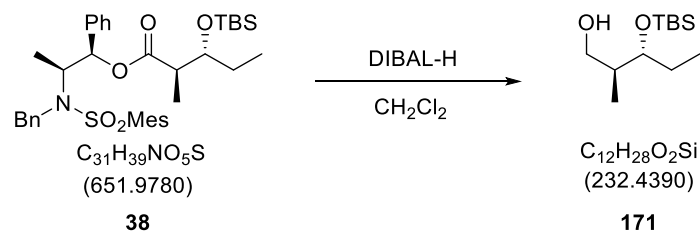
Masamune alcohol (5.3 g, 9.95 mmol, 1.0 eq.) was solved in dry dichloromethane (100 ml) and cooled down to 0°C. 2,6 – Lutidine (4.63 ml, 39.8 mmol, 4 eq.) was added. The mixture was cooled down to -78°C and TBSOTf (4.3 ml, 19.9 mmol, 2 eq.) was added dropwise over a period of 30 min. After 5 min. the reaction mixture was warmed up to 0°C. After stirring for further 1.5 hour, a pH buffer and a saturated aqueous solution of NH₄Cl were added. The water phases were extracted three times with CH₂Cl₂. The combined organic layers were washed with brine, dried over Na₂SO₄ and the solvent evaporated. The crude product was purified by means of column chromatography (PE:EA – 20:1 then 10:1) to yield the pure protected alcohol as colorless thick oil (6.4 g, 10.24 mmol, 98%).

¹H-NMR (400 MHz, CDCl₃): δ 7.33-7.40 (m, 8H, Ar-H), 6.85 (m, 4H, Ar-H), 5.74 (d, 1H, *J* = 5.1 Hz, OCH), 4.82 (d, 1H, *J* = 16.4 Hz, NCH₂), 4.49 (d, 1H, *J* = 16.4 Hz, NCH₂), 4.10 (m, 1H, NCH), 3.88 (m, 1H, CH(OTBS)), 2.54 (m, 1H, C(O)CHCH₃), 2.46 (s, 6H, *o*-Mes-CH₃), 2.29 (s, 3H, *p*-Mes-CH₃), 1.42 (m, 1H, CH₂CH₃), 1.32 (m, 1H, CH₂CH₃), 1.18 (d, 3H, *J* = 6.8 Hz, NCHCH₃), 1.03 (d, 3H, *J* = 7.1 Hz, C(O)CHCH₃), 0.88 (s, 9H, TBS), 0.82 (t, 3H, *J* = 7.2 Hz, CH₂CH₃), 0.06 (ds, 6H, TBS) ppm;

HRMS (ESI): *m/z*: calculated for C₃₇H₅₃NO₅SiSNa: 674.3311 [M + Na]⁺; found: 674. 3307 [M + Na]⁺.

The analytical data are consistent with those reported in the literature.^{27,28}

[2S,3R-3-(tert-butyldimethylsilyl)oxy]-2-methylpentan-1-ol [171]:



The TBS-protected aldol ester (0.500 g, 0.77 mmol, 1 eq.) was dissolved in dry dichloromethane and cooled down to $-78^{\circ}C$. DIBAL-H (3.1 ml, 3.07 mmol, 4 eq.) was slowly added (over 40 min.) and the mixture was stirred for further 3 hours. Ethyl acetate and a saturated solution of K-Na tartrate were slowly added and the reaction mixture was stirred overnight at room temperature. The water phase was then extracted three times with CH_2Cl_2 and the combined organic layers were washed with brine, dried over Na_2SO_4 and the solvent evaporated. The crude product was purified via column chromatography (PE:EA – 12:1) to give the desired product as colorless oil (0.12 g, 0.52 mmol, 68%), $R_f = 0.35$ (PE:EE = 4:1).

1H -NMR (400 MHz, $CDCl_3$): δ 3.78 (m, aH, CH_2OH), 3.62 (dt, 1H, $J = 5.5$ Hz, $CH(OTBS)$), 3.54 (m, 1H, CH_2OH), 1.78 (m, 1H, CH_3CH), 1.59 (m, 2H, CH_2CH_3), 0.99 (d, 3H, $J = 6.8$ Hz, $CHCH_3$), 0.90 (s, 9H, TBS), 0.87 (t, 3H, CH_2CH_3), 0.09 (s, 6H, TBS) ppm;

^{13}C -NMR (400 MHz, $CDCl_3$, $CDCl_3 = 77.0$ ppm) δ 205.4, 74.9, 50.8, 27.6, 25.9, 10.7, 9.1, -4.1, -4.6.

The analytical data are consistent with those reported in the literature.^{27,28}

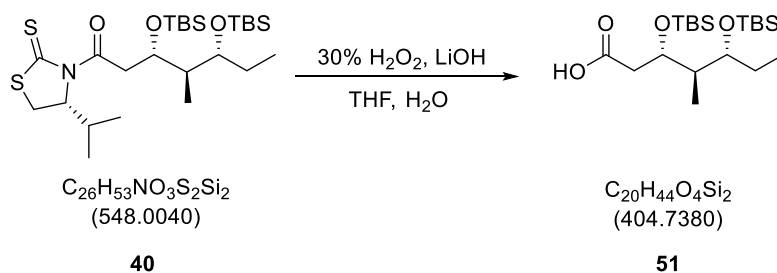
very slowly over a period of 40 min. The mixture was warmed up to room temperature after 5 min and stirred for further 1 hour. A solution of pH-buffer was added and the aqueous phase was extracted multiple times with CH₂Cl₂. The organic layers were combined, dried over Na₂SO₄ and the solvent was evaporated. The crude product was purified by means of column chromatography (PE:EA – 20:1) to yield the pure product as yellow oil (0.040 g, 0.073 mmol, 36%), R_f = 0.60 (PE:EA = 3:1).

¹H-NMR (400 MHz, CDCl₃): δ 5.07 (brt, *J* = 6.8 Hz, CH₂CHCH, 1H), 4.61 (ddd, *J* = 9.6, 3.9, 1.9 Hz, CCH₂CH(OTBS), 1H), 3.56 - 3.44 (m, SCH₂, CCH₂CH, CH(OTBS)CH₂CH₃, 1H), 3.04-2.99 (m, SCH₂, CCH₂CH, 1H), 2.44 – 2.35 (m, CH(CH₃)₂, 1H), 1.89 – 1.80 (m, CHCH₃, 1H), 1.56 - 1.50 (m, CH₂CH₃, 2H), 1.06 (d, *J* = 6.8 Hz, CH(CH₃)₂, 3H), 0.97 (d, *J* = 7.2 Hz, 3H, CH(CH₃)₃), 0.89 (s, OSiC(CH₃)₃, 9H), 0.87 (t, *J* = 7.2 Hz CH₂CH₃, 3H), 0.84 (s, OSiC(CH₃)₃, 9H), 0.82 (d, *J* = 7.2 Hz, CHCH₃, 3H), 0.07 (s, OSiCH₃, 3H), 0.03 (s, OSiCH₃, 3H), 0.02 (s, OSiCH₃, 3H) ppm;

HRMS (ESI): *m/z*: calculated for C₂₆H₅₃NO₃NaS₂Si: 570.2903 [M + Na]⁺: found: 570.2902 [M + Na]⁺.

The analytical data are consistent with those reported in the literature.^{27,28}

[3*S*,4*R*,5*R*-3,5-Bis(*tert*-butyldimethylsilyloxy)-4-methylheptanoic acid [51]:



A 30%-aqueous solution of H₂O₂ (0.01 ml, 0.3 mmol, 8 eq.) and a 1M LiOH solution (0.146 ml, 0.146 mmol, 4 eq.) were added stepwise to a solution of Nagao-aldol amide (0.020, 0.037 mmol, 1 eq.) in THF/H₂O (0.6 ml, 4:1) at 0°C. The reaction mixture was warmed up to room temperature, stirred overnight and terminated by adding a saturated aqueous solution of Na₂SO₃. The aqueous phase was extracted with Et₂O. The combined organic layers were dried over Na₂SO₄, filtered and the solvent was evaporated. Purifying the crude product by column chromatography (PE:EA = 8:1) yielded acid **51** as colorless oil (0.007 g, 0.01 mmol, 50%).

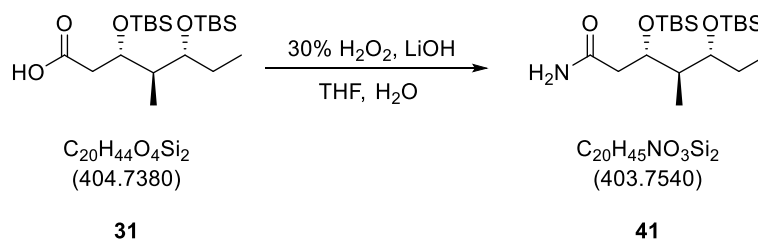
¹H-NMR (400 MHz, CDCl₃): δ 4.39 (ddd, *J* = 8.4, 4.6, 3.5 Hz, C(O)CH₂CH(OTBS), 1H), 3.54 (dt, *J* = 6.8, 4.9 Hz, CH₃CH₂CH(OTBS), 1H), 2.52 (dd, *J* = 15.0, 3.5 Hz, C(O)CH₂CH, 1H), 2.39 (dd, *J* = 15.0, 8.4 Hz, C(O)CH₂CH, 1H), 1.89 (m, CH(OTBS)CHCH₃, 1H), 1.42 (m, CH(OTBS)CH₂CH₃, 2H), 0.89 (s, C(CH₃)₃, 9H), 0.87 (t, *J* = 5.1 Hz, CH₂CH₃, 3H), 0.86 (s, C(CH₃)₃, 9H), 0.82 (d, *J* = 7.2 Hz, CHCH₃, 3H), 0.07 (s, OSiCH₃, 3H), 0.05 (s, OSiCH₃, 6H), 0.04 (s, OSiCH₃, 3H) ppm.

¹³C-NMR (400 MHz, CDCl₃, CDCl₃ = 77.0 ppm) δ 168.6, 74.6, 68.8, 42.3, 35.6, 26.05, 26, 25.7, 18.2, 18.15, 10.2, 8.3, -3.9, -4.4, -4.5, -4.6.

HRMS (ESI): *m/z*: calculated for C₂₀H₄₄O₄Si₂: 403.2700 [M - H]⁻; found: 403.2699 [M - H]⁻.

The analytical data are consistent with those reported in the literature.^{27,28}

[3*S*,4*R*,5*R*-3,5-Bis(*tert*-butyldimethylsilyloxy)-4-methylheptanamide **[41]:**



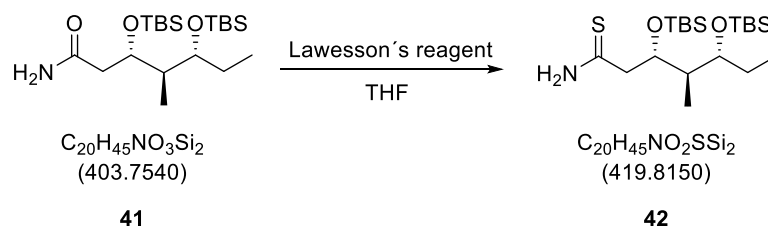
A 30%-aqueous solution of H₂O₂ (0.01 ml, 0.3 mmol, 8 eq.) and 1M LiOH solution (0.146 ml, 0.146 mmol, 4 eq.) were added stepwise to a solution of Nagao-aldol amide (0.020, 0.037 mmol, 1 eq.) in THF/H₂O (0.6 ml, 4:1) at 0°C. The reaction mixture was warmed up to room temperature, stirred overnight and terminated by adding a saturated aqueous solution of Na₂SO₃. The aqueous phase was extracted with Et₂O. The combined organic layers were dried over Na₂SO₄, filtered and the solvent was evaporated. Purifying the crude product via column chromatography (PE:EA = 8:1) yielded acid **41** as colorless oil (0.007 g, 0.01 mmol, 50%).

¹H-NMR (400 MHz, CDCl₃, CHCl₃ = 7.26 ppm): *d* = 6.24 (bs, 1H, NH₂), 5.36 (bs, 1H, NH₂), 4.11 (ddd, *J* = 6.4, 6.4, 3.7 Hz, 1H, H-18), 3.67 (dt, *J* = 5.4, 5.3 Hz, 1H, H-20), 2.46 (dd, *J* = 15.0, 3.7 Hz, 1H, H-17), 2.31 (dd, *J* = 15.0, 3.7 Hz, 1H, H-17'), 1.96 (m, 1H, H-19), 1.44 (dq, *J* = 5.4, 7.3 Hz, 2H, H-21), 0.91 (s, 9H, TBS), 0.89 (s, 9H, TBS), 0.87 (pt, *J* = 7.3 Hz, 3H, H-22), 0.82 (d, *J* = 7.2 Hz, 3H, H-23), 0.10 (s, 3H, TBS), 0.09 (s, 3H, TBS), 0.05 (s, 3H, TBS), 0.04 (s, 3H, TBS) ppm.

HRMS (ESI): *m/z*: calculated for C₂₀H₄₆NO₃Si₂: 404.3016 [M+H]⁺, found: 404.3016 [M+H]⁺

The analytical data are consistent with those reported in the literature.^{27,28}

[3*S*,4*R*,5*R*-3,5-Bis(*tert*-butyldimethylsilyl)oxy]-4-methylheptanethioamide [42]:

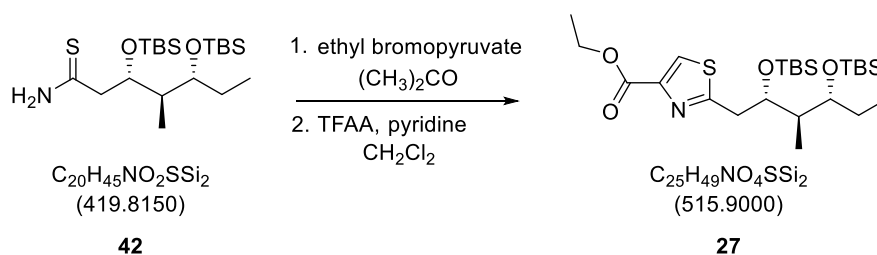


Lawesson's reagent (0.004 g, 0.09 mmol, 0.6 eq.) was added to a solution of (3*S*,4*R*,5*R*)-3,5-Bis(*tert*-butyldimethylsilyl)oxy-4-methylheptanamide (6 mg, 0.015 mmol, 1 eq.) in THF (0.1 ml) at room temperature. After stirring for 4 hours, brine was added to the mixture. The organic phase was extracted with Et₂O, dried over Na₂SO₄, filtered and the solvent was evaporated. Purification by flash chromatography (PE:EA = 10:1) furnished thioamide **42** as a yellow oil.

¹H-NMR (400 MHz, CDCl₃, CHCl₃ = 7.26 ppm): d 7.99 (bs, 1H, NH₂), 7.37 (bs, 1H, NH₂), 4.15 (ddd, *J* = 6.1, 6.1, 4.3 Hz, 1H, H-18), 3.72 (dt, *J* = 5.4, 5.5 Hz, 1H, H-20), 2.89-2.87 (m, 2H, H-17), 1.97-1.92 (m, 1H, H-19), 1.41 (dq, *J* = 7.2, 5.4 Hz, 2H, H-21), 0.88 (s, 9H, TBS), 0.87 (s, 9H, TBS), 0.86 (pt, *J* = 7.2 Hz, 3H, H-22), 0.83 (d, *J* = 7.2 Hz, 3H, H-23), 0.09 (s, 3H, TBS), 0.08 (s, 3H, TBS), 0.05 (s, 3H, TBS), 0.03 (s, 3H, TBS) ppm;

The analytical data are consistent with those reported in the literature.^{27,28}

[(2*S*,3*R*,4*R*)-2,4-Bis(*tert*-butyldimethylsilyloxy)-3-methylhexyl]-thiazole-4-carbonic acid ethylester [27]:



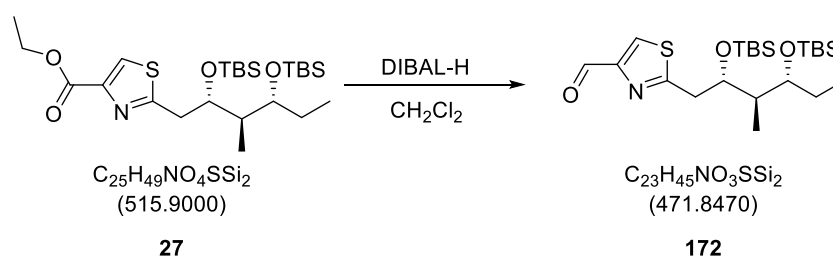
To a solution thioamide **42** (2.2 g, 5.20 mmol, 1.0 eq) in acetone (8.5 mL) was added ethyl bromopyruvate (0.7 mL g, 5.88 mmol, 1.1 eq) at -10 °C. After stirring for 2 h CHCl₃ and a sat. aq. solution of NaHCO₃ were added. After extraction with CH₂Cl₂, the combined organic extracts were dried over MgSO₄, filtered and concentrated under reduced pressure. The residue was taken up in CH₂Cl₂ (14.0 mL) and pyridine (0.9 mL, 11.44. mmol, 2.2 eq) and trifluoroacidic anhydride (0.8 mL, 5.72 mmol, 2.2 eq) were sequentially added at -30 °C. The reaction mixture was allowed to warm up to room temperature over 4 h. After stirring for 14 h at room temperature CH₂Cl₂ and a sat. aq. solution of NaHCO₃ were added. After extraction with CH₂Cl₂, the combined, organic extracts were washed with an aq. solution of KHSO₄ (10%), dried over MgSO₄ and concentrated under reduced pressure. Purification by flash chromatography (PE:EA = 15:1) furnished thiazole **27** as a light yellow oil (2.4 g, 4.59 mmol, 88%).

¹H-NMR (400 MHz, CDCl₃, CHCl₃ = 7.26 ppm): d = 8.14 (s, 1H), 4.38 (dt, *J* = 8.2, 4.4 Hz, 1H), 3.90 (s, 3H), 3.61 (dt, *J* = 5.7, 5.8 Hz, 1H), 2.97 (dd, *J* = 14.8, 4.4 Hz, 1H), 2.92 (dd, *J* = 14.9, 8.2 Hz, 1H), 1.94-1.86 (m, 1H), 1.60-1.48 (m, 2H), 0.90-0.87 (m, 15H), 0.78 (s, 9H), 0.04 (s, 6H), -0.02 (s, 3H), -0.24 (s, 3H) ppm

HRMS (ESI): *m/z*: calculated for C₂₅H₄₉NO₄Si₂SNa: 538.2819 [M+Na]⁺, found: 538.2839 [M+Na]⁺.

The analytical data are consistent with those reported in the literature.^{27,28}

[(2*S*,3*R*,4*R*)-2,4-Bis(*tert*-butyldimethylsilyloxy)-3-methylhexyl]-thiazol-4-carbaldehyde **[172]:**



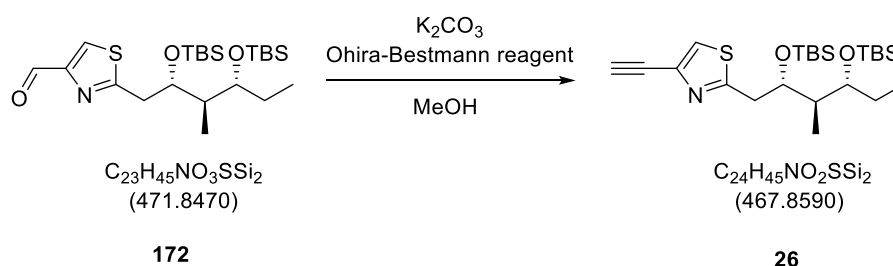
To a solution of **27** (31 mg, 0.06 mmol, 1.0 eq) in CH_2Cl_2 (0.8 mL) was added DIBAL-H (1.2 mol/L in toluene, 50 μ L, 0.06 mmol, 1.0 eq) within 1 h at $-78^\circ C$. After 1 h, DIBAL-H (1.2 mol/L in toluene, 50 μ L, 0.06 mmol, 1.0 eq) was added again and the reaction mixture stirred for 1 h. DIBAL-H (1.2 mol/L in toluene, 25 μ L, 0.03 mmol, 0.5 eq) was added a second time and the reaction was terminated after 30 min by addition of methanol (5 mL). A sat. aq. solution of Rochelle's salt was added and the mixture was stirred at room temperature for 14 h. After extraction with CH_2Cl_2 , the combined organic extracts were dried ($MgSO_4$), filtered and concentrated under reduced pressure. Purification by flash chromatography (PE:EA = 20:1) furnished aldehyde **172** as colorless oil (28 mg, 0.06 mmol, quant).

1H -NMR (400 MHz, $CDCl_3$, $CHCl_3 = 7.26$ ppm) d 10.00 (s, 1H, H-13), 8.07 (s, 1H, H-15), 4.24 (ddd, $J = 6.2, 6.2, 3.8$ Hz, 1H, H-18), 3.71 (dt, $J = 6.0, 4.4$ Hz, 1H, H-20), 3.20 (d, $J = 6.2$ Hz, 1H, H-17), 3.18 (d, $J = 3.8$ Hz, 1H, H-17'), 1.88-1.80 (m, 1H, H-19), 1.53-1.45 (m, 2H, C-21), 0.87-0.80 (m, 24H, TBS, H-22, H-23), 0.07 (s, 3H, TBS), 0.04 (s, 3H, TBS), 0.03 (s, 3H, TBS), 0.01 (s, 3H, TBS) ppm.

HRMS (ESI): m/z : calculated for $C_{23}H_{45}NO_3Si_2SNa$: 494.2556 $[M+Na]^+$, found: 494.2561 $[M+Na]^+$.

The analytical data are consistent with those reported in the literature.^{27,28}

[(2*S*,3*R*,4*R*)-2,4-Bis(*tert*-butyldimethylsilyloxy)-3-methylhexyl]-4-ethynylthiazole [26]:



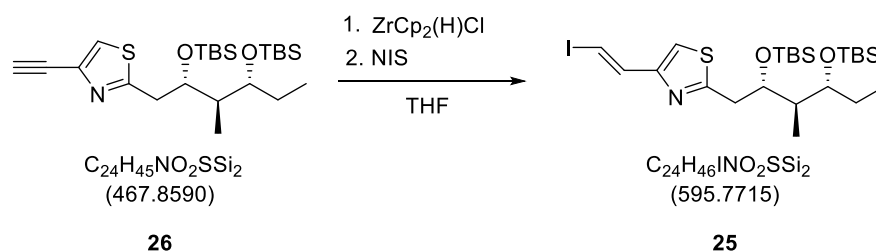
To a solution of aldehyde **172** (22 mg, 0.05 mmol, 1.0 eq) in MeOH (0.5 mL) were sequentially added K_2CO_3 (16 mg, 0.12 mmol, 2.5 eq) and the OHIRA-BESTMANN **49** reagent^{xx} (13 mg, 0.07 mmol, 1.5 eq) at 0 °C. After 14 h the reaction was terminated by addition of Et_2O and H_2O . After extraction with Et_2O , the combined, organic extracts were dried over MgSO_4 and concentrated under reduced pressure. Purification by flash chromatography (PE:EA = 15:1) furnished alkyne **26** as a colorless oil (21 mg, 0.05 mmol, 96%).

¹H-NMR (400 MHz, CDCl_3 , $\text{CHCl}_3 = 7.26$ ppm) d 7.40 (s, 1H, H-15), 4.17 (ddd, $J = 6.5, 6.4, 4.0$ Hz, 1H, H-18), 3.72 (ddd, $J = 6.0, 6.0, 4.3$ Hz, 1H, H-20), 3.17 (d, $J = 6.4$ Hz, 1H, H-17), 3.14 (d, $J = 4.0$ Hz, 1H, H-17'), 3.08 (s, 1H, H-12), 1.87-1.78 (m, 1H, H-19), 1.51-1.42 (m, 2H, H-21), 0.87 (s, 9H, TBS), 0.86 (s, 9H, TBS), 0.85 (s, 3H, H-22), 0.82 (d, $J = 4.1$ Hz, 3H, H-23), 0.07 (s, 3H, TBS), 0.03 (s, 3H, TBS), 0.00 (s, 3H, TBS), -0.12 (s, 3H, TBS) ppm.

HRMS (ESI): m/z : calculated for $\text{C}_{24}\text{H}_{46}\text{NO}_2\text{Si}_2\text{S}$: 468.2788 $[\text{M}+\text{H}]^+$, found: 468.2797 $[\text{M}+\text{H}]^+$.

The analytical data are consistent with those reported in the literature.^{27,28}

[(2*S*,3*R*,4*R*)-2,4-Bis(*tert*-butyldimethylsilyloxy)-3-methylhexyl]-4-[(*E*)-2-iodovinyl]thiazole [25]:



To a suspension of the SCHWARTZ reagent (496 mg, 1.92 mmol, 3.0 eq) in THF (6.0 mL) was added **26** (300 mg, 0.64 mmol, 1.0 eq) in THF (4.5 mL) at 0 °C. After 1 h NIS (432 mg, 1.92 mmol, 3.0 eq) in THF (4.5 mL) was added at -78 °C and the reaction mixture was stirred in the dark for 20 min. The reaction was terminated by addition of a sat. aq. $\text{Na}_2\text{S}_2\text{O}_3$ solution and the aqueous layer was extracted with Et_2O . The combined, organic extracts were dried over MgSO_4 , filtered and concentrated under reduced pressure. Purification by flash chromatography (PE:EA = 30:1) furnished vinyl iodide **25** as a colorless oil (346 mg, 0.58 mmol, 89%).

$^1\text{H-NMR}$ (400 MHz, CDCl_3 , $\text{CHCl}_3 = 7.26$ ppm) d 7.33 (d, $J = 14.3$ Hz, 1H, H-12), 7.17 (d, $J = 14.3$ Hz, 1H, H-13), 4.25 (ddd, $J = 6.9, 5.5, 3.8$ Hz, 1H, H-18), 3.70-3.67 (m, 1H, H-20), 3.08 (d, $J = 3.8$ Hz, 1H, H-17), 3.06 (d, $J = 6.9$ Hz, 1H, H-17'), 1.88- 1.84 (m, 1H, H-19), 1.52-1.46 (m, 2H, C-21), 0.88 (s, 9H, TBS), 0.86 (s, 3H, H-22), 0.83 (s, 9H, TBS), 0.82 (d, $J = 4.3$ Hz, 3H, H-23), 0.05 (s, 6H, 2x TBS), -0.01 (s, 3H, TBS), -0.22 (s, 3H, TBS) ppm;

HRMS (ESI): m/z : calculated for $\text{C}_{24}\text{H}_{46}\text{INO}_2\text{Si}_2\text{S}$: 596.1925 $[\text{M}+\text{H}]^+$, found: 596.1923 $[\text{M}+\text{H}]^+$.

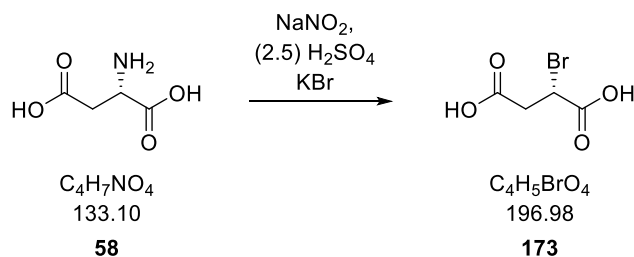
$[\alpha]_{\text{D}}^{20}$ -20.5 (c 1.0 in CHCl_3) (lit. $[\alpha]_{\text{D}}^{20}$ -20.9 (c 1.0 in CHCl_3));

The analytical data are consistent with those reported in the literature.^{27,28}

7.3. Synthesis of Western fragment [24]:

Synthesis of chiral oxirane [32]:

(S)-2-Bromosuccinic acid [173]:

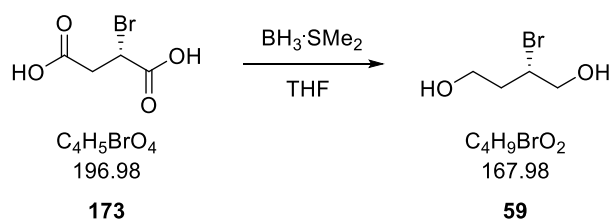


L-aspartic acid **58** and potassium bromide were dissolved in 2.5 M sulfuric acid and the mixture was cooled down to $-5\text{ }^\circ\text{C}$. Sodium nitrite was dissolved in water and slowly added. The reaction mixture was let to stir overnight at $-5\text{ }^\circ\text{C}$. Ethyl acetate was added and the mixture warmed to room temperature. The organic phase was separated and extracted three more times with ethyl acetate. The combined organic phases were dried over Na_2SO_4 , filtered and the solvent was evaporated to give the bromide **173** as colorless oil, which was used without any further purification.

$^1\text{H-NMR}$ (400 MHz, MeOD): δ 4.56 (dd, 1H, $J = 8.6, 6.3$ Hz, H-2), 3.19 (dd, 1H, $J = 17.0, 8.6$ Hz, H-3), 2.94 (dd, 1H, $J = 17.0, 6.3$ Hz, H-3) ppm.

The analytical data are consistent with those reported in the literature.^{27,28}

(S)-2-Bromobutane-1,4-diol [59]:



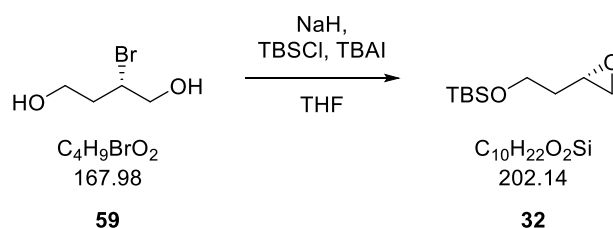
(S)-2-bromosuccinic acid **173** (7.00 g, 35.94 mmol, 1.0 eq.) was dissolved in dry THF (55 mL) at $0\text{ }^\circ\text{C}$. A solution of borane dimethylsulfide complex (10.4 mL, 3.0 eq.) in dry THF (100 mL) was added to the mixture at $0\text{ }^\circ\text{C}$, over one hour. The reaction was stirred at room temperature for 12 h and then terminated by addition of a THF/water mixture (50 mL, 1:1) at $0\text{ }^\circ\text{C}$. Potassium

carbonate (23 g) was added and the mixture was stirred at 0 °C for 30 minutes. After filtration the solid was washed with Et₂O, the filtrate was dried over Na₂SO₄ and concentrated under reduced pressure. Product **59** (5.19 g, 27.16 mmol, 76 %) was obtained as colourless oil. Compound **59** was used without further purification.

¹H-NMR (400 MHz, MeOD): δ 4.86 (s, 2H, OH), 4.20 (ddd, 1H, *J* = 15.5, 5.8, 3.9 Hz, H-2), 3.67-3.84 (m, 4H, H-1, H-4), 2.17 (m, 1H, *J* = 14.7, 8.2, 6.5, 3.4 Hz, H-3), 1.90 (m, 1H, *J* = 9.9, 9.8, 4.8 Hz, H-3) ppm.

The analytical data are consistent with those reported in the literature.^{27,28}

(S)-tert-Butyldimethyl[2-(oxiran-2-yl)]ethoxysilane [32]:

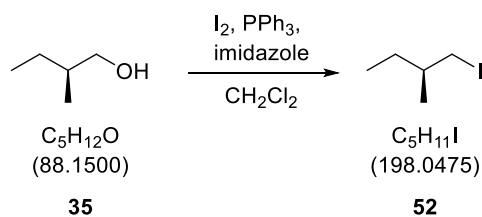


A solution of (*R*)-2-bromobutane-1,4-diol **32** (5.12 g, 27.16 mmol, 1.0 eq.) in dry THF (2 mL) was slowly added to a suspension of sodium hydride (2.02 g, 84.14 mmol, 3.1 eq.) in THF (20 mL) at -10 °C. After 30 minutes tetrabutylammonium iodide (1.01 g, 2.72 mmol, 0.1 eq.) and TBS-Cl (4.51 g, 29.88 mmol, 1.1 eq.) were added and stirring was continued at -10 °C for 15 minutes. The reaction was allowed to warm up to room temperature and was stirred for another hour. The reaction was terminated by addition of an ammonium chloride solution (aq. sat. 10 mL) and the aqueous layer was extracted with EtOAc (3 x 30 mL). The combined organic layers were washed with brine (100 mL), dried over MgSO₄, filtered and concentrated under reduced pressure. Column chromatography (hexanes/EtOAc = 10:1) afforded product **32** (1.84 g, 9.09 mmol, 34 %) as colorless liquid.

¹H-NMR (400 MHz, CDCl₃): δ 3.77 (t, 2H, *J* = 6.0 Hz, H-4), 3.01-3.09 (m, 1H, H-2), 2.78 (t, 1H, *J* = 4.7, H-1), 2.51 (dd, 1H, *J* = 4.7, 2.7 Hz, H-1), 1.64-1.82 (m, 2H, H-3), 0.89 (s, 9H, TBS), 0.06 (s, 6H, TBS) ppm.

The analytical data are consistent with those reported in the literature.^{27,28}

(S)-1-Iodo-2-methylbutane [52]:



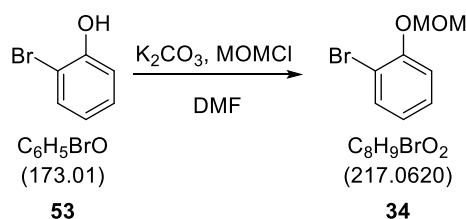
(S)-(-)-2-Methyl-1-butanol **35** (1.21 ml, 11.3 mmol, 1 eq.) was solved in dry CH_2Cl_2 (25 ml) at room temperature. Triphenyl phosphine (4.6 g, 17.6 mmol, 1.55e q.), imidazole (1.15 g, 17 mmol, 1.5 eq.) and iodine (2.87 g, 11.3 mmol, 1.25 eq.) were added slowly one after another and the reaction mixture was stirred for 2 hours. CH_3OH (0.7 ml) was added slowly (suspension changes color from pale yellow to colorless). The mixture was washed with water and extracted three times with pentane. The combined organic phases were dried over Na_2SO_4 , filtered and the solvent was evaporated. Distillation under reduced pressure (58 mbar, 55-60°C) afforded the pure product **52** as pale yellow liquid (1.34 ml, 10.3 mmol, 83%).

$^1\text{H-NMR}$ (400 MHz, CDCl_3): δ 3.23 (td, 2H, CH_2I), 1.38 (m, 2H, $\text{CH}_3\text{CH}_2\text{CH}$), 1.33 (m, 1H, $\text{CH}_3\text{CH}_2\text{CH}$), 0.99 (d, 3H, CH_3CH), 0.92 (t, 1H, CH_3CH_2) ppm;

HRMS (GC MS): m/z : calculated for $\text{C}_5\text{H}_{11}\text{I}$: 197.80 $[\text{M} + \text{H}]^+$: found: 197.80 $[\text{M} + \text{H}]^+$.

The analytical data are consistent with those reported in the literature.^{27,28}

1-Bromo-2-(methoxymethoxy)benzene [34]:



MOMCl (6.6 ml, 86.90, 1.5 eq.) was added dropwise (over 40 min) at 0°C to a mixture of potassium carbonate (32 g, 231.3 mmol, 4 eq., 80%) and 2-bromophenol **53** (6.7 ml, 57.8 mmol, 1 eq.) in DMF (60 ml). The resultant colorless suspension was stirred for 2 hours at room temperature. Water (1 L) and MTBE (400 ml) were added, the organic phase was further washed with water (x2) and brine, dried over Na₂SO₄, filtered and the solvent was evaporated. Purifying the crude product by means of column chromatography (PE:EE = 14:1) afforded the pure MOM-protected bromophenol **34** as colourless liquid (12.3 g, 56.9 mmol, 99%).

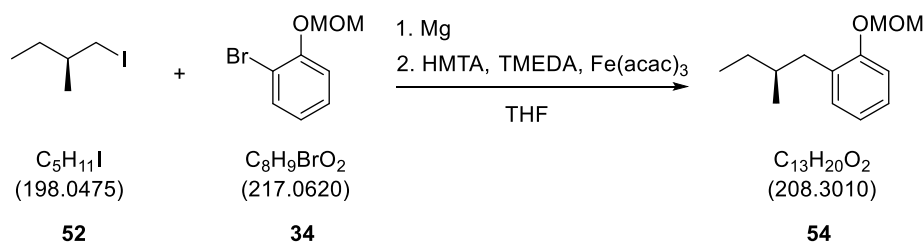
¹H-NMR (400 MHz, CDCl₃): δ 7.66 - 7.67 (dd, 1H, Ar-H), 7.27 (m, 2H, Ar-H), 6.95 (td, 1H, Ar-H), 5.35 (s, 2H, Ar-O-CH₂), 3.62 (s, 3H, Ar-O-CH₂-O-CH₃) ppm;

¹³C-NMR (400 MHz, CDCl₃, CDCl₃ = 77.0 ppm) δ 153.8, 133.4, 128.5, 123.1, 116.2, 112.9, 95.1, 56.4.

HRMS-ESI: *m/z*: calculated for C₈H₉O₂Br: 215.9786 [M + H]⁺: found: 215.9782 [M + H]⁺.

The analytical data are consistent with those reported in the literature.^{27,28}

(S)-1-(Methoxymethoxy)-2-(2-methylbutyl)benzene [54]:



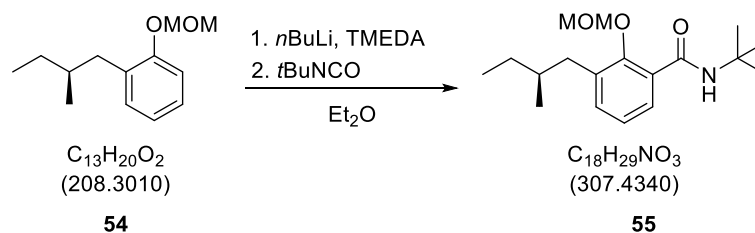
Magnesium turnings (3.1 g, 128.2 mmol, 6.0 eq.) were put in a 100 ml round-bottom Schlenk-flask. The flask was evacuated three times and a solution of 1-bromo-2-(methoxymethoxy)benzene **34** (6.5 ml, 42.8 mmol, 2.0 eq.) in dry THF (50 ml) was added. The mixture was refluxed for 2 hours (yellow-greenish color) and then slowly added (over 50 min.) at 0°C to a solution of (*S*)-1-iodo-2-methylbutane **52** (2.8 ml, 21.4 mmol, 1.0 eq.), $Fe(acac)_3$ (0.378 g, 1.07 mmol, 0.05 eq), TMEDA (0.32 ml, 2.14 mmol, 0.1 eq.) and HMTA (0.150 g, 1.07 mmol, 0.05 eq.) in dry THF (35 ml) (caramel color). The resultant suspension was stirred for further 1.5 hour at 0°C and then hydrolyzed with a saturated aqueous solution of NH_4Cl and 1M HCl. The water phase was extracted three times with Et_2O , the combined organic phases were dried over Na_2SO_4 , filtered and the solvent evaporated under reduced pressure. Column chromatography (PE:EA = 4:1) afforded the pure product **54** (2.8 g, 13.5 mmol, 63%) as colorless oily solid.

1H -NMR (200 MHz, $CDCl_3$): δ 7.10 (m, 3H, Ar-H), 6.92 (m, 1H, Ar-H), 5.19 (s, 2H, $-OCH_2OCH_3$), 3.48 (s, 3H, OCH_2OCH_3), 2.67 (dd, $J = 13.25$ Hz, 1H, $-CH_2CH(CH_3)CH_2CH_3$), 2.39 (dd, $J = 13.25$ Hz, 1H, $-CH_2CH(CH_3)CH_2CH_3$), 1.70 (m, 1H, $-CH_2CH(CH_3)CH_2CH_3$), 1.39 (m, 1H, $-CH_2CH(CH_3)CH_2CH_3$), 1.19 (m, 1H, $-CH_2CH(CH_3)CH_2CH_3$), 0.92 (t, 3H, $-CH_2CH(CH_3)CH_2CH_3$), 0.85 (d, 3H, $-CH_2CH(CH_3)CH_2CH_3$) ppm.

^{13}C -NMR (400 MHz, $CDCl_3$, $CDCl_3 = 77.0$ ppm) δ 155.5, 131.1, 131, 129.6, 127, 122, 121.4, 116.4, 113.9, 94.5, 56, 37.6, 35.6, 29.6, 19.3, 11.7.

The analytical data are consistent with those reported in the literature.^{27,28}

(S)-N-(tert-Butyl)-2-(methoxymethoxy)-3-(2-methylbutyl) benzamide [55]:



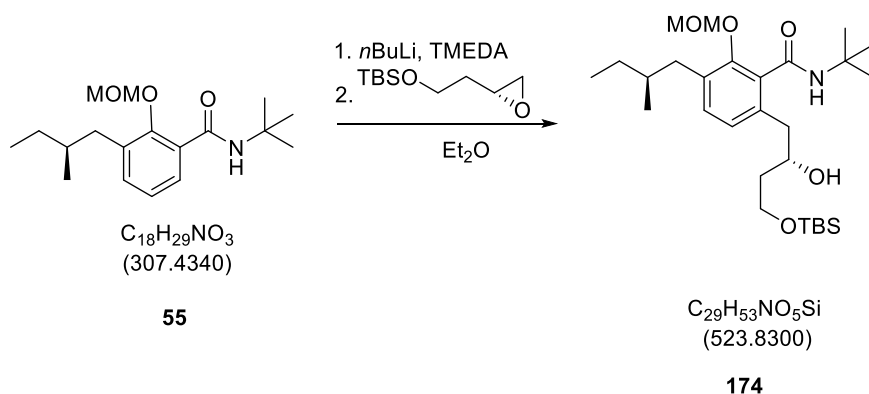
N,N,N',N'-Tetramethylethylenediamine (0.41 ml, 2.56 mmol, 1.3 eq.) and *n*-butyllithium (1 ml, 2.56 mmol, 1.3 eq.) were slowly added to a solution of (*S*)-1-(methoxymethoxy)-2-(2-methylbutyl)benzene **54** (0.41, 1.97 mmol, 1 eq.) in Et_2O (9 ml) at $-30^\circ C$. After 2 hours the reaction mixture was warmed up to $-5^\circ C$. After additional three hours, *t*-butyl isocyanide (2 ml, 17.7 mmol, 9 eq.) was added dropwise. The resultant reaction mixture was slowly warmed up to room temperature and stirred overnight. The reaction was terminated by the addition of 1M HCl. The aqueous phase was extracted with diethyl ether and the combined organic layers were dried over Na_2SO_4 , filtered and the solvent was evaporated. Column chromatography (PE:EA = 12:1 then 4:1) afforded the pure product **55** (0.43 g, 1.41 mmol, 71%) as colorless crystals.

1H -NMR (200 MHz, $CDCl_3$): δ 7.77 (dd, 1H, Ar-H), 7.22 (d, 1H, Ar-H), 7.13 (t, 1H, Ar-H), 4.96 (s, 2H, $-OCH_2OCH_3$), 3.58 (s, 3H, OCH_2OCH_3), 2.70 (dd, $J = 13.25$ Hz, 1H, $-CH_2CH(CH_3)CH_2CH_3$), 2.45 (dd, $J = 13.25$ Hz, 1H, $-CH_2CH(CH_3)CH_2CH_3$), 1.76 (m, 1H, $-CH_2CH(CH_3)CH_2CH_3$), 1.47 (s, 9H, *t*-butyl), 1.36 (m, 1H, $-CH_2CH(CH_3)CH_2CH_3$), 1.18 (m, 1H, $-CH_2CH(CH_3)CH_2CH_3$), 0.92 (t, 3H, $-CH_2CH(CH_3)CH_2CH_3$), 0.85 (d, 3H, $-CH_2CH(CH_3)CH_2CH_3$) ppm;

HRMS-ESI: m/z : calculated for $C_{18}H_{29}NO_3$: 330.2045 $[M + Na]^+$; found: 330.2048 $[M + Na]^+$.

The analytical data are consistent with those reported in the literature.^{27,28}

***N*-{*tert*-Butyl-6-[(*S*)-4-(*tert*-butyldimethylsilyl)oxy-2-hydroxybutyl-2-(methoxymethoxy)-3-(*S*)-2-methylbutyl]} benzamide [174]:**



N,N,N',N'-Tetramethylethylenediamin (0.58 ml, 3.9 mmol, 3 eq.) and *n*-butyllithium (1.56 ml, 3.9 mmol, 3 eq.) were slowly added to a solution of (*S*)-*N*-(*tert*-butyl)-2-(methoxymethoxy)-3-(2-methylbutyl) benzamide **55** (0.4, 1.3 mmol, 1 eq.) in degassed Et₂O (8 ml) at -78°C. The reaction mixture was warmed up to -40°C. (2*R*)-2-(2-*tert*-Butyldimethylsilyloxyethyl) oxiran (0.53 g, 2.6 mmol, 2 eq.) was added after 2 hours at -78°C. The resultant mixture was stirred at -40°C overnight. The reaction was ended by adding saturated solution of NH₄Cl. The water phase was extracted with diethyl ether, dried over Na₂SO₄, filtered and the solvent evaporated. Purification by column chromatography afforded the pure product **174** (0.18 g, 0.35 mmol, 37%) as colorless crystals.

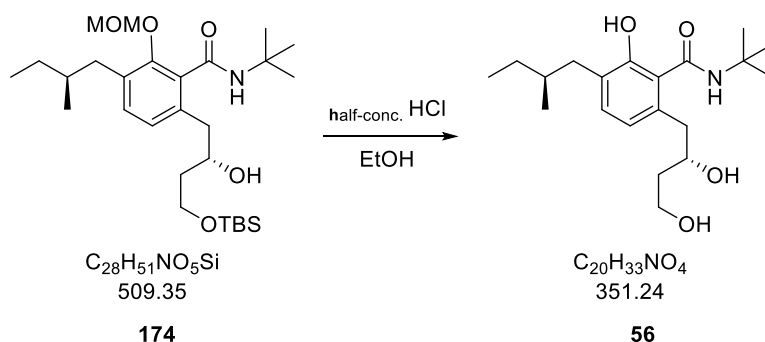
¹H-NMR (200 MHz, CDCl₃): δ 7.10 (d, *J* = 7.8 Hz, 1H), 6.95 (d, *J* = 7.8 Hz, 1H), 6.43 (bs, 1H, NH), 5.03 (s, 2H), 4.04 (m, 1H), 3.90 (m, 2H), 3.55 (s, 3H), 2.75 (m, 3H), 2.39 (dd, *J* = 13.7, 8.2 Hz, 1H), 1.73 (m, 3H), 1.46 (s, 9H, *t*-butyl), 1.39 (m, 1H), 1.13 (m, 2H), 0.90 (m, 15H), 0.07 (s, 6H, TBS) ppm;

¹³C-NMR (400 MHz, CDCl₃, CDCl₃ = 77.0 ppm) δ 168, 152.5, 135.6, 133.4, 133.2, 131.5, 125.7, 100.7, 72.8, 62.5, 57.8, 52, 40.6, 39.7, 37.6, 35.3, 29.7, 28.8, 26, 22.8, 19.2, 18.3, 11.6, -5.3, -5.3.

HRMS-ESI: *m/z*: calculated for C₂₈H₅₁NO₅SiNa: 510.3615 [M + H]⁺: found: 510.3614 [M + H]⁺.

The analytical data are consistent with those reported in the literature.^{27,28}

***N*-(*tert*-Butyl)-6-[(*S*)-2,4-dihydroxybutyl]-2-hydroxy-3-(*S*)-2-methylbutyl} benzamide
[56]:**



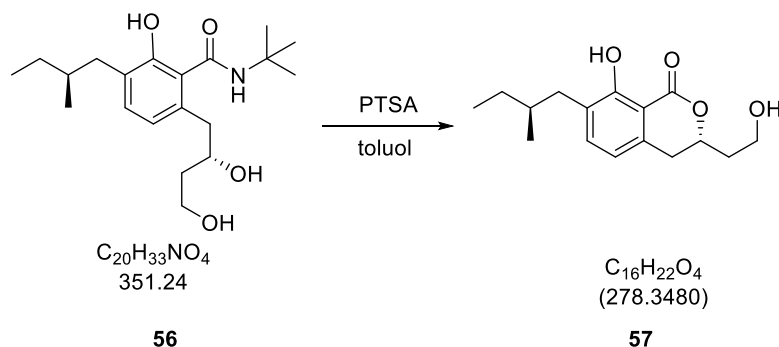
Half-concentrated hydrochloric acid (1.5 ml) was added to a solution of *N*-(*tert*-butyl)-6-((*S*)-4-((*tert*-butyldimethylsilyl)oxy)-2-hydroxybutyl)-2-(methoxymethoxy)-3-((*S*)-2-methylbutyl) benzamide **174** (0.18 g, 0.35 mmol, 1 eq.) in EtOH and the mixture was stirred for 1 hour at 50°C. The reaction was hydrolyzed by addition of saturated aqueous solution of NaHCO₃. The aqueous phase was extracted with ethyl acetate. The combined organic phases were dried over Na₂SO₄ and the solvent evaporated. Column chromatography (PE:EA = 4:1 then 1:1) afforded the pure product **56** (0.07 g, 0.18 mmol, 53%) as colorless oil.

¹H-NMR (200 MHz, CDCl₃): δ 10.24 (s, 1H), 8.48 (s, 1H, NH), 7.05 (d, $J = 7.7\text{Hz}$, 1H), 6.64 (d, $J = 7.7\text{ Hz}$, 1H), 4.29 (m, 1H), 4.02 (m, 1H), 3.94 (m, 1H), 3.70 (s, 1H), 3.05 (dd, $J = 13.8, 10.1$, 1H), 2.68 (dd, $J = 13.8, 3.2$, 3H), 2.60 (dd, $J = 13.3, 6.1\text{ Hz}$, 1H), 2.38 (dd, $J = 13.2, 8.3\text{ Hz}$, 1H), 1.89 (m, 2H), 1.74 (m, 1H), 1.47 (s, 9H, *t*-butyl), 1.41 (m, 1H), 1.17 (m, 1H), 0.90 (t, $J = 7.4\text{ Hz}$, 3H), 0.85 (d, $J = 6.5\text{ Hz}$, 3H), 0.89 (s, 9H, TBS), 0.06 (s, 6H, TBS) ppm;

HRMS-ESI: m/z : calculated for C₂₀H₃₄NO₄: 352.2488 [M + H]⁺; found: 352.2481 [M + H]⁺.

The analytical data are consistent with those reported in the literature.^{27,28}

(S)-8-Hydroxy-3-(2-hydroxyethyl)-7-[(S)-2-methylbutyl]isochroman-1-one [57]:



p-Toluenesulfonic acid (11 mg, 0.06 mmol, 2 eq.) was added to a solution of *N*-(*tert*-butyl)-6-((*S*)-2,4-dihydroxybutyl)-2-(methoxymethoxy)-3-((*S*)-2-methylbutyl) benzamide **56** (10 mg, 0.03 mmol, 1 eq.) in toluol (0.5 ml) and the mixture was heated under refluxing conditions for 50 min. The solvent was evaporated and column chromatography (PE:EA = 3:1 then 1:1) afforded the pure product (5 mg, 0.015 mmol, 62 %) as colorless oil.

¹H-NMR (200 MHz, CDCl₃): δ 11.21 (s, 1H, ArOH), 7.23 (d, *J* = 7.5 Hz, 1H), 6.60 (d, *J* = 7.5 Hz, 1H), 4.82 (m, 1H), 3.95 (m, 1H), 3.89 (m, 1H), 2.98 (ddd, *J* = 16.2, 10.5, 0.8 Hz, 1H), 2.92 (ddd, *J* = 16.2, 4.3, 0.6 Hz, 1H), 2.66 (dd, *J* = 13.3, 6.2 Hz, 1H), 2.37 (dd, *J* = 13.3, 8.2 Hz, 1H), 2.12 (m, 1H), 1.98 (m, 1H), 1.74 (m, 1H), 1.39 (m, 1H), 1.19 (m, 1H), 0.90 (t, *J* = 7.4 Hz, 3H), 0.85 (d, *J* = 6.7 Hz, 3H) ppm.

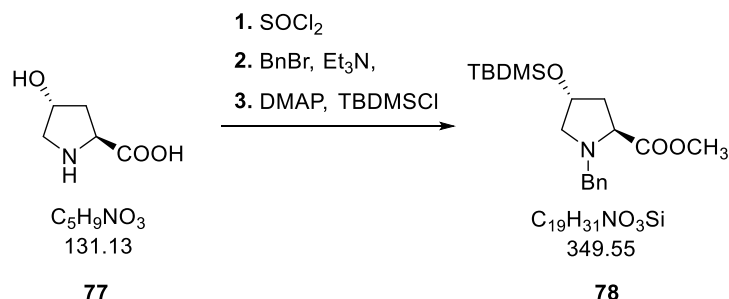
¹³C-NMR (400 MHz, CDCl₃, CDCl₃ = 77.0 ppm) δ 170.2, 160.6, 137.2, 136.6, 128.9, 117, 107.7, 58.6, 37.3, 36.8, 34.7, 33.1, 29.4, 19, 11.5.

[α]_D²⁰ -21 (c 1.0 in CHCl₃) (lit. [α]_D²⁰ -21.5 (c 0.8 in CHCl₃));

The analytical data are consistent with those reported in the literature.^{27,28}

7.4. Chiral ligands

Methyl (2*S*,4*R*)-1-benzyl-4-(*tert*-butyldiphenylsilyloxy)pyrrolidine-2-carboxylate [78]:



To a stirred suspension of (2*R*,4*R*)-4-hydroxy-2-methoxycarbonylpyrrolidine **77** (0.8 g, 6.1 mmol, 1.0 equiv) in MeOH (20 mL) at 0 °C thionyl chloride (0.54 mL, 7.4 mmol, 1.2 equiv) was added dropwise. After 72 h at RT, the organic solvent was removed in vacuo to afford a white solid.

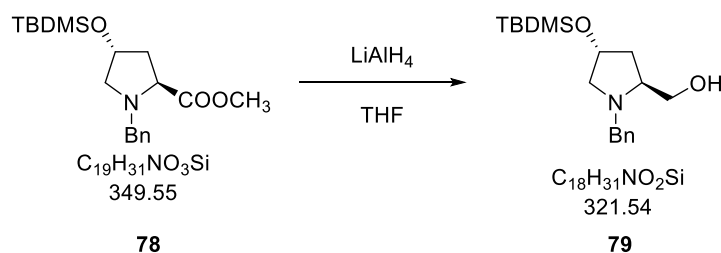
To a stirred suspension of the resulting white solid in CH₂Cl₂ (10 mL) at rt was added Et₃N (2.4 mL, 17 mmol, 4 equiv), followed by BnBr (0.6 mL, 5.1 mmol, 1.2 equiv). After 10 min at RT, the reaction mixture was heated under refluxing conditions for 5 h and cooled to rt.

DMAP (0.5 mg, 0.4 mmol, 0.1 equiv) and TBDMSO (0.77 g, 5.1 mmol, 1.2 equiv) were added. After 12 h at RT, the reaction was terminated by addition of a saturated aqueous Na₂CO₃ solution until pH 10 was reached. The aqueous layer was extracted with CH₂Cl₂ and EtOAc and the combined organic phases were dried over MgSO₄ and filtered. The solvent was removed in vacuo to afford an oil, which was purified by flash column chromatography on silica gel (EtOAc/pentane = 1:3) to give **78b** (0.9 g, 2.6 mmol, 43% yield) as a colorless oil.

¹H-NMR (200 MHz, CDCl₃): δ 7.35–7.21 (5H), 4.41 (m, 1H), 3.91 (d, *J* = 12.5 Hz, 1H), 3.65 (s, 3H), 3.60 (d, *J* = 12.5 Hz, 1H), 3.53 (t, *J* = 8.1 Hz, 1H), 3.27 (dd, *J* = 9.6, 5.7 Hz, 1H), 2.37 (dd, *J* = 9.6, 5.2 Hz, 1H), 2.19 (ddd, *J* = 13.1, 7.5, 7.3 Hz, 1H), 2.03 (ddd, *J* = 12.8, 8.5, 4.0 Hz, 1H), 0.8 (s, 9H), 0.03 (s, 3H), 0.02 (s, 3H).

The analytical data are consistent with those reported in the literature.⁷⁸

{(2*S*, 4*R*)-1-Benzyl-4-[(*tert*-butyldiphenylsilyl) oxy] pyrrolidin-2-yl} methanol [79]:



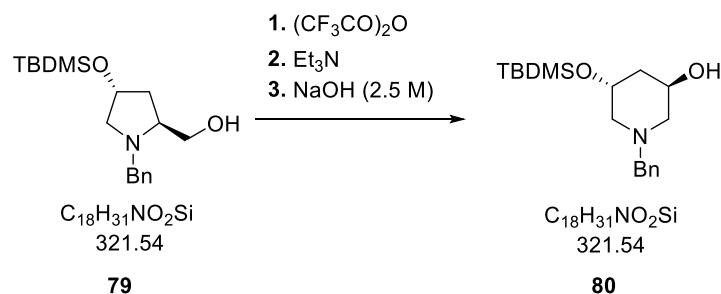
To a suspension of LiAlH₄ (0.11 g; 2.8 mmol, 2.0 equiv) in THF (2 mL) at 0 °C, a solution of pyrrolidine **78** (0.5 g, 1.4 mmol, 1.0 equiv) in THF (3 mL) was added dropwise.

After stirring at 0 °C for 10 min, the reaction mixture was heated under refluxing conditions for 2 h and then cooled to 0 °C. Water (0.01 mL), an aqueous 3.75 M NaOH solution (0.3 mL), and water (0.1 mL) were successively added. The obtained precipitate was collected on a pad of celite and washed with THF. The organic solvent was removed in vacuo to give **79** (0.23 g, 0.7 mmol, 52% yield) as a colorless oil.

¹H-NMR (200 MHz, CDCl₃): δ 7.37–7.27 (5H), 4.27 (m, 1H), 3.97 (d, $J = 13.2$ Hz, 1H), 3.67 (dd, $J = 11.0, 3.3$ Hz, 1H), 3.47 (d, $J = 13.2$ Hz, 1H), 3.39 (d, $J = 11.0$ Hz, 1H), 3.14 (dd, $J = 9.9, 5.5$ Hz, 1H), 3.07 (m, 1H), 2.65 (s, 1H), 2.37 (dd, $J = 9.9, 5.7$ Hz, 1H), 2.09 (ddd, $J = 12.9, 7.4, 7.4$ Hz, 1H), 1.84 (ddd, $J = 13.0, 8.6, 4.6$ Hz, 1H), 0.8 (s, 9H), 0.03 (s, 3H), 0.02 (s, 3H).

The analytical data are consistent with those reported in the literature.⁷⁸

(3*R*, 5*R*)-1-Benzyl-5-[(*tert*-butyldiphenylsilyl) oxy] piperidin-3-ol [80]:

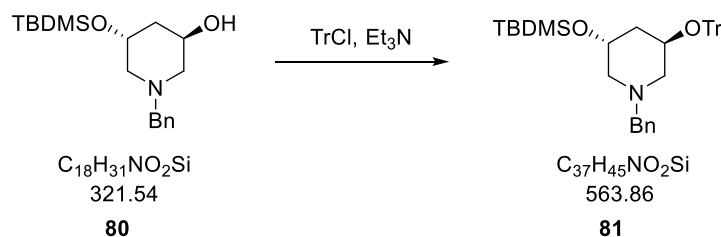


Trifluoroacetic anhydride (0.12 mL, 0.86 mmol, 1.2 equiv) was added dropwise to a solution of pyrrolidine **79** (0.23 g, 0.7 mmol, 1.0 equiv) in THF (7 mL), cooled to 0 °C. After 1 h, Et₃N (0.4 mL, 2.8 mmol, 4.0 equiv) was added dropwise. The reaction mixture was stirred for 20 min at 0 °C and then heated under refluxing conditions for 72 h. After addition of an aqueous 2.5 M NaOH solution (3 mL), the mixture was stirred for 2 h at RT and then extracted with EtOAc, dried with MgSO₄, and evaporated to dryness in vacuo. The residue was purified by flash column chromatography on silica gel (EtOAc/ pentane 1:3) to give **80** (0.154 g, 0.5 mmol, 70% yield) as an oil.

¹H-NMR (200 MHz, CDCl₃): δ 7.37–7.24 (5H), 4.05 (h, *J* = 4.8 Hz, 1H), 3.96 (s, 1H), 3.63 (d, *J* = 13.2 Hz, 1H), 3.53 (d, *J* = 13.2 Hz, 1H), 2.90 (m, 1H), 2.75 (m, 1H), 2.50 (br s, 1H), 2.19 (dd, *J* = 11.4, 1.84 Hz, 1H), 2.09 (m, 1H), 1.97 (t, *J* = 10.1 Hz, 1H), 1.38 (ddd, *J* = 13.0, 10.3, 2.6 Hz, 1H), 0.88 (s, 9H), 0.06 (s, 3H), 0.04 (s, 3H).

The analytical data are consistent with those reported in the literature.⁷⁸

(3*R*, 5*R*)-1-Benzyl-3-[(*tert*-butyldiphenylsilyl) oxy]-5-(trityloxy) piperidine [81]:

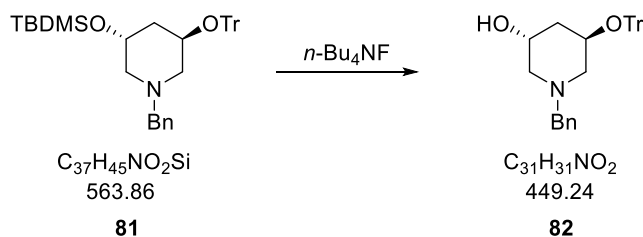


To a stirred solution of piperidine **80** (0.15 g, 0.5 mmol, 1.0 equiv) in CH_2Cl_2 (3 mL) at RT was added triphenylmethyl chloride (0.09 g, 0.5 mmol, 1.1 equiv), followed by the addition of Et_3N (0.13 mL, 0.9 mmol, 2.0 equiv). After stirring at RT for 48 h, the reaction was terminated by addition of an aqueous 3.75 M NaOH solution (3 mL). After extraction with EtOAc, the combined organic layers were dried with MgSO_4 and filtered. The solvent was removed in vacuo to afford a yellow oil, which was purified by flash column chromatography on silica gel (EtOAc/petroleum ether = 1:4) to give **81** (0.22 g, 0.32 mmol, 83% yield) as an amorphous solid.

$^1\text{H-NMR}$ (200 MHz, CDCl_3): δ 7.54–7.47 (5H), 7.34–7.16 (15H), 4.16 (m, 1H), 3.89 (m, 1H), 3.53 (d, $J = 13.6$ Hz, 1H), 3.33 (d, $J = 13.6$ Hz, 1H), 2.65 (dd, $J = 10.6, 3.3$ Hz, 1H), 2.17 (dd, $J = 11.6, 5.5$ Hz, 1H), 2.12 (dd, $J = 10.8, 3.3$ Hz, 1H), 1.86 (dd, $J = 11.4, 2.6$ Hz, 1H), 1.42 (m, 1H), 1.19 (m, 1H), 0.85 (s, 9H), 0.00 (s, 3H), -0.01 (s, 3H)

The analytical data are consistent with those reported in the literature.⁷⁸

(3*R*, 5*R*)-1-Benzyl-5-(trityloxy) piperidin-3-ol [82]:

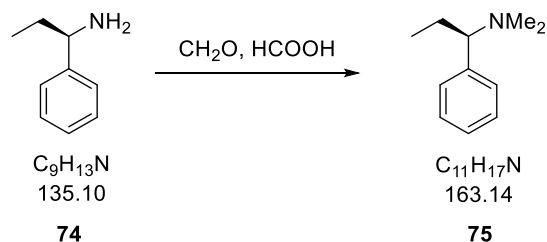


To a stirred solution of piperidine **81** (0.19 g, 0.34 mmol, 1.0 equiv) in THF (1 mL) at RT was added a solution of *tetra-N*-butylammonium fluoride 1 M in THF (1.35 mL, 1.35 mmol, 4.0 equiv). After stirring at RT for 72 h, the reaction was terminated by addition of water (6 mL). After extraction with EtOAc, the combined organic layers were dried with MgSO₄ and filtered. The solvent was removed in vacuo to afford a yellow gum, which was purified by flash column chromatography on silica gel (EtOAc/petroleum ether = 1:3) to give **82** (0.92 g, 0.2 mmol, 60% yield) as a white solid.

¹H-NMR (200 MHz, CDCl₃): δ 7.52–7.44 (15H), 7.33–7.09 (5H), 3.95–3.82 (2H), 3.37 (d, *J* = 12.9 Hz, 1H), 3.27 (d, *J* = 13.2 Hz, 1H), 2.64 (m, 1H), 2.24–1.94 (4H), 1.84–1.69 (2H).

The analytical data are consistent with those reported in the literature.⁷⁸

(R)-N, N-Dimethyl-1-phenylpropan-1-amine [75]:

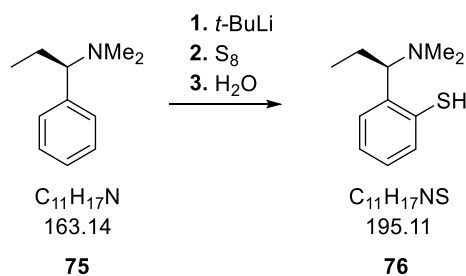


To (*R*)- α -ethylbenzylamine **74** (2 g, 14.8 mmol, 1 eq) was added dropwise 5,2 mL of an aqueous formaldehyde solution (37%) followed by dropwise addition of 6 mL of an aqueous formic acid solution (89%). The mixture was heated under refluxing conditions for 24 h, cooled to RT, basified with NaOH pellets and extracted with Et₂O (3x). The combined Et₂O layers were dried (MgSO₄), filtered and then concentrated under reduced pressure to give a light yellow oil. This oil was purified by means of column chromatography (PE:EA = 1:1) to yield 79% of **75** (1,9 g, 11,6 mmol) as a colorless oil.

¹H-NMR (200 MHz, CDCl₃): δ 7.33-7.20 (m, 5 H), 3.03 (dd, 1 H, $J = 4.8$ Hz), 2.17 (s, 6 H), 2.00- 1.67 (m, 2 H), 0.72 (t, 3 H, $J = 7.4$ Hz).

The analytical data are consistent with those reported in the literature.^{73, 74}

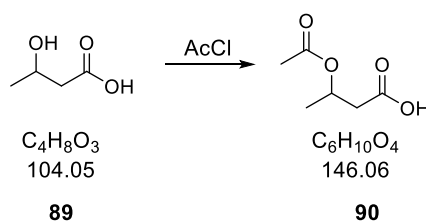
(R)-2-[1-(Dimethylamino) propyl] benzenethiol [76]:



To a solution of **75** (1 g, 6.1 mmol, 1 eq) in 8 mL dry hexane (freshly distilled) under N₂ was added dropwise *t*-BuLi (3.7 mL, 7 mmol, 1.15 eq) at RT and stirred for 24 h. This mixture was then added dropwise at -78 °C under N₂ to a suspension of sublimed sulphur (0.180 g, 5.6 mmol, 0.95 eq) in 5 mL of THF. The mixture was allowed to warm slowly to 0 °C. The solution was kept at 0 °C for 9 h before warming to RT. The mixture was terminated by addition of an equal volume of water and washed with Et₂O. The aq. layer was then neutralized with a minimum amount of conc. HCl. The neutral aq. layer was then washed again with Et₂O. The yellow Et₂O wash was discarded. The aq. layer was then extracted with CH₂Cl₂ (3x), dried over MgSO₄ and concentrated to yield 0.53 g of **76** as crude white solid.

7.5. Test substrate

3-Acetoxybutanoic acid [175]:

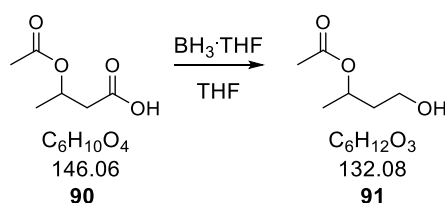


3-Hydroxybutanoic acid **89** (2 g, 104.1 mmol, 1 eq) was dissolved in acetyl chloride (6.8 mL, 78.5 mmol, 5 eq), the mixture was warmed up to 40 °C and stirred for 5 hours. The mixture was then concentrated under vacuum, water (4 mL) was added and the solution was warmed to 50 °C and stirred for 1 hour. After cooling down to RT, the crude mixture was extracted with ethyl acetate (6 x 20 mL), the solvent was evaporated to yield the final product as a colorless oil **90** which was directly used without any further purification.

¹H-NMR (200 MHz, CDCl₃): δ 5.14-5.05 (m, 1 H), 3.65-3.56 (m, 2 H), 2.2 (s, 1 H), 2.05 (s, 3 H), 1.8 – 1.73 (m, 2 H), 1.28 (d, 3H, *J* = 6.0 Hz).

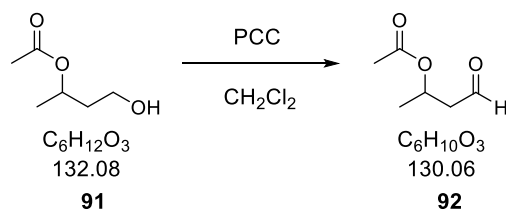
The analytical data are consistent with those reported in the literature.¹³²

4-Hydroxybutan-2-yl acetate [91]:



90 (2.4 g, 16.42 mmol, 1 eq) was dissolved in dry THF and cooled down to 0 °C. Borane tetrahydrofuran solution (29.6 mL, 29.6 mmol, 1.8 eq) was slowly added and the reaction mixture was stirred for 1.5 h at 0 °C. It was then warmed up to RT and stirred for another hour before cooling down to 0°C. Water (1 mL) was slowly added and K₂CO₃ (1.3 g). The mixture was stirred for 15 min at RT and filtered through a plug of silica and washed with ethyl acetate. The solvent was evaporated to yield the pure product **91** in 75% (1.67g, 12.6 mmol) as colorless oil that was subsequently used without any further purification.

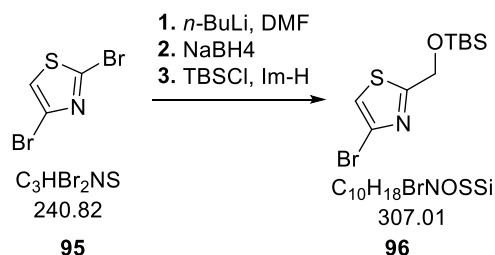
4-Oxobutan-2-yl acetate [92]:



PCC and Celitin were suspended in dichloromethane. **91** dissolved in CH_2Cl_2 was slowly added to the PCC/Celitin mixture and stirred at RT for 30 min. The reaction mixture was then diluted with diethyl ether and filtered through a pad of Celitin/silica gel, washed with more Et_2O . After filtering through silica (PE/ $EtOAc$ = 3:1) the pure aldehyde **92** (TLC monitored) was collected as a colorless oil and used directly without any further purification.

The analytical data are consistent with those reported in the literature.¹³³

4-Bromo-2-[(*tert*-butyldimethylsilyl) oxy] methyl thiazole **96**:



2, 4 – Dibromothiazole **95** (2.5 g, 10.3 mol, 1 eq.) was solved in dry diethyl ether (50 ml) and cooled down to -78 °C. *n* -BuLi (4.9 mL, 12.35 mol, 1.2 eq.) was added slowly dropwise. The mixture was stirred at -78 °C for 30 min before DMF (1.6 mL, 20.6 mol, 2 eq) was slowly added and the solution was stirred for further 30 min at -78 °C. The temperature was then slowly raised to RT over 2 hours. Hexane (15 mL) was added and the reaction mixture stirred for 10 min, before it was passed through a silica gel cake, eluting with a mixture of hexane/ethyl acetate = 3:1. The solvents were evaporated to yield the resultant aldehyde as colorless liquid in 99% (1.95 g, 10.2 mol) crude yield and was used in the next step without any further purification.

The aldehyde produced in the procedure described above (1.95 g, 10.2 mol, 1 eq.) was solved in methanol (100 mL) and NaBH₄ (0.73 g, 37.8 mmol, 1.9 eq) was added. The mixture was stirred at RT for 30 min and ethyl acetate (25 mL) and hexane (50 mL) were added. The mixture was passed through silica and eluted with pure ethyl acetate. The solvent was evaporated and the resultant oil was purified by column chromatography (PE:EA = 5:1 then 1:1) to yield the resultant alcohol in 94% (1.8 g, 9.3 mol) yield.

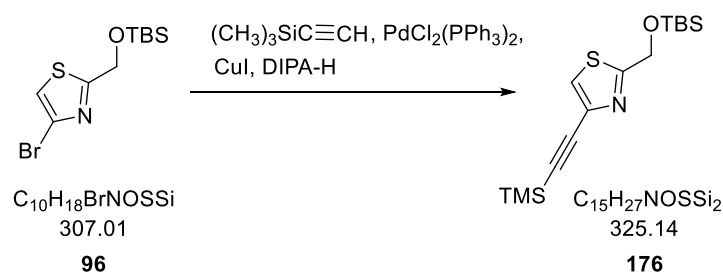
The resultant alcohol (0.25 g, 1.29 mmol, 1 eq) was dissolved in dichloromethane (20 mL). Imidazole (0.13 g, 0.68 mmol, 1.5 eq) and TBSCl (0.25 g, 1.5 mol, 1.3 eq) were added and the mixture was stirred for 30 min at RT. The reaction was quenched with methanol (0.4 mL). It was then filtered through a silica plug, washing with dichloromethane. Solvent was then evaporated to yield the pure product **96** in 90% (0.35 g, 1.14 mol) yield as colorless oil.

¹H NMR (400 MHz, CDCl₃): δ (ppm) 7.16 (s, 1H), 4.93 (s, 2H), 0.94 (s, 9H), 0.12 (s, 6H);

¹³C NMR (100 MHz CDCl₃): δ (ppm) 174.5, 124.2, 116.4, 62.9, 25.7, 18.2, -5.5.

The analytical data are consistent with those reported in the literature.¹²⁶

2-[[*tert*-Butyldimethylsilyl] oxy] methyl]-4-ethynylthiazole [**176**]:

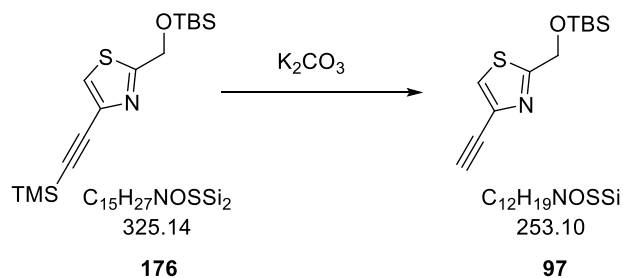


96 (0.250 g, 308.3 mmol, 1 eq) was solved in freshly distilled diisopropylamine (14 mL). Argon was bubbled through the solution for 30 min. Ethynyltrimethylsilane was added, followed by $\text{PdCl}_2(\text{PPh}_3)_2$ (0.01 g, 701.9 mmol, 0.02 eq) and copper iodide (0.003 g, 190.4 mmol, 0.02 eq). The reaction mixture was then heated to 60 °C and stirred at that temperature for 7 h. It was then cooled down to RT and purified by column chromatography (PE) to yield the TMS protected product **176** in 90% yield.

$^1\text{H NMR}$ (400 MHz, CDCl_3): δ (ppm) 7.42 (s, 1H), 4.93 (s, 2H), 0.95 (s, 9H), 0.25 (s, 9H), 0.12 (s, 6H);

The analytical data are consistent with those reported in the literature.¹²⁷

2-[[*tert*-Butyldimethylsilyl] oxy] methyl]-4-ethynylthiazole **[97]**:



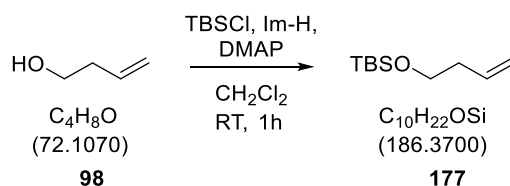
176 (0.17 g, 52 mmol, 1 eq) was solved in 1 mL dry methanol. K_2CO_3 (0.15 g, 138.6 mmol, 1.5 eq) was suspended in dry methanol (5 mL) and cooled down to 0 °C. The TMS protected alkyne (0.23 g, 325.6 mmol, 1 eq) was then added dropwise to the cold mixture. The reaction was stirred for 5 min at 0 °C and then warmed up to RT and stirred further 50 min. Water (10 mL) and ethyl acetate (10 mL) were then added and the mixture was extracted 2 times with ethyl acetate (20 mL). The solvent was evaporated and the crude product was purified via column chromatography (PE:EA = 30:1) to yield the pure product **97** as colorless oil in 68 % yield.

^1H NMR (400 MHz, CDCl_3): δ (ppm) 7.46 (s, 1H), 4.93 (s, 2H), 3.09 (s, 1H), 0.94 (s, 9H), 0.13 (s, 6H);

HRMS-ESI: m/z : calculated for $\text{C}_{12}\text{H}_{19}\text{NOSSi}$: 254.1035 $[\text{M} + \text{H}]^+$; found: 254.1034 $[\text{M} + \text{H}]^+$.

Sharpless chemistry:

But-3-en-1-yloxy(tert-butyl) dimethylsilane [177]:

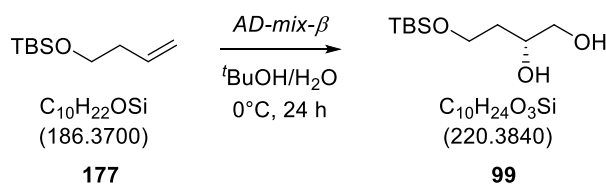


A 250 mL round-bottom flask was charged with buten-1-ol **98** (10.0 g, 138.7 mmol, 1.0 eq) and dissolved in CH₂Cl₂ (130 mL). The reaction was then charged sequentially with *tert*-butyldimethylsilyl chloride (20.9 g, 138.7 mmol, 1.0 eq), imidazole (14.2 g, 208.0 mmol, 1.5 eq) and DMAP (0.85 g, 6.9 mmol, 0.05eq) and stirring was continued for 1 h. The reaction slurry was then filtered through a pad of silica, eluting with a mixture of PE:EA (100:1), and concentrated in vacuo to afford the title compound **177** as colorless liquid (24.5 g, 131.5 mmol, 95 %), *R_f* = 0.84 (PE:EA = 10:1).

¹H-NMR (400 MHz, CDCl₃): δ 5.92-5.72 (ddt, 1 H), 5.12-4.99 (m, 2 H), 3.66 (t, 2 H), 1.93 (qt, 2 H), 0.79 (s, 9 H), 0.05 (s, 6H).

The analytical data are consistent with those reported in the literature.¹²⁸

(*R*)-4-[(*tert*-Butyldimethylsilyl)oxy]butane-1,2-diol [99]:

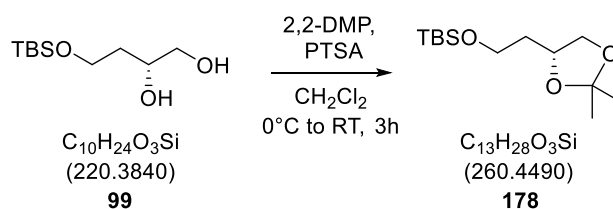


To a solution of **177** (4.0 g, 21.5 mmol, 1.0 eq) in *tert*BuOH/H₂O 1:1 (190 mL) was added AD-mix-β (24.6 g, K₂OsO₂(OH)₄, K₃Fe(CN)₆, K₂CO₃, (DHQ)₂PHAL) at 0°C. The mixture was stirred at the same temperature for 18 h. The ice-bath was then removed and stirring was continued for further 3 h. Na₂SO₃ (28.6 g) was added to this mixture, which was stirred for additional 30 min. The organic layer was separated and the aqueous layer was extracted with EtOAc (3 x 20 mL). The combined organic layers were dried over Na₂SO₄ and the solvent was removed under reduced pressure. The residue was purified by means of column

chromatography (PE:EA = 4:1) to afford the pure product **99** as a colorless oil (4.16 g, 22.7 mmol, 89%), $R_f = 0.55$ (EA).

$^1\text{H-NMR}$ (400 MHz, CDCl_3): δ 3.95-3.91 (m, 1 H), 3.88-3.83 (m, 2 H), 3.62 (dd, 1 H), 3.51 (dd, 1 H), 3.47 (bs, 1 H), 2.35 (bs, 1 H), 1.78 – 1.71 (m, 1H), 1.68 – 1.62 (m, 1H), 0.9 (s, 9 H), 0.08 (s, 6H).

(R)-tert-Butyl[2-(2,2-dimethyl-1,3-dioxolan-4-yl)ethoxy]dimethylsilane [178]:

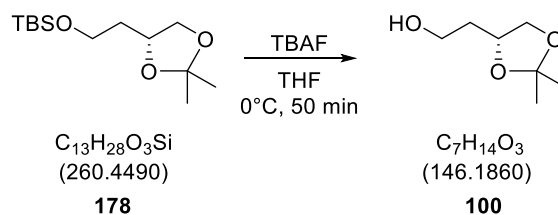


To a stirred solution of **99** (3.5 g, 15.9 mmol, 1.0 eq) in dry CH_2Cl_2 (100mL) at 0°C were added 2,2-DMP (3.3 g, 31.8 mmol, 2.0 eq) and a catalytic amount of PTSA (0.2 g, 1.3 mmol, 0.08 eq). The mixture was stirred for additional three hours at room temperature. Saturated aqueous solution of NaHCO_3 was added and the aqueous layer extracted with CH_2Cl_2 (3 x 50 mL). The combined organic layers were washed with brine and dried over anhydrous Na_2SO_4 . Filtration and removal of the solvent gave a crude product, which was purified by column chromatography (PE:EA = 10:1) to afford the pure product **178** as a colorless liquid (2.1 g, 14.4 mmol, 51%). $R_f = 0.69$ (PE:EA = 4:1).

$^1\text{H-NMR}$ (400 MHz, CDCl_3): δ 4.19 (m, 1 H), 4.08 (m, 1 H), 3.72 (m, 2 H), 3.57 (t, 1 H), 1.18 (m, 2 H), 1.4 (s, 3 H), 1.36 (s, 3H), 0.91 (s, 9H), 0.07 (s, 6H).

$^{13}\text{C-NMR}$ (400 MHz, CDCl_3 , $\text{CDCl}_3 = 77.0$ ppm) δ 108.4, 74, 70, 60, 36.8, 27, 26.1, 26, 25.9, 18.4, -5.3.

(R)-2-(2, 2-Dimethyl-1,3-dioxolan-4-yl)ethan-1-ol [100]:

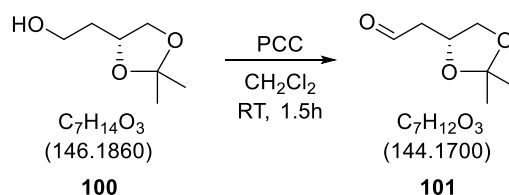


To a stirred solution of silyl ether **178** (0.8 g, 3.1 mmol, 1.0 eq) in dry THF (15 mL) at 0°C was added *tetra-N*-butylammoniumfluoride (4.6 mL, 4.6 mmol, 1.5 eq). After stirring for 50 min at 0°C, a saturated aqueous NH_4Cl was added and the aqueous phase was extracted with Et_2O (2 x 15 mL). The combined organic layers were dried over anhydrous Na_2SO_4 , filtered, the solvent was removed and the residue was purified by column chromatography (PE:EA = 1:1) to afford the pure product **100** as a colorless liquid (0.41 g, 2.8 mmol, 91%), $R_f = 0.57$ (EA), $[\alpha]_D^{20} +2.8$ (c 1.0 in $CHCl_3$) (lit. $[\alpha]_D^{20} +3.1$ (c 0.9 in $CHCl_3$));

1H -NMR (400 MHz, $CDCl_3$): δ 4.27 (m, 1 H), 4.09 (m, 1 H), 3.79 (m, 2 H), 3.59 (t, 1 H), 2.21 (bs, 1H), 1.81 (m, 2 H), 1.42 (s, 3 H), 1.36 (s, 3H).

The analytical data are consistent with those reported in the literature.¹³⁴

(R)-2-(2,2-Dimethyl-1,3-dioxolan-4-yl)acetaldehyde [101]:



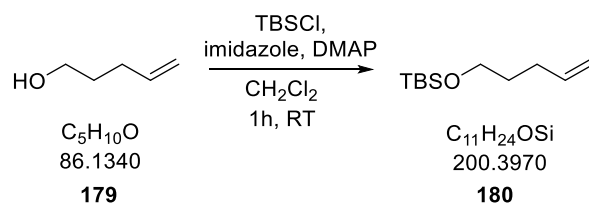
To a stirred suspension of pyridinium chlorochromate (0.74 g, 3.4 mmol, 2.0 eq) and molecular sieves (3 A, freshly activated, 0.74 g) in CH_2Cl_2 (5 mL) was added alcohol **100** (0.25 g, 1.7 mmol, 1.0 eq) in CH_2Cl_2 (2 mL). After being stirred for 1.5 hours at room temperature the mixture was diluted with Et_2O and filtered through a pad of Celitin/silica gel. The solvent was evaporated to yield the pure aldehyde **101** (0.21 g, 1.5 mmol, 88%) as pale yellow liquid, $R_f = 0.69$ (EA).

¹H-NMR (400 MHz, CDCl₃): δ 9.82 (s, 1 H), 4.54 (m, 1 H), 4.2 (m, 1 H), 3.6 (m, 1 H), 2.86 (ddd, 1 H), 2.67 (dd, 1 H), 1.43(s, 3 H), 1.37 (s, 3H).

¹³C-NMR (100 MHz, CDCl₃, CDCl₃ = 77.0 ppm) δ 200.1, 109.4, 70.8, 69.3, 48, 26.9, 25.6.

The analytical data are consistent with those reported in the literature.¹³⁵

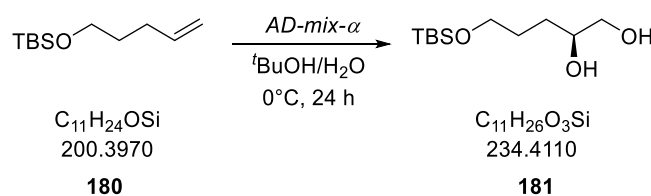
***tert*-Butyldimethyl(pent-4-en-1-yloxy)silane [180]:**



A 100 mL round-bottom flask was charged with penten-1-ol **179** (3.0 g, 34.8 mmol, 1.0 eq) and dissolved in CH₂Cl₂ (35mL). The reaction was then charged sequentially with *tert*-butyldimethylsilyl chloride (5.25 g, 34.8 mmol, 1.0 eq), imidazole (3.56 g, 52.2 mmol, 1.5 eq) and DMAP (0.21 g, 1.74 mmol, 0.05eq), and allowed to stir for 1 h. The reaction slurry was then filtered through a pad of silica, eluted with a mixture of PE:EA (100:1), and concentrated in vacuo to afford the title compound **180** as colorless liquid (6.29 g, 31.4 mmol, 90 %), R_f = 0.84 (PE:EA = 10:1).

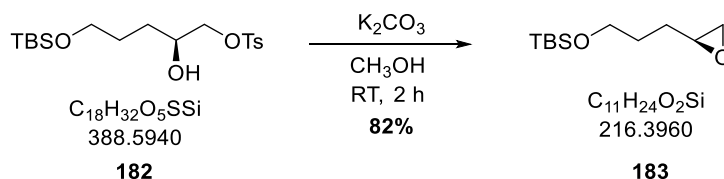
The analytical data are consistent with those reported in the literature.¹²⁹

(*S*)-5-[(*tert*-Butyldimethylsilyl) oxy] pentane-1, 2-diol [181]:



To a solution of **180** (0.5 g, 2.5 mmol, 1.0 eq) in *tert*BuOH/H₂O 1:1 (25 mL) was added *AD*-mix- α (3.09 g, K₂O₅O₂(OH)₄, K₃Fe(CN)₆, K₂CO₃, (DHQ)₂PHAL) at 0°C. The mixture was stirred at the same temperature for 18 h. The ice-bath was then removed and stirring was continued for additional three hours. Na₂SO₃ (3.25 g) was added to the mixture and stirring was continued for 30 min. The organic layer was separated and the aqueous layer was extracted with

(S)-tert-Butyldimethyl[3-(oxiran-2-yl)propoxy]silane [183]:

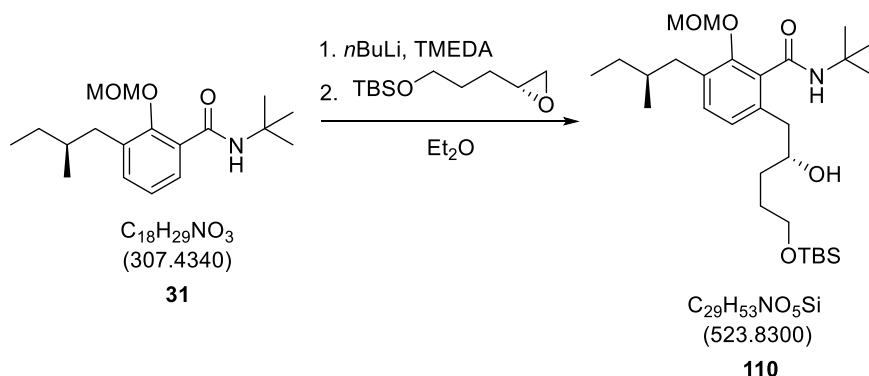


To a stirred solution of **182** (0.5 g, 2.5 mmol, 1.0 eq) in dry CH₃OH (mL) was added K₂CO₃ () under Ar and the mixture was stirred for 2 h at RT. After completion of the reaction, CH₃OH was removed under reduced pressure. The residue was diluted with H₂O (40 mL) and extracted with CH₂Cl₂ (2 x 30 mL). The combined organic phases were dried over Na₂SO₄, filtered and the solvent was evaporated under reduced pressure. The crude residue was purified by column chromatography (PE:EA = 15:1) to give the desired compound **183** as a colorless liquid (0.22 g, 2.5 mmol, 82%). *R_f* = 0.67 (PE:EE = 4:1), [α]²⁰_D -3.8 (c 0.2 in CHCl₃) (lit.[α]²⁰_D -4.3 (c 0.2 in CHCl₃));

¹H-NMR (200 MHz, CDCl₃): δ 3.72 – 3.61 (m, 2H), 3.01 – 2.87 (m, 1H), 2.75 (dd, *J* = 5.0, 4.0 Hz, 1H), 2.47 (dd, *J* = 5.0, 2.7 Hz, 1H), 1.78 – 1.63 (m, 2H), 1.63 – 1.52 (m, 2H), 0.93 – 0.86 (m, 9H), 0.09 – 0.01 (m, 6H).

The analytical data are consistent with those reported in the literature.¹³⁷

***N*-(*tert*-Butyl)-6-[(*R*)-5-[(*tert*-butyldimethylsilyl) oxy]-2-hydroxypentyl]-2-(methoxymethoxy)-3-(*S*)-2-methylbutyl} benzamide **110**:**

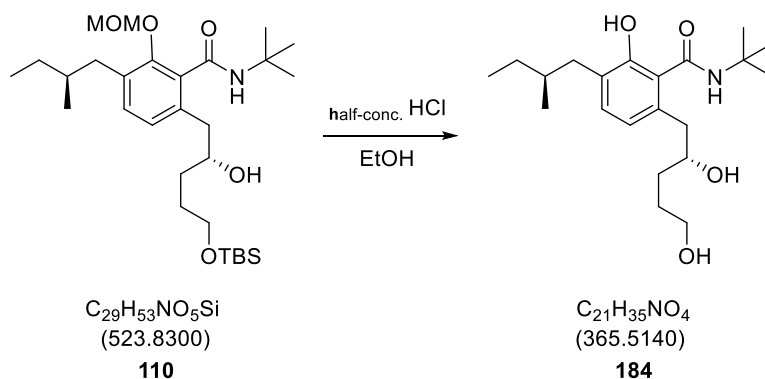


N,N,N',N' - Tetramethylethylenediamin (0.87 ml, 5.8 mmol, 3 eq.) and *n*-butyllithium (2.3 ml, 5.8 mmol, 3 eq.) were slowly added to a solution of (*S*)-*N*-(*tert*-butyl)-2-(methoxymethoxy)-3-(2-methylbutyl) benzamide **31** (0.6 g, 1.9 mmol, 1 eq.) in degassed Et₂O (11 ml) at -78°C. The reaction mixture was warmed up to -30°C. (2*R*)-2-(2-*tert*-Butyldimethylsilyloxyethyl) oxiran (1.26 g, 5.8 mmol, 3 eq.) was added after 2 hours at -78°C. The resulting mixture was stirred at -30°C overnight and the reaction was terminated by adding a saturated solution of NH₄Cl. The aqueous phase was extracted with diethyl ether, dried over Na₂SO₄, filtered and the solvent was evaporated. Purification by column chromatography (PE:EA = 30:1) afforded the pure product **110** (0.34 g, 0.65 mmol, 34%) as colorless crystals.

¹H-NMR (400 MHz, CDCl₃): δ 7.11 (d, *J* = 7.9 Hz, 1H), 6.94 (d, *J* = 7.9 Hz, 1H), 6.18 (s, 1H), 5.1 (q, 2H), 3.78 (bs, 1H), 3.67 (t, *J* = 6.0 Hz, 2H), 3.53 (s, 3H), 2.81 – 2.58 (m, 3H), 2.38 (dd, *J* = 13.6, 8.3 Hz, 1H), 1.78 – 1.63 (m, 4H), 1.56 (m, 2H), 1.46 (s, 9H), 1.27 – 1.12 (m, 2H), 0.92 (dd, *J* = 7.3, 2.5 Hz, 3H), 0.89 (s, 9H), 0.85 (d, *J* = 2.3 Hz, 3H), 0.05 (s, 6H).

¹³C-NMR (100 MHz, CDCl₃, CDCl₃ = 77.0 ppm) δ 168.3, 152.2, 136.5, 133.3, 132.8, 131.7, 126, 100.7, 72.6, 63.6, 63.6, 57.9, 52.1, 37.5, 35.3, 35.2, 29.7, 29.4, 28.8, 26.1, 19.2, 18.5, 11.6, 5.1, 5.1.

N-(*tert*-Butyl)-6-[(*R*)-2,5-dihydroxypentyl-2-hydroxy-3-(*S*)-2-methylbutyl] benzamide
[184]:

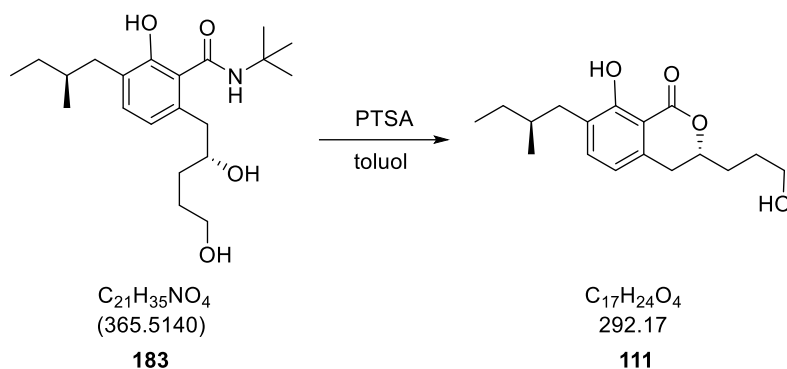


Half-concentrated hydrochloric acid (3.4 ml) was added to a solution of *N*-(*tert*-butyl)-6-((*S*)-4-((*tert*-butyldimethylsilyloxy)-2-hydroxybutyl)-2-(methoxymethoxy)-3-((*S*)-2-methylbutyl) benzamide **110** (0.33 g, 0.63 mmol, 1 eq.) in EtOH (15 ml) and the mixture was stirred for 1 hour at 50°C. The reaction was hydrolyzed by addition of a saturated aqueous solution of NaHCO₃. The aqueous phase was extracted with ethyl acetate. The combined organic phases were dried over Na₂SO₄, filtered and the solvent was evaporated. Column chromatography (PE:EA = 4:1 then 1:1) afforded the pure product **184** (0.23 g, 0.63 mmol, 98%) as a pink oil.

¹H-NMR (400 MHz, CDCl₃) δ 10.29 (bs, 1H), 8.57 (s, 1H), 7.04 (d, *J* = 7.7 Hz, 1H), 6.62 (d, *J* = 8.0 Hz, 1H), 4.03 (tt, 1H), 3.87 – 3.78 (m, 1H), 3.69 (m, 1H), 3.00 (dd, *J* = 13.9, 10.8 Hz, 1H), 2.74 – 2.56 (m, 2H), 2.35 (ddd, *J* = 23.6, 13.3, 8.0 Hz, 1H), 1.95 – 1.79 (m, 2H), 1.79 – 1.71 (m, 2H), 1.65 (m, 2H), 1.46 (s, 9H), 1.40 (m, 1H), 1.31 – 1.11 (m, 2H), 0.90 (t, 3H), 0.85 (d, *J* = 6.7 Hz, 3H).

¹³C-NMR (100 MHz, CDCl₃, CDCl₃ = 77.0 ppm) δ 169.8, 156.7, 134.5, 132.6, 127.6, 121.4, 120.2, 74.88, 63.3, 52.3, 40.7, 37.4, 36.0, 34.7, 29.0, 21.2, 19.3, 11.6.

(R)-8-Hydroxy-3-(3-hydroxypropyl)-7-[(S)-2-methylbutyl] isochroman-1-one [111]:

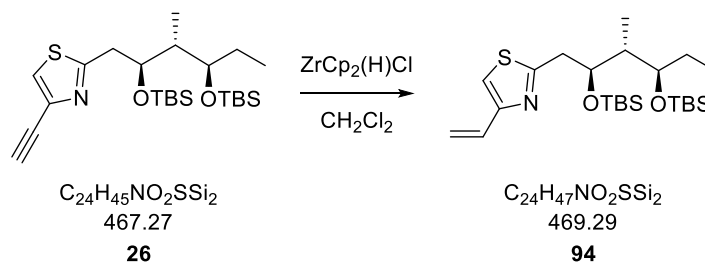


p-Toluenesulfonic acid (23 mg, 1.2 mmol, 2 eq.) was added to a solution of *N*-(*tert*-butyl)-6-((*S*)-2,4-dihydroxybutyl)-2-(methoxymethoxy)-3-((*S*)-2-methylbutyl) benzamide **183** (22 mg, 0.6 mmol, 1 eq.) in toluene (10 ml) and the mixture was heated under refluxing conditions for 30 min. The solvent was evaporated and column chromatography (PE:EA = 3:1 then 1:1) afforded the pure product **111** (14 mg, 0.48 mmol, 81 %) as a yellow oil.

$^1\text{H-NMR}$ (400 MHz, CDCl_3) δ 11.22 (s, 1H), 7.23 (d, $J = 7.5$ Hz, 1H), 6.61 (d, $J = 7.5$ Hz, 1H), 4.66 – 4.53 (m, 1H), 4.18 – 4.09 (m, 1H), 3.74 (t, $J = 5.1$ Hz, 1H), 2.99 – 2.84 (m, 2H), 2.70 – 2.60 (m, 1H), 2.44 – 2.35 (m, 1H), 1.97 – 1.88 (m, 2H), 1.88 – 1.78 (m, 2H), 1.74 (m, 1H), 1.40 (m, 1H), 1.23 – 1.15 (m, 1H), 0.91 (t, $J = 7.4$ Hz, 3H), 0.86 (d, $J = 6.6$ Hz, 3H).

$^{13}\text{C-NMR}$ (100 MHz, CDCl_3 , $\text{CDCl}_3 = 77.0$ ppm) δ 170.4, 160.7, 137.3, 136.6, 129.1, 117.1, 107.9, 63.9, 36.9, 34.9, 33.0, 31.5, 29, 21.2, 19.3, 11.6.

2-[(2*S*, 3*R*, 4*R*)-2, 4-Bis [(*tert*-butyldimethylsilyl) oxy]-3-methylhexyl]-4-vinylthiazole [94]:



26 (0,3 g, 0,64 mmol, 1 eq) was dissolved in dichloromethane (1 mL) and zirconocene hydrochloride (0,18 g, 0,7 mmol, 1,1 eq) suspended in dichloromethane (4 mL) was slowly added. The suspension was stirred at RT for 1 h and water (5 mL) was added. The mixture was extracted with dichloromethane (3 x 15 mL), the solvent was evaporated and the crude product **94** was purified by column chromatography (PE:EA = 4:1) to yield 99% (0.3 g, 0.63mmol) of the product as colorless oil.

¹H-NMR (400 MHz, CDCl₃): δ 6.94 (s, 1H), 6.65 (dd, 1H), 6.03 (dd, 1H), 5.33 (dd, 1H), 4.26 (td, 1H), 3.69 (m, 1H), 3.10 (m, 2H), 1.87 (m, 1H), 1.50 (m, 2H), 0.91 (m, 3H), 0.88 (m, 6H), 0.85 (m, 6H), 0.82 (m, 3H), 0.05 (m, 6H), -0.01 (s, 3H), -0.20 (s, 3H) ppm.

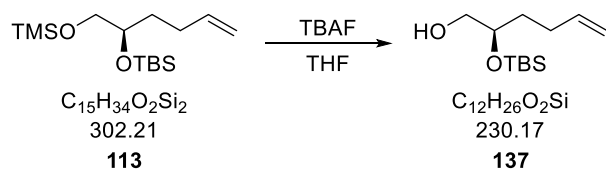
The analytical data are consistent with those reported in the literature.¹³⁹

was used directly without any further purification. It was dissolved in DMF and imidazole (0.13g, 1.9 mmol, 1.1 eq) and TBSCl (0.28 g, 1.9 mmol, 1.1 eq) were added. Then the mixture was stirred for 1.5 h at RT and water was added. The extract was concentrated under vacuum and purified via column chromatography (PE: EA = 5:1) to yield the product **113** as a pale yellow oil in 82 % (0.4 g, 1.3 mmol). The product was subsequently used for the preparation of substrate **137**.

¹H-NMR (400 MHz, CDCl₃): δ 5.92 – 5.72 (m, 1H), 5.08 – 4.88 (m, 2H), 3.73 – 3.61 (m, 1H), 3.57 – 3.34 (m, 2H), 2.24 – 2.13 (m, 1H), 2.10 – 1.98 (m, 1H), 1.71 – 1.59 (m, 1H), 1.50 – 1.37 (m, 1H), 0.93 – 0.86 (m, 9H), 0.16 – 0.07 (m, 8H), 0.05 (q, *J* = 2.1 Hz, 6H).

¹³C-NMR (100 MHz, CDCl₃, CDCl₃ = 77.0 ppm) δ 139, 114.5, 72.9, 67.8, 33.5, 29.8, 26.2, 18.6, 0.6, -5.1, -5.2.

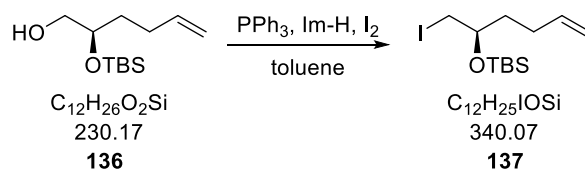
(*R*)-2-[(*tert*-Butyldimethylsilyl)oxy]hex-5-en-1-ol [136]:



To a solution of **113** (0.2 g, 0.66 mmol, 1 eq) in THF was added TBAF (0.7 mL, 0.69 mmol, 1.05 eq) slowly at 0 °C. The mixture was then slowly warmed up to RT over 45 min and stirred for additional 30 min at RT. Then water and aqueous solution of NH₄Cl was added and the crude extract was concentrated under vacuum to be purified via column chromatography (PE: EA = 4:1) to yield 98% (0.15 g, 0.65 mmol) of the product **136** as a colorless oil. The product was subsequently used for the preparation of substrate **137**.

¹H-NMR (400 MHz, CDCl₃): δ 5.83 (ddt, *J* = 16.9, 10.2, 6.6 Hz, 1H), 5.10 – 4.90 (m, 2H), 3.65 (ddd, *J* = 18.4, 9.2, 3.4 Hz, 2H), 3.46 – 3.34 (m, 1H), 2.33 – 2.19 (m, 2H), 2.18 – 2.06 (m, 1H), 1.62 – 1.40 (m, 2H), 0.91 – 0.87 (m, 9H), 0.08 (d, *J* = 2.9 Hz, 6H).

(R)-tert-Butyl[(1-iodohex-5-en-2-yl)oxy]dimethylsilane [137]:

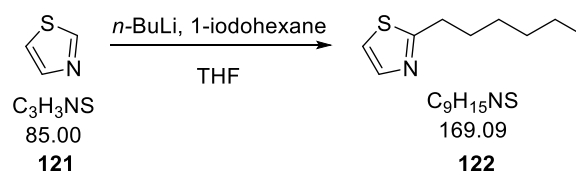


Imidazole (0.06 g, 0.9 mmol, 1.5 eq) and PPh₃ (0.24 g, 0.9 mmol, 1.5 eq) were added to a solution of **136** (0.14 g, 0.6 mmol, 1 eq) in dichloromethane (5 mL). Iodine (0.23 g, 0.9 mmol, 1.5 eq) was carefully added at 0 °C and the reaction mixture was stirred for 45 min at 0 °C. An aqueous solution of Na₂S₂O₃ (10 mL) was added and the aqueous phase was extracted with dichloromethane (3 x 15 mL). The extract was dried over Na₂SO₄, filtered, concentrated under vacuum and purified by column chromatography (PE: EA = 4:1) to yield the product **137** as a pale yellow oil in 97% (0.19 g, 0.55 mmol) yield, $[\alpha]^{20}_{\text{D}} +11.3$ (c 1.0 in CHCl₃) (lit. $[\alpha]^{20}_{\text{D}} +12.8$ (c 1.66 in CHCl₃));

¹H-NMR (400 MHz, CDCl₃): δ 5.81 (m, 1H), 5.00 (m, 2H), 3.65 (m, 1H), 3.61 (m, 1H), 3.41 (m, 1H), 2.17 (m, 2H), 1.49 (m, 2H), 0.89 (s, 9H), 0.07 (s, 6H).

The analytical data are consistent with those reported in the literature.¹³⁰

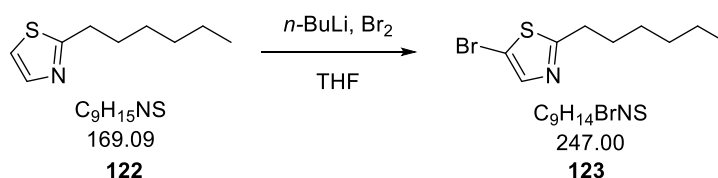
2-Hexylthiazole [122]:



n-BuLi (11.3 mL, 28.2 mmol, 1.2 eq) was added dropwise to a thiazole **121** (1.67 mL, 23.5 mL, 1 eq) solution in THF (100 mL) at -78 °C. The mixture was stirred for 30 min and 1-iodohexane (3.97 mL, 25.8 mmol, 1.1 eq) was added slowly. The reaction mixture was stirred for additional 30 min at -78 °C and warmed up to RT and stirring was continued for another 2 hours. Water was added and extracted with ethyl acetate. The extract was dried with Na₂SO₄, filtered and concentrated under vacuum. The crude residue was purified via column chromatography (PE) to yield the product **122** as pale yellow oil in 40% yield (1.48 g, 8.7 mmol). The product was subsequently used as substrate for the next reaction step.

¹H-NMR (400 MHz, CDCl₃): δ 7.66 (d, *J* = 3.6 Hz, 1H), 7.17 (d, *J* = 3.1 Hz, 1H), 3.01 (dd, *J* = 9.0, 6.4 Hz, 2H), 1.84 – 1.74 (m, 2H), 1.37 (m, 2H), 1.28 (m, 4H), 0.89 – 0.81 (t, 3H).

5-Bromo-2-hexylthiazole [123]:

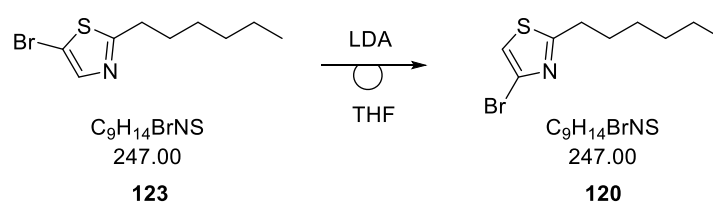


n-BuLi (1.44 mL, 2.3 mmol, 1.3 eq) was added dropwise to **122** (1.67 mL, 23.5 mL, 1 eq) solved in THF (6 mL) at -78 °C. Bromine (0.12 mL, 2.3 mmol, 1.3 eq) was added dropwise after 30 min at the same temperature and the mixture was stirred for additional 30 min at -78 °C. The mixture was then stirred for another 50 min at RT and water was added. The aqueous phase was extracted with ethyl acetate, dried over Na₂SO₄, filtered and concentrated under vacuum. The crude residue was purified by column chromatography (PE) to yield the product **123** in 80 % (0, 47 g, 1,9 mmol) yield.

¹H-NMR (400 MHz, CDCl₃): δ 7.53 (s, 1H), 2.99 – 2.91 (m, 2H), 1.75 (dt, *J* = 15.3, 7.7 Hz, 2H), 1.41 – 1.36 (m, 2H), 1.29 (dd, *J* = 6.9, 4.1 Hz, 4H), 0.90 – 0.86 (m, 3H).

¹³C-NMR (100 MHz, CDCl₃, CDCl₃ = 77.0 ppm) δ 173.4, 143.4, 107.2, 34, 31.8, 29.9, 29.1, 29.06, 22.8, 14.2.

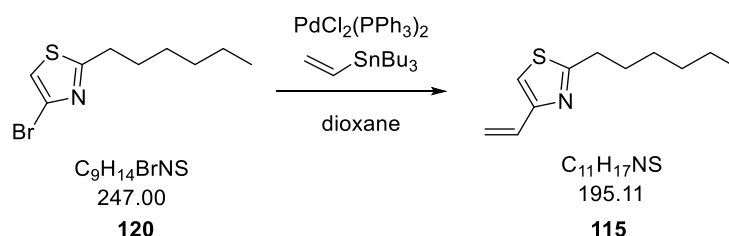
4-Bromo-2-hexylthiazole [120]:



123 (0.4 g, 1.6 mmol, 1 eq) was dissolved in THF (10 mL) and cooled down to -78 °C. Freshly prepared LDA (2.7 mL, 1.9 mmol, 1.2 eq) was added very slowly and the resultant mixture was stirred for 1 hour at -78 °C. Water was then added and the reaction vessel was slowly warmed up to RT while stirring. THF was removed under vacuum and the remaining aqueous layer was extracted with diethyl ether, washed with brine, dried over Na₂SO₄, filtered and evaporated under vacuum. The crude material was purified by column chromatography (PE) to yield the product **120** as pale yellow oil in 50% (0.21 g, 0.85 mmol) yield.

¹H-NMR (400 MHz, CDCl₃): δ 7.06 (d, *J* = 3.4 Hz, 1H), 3.04 – 2.93 (m, 2H), 1.83 – 1.73 (m, 2H), 1.42 – 1.35 (m, 2H), 1.34 – 1.27 (m, 4H), 0.87 (dd, *J* = 6.1, 4.3 Hz, 3H).

2-Hexyl-4-vinylthiazole [115]:



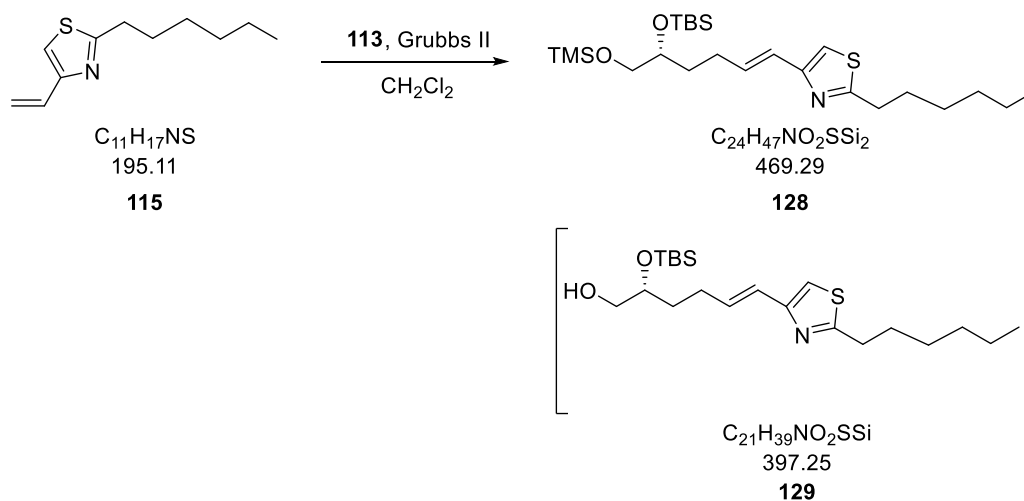
PdCl₂(PPh₃)₂ (0.002 g, 0.003 mmol, 0.002 eq) was added to a solution of **120** (0.04 g, 0.16 mmol, 1 eq) in dioxane (1 mL) and allyltributylstannane (0.05 mL, 0.18 mmol, 1.1 eq) was

added dropwise. The mixture was then stirred for 16 hours at 100 °C, then it was diluted with diethyl ether (2 mL), washed with water (2 x 2 mL), dried over Na₂SO₄, filtered and concentrated under vacuum. The crude product **115** was purified by column chromatography to yield a yellow oil in 94 % (0.03 g, 0.15 mmol).

¹H-NMR (400 MHz, CDCl₃): δ 7.4 (s, 1 H), 6.63 (dd, 1H), 5.87 (d, 1H), 5.43 (d, 1H), 2.86 (m, 2 H), 1.65 (m, 4 H), 1.3 (m, 4 H), 0.87 (m, 3 H).

UPLC-MS (LC MS): *m/z*: calculated for C₁₁H₁₈NS: 196.1160 [M + H]⁺: found: 196.1152 [M + H]⁺.

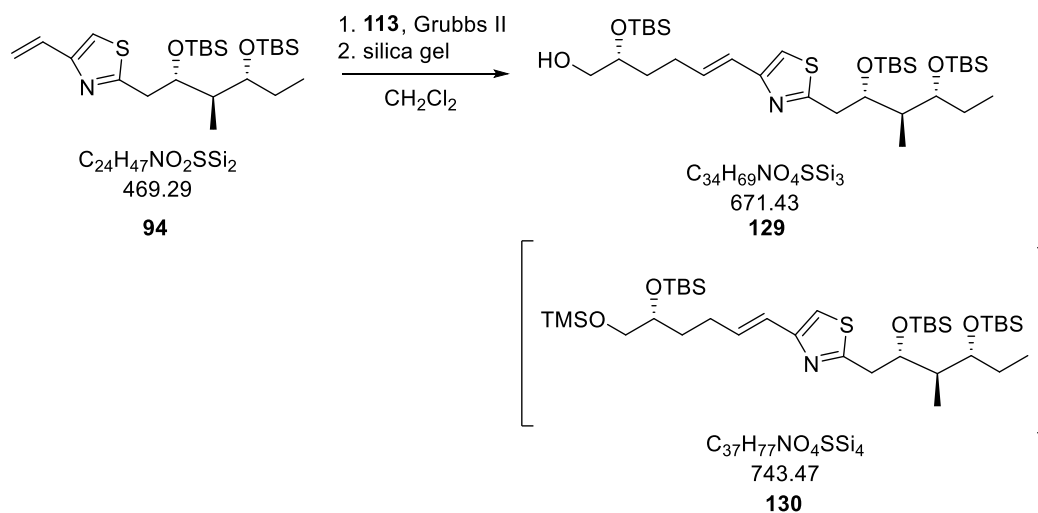
(*R, E*)-4-(5-[(*tert*-Butyldimethylsilyl) oxy]-6-[(trimethylsilyl) oxy] hex-1-en-1-yl)-2-hexylthiazole [128] and (*R, E*)-2-[(*tert*-Butyldimethylsilyl) oxy]-6-(2-hexylthiazol-4-yl) hex-5-en-1-ol [129]:



115-thiazole (0.03g, 0.15 mmol, 2 eq) was solved in dichloromethane (2 mL), **113** (0.025g, 0.07 mmol, 1 eq) was added as well as Grubbs 2nd generation catalyst (0.04 g, 0.045 mmol, 0.3 eq). The mixture was warmed up to 40 °C and stirred overnight at this temperature. The solvent was then evaporated under vacuum and the residue was purified via column chromatography (PE:EA = 10:1).

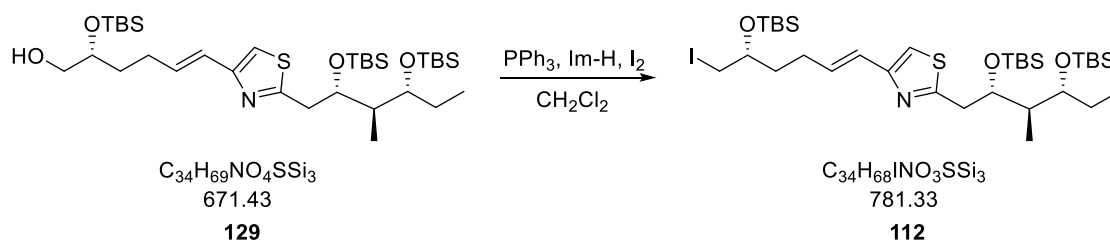
No further analytical evaluation was carried out.

(*R,E*)-6-[2-((2*S*,3*R*,4*R*)-2,4-Bis[(*tert*-butyldimethylsilyl)oxy]-3-methylhexyl)thiazol-4-yl]-2-[(*tert*-butyldimethylsilyl)oxy]hex-5-en-1-ol [129] and 2-((2*S*,3*R*,4*R*)-2,4-Bis[(*tert*-butyldimethylsilyl)oxy]-3-methylhexyl)-4-((*R,E*)-5-[(*tert*-butyldimethylsilyl)oxy]-6-(trimethylsilyl)oxy)hex-1-en-1-yl}thiazole [130]:



94-thiazole (0.03g, 0.15 mmol, 2 eq) was dissolved in dichloromethane (2 mL), **113** (0.025 g, 0.07 mmol, 1 eq) was added as well as Grubbs 2nd generation catalyst (0.04 g, 0.045 mmol, 0.3 eq). The mixture was warmed up to 40 °C and stirred overnight at this temperature. Silica gel was added and the suspension stirred at RT for further 2 hours. The mixture was filtered through a thin pad of silica gel, the solvent was evaporated under vacuum and the residue was purified by column chromatography (PE:EA = 6:1). The product **129** and side-product **130** were elucidated via means of LC-MS. The product was directly used without further analytical assignments.

2-[(2*S*, 3*R*, 4*R*)-2, 4-Bis(*tert*-butyldimethylsilyloxy)-3-methylhexyl]-4-[(*R,E*)-5-[(*tert*-butyldimethylsilyloxy)-6-iodohex-1-en-1-yl]thiazole [112]:



Imidazole (0.006 g, 0.09 mmol, 1.4 eq) and PPh_3 (0.025 g, 0.094 mmol, 1.4 eq) were added to a solution of **129** (0.045 g, 0.067 mmol, 1 eq) in dichloromethane (1 mL). Iodide (0.024 g, 0.094 mmol, 1.4 eq) was then slowly added at 0 °C and the mixture was stirred for 30 min at the same temperature. An aqueous solution of $Na_2S_2O_3$ (1 mL) was then added and the aqueous phase was extracted with dichloromethane (2 x 5 mL). Purification via column chromatography (PE) yielded the product **112** as a yellow oil in 40% (0.02g, 0.025 mmol) yield.

The product was analyzed by LC-MS.

8. Liposome assays

8.1. Synthesis of the pGST-P7 fusion protein

A pGEX-4T vector with a built-in sequence for P7-GST serves as the basis for the heterologous expression of the P7-GST fusion protein. This vector is transformed into heat-competent Rosetta Nova Blue BL21 *E. coli* cells. For this, 4 μ l of the plasmid vector are incubated with competent *E. coli* cells on ice for 10 min. The heat pulse occurs for 30 seconds at 42 °C. After incubation for 2 minutes on ice, 250 μ l S.O.C is added to the cells. This is followed by incubation for one hour at 37 °C. and 140 rpm. Spread on LB agar plates containing ampicillin (100 μ g/ml) and chloramphenicol (35 μ g/ml) and incubate at 37 °C overnight. Clones are transferred from the plate into 100 ml LB medium containing ampicillin (100 μ g/ml) and chloramphenicol (35 μ g/ml), and incubated at 37 °C, at 140 rpm for 8 h. Afterwards, the preculture is cultured in 1.5 l of TB medium, ampicillin (100 μ g/ml) and chloramphenicol (35 μ g/ml) at 37 °C. The induction then takes place by adding IPTG (1 mM) and cultivation is continued at 30 °C for 5 hours. The cells were collected by centrifugation at 8,500xg for 15 min and the supernatant was removed.

8.2. Isolation of the fusion protein GST-P7

The cells (10g) are disrupted mechanically in lysis buffer using a French press at 12,000-14,000 p.s.i. The lysate is adjusted to 1% *N*-lauroylsarcosine (NLS) and stirred on ice at 140 rpm. After centrifugation at 14,000xg for 20 minutes, the supernatant is removed and diluted to 0.3% NLS. The supernatant is then incubated on a GST-binding matrix and unbound protein is washed off at a flow rate of 2 ml / min (GST washing buffer 1x TBS, 30 mM octylglucoside, pH 7.4). Bound proteins are then eluted from the column with reduced glutathione (GST elution buffer 50 mM Tris-HCl, 10 mM reduced glutathione 30 mM octylglucoside pH 8.0). The purification is optically monitored at OD280. The proteins transferred into concentrators YM10 and concentrated to a final concentration of 2 mg/ml.

To separate the GST fusion tag, PreScission Protease (protease in 50 mM Tris-HCl (pH8), 150mM NaCl, 10mM EDTA, 1mM DTT, 20% glycerol) was added to 300 μ l of the concentrated protein solution (2 mg/ml) and incubated at 4 °C for 16 h.

The phospholipid is first dissolved in chloroform at 10 mg / ml. This is followed by lyophilization at 50 °C in vacuo for 30 minutes and one-minute nitrogen gassing. Multilamellar vesicles are formed by hydrogenating the lipid film with a solution containing the desired fluorescent indicator. Unilamellar liposomes are formed by sonification for 10 min at 40%

amplitude using a Branson Sonifier 250 (Branson). The liposomes are reconstituted at about 100 µg/ml overnight with purified p7 protein. This is followed by three washing steps with centrifugation at 150,000 xg for 30 min. The pellets are resuspended in assay buffer.

8.3. Preparation of unilamellar liposomes.

8.3.1. Reverse-phase evaporation method

8.3.1.1. General procedure

An ethanol solution of phospholipide POPC (1-Palmitoyl-2-Oleoyl-Sn-Glycero-3-Phosphocholin) and cholesterol (1:1 lipid mixture) was evaporated at 30 °C water bath and the residue lipid film was flushed with N₂. The remaining lipid film was resolved in diethyl ether. The organic lipid mixture was then suspended in pH 7 detergent buffer (Tris HCl/Glycine) and fluorescent dye was added under nitrogen at 0 °C. Unilamellar liposomes were achieved after sonification at 50% amplitude with Branson Sonifier 250 until either a clear one-phase dispersion or a homogenous opalescent that does not separate for at least 30 min was formed. The organic solvent was the evaporated, the resultant suspension was split in separate vessels and the reconstituted p7 protein was added at this point to an individual vessel. All vessels were incubated at 0 °C for 18 h. Then they were centrifuged two times for 15 min at 60 000 rpm, while resuspended in a pH 7 buffer (Tris HCl/Glycine).

8.3.2. Lipid hydration method

8.3.2.1. General procedure

A chlorophorm solution of phospholipide POPC (1-Palmitoyl-2-Oleoyl-Sn-Glycero-3-Phosphocholin) was evaporated at 30 °C water bath for 40 min and the residue lipid film was flushed with N₂. The remaining lipid film was dispersed in pH 7 detergent buffer (Tris HCl/Glycine) and fluorescent dye was added. Unilamellar liposomes were achieved after sonification for 5 min at 50% amplitude with Branson Sonifier 250. The resultant suspension was split in separate vessels and the reconstituted p7 protein was added at this point to an individual vessel. All vessels were incubated at 0 °C for 18 h. Then they were centrifuged two times for 15 min at 65 000 rpm, while resuspended in a pH 7 buffer (Tris HCl/Glycine).

The following fluorimetric screenings were carried out in black-walled, flat-bottomed black-base 96-well plates. Dye release measured by increased fluorescence was taken as an indicator of ion-channel-induced membrane permeability (activity).

Reactions for each condition were carried out in duplicate wells with two independent experimental repeats. Endpoint measurements were used for the analysis with the average of the duplicate wells taken.

8.4. HTPS trials

8.4.1. Effects of protein content

Liposomes were prepared according to the general procedure of the lipid hydration method. Fluorimetric measurements were conducted to define the activity base lines for the two different p7 proteins versus a control. The measurements were done at excitation wavelength of 355 nm and emission wavelength of 460 nm. The liposomes contained internally 50 μ M HTPS dye and were suspended in buffer 10 mM Tris pH 7.0. After 10 s 10 μ l 20 mM KOH was injected to the running kinetics.

Entry	Content
P7_horse	35 μ l Buffer; 5 μ l P7 (horse) liposome, inject 10 μ l 20 mM KOH
P7_human	35 μ l Buffer; 5 μ l P7 (human) liposome, inject 10 μ l 20 mM KOH
P7_control	35 μ l Buffer; 5 μ l control liposome (no P7), inject 10 μ l 20 mM KOH

Table 12 Conditions of fluorimetric measurements of liposomes with different P7 protein content.

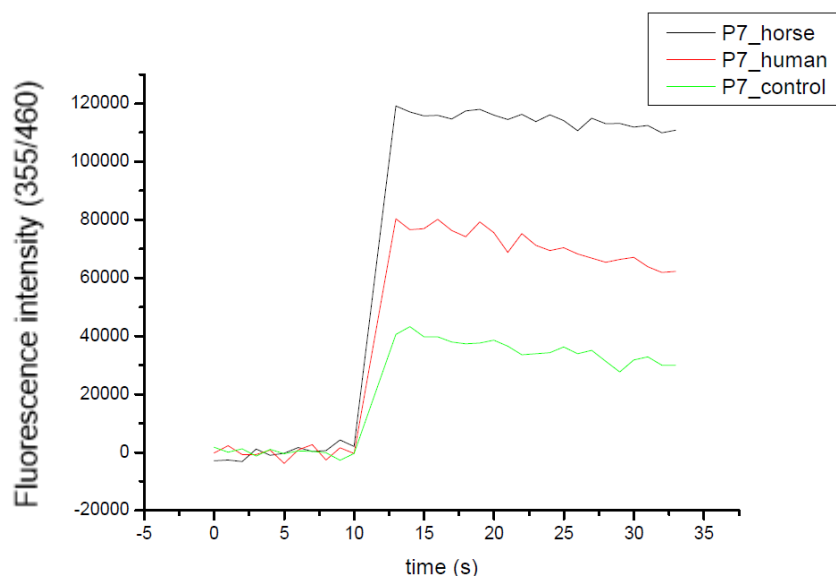


Figure 31 Potassium mediated transport activities of horse (NHCV) and human (HCV) p7.

8.4.2. Effects of ion-channel inhibitors content

After establishing the base-lines for the two different p7 proteins, 1 mM solutions of Amantadine and Rimandatine were injected into the kinetics to test their inhibitory activity for the horse p7 ion channel.

Entry	Content
P7_horse	35 μ l Buffer, 5 μ l P7 (horse) liposome, Inject 10 μ l 50 mM KOH
P7_control	35 μ l Buffer, 5 μ l control liposome, inject 10 μ l 50 mM KOH
P7_horse+Aman	34, 5 μ l Buffer, 5 μ l P7 (horse) liposome, 0, 5 μ l Aman (1 mM Stock), inject 10 μ l 50 mM KOH
P7_control+Aman	34, 5 μ l Buffer, 5 μ l control liposome, 0, 5 μ l Aman (1 mM Stock), inject 10 μ l 50 mM KOH
P7_horse+Riman	34, 5 μ l Buffer, 5 μ l P7 (horse) liposome, 0, 5 μ l Riman (1 mM Stock), inject 10 μ l 50 mM KOH
P7_control+Riman	34, 5 μ l Puffer, 5 μ l control liposome, 0, 5 μ l Riman (1 mM Stock), inject 10 μ l 50 mM KOH

Table 13 Conditions of fluorimetric measurements of liposomes with P7 horse protein content and Amantadine and Rimandatine as inhibitory molecules.

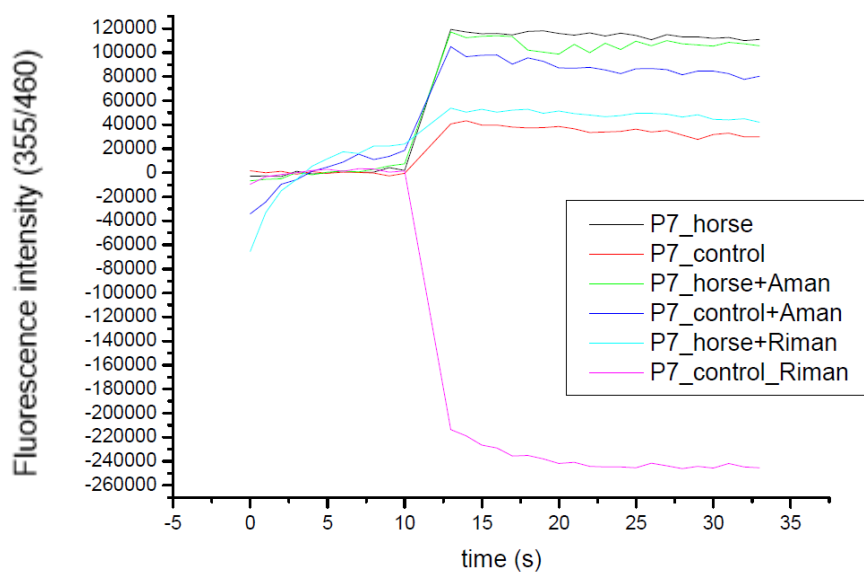


Figure 32 Potassium mediated transport activities of horse (NHCV) p7 in the presence of Amantadine and Rimandatine.

8.5. PBF1 trials

8.5.1. Effects of different pH buffer (4.8 pH gives stable result)

Liposomes were prepared according to the general procedure of the lipid hydration method. Fluorimetric measurements were conducted to define the most stable pH conditions. The measurements were done at excitation wavelength of 355 nm and emission wavelength of 460 nm. The liposomes contained internally 10 μ M PBF1 dye and there were two batches, one suspended in buffer 100 mM Tris pH 4.8 and another suspended in 100 mM Tris pH 6.0. After 10 s 40 μ l 1 M KCl was injected to the running kinetics.

Entry	Content
PBF1_lipos_pH4.8	150 μ l 100 mM MES, pH 4.8; 10 μ l PBF1 liposomes
PBF1_lipos_pH6.0	150 μ l 100 mM MES, pH 6.0; 10 μ l PBF1 liposomes
PBF1_P7_lipos_pH4.8	150 μ l 100 mM MES, pH 4.8; 10 μ l PBF1 P7 liposomes
PBF1_P7_lipos_pH6.0	150 μ l 100 mM MES, pH 6.0; 10 μ l PBF1 P7 liposomes

Table 14 Conditions of fluorimetric measurements of liposomes with P7 protein at two different pH.

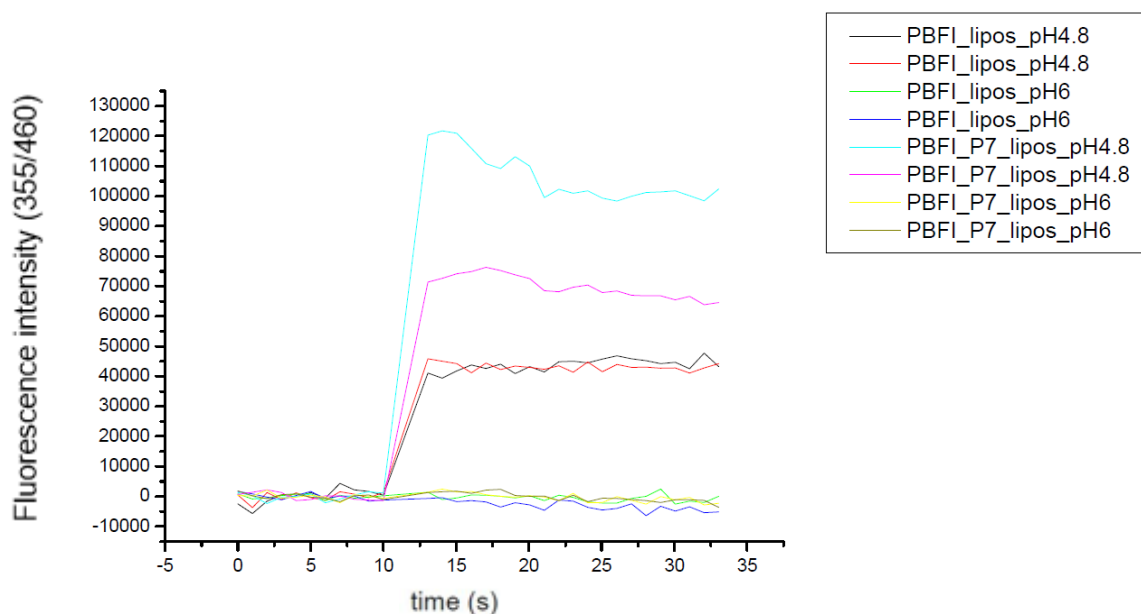


Figure 33 Potassium mediated transport activities of human (HCV) p7 at different pH values.

8.5.2. Effects of different concentration of liposomes (5 μ l gives stable result)

Liposomes were prepared according to the general procedure of the lipid hydration method. Fluorimetric measurements were conducted to define what liposome concentration provided the most stable signal result. The measurements were done at excitation wavelength of 355 nm and emission wavelength of 460 nm. The liposomes contained internally PBF1 dye at different concentration (five different batches) and all were suspended in buffer 100 mM Tris pH 4.8. After 10 s 40 μ l 1 M KCl was injected to the running kinetics.

Entry	Content
2.5 μ l lipos	157,5 μ l 100 mM MES, pH 4.8; 2.5 μ l PBFI liposomes
5 μ l lipos	155 μ l 100 mM MES, pH 4.8; 5 μ l PBFI liposomes
10 μ l lipos	150 μ l 100 mM MES, pH 4.8; 10 μ l PBFI liposomes
12.5 μ l lipos	147,5 μ l 100 mM MES, pH 4.8; 12,5 μ l PBFI liposomes
15 μ l lipos	145 μ l 100 mM MES, pH 4.8; 15 μ l PBFI liposomes
2.5 μ l P7	157,5 μ l 100 mM MES, pH 4.8; 2.5 μ l PBFI P7 liposomes
5 μ l P7	155 μ l 100 mM MES, pH 4.8; 5 μ l PBFI P7 liposomes
10 μ l P7	150 μ l 100 mM MES, pH 4.8; 10 μ l PBFI P7 liposomes
12.5 μ l P7	147,5 μ l 100 mM MES, pH 4.8; 12,5 μ l PBFI P7 liposomes
15 μ l P7	145 μ l 100 mM MES, pH 4.8; 15 μ l PBFI P7 liposomes

Table 15 Conditions of fluorimetric measurements of liposomes with PBFI at different concentrations.

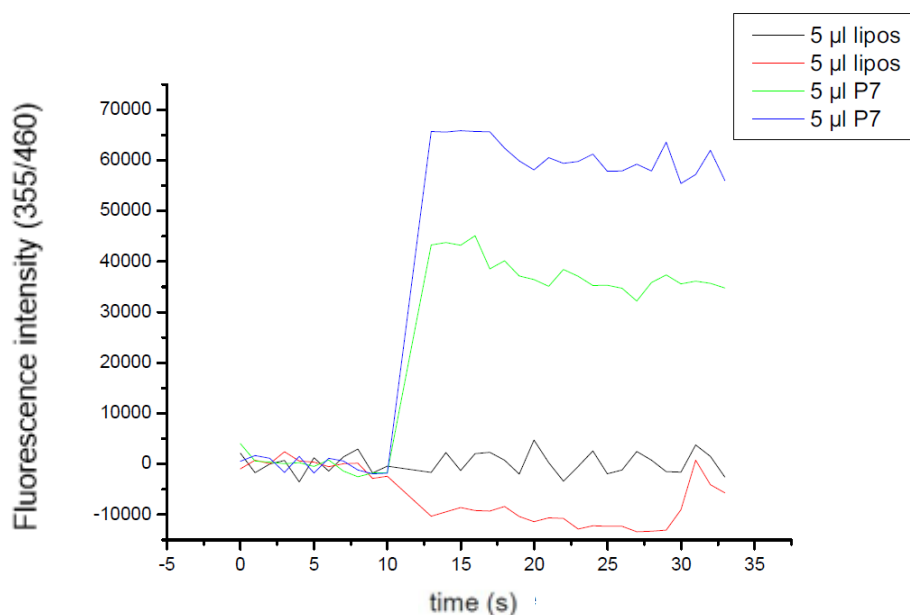


Figure 34 Potassium mediated transport activities of liposomes with and without human (HCV) p7.

8.5.3. Effects of different quinidine inhibitors

Liposomes were prepared according to the general procedure of the lipid hydration method. Fluorimetric measurements were conducted to screen a small set of commercially available quinidines for potential inhibitory activity of P7. The measurements were done at excitation wavelength of 355 nm and emission wavelength of 460 nm. The liposomes contained internally 5 μ l PBF1 dye and were suspended in buffer 100 mM Tris pH 4.8. All inhibitors were used as 10 μ M solutions. After 10 s 40 μ l 1 M KCl was injected to the running kinetics.

Entry	Content
lipos	155 μ l 100 mM MES, pH 4.8; 5 μ l PBF1 liposomes
lipos+Quin1	153 μ l 100 mM MES, pH 4.8; 2 μ l Quin 1; 5 μ l PBF1 liposomes
lipos+Quin2	153 μ l 100 mM MES, pH 4.8; 2 μ l Quin 2; 5 μ l PBF1 liposomes
lipos+Quin3	153 μ l 100 mM MES, pH 4.8; 2 μ l Quin 3; 5 μ l PBF1 liposomes
lipos+Quin4	153 μ l 100 mM MES, pH 4.8; 2 μ l Quin 4; 5 μ l PBF1 liposomes
lipos+Quin5	153 μ l 100 mM MES, pH 4.8; 2 μ l Quin 5; 5 μ l PBF1 liposomes
lipos+Quin6	153 μ l 100 mM MES, pH 4.8; 2 μ l Quin 6; 5 μ l PBF1 liposomes
lipos+Quin7	153 μ l 100 mM MES, pH 4.8; 2 μ l Quin 7; 5 μ l PBF1 liposomes
lipos+Quin8	153 μ l 100 mM MES, pH 4.8; 2 μ l Quin 8; 5 μ l PBF1 liposomes
lipos+Quin15	153 μ l 100 mM MES, pH 4.8; 2 μ l Quin 15; 5 μ l PBF1 liposomes
P7_lipos	155 μ l 100 mM MES, pH 4.8; 5 μ l PBF1 liposomes
P7_lipos+Quin1	153 μ l 100 mM MES, pH 4.8; 2 μ l Quin 1; 5 μ l PBF1 liposomes
P7_lipos+Quin2	153 μ l 100 mM MES, pH 4.8; 2 μ l Quin 2; 5 μ l PBF1 liposomes
P7_lipos+Quin3	153 μ l 100 mM MES, pH 4.8; 2 μ l Quin 3; 5 μ l PBF1 liposomes
P7_lipos+Quin4	153 μ l 100 mM MES, pH 4.8; 2 μ l Quin 4; 5 μ l PBF1 liposomes
P7_lipos+Quin5	153 μ l 100 mM MES, pH 4.8; 2 μ l Quin 5; 5 μ l PBF1 liposomes
P7_lipos+Quin6	153 μ l 100 mM MES, pH 4.8; 2 μ l Quin 6; 5 μ l PBF1 liposomes

P7_lipos+Quin7	153 μ l 100 mM MES, pH 4.8; 2 μ l Quin 7; 5 μ l PBF1 liposomes
P7_lipos+Quin8	153 μ l 100 mM MES, pH 4.8; 2 μ l Quin 8; 5 μ l PBF1 liposomes
P7_lipos+Quin15	153 μ l 100 mM MES, pH 4.8; 2 μ l Quin 15; 5 μ l PBF1 liposomes

Table 16 Conditions of fluorimetric measurements of the inhibitory activity towards HCV p7 of a set of quinidine derivatives.

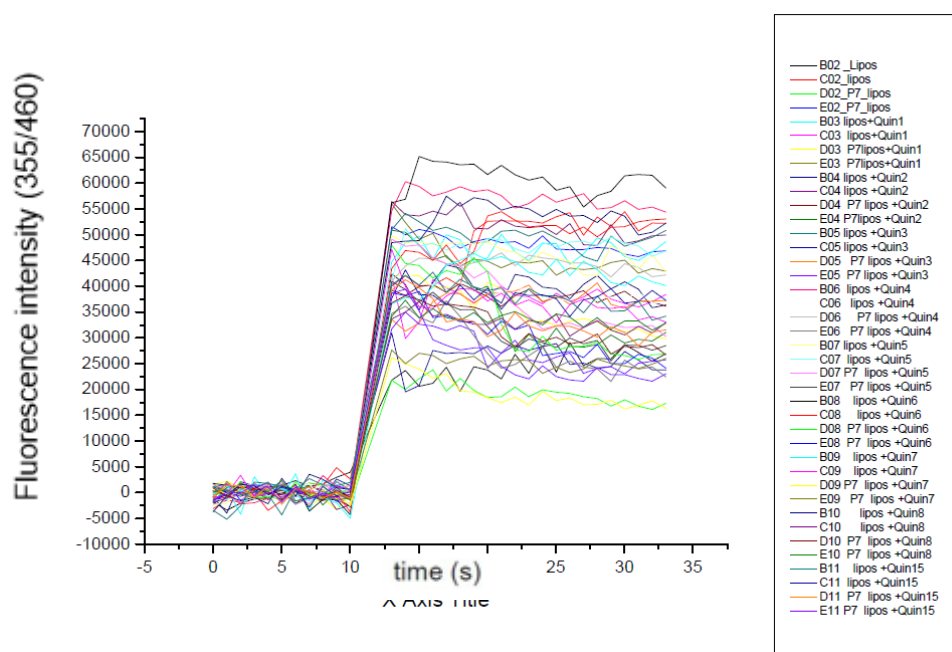


Figure 35 Potassium mediated transport activities of HCV p7 in the presence of Quinidine derivatives – two parallel sample measurements.

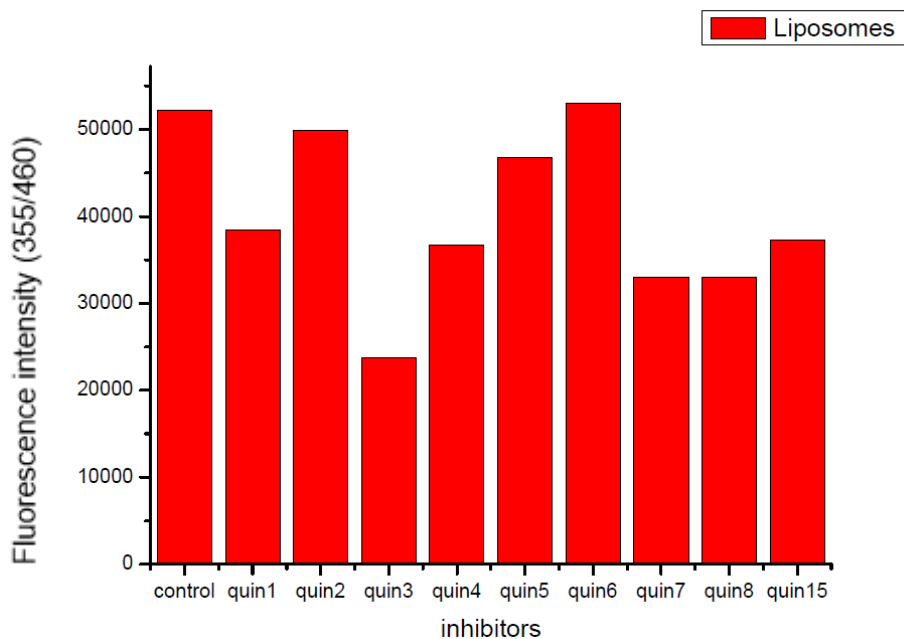


Figure 36 Statistical overview of Quinidine derivatives inhibitor activity of the HCV p7 viroporin – averaged results from two parallel measurements.

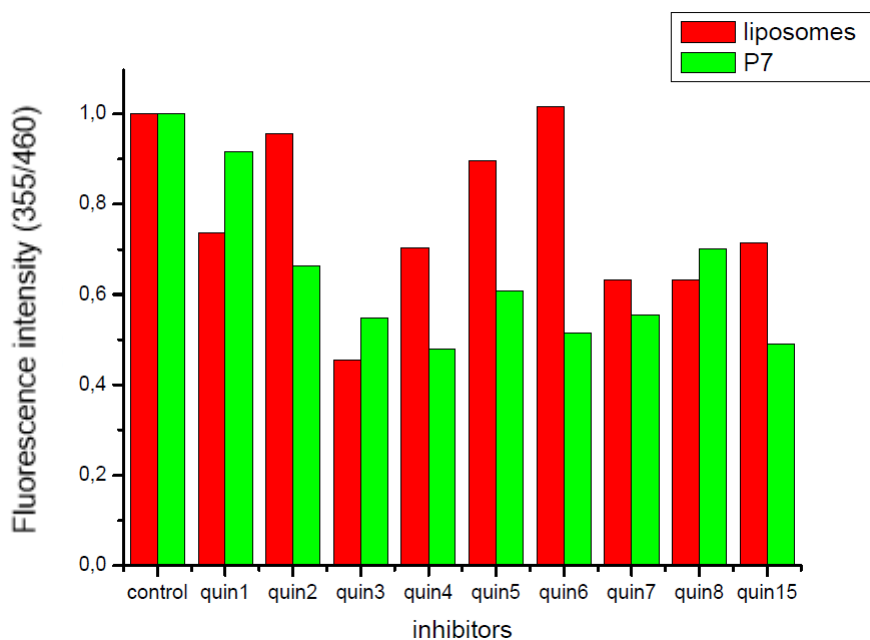


Figure 37 Statistical overview of Quinidine derivatives inhibitor activity of the HCV p7 viroporin – deviations of two parallel measurements.

9.5.4. Effects of different noricumazole inhibitors

Liposomes were prepared according to the general procedure of the lipid hydration method. Fluorimetric measurements were conducted to screen a small set of noricumazole derivatives

for potential inhibitory activity of P7. The measurements were done at excitation wavelength of 355 nm and emission wavelength of 460 nm. The liposomes contained internally 5 μ l PBF1 dye and were suspended in buffer 100 mM Tris pH 4.8. The inhibitors were used as 10 μ M solutions. After 10 s 40 μ l 1 M KCl was injected to the running kinetics.

Entry	Content
lipos_control	155 μ l 100 mM MES; 5 μ l PBF1 liposomes
contr_Nori1	153 μ l 100 mM MES; 2 μ l Nori 1; 5 μ l PBF1 liposomes
contr_Nori2	153 μ l 100 mM MES; 2 μ l Nori 2; 5 μ l PBF1 liposomes
contr_Nori6	153 μ l 100 mM MES; 2 μ l Nori 6; 5 μ l PBF1 liposomes
contr_Nori7	153 μ l 100 mM MES; 2 μ l Nori 7; 5 μ l PBF1 liposomes
contr_Nori8	153 μ l 100 mM MES; 2 μ l Nori 8; 5 μ l PBF1 liposomes
contr_Nori9	153 μ l 100 mM MES; 2 μ l Nori 9; 5 μ l PBF1 liposomes
contrl_Nori10	153 μ l 100 mM MES; 2 μ l Nori 10; 5 μ l PBF1 liposomes
contrl_Nori11	153 μ l 100 mM MES; 2 μ l Nori 11; 5 μ l PBF1 liposomes
contrl_Nori12	153 μ l 100 mM MES; 2 μ l Nori 12; 5 μ l PBF1 liposomes
contrl_Nori13	153 μ l 100 mM MES; 2 μ l Nori 13; 5 μ l PBF1 liposomes
contrl_Nori14	153 μ l 100 mM MES; 2 μ l Nori 14; 5 μ l PBF1 liposomes
contrl_Nori16	153 μ l 100 mM MES; 2 μ l Nori 16; 5 μ l PBF1 liposomes
contrl_Nori16a	153 μ l 100 mM MES; 2 μ l Nori 16a; 5 μ l PBF1 liposomes
contrl_Nori17	153 μ l 100 mM MES; 2 μ l Nori 17; 5 μ l PBF1 liposomes
contrl_Nori18	153 μ l 100 mM MES; 2 μ l Nori 18; 5 μ l PBF1 liposomes
contrl_Nori19	153 μ l 100 mM MES; 2 μ l Nori 19; 5 μ l PBF1 liposomes
contrl_Nori20	153 μ l 100 mM MES; 2 μ l Nori 20; 5 μ l PBF1 liposomes
contrl_Nori21	153 μ l 100 mM MES; 2 μ l Nori 21; 5 μ l PBF1 liposomes

contrl_Nori22	153 μ l 100 mM MES; 2 μ l Nori 22; 5 μ l PBFi liposomes
contrl_Nori23	153 μ l 100 mM MES; 2 μ l Nori 23; 5 μ l PBFi liposomes
contrl_Quin	153 μ l 100 mM MES; 2 μ l Quin; 5 μ l PBFi liposomes
contrl_Rim	153 μ l 100 mM MES; 2 μ l Rim; 5 μ l PBFi liposomes
contrl_Aman	153 μ l 100 mM MES; 2 μ l Aman; 5 μ l PBFi liposomes
P7	155 μ l 100 mM MES; 5 μ l P7 PBFi liposomes
Nori1	153 μ l 100 mM MES; 2 μ l Nori 1; 5 μ l P7 PBFi liposomes
Nori2	153 μ l 100 mM MES; 2 μ l Nori 2; 5 μ l P7 PBFi liposomes
Nori6	153 μ l 100 mM MES; 2 μ l Nori 6; 5 μ l P7 PBFi liposomes
Nori7	153 μ l 100 mM MES; 2 μ l Nori 7; 5 μ l P7 PBFi liposomes
Nori8	153 μ l 100 mM MES; 2 μ l Nori 8; 5 μ l P7 PBFi liposomes
Nori9	153 μ l 100 mM MES; 2 μ l Nori 9; 5 μ l P7 PBFi liposomes
Nori10	153 μ l 100 mM MES; 2 μ l Nori 10; 5 μ l P7 PBFi liposomes
Nori11	153 μ l 100 mM MES; 2 μ l Nori 11; 5 μ l P7 PBFi liposomes
Nori12	153 μ l 100 mM MES; 2 μ l Nori 12; 5 μ l P7 PBFi liposomes
Nori13	153 μ l 100 mM MES; 2 μ l Nori 13; 5 μ l P7 PBFi liposomes
Nori14	153 μ l 100 mM MES; 2 μ l Nori 14; 5 μ l P7 PBFi liposomes
Nori16	153 μ l 100 mM MES; 2 μ l Nori 16; 5 μ l P7 PBFi liposomes
Nori16a	153 μ l 100 mM MES; 2 μ l Nori 16a; 5 μ l P7 PBFi liposomes
Nori17	153 μ l 100 mM MES; 2 μ l Nori 17; 5 μ l P7 PBFi liposomes
Nori18	153 μ l 100 mM MES; 2 μ l Nori 18; 5 μ l P7 PBFi liposomes
Nori19	153 μ l 100 mM MES; 2 μ l Nori 19; 5 μ l P7 PBFi liposomes
Nori20	153 μ l 100 mM MES; 2 μ l Nori 20; 5 μ l P7 PBFi liposomes
Nori21	153 μ l 100 mM MES; 2 μ l Nori 21; 5 μ l P7 PBFi liposomes

Nori22	153 μ l 100 mM MES; 2 μ l Nori 22; 5 μ l P7 PBFI liposomes
Nori23	153 μ l 100 mM MES; 2 μ l Nori 23; 5 μ l P7 PBFI liposomes
Quin	153 μ l 100 mM MES; 2 μ l Quin; 5 μ l P7 PBFI liposomes
Rim	153 μ l 100 mM MES; 2 μ l Rim; 5 μ l P7 PBFI liposomes
Aman	153 μ l 100 mM MES; 2 μ l Aman; 5 μ l P7 PBFI liposomes

Table 17 Conditions of fluorimetric measurements of the inhibitory activity towards HCV p7 of a set of quinidine derivatives.

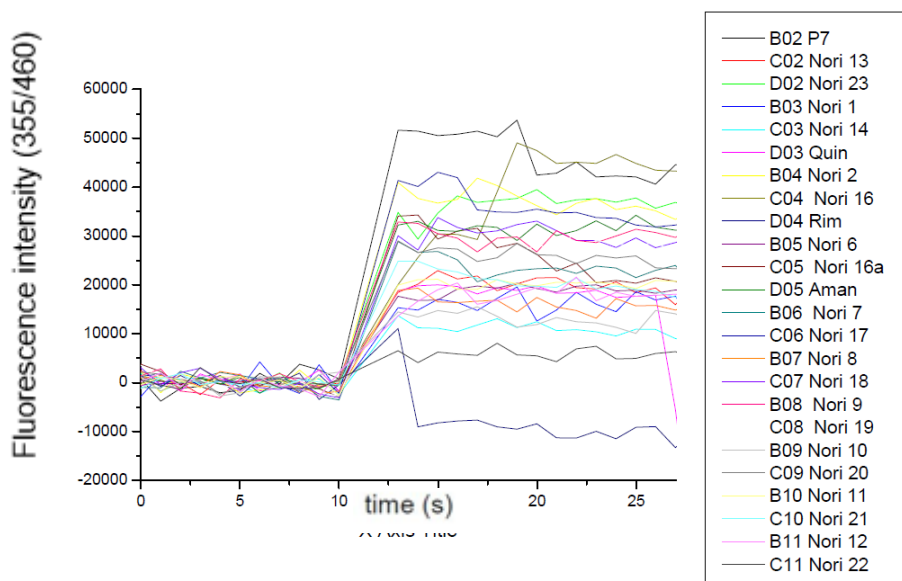


Figure 38 Potassium mediated transport activities of HCV p7 in the presence of Noricumazole derivatives.

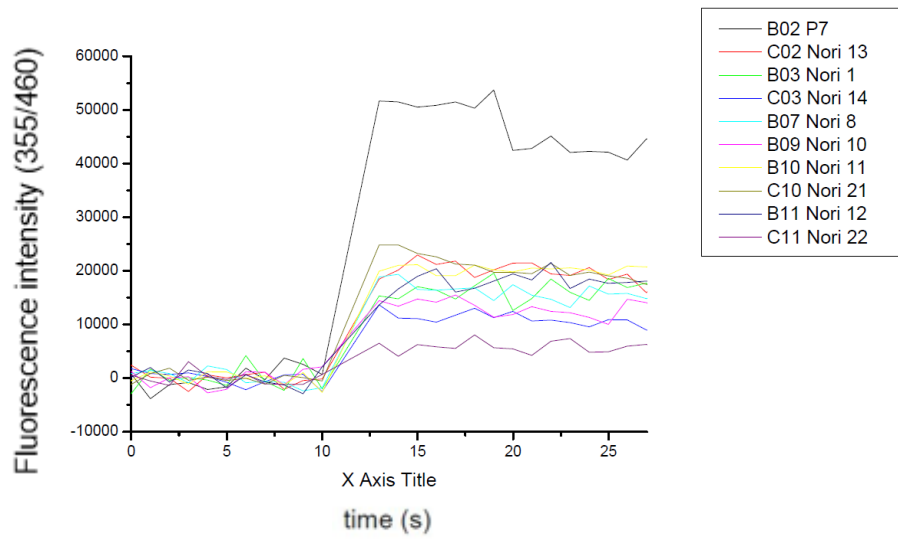


Figure 39 Potassium mediated transport activities of HCV p7 in the presence of Noricumazole derivatives – best of best Noricumazole inhibitors.

9. References

- ¹ M. Jefferies, B. Rauff, H. Rashid, T. Lam, S. Rafiq, *World J. Clin. Cases* **2018**, *6*, 589-599.
- ² S. Saab, Y. Challita, P. H. Chen, M. A. Jimenez, A. D. Lee, E. G. Saab, T. Ahn, G. Choi, F. A. Durazo, M. M. El-Kabany, S. B. Han, J. Grotts, V. G. Agopian, R. W. Busuttil, *J. Clin. Trans. Hepatology* **2018**, *6*, 247-250.
- ³ J. Gentsch, C. Brohm, E. Steinmann, M. Friesland, N. Menzel, G. Vieyres, P. M. Perin, A. Frentzen, L. Kaderali, T. Pietschmann, *PLoS Pathogens* **2013**, *9*, 1-14.
- ⁴ A. M. Atoom, N. G. A. Taylor, R. S. Russel, *Virology* **2014**, 462-463, 377-387.
- ⁵ a) M. E. Burlone, A. Budkowska, *J. Gen. Virol.* **2009**, *90*, 1055-1070; b) P. Georgel, C. Schuster, M. B. Zeisel, F. Stoll-Keller, T. Berg, S. Bahram, T. F. Baumert, *Trends Mol. Med.* **2010**, *16*, 277-286.
- ⁶ R. Bartenschlager, V. Lohmann, *J. Gen. Virol.* **2000**, *81*, 1631-1648.
- ⁷ Journal of Online Hepatology, *Lecture: HCV viral kinetics*, (February **2011**).
- ⁸ Robert Koch Institute (RKI), *Epidemiologisches Bulletin* **2011**, Nr. 29.
- ⁹ S. M. Lynch, G. Y. Wu, *J. Clin. Trans. Hepatology* **2016**, *4*, 310-319.
- ¹⁰ Drug Bank, *Open Data Drug & Drug Target Database*, <http://www.drugbank.ca/drugs/DB00105>, November, **2011**.
- ¹¹ a) R. T. Chung, M. Gale Jr., S. J. Polyak, S. M. Lemon, T. J. Liang, J. H. Hoofnagle, *Hepatology* **2008**, *47*, 306-320; b) R. M. Friedman, S. Couteute, *Hepat. Res. Treat.* **2010**, Art. ID 323926.
- ¹² F. G. Njoroge, K. X. Chen, N. Shih, J. J. Piwinski, *Acc. Chem. Res.* **2008**, *41*, 50-59.
- ¹³ a) C. Lin, A. D. Kwong, R. B. Perni, *Inf. Disorders – Drug Targets* **2006**, *6*, 3-16; b) J. J. Kim, C. M. Culley, R. A. Mohammad, *Am. J. Health – System Pharmacy* **2012**, *1*, 19-33.
- ¹⁴ a) S. M. Lynch, G. Y. Wu, *J. Clin. Trans. Hepatology* **2016**, *4*, 310-319.
- ¹⁵ A. Majumdar, M. T. Kitson, S. K. Roberts, *Aliment Pharmacol. Ther.* **2016**, *43*, 1276-1292.
- ¹⁶ J. Zhang MD, D. Nguyen MD, K. Hu MD, *N. Am. J. Med. Sc.* **2016**, *9*, 47-54.
- ¹⁷ K. Weissman, R. Müller, *Bioorg. Med. Chem.* **2009**, *17*, 2121-2136.
- ¹⁸ H. Reichenbach, *J. Ind. Microbiol. & Biotech.* **2001**, *27*, 149-156.
- ¹⁹ S. Grabley, R. Thiericke, *Drug discovery from nature* **1999**, 149-150.
- ²⁰ H. Reichenbach, *Encyclopedia of Industrial Biology* **2010**.
- ²¹ R. Müller et al., *Nature Biotechn.* **2007**, *25*, 1281-1289.
- ²² a) K. Weissman, R. Müller, *Bioorg. Med. Chem.* **2009**, *17*, 2121-2136; b) J. Diez, J. Martinez, *Biomed Central* **2012**, *11*, 52-54.

- ²³ K. C. Nicolaou, N. Winssinger, J. Pastor, S. Ninkovic, F. Sarabia, Y. He, D. Vourloumis, Z. Yang, T. Li, P. Giannakaku, E. Hamel, *Nature* **1997**, *387*, 268-272.
- ²⁴ H. Irschik, R. Jansen, K. Gerth, G. Höfle, H. Reichenbach, *J. Antibiol.* **1987**, *40*, 7-13.
- ²⁵ R. Jansen, H. Irschik, V. Huch, D. Schummer, H. Steinmetz, M. Bock, T. Schmidt, A. Kirschning, R. Müller, *Eur. J. Org. Chem.* **2010**, 1284-1289.
- ²⁶ J. Herrmann, A. Abou Fayad, R. Müller, *Nat. Prod. Rep.* **2017**, *34*, 135-160.
- ²⁷ J. Barbier, R. Jansen, H. Irschik, S. Benson, K. Gerth, B. Böhlendorf, G. Höfle, H. Reichenbach, J. Wegner, C. Zeilinger, A. Kirschning, R. Müller, *Angew. Chem.* **2011**, *51*, 1256-1260.
- ²⁸ J. Barbier, J. Wegner, S. Benson, J. Gentzsch, T. Pietschmann, A. Kirschning, *Chem. Eur. J.* **2012**, *18*, 9083-9090.
- ²⁹ J. Gentzsch, Ch. Brohm, E. Steinmann, M. Friesland, N. Menzel, G. Vieyres, P. M. Perin, A. Frentzen, L. Kaderall, T. Pietschmann, *PLOS Pathogens* **2013**, *9*, e1003355.
- ³⁰ H. Reichenbach, G. Höfle, S. Grabley, R. Thieriecke, *Drug discovery from nature* **1999**, Springer Verlag, 149-179.
- ³¹ J. Gentzsch, B. Hinkelmann, L. Kaderali, H. Irschik, R. Jansen, F. Sasse, R. Frank, T. Pietschmann, *Antiviral Res.* **2011**, *89*, 136-148.
- ³² J. L. Nieto-Torres, C. Verdia-Baguena, C. Castano-Rodriguez, V. M. Aguilera, L. Enjuanes, *Viruses* **2015**, *7*, 3552-3573.
- ³³ K. Wang, S. Xie, B. Sun, *Biochem Biophys Acta* **2011**, 510-515.
- ³⁴ S. K. Bagal, A. D. Brown, P. J. Cox, K. Omoto, R. M. Owen, D.C. Pryde, B. Sidders, S. E. Skerratt, E. B. Stevens, R. I. Storer, N. A. Swain, *J. Med. Chem.* **2013**, *56* (3), 593-624.
- ³⁵ J. Wegner, *Diplomarbeit, Leibniz Universität Hannover*, Hannover **2008**.
- ³⁶ R. H. Spencer, D. C. Rees, *Annu. Rev. Biophys. Biomol. Struct.* **2002**, *31*, 207-233.
- ³⁷ I. M. Williamson, S. J. Alvis, J. M. East, A. G. Lee, *Cell. Mol. Life Sci.* **2003**, *60*, 1581-1590.
- ³⁸ C. Zeilinger, *FEBS Lett.* **1994**, *348*, 278-282.
- ³⁹ F. I. Valiyaveetil, Y. Zhou, R. MacKinnon, *Biochemistry* **2002**, *41*, 10771-10777.
- ⁴⁰ M. L. Renart, F. N. Barrera, M. L. Molina, J. A. Encinar, J. A. Poveda, A. M. Fernandez, J. Gomez, J. M. Gonzalez-Ros, *J. Biol. Chem.* **2006**, *281*, 29905-29915.
- ⁴¹ L. Heginbotham, M. LeMasurier, L. Kolmakova-Partensky, C. J. Miller, *Gen. Physiol.* **1999**, *114*, 551-560.
- ⁴² Carsten Zeilinger, unpublished results

- ⁴³ S. Walter, A. Bollenbach, J. Poerrbecker, S. Pfaender, R. J. P. Brown, G. Vieyres, C. Scott, R. Foster, A. Kumar, N. Zitzmann, S. Griffin, F. Penin, T. Pietschmann, E. Steinmann, J. *Virology* **2016**, 5075-5089.
- ⁴⁴ T. L. Foster, G. S. Thompson, A. P. Kalverda, J. Kankanala, M. Bentham, L. F. Wetherhill, J. Thompson, A. M. Baker, D. Clarke, M. Noerenberg, A. R. Pearson, D. J. Rowlands, S. W. Homans, M. Harris, R. Foster, S. Griffin, *Hepatology* **2014**, *59*, 408-422.
- ⁴⁵ V. Madan, R. Bartenschlager, *Viruses* **2015**, *7*, 4461 – 4481.
- ⁴⁶ P. Luik, C. Chew, J. Aittoniemi, J. Chang, P. Wentworth, R. A. Dwek, P. C. Biggin, C. Venien-Bryan, N. Zitzmann, *PNAS* **2009**, *106*, 12712-12716.
- ⁴⁷ D. Clarke, S. Griffin, L. Beales, C. S. Gelais, S. Burgess, M. Harris, D. Rowlands, *J. Biol. Chem.* **2006**, *281*, 37057-37068.
- ⁴⁸ D. E. Chandler, F. Penin, K. Schulten, C. Chipot, *PLoS Comput. Biol.* **2012**, *8*, 1-10.
- ⁴⁹ E. Steinmann, T. Pietschmann, *Viruses* **2010**, *2*, 2078-2095.
- ⁵⁰ L. W. Meredith, N. Zitzmann, J. A. McKeating, *Antiviral Research* **2013**, *100*, 636-639.
- ⁵¹ C. StGelais, T. L. Foster, M. Verow, E. Atkins, C. W. G. Fishwick, D. Rowlands, M. Harris, S. Griffin, *J. Virology* **2009**, *83*, 7970 – 7981.
- ⁵² C. StGelais, T. J. Tuthill, D. S. Clarke, D. J. Rowlands, M. Harris, S. Griffin, *Antivir. Res.* **2007**, *76*, 48-58.
- ⁵³ Q. Du, S. Wang, D. Chen, J. Meng, R. Huang, *PLOS ONE* **2014**, *9*, 1-7.
- ⁵⁴ C. A. Luscombe, Z. Huang, M. G. Murray, M. Miller, J. Wilkinson, G. D. Ewart, *Antivir. Res.* **2010**, *86*, 144-153.
- ⁵⁵ S. Griffin, C. StGelais, A. M. Owsiake, A. H. Patel, D. Rowlands, M. Harris, *Hepatology* **2008**, *48*, 1779-1790.
- ⁵⁶ J. Shaw, R. Gosein, M. M. Kalita, T. L. Foster, J. Kankanala, D. Ram Mahato, C. Scott, B. J. King, E. Brown, M. J. Bentham, L. Wetherill, A. Bloy, A. Samson, M. Harris, J. Mankonri, D. Rowlands, A. Macdonald, A. W. Tarr, W. B. Fischer, R. Foster, S. Griffin, *BioRxiv* **2018**, preprint synth./discussion.
- ⁵⁷ A. Abiko, J. Liu, S. Masamune, *J. Am. Chem. Soc.* **1997**, *119*, 10, 2586-2587.
- ⁵⁸ a) E. Fujita, Y. Nagao, *Adv. Heterocycl. Chem.* **1989**, *45*, 1-36; b) Y. Nagao, T. Kamagai, Y. Nagase, S. Tamai, Y. Ivone, M. Shiro, *J. Org. Chem.* **1992**, *57*, 4232.
- ⁵⁹ a) D. Seyferth, R. S. Marmor, P. Hilbert, *J. Org. Chem.* **1971**, *36*, 10, 1379-1386; b) J. C. Gibert, U. Weerasooriya, *J. Org. Chem.* **1982**, *47*, 10, 1837-1845.
- ⁶⁰ B. S. Kwon, J. Tae, *Heterocycles* **2004**, *62*, 137-141.
- ⁶¹ J. A. Frick, J. B. Klassen, A. Bathe, J. M. Abramson, H. Rapoport, *Synthesis* **1992**, 621-623.

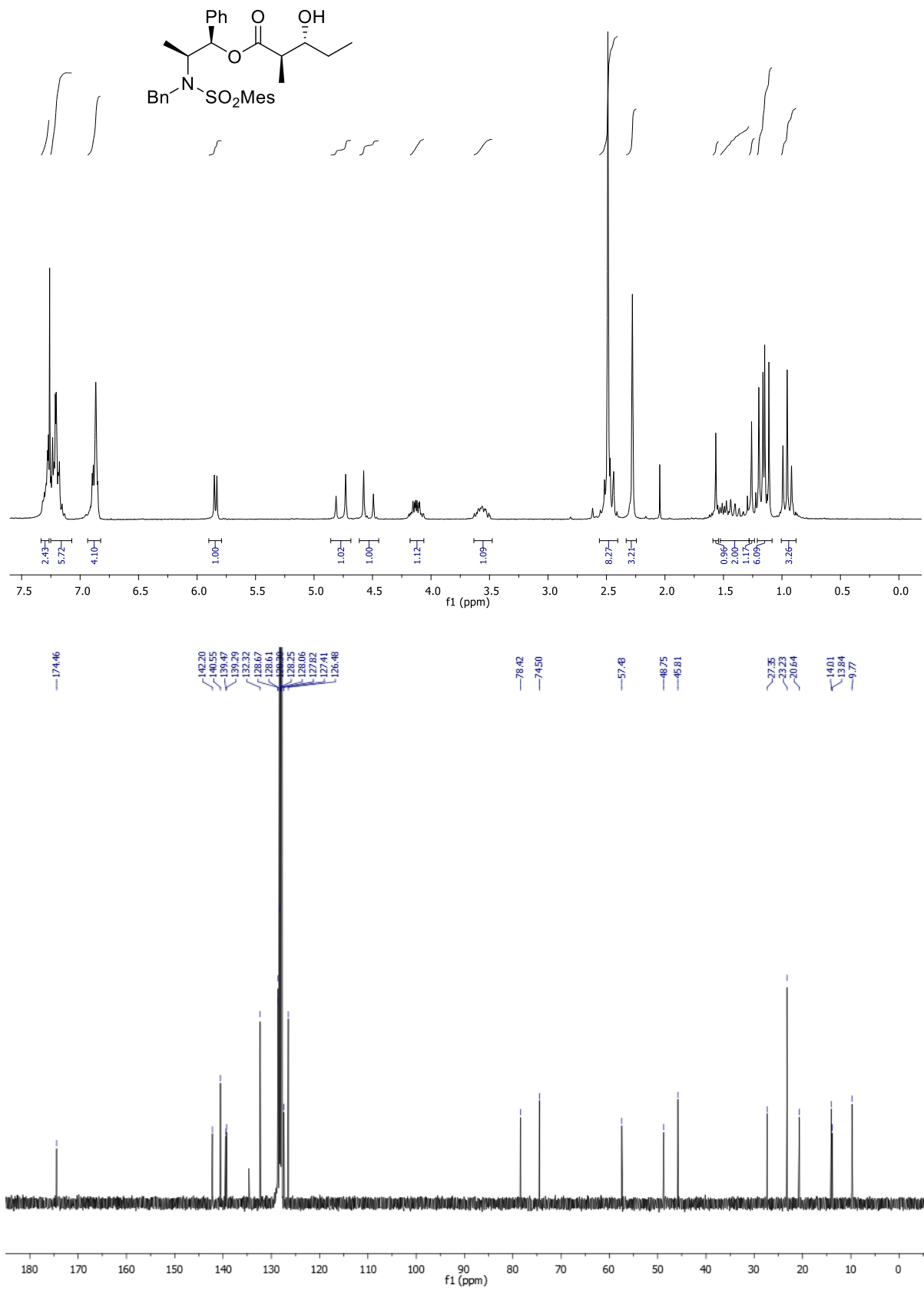
- ⁶² K. Mori, M. Ikunaka, *Tetrahedron* **1984**, *40*, 3471-3479.
- ⁶³ S. Benson, *Diplomarbeit, Leibniz Universität Hannover*, Hannover, **2007**.
- ⁶⁴ S. V. Ley, A. Priour, *Eur. J. Org. Chem.* **2002**, 3995-4004.
- ⁶⁵ Z. Kaleta, B. T Makowski, T. Soos, R. Dembinski, *Org. Lett.* **2006**, *8*, 1625-1628.
- ⁶⁶ S. Müller, B. Liepold, G. J. Roth, H. J. Bestmann, *Synlett.* **1996**, 521-522.
- ⁶⁷ a) J. Schwartz, J. A. Labinger, *Angew. Chem. Int. Ed.* **2003**, *15*, 330-340; b) D. W. Hart, J. Schwartz, *Am. Chem. Soc.* **1974**, *96*, 8115-8116; c) D. W. Hart, T. F. Blackburn, J. Schwartz, *J. Am. Chem. Soc.* **1975**, *97*, 679-680.
- ⁶⁸ a) K. Tamao, K. Sumitani, M. Kumada, *J. Am. Chem. Soc.* **1972**, *94*, 4374; b) M. Tamura, J. K. Kochi, *J. Am. Chem. Soc.* **1971**, *93*, 1487; c) R. S. Smith, J. K. Kochi, *J. Org. Chem.* **1975**, *40*, 599.
- ⁶⁹ D. B. Dess, J. C. Martin, *J. Org. Chem.* **1983**, *48*, 4155-4156.
- ⁷⁰ C. M. Binder, B. Singaram, *Org. Prep. & Proc. Int.* **2011**, *43*, 139-208.
- ⁷¹ P. V. Ramachandran, A. Srivastava, D. Hazra, *Org. Lett.* **2007**, *9*, 157-160.
- ⁷² D. A. Evans, M. J. Dart, J. L. Duffy, M. G. Yang, *J. Am. Chem. Soc.* **1996**, *118*, 4322-4343.
- ⁷³ a) P. Wipf, W. Xu, *Tetrahedron Lett.* **1994**, *35*, 5197; b) P. Wipf, W. Xu, *Org. Synth.* **1996**, *74*, 205.
- ⁷⁴ P. Wipf, R. Seth, *J. Org. Chem.* **1998**, *63*, 19, 6454-6455.
- ⁷⁵ a) W. Eschweiler, *Berichte der deutschen chemischen Gesellschaft* **1905**, *38*, 1, 880-882; b) H. T. Clarke, H. B. Gillespie, S. Z. Weisshaus, *J. Am. Chem. Soc.* **1933**, *55*, 11, 4571-4587.
- ⁷⁶ R. Roudeau, D. G. Pardo, J. Cossy, *Tetrahedron* **2006**, *62*, 2388-2394.
- ⁷⁷ J. Cossy, *Chem. Rec.* **2005**, *5*, 70-80.
- ⁷⁸ J. Cossy, C. Dumas, P. Michel, D. G. Pardo, *Tetrahedron Lett.* **1995**, *36*, 4, 549-552.
- ⁷⁹ A. Cochi, D. G. Pardo, J. Cossy, *Eur. J. Org. Chem.* **2012**, 2023-2040.
- ⁸⁰ H. C. Brown, S. Krishnamurthy, T. P. Stocky, *J. Org. Chem.* **1973**, *38*, 16, 2786-2792.
- ⁸¹ L. Pu, H-B. Yu, *Chem. Rev.* **2001**, *101*, 757-824.
- ⁸² K. C. Nicolaou, D. Rhoades, Y. Wang, R. Bai, E. Hamel, M. Aujay, J. Sandoval, J. Gavrilyuk, *J. Am. Chem. Soc.* **2017**, *139*, 7318-7334.
- ⁸³ K. C. Nicolaou, W. Marsch, *Patent Nr. WO2018191394*.
- ⁸⁴ K. Sonogashira, *J. Organometallic Chem.* **2002**, *653*, 46-49.
- ⁸⁵ E. N. Jacobsen, I. Marko, W. S. Mungall, G. Schroeder, K. B. Sharpless, *J. Am. Chem. Soc.* **1988**, *110*, 6, 1968-1970.
- ⁸⁶ H. C. Kolb, M. S. VanNienwenhze, K. B. Sharpless, *Chem. Rev.* **1994**, *94*, 8, 2483-2547.
- ⁸⁷ C. Wang, Z. Xi, *Chem. Soc. Rev.* **2007**, *36*, 1395-1406.

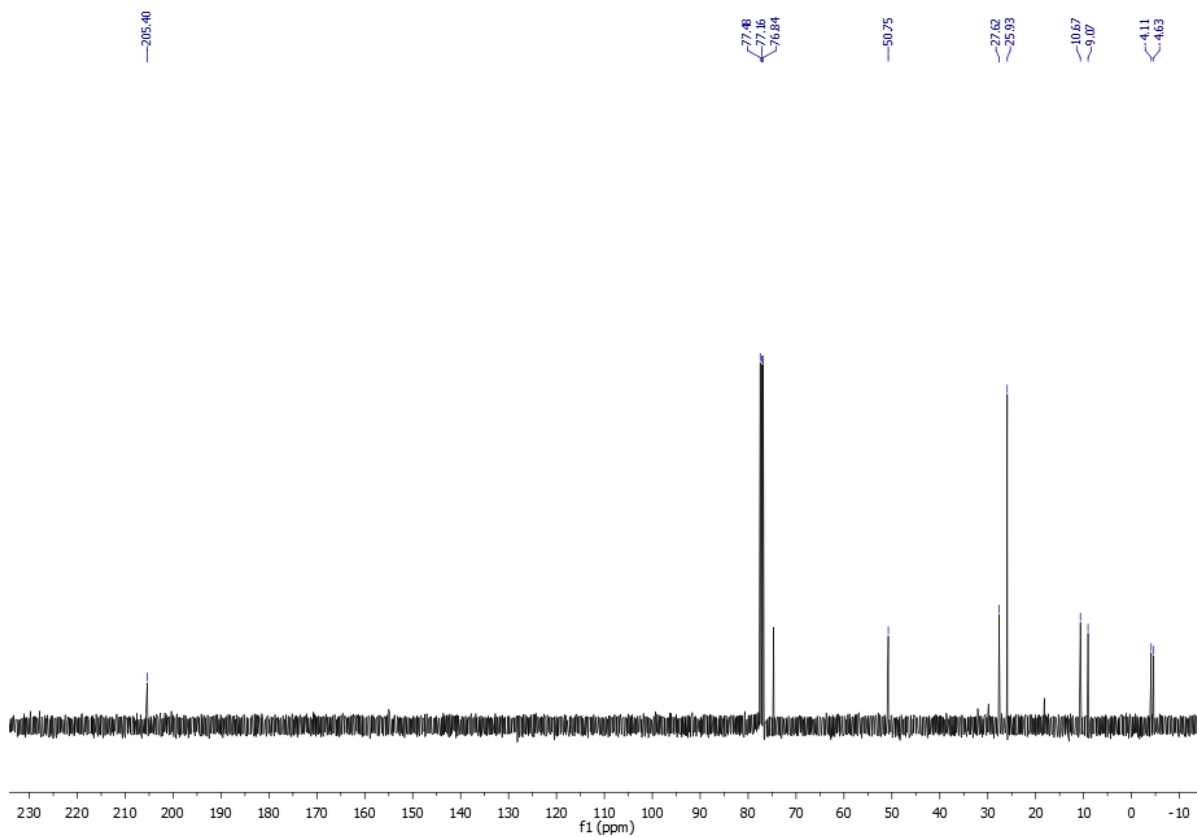
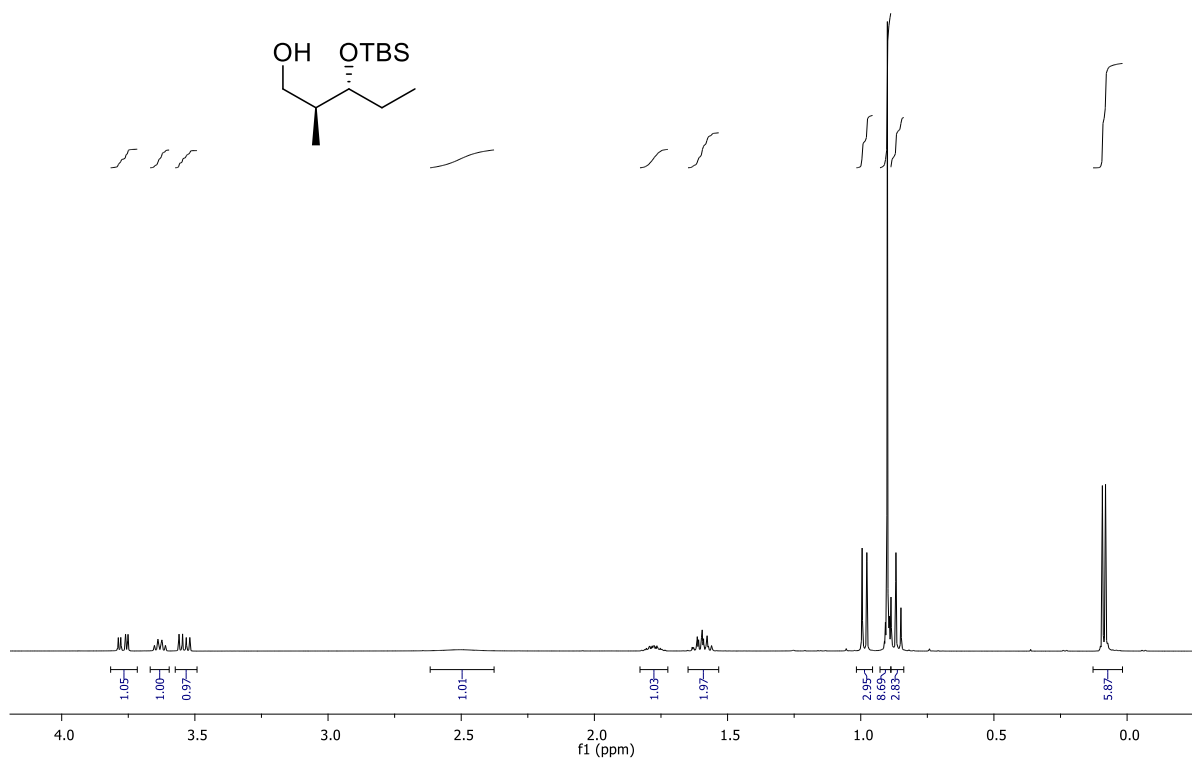
- ⁸⁸ H. Maeta, T. Hashimoto, T. Hasegawa, K. Sozuki, *Tetrahedron Lett.* **1992**, *40*, 5965-5968.
- ⁸⁹ J. Hermans *Protokol zum Forschungspraktikum, Hannover*, **2010**.
- ⁹⁰ a) K. Omura, D. Swern, *Tetrahedron* **1978**, *34*, 11, 1651-1660; b) A. J. Mancuso, D. S. Brownfain, D. Swern, *J. Org. Chem.* **1979**, *44*, 23, 4148-4150.
- ⁹¹ J. R. Parikh, W. V. E. Doering, *J. Am. Chem. Soc.* **1967**, *89*, 21, 5505-5507.
- ⁹² R. A. Sheldon, I. W. C. E. Arends, G. J. T. Brink, A. Dijkman, *Acc. Chem. Res.* **2002**, *35*, 774-781.
- ⁹³ S. V. Ley, J. Normann, W. P. Griffith, S. P. Marsden, *Synthesis*, **1994**, 639-665.
- ⁹⁴ E. J. Corey, J. W. Suggs, *Tetrahedron Lett.* **1975**, *16*, 31, 2647-2650.
- ⁹⁵ S. G. Wierschke, J. Chandrasekhar, W. L. Jorgensen, *J. Am. Chem. Soc.* **1985**, *107*, 6, 1496-1500.
- ⁹⁶ C. Najera, M. Yus, *Curr. Org. Chem.* **2003**, *7*, 867-926.
- ⁹⁷ a) A. O. King, N. Okukado, E. Negishi, *J. C. S. Chem. Comm.* **1977**, 683-684; b) D. Haas, J. M. Hamann, R. Greiner, P. Knochel, *ACS Catal.* **2016**, *6*, 1540-1552.
- ⁹⁸ D. R. Armstrong, P. Garcia-Alvarez, A. R. Kennedy, R. E. Mulvey, J. A. Parkinson, *Angew. Chem. Int. Ed.* **2010**, *49*, 3185-3188.
- ⁹⁹ R. L-Y Bao, R. Zhao, L. Shi, *Chem. Comm.* **2015**, *51*, 6884-6900.
- ¹⁰⁰ Y. Ie, *PCT Int. Appl. Sept.* **2011**, Patent Nr. WO2011108646.
- ¹⁰¹ E. L. Stangelang, T. Sammkia, *J. Org. Chem.* **2004**, *69*, 7, 2381-2385.
- ¹⁰² a) A. Vaitiekunas, F. F. Nord, *J. Am. Chem. Soc.* **1953**, *75*, 1764-1768; b) M. Schlosser, *Angew. Chem. Int. Ed.* **2005**, *44*, 376-393.
- ¹⁰³ M. Schürch, M. Spina, A. Khan, M. D. Mihovilovic, P. Stanetty, *Chem. Soc. Rev.* **2007**, *36*, 1046-1057.
- ¹⁰⁴ a) J. K. Stille, D. Milstein, *J. Am. Chem. Soc.* **1978**, *100*, 3636; b) J. K. Stille, D. Milstein, *J. Am. Chem. Soc.* **1979**, *101*, 4992.
- ¹⁰⁵ S. P. H. Mee, V. Lee, J. E. Baldwin, *Chem. Eur. J.* **2005**, *11*, 3294-3308.
- ¹⁰⁶ A. Suzuki, N. Miyaura, K. Yamada, *Tetrahedron Lett.* **1979**, *20*, 3437
- ¹⁰⁷ O. M. Ogbay, N. C. Warner, D. J. O'Leary, R. H. Grubbs, *Chem. Soc. Rev.* **2018**, *47*, 4510-4544.
- ¹⁰⁸ R. Appel, *Angew. Chem. Int. Ed.* **1975**, *14*, 12, 801-811.
- ¹⁰⁹ R. W. Sabuis Ph. D., *8-Hydroxypyrene-1,3,6-trisulfonic acid trisodium salt (HPTS)*, Chapter 90, first published 20. Feb. **2015**.
- ¹¹⁰ S. Bransburg-Zabary, E. Nachliel, M. Gutman, *J. Biophys.* **2002**, *83*, 6, 3001-3011.
- ¹¹¹ C. I. Trigoso, J. Espada, J. C. Stockert, *Histochem. Cell. Biol.* **1995**, *104*, 1, 69-73.

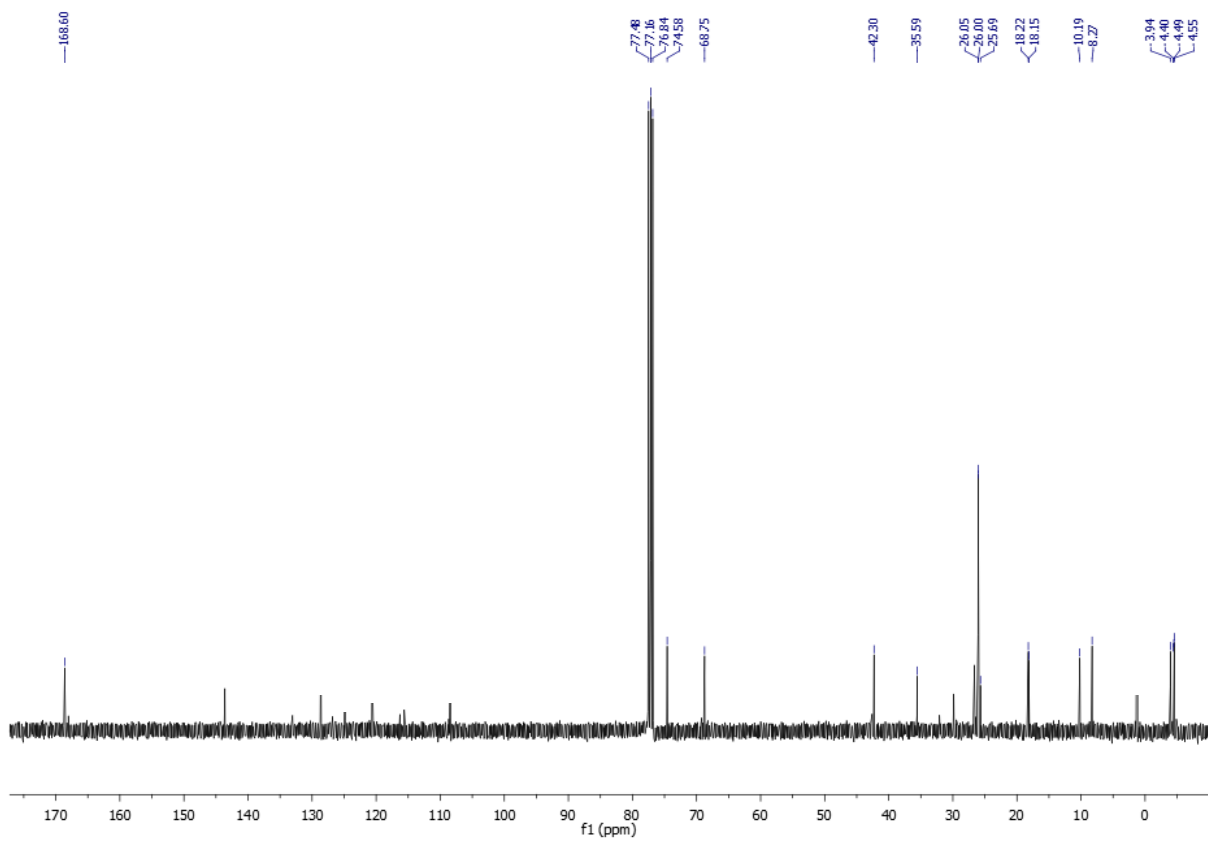
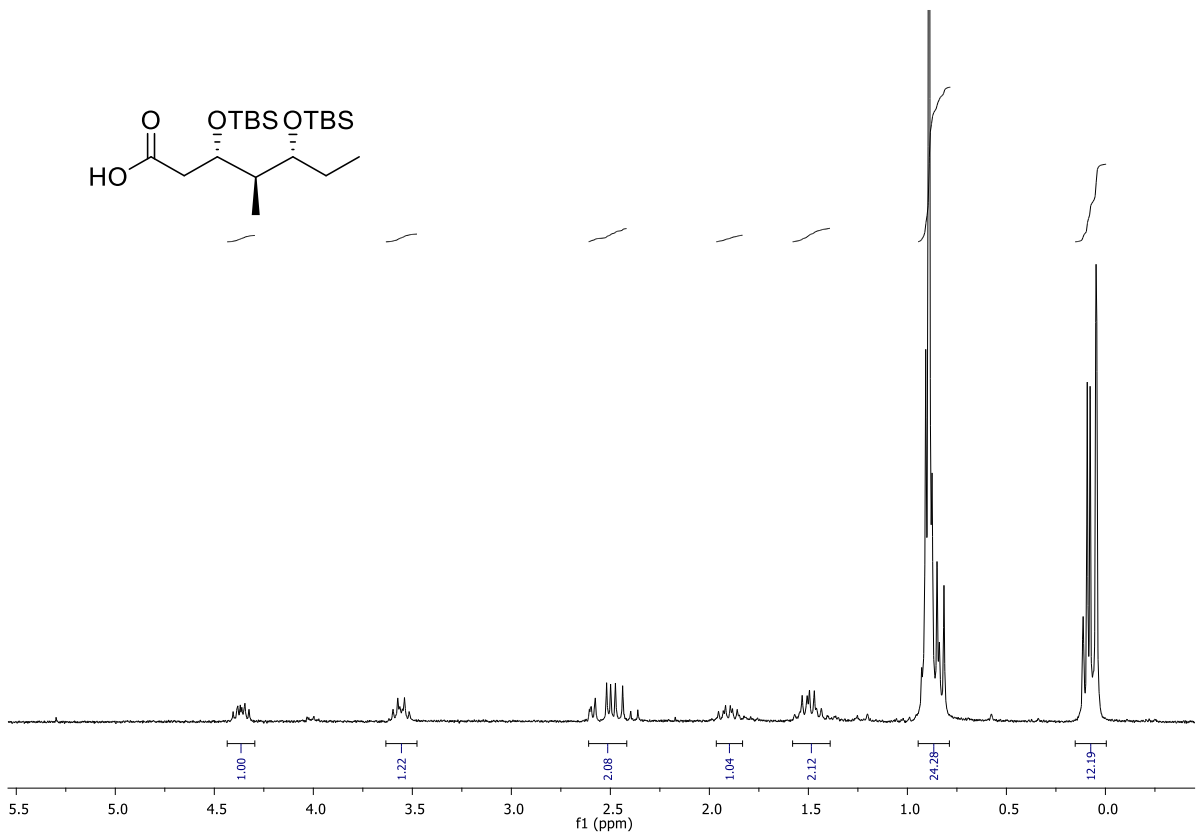
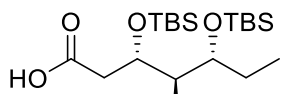
- ¹¹² J. E. Melanson, C. A. Boulet, C. A. Lucy, *Anal. Chem.* **2001**, *73*, 8, 1809-1813.
- ¹¹³ J. Han, K. Burgess, *Chem. Rev.* **2010**, *110*, 2709-2728.
- ¹¹⁴ B. Alberts, A. Johnson, J. Lewis, *Molecular Biology of the Cell*, 4th edition, **2002**, Chapter: *Ion channels and the electrical properties of membranes.*
- ¹¹⁵ V. Sriram, C. T. Rhodes, *Pharmaceut. Acta Helvet.* **1995**, *70*, 95-111.
- ¹¹⁶ A. Laouini, C. Jaafar-Maalej, I. Limayem-Blouza, S. Sfar, C. Charcosset, H. Fessi, *J. Colloid Sc. Biotech.* **2012**, *1*, 147-168.
- ¹¹⁷ U. Mihm, N. Grigorian, C. Welsch, E. Hermann, B. Kronenberger, G. Tenber, M. Wagner, W. P. Hofmann, M. Albrecht, T. Lengauer, S. Zenzem, C. Sarrazin *Antivir. Ther.* **2006**, *11*, 507-519.
- ¹¹⁸ a) E. Steinmann, T. Whitfield, S. Kallis, R. A. Dwek, N. Zitzmann, T. Pietschmann, R. Bartenschlager, *Hepatology* **2007**, *46*, 330-338; b) C. StGelais, T. L. Foster, M. Verow, E. Atkins, C. W. G. Fishwick, D. Rowlands, M. Harris, S. Griffin, *J. Virol.* **2009**, *83*, 16, 7970-7981.
- ¹¹⁹ J. P. Zoeteweyj, B. Van De Water, H. J. De Bout, J. F. Nagelkerke, *Biochem. J.* **1994**, *299*, 539-543.
- ¹²⁰ X. Zhou, F. Su, Y. Tian, C. Youngbull, R. H. Johnson, D. R. Meldrum, *J. Am. Chem. Soc.* **2011**, *133*, 46, 18530-18533.
- ¹²¹ F. Gomez-Lagunas, *J. Physiol.* **2010**, *588*, 2691-1706.
- ¹²² S. Wang, M. J. Morales, Y.-J. Qu, G. C. L. Bett, H. C. Strauss, R. L. Rasmussen, *J. Physiol.* **2003**, *546*, 387-401.
- ¹²³ N. Calland, J. Dubuisson, Y. Ronille, K. Seron, *Viruses* **2012**, *4*, 2197-2217.
- ¹²⁴ a) P. Intharathap, C. Laohppongspaisan, T. Rungrotmongki, A. Loisuangsin, M. Malaisree, P. Decha, D. Aruksakunwong, K. Chuenpennit, N. Kaiyawet, P. Sompornpisut, S. Pianwauit, S. Hannougbua, *J. Mol. Graph. Model* **2008**, *27*, 342-348; b) R. Dolin, R. C. Reichman, H. P. Madore, R. Maynard, P. N. Linton, J. Webber-Jones, *New Engl. J. Med.* **1982**, *307*, 580-584.
- ¹²⁵ P. Albert, *Optimierung eines optischen Testverfahrens zur biophysikalischen Analyse der Ionenkanalfunktion, Bachelorarbeit, Hannover*, **2014**.
- ¹²⁶ K. C. Nicolaou, D. Rhoades, Y. Wang, R. Bai, E. Hamel, M. Aujay, J. Sandoval, J. Gavrilynk, *J. Am. Chem. Soc.* **2017**, *139*, 7318-7334.
- ¹²⁷ M. B. Gopinathan, C. Jin, K. S. Rehder, *Synthesis* **2009**, *12*, 1979-1982.
- ¹²⁸ L. Yan, J. P. Morken, *Org. Lett.* **2019**, *21*, 3760-3763.
- ¹²⁹ W. Yan, Z. Li, Y. Kishi, *J. Am. Chem. Soc.* **2015**, *137*, 6219-6225.

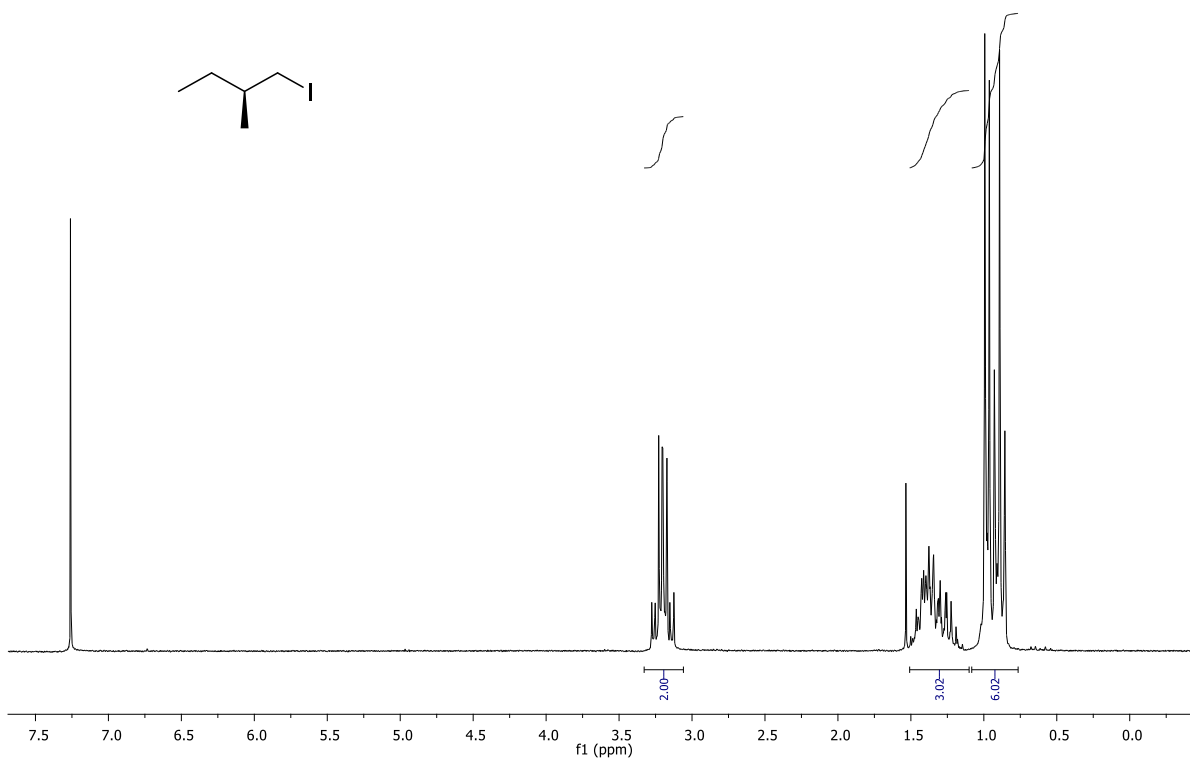
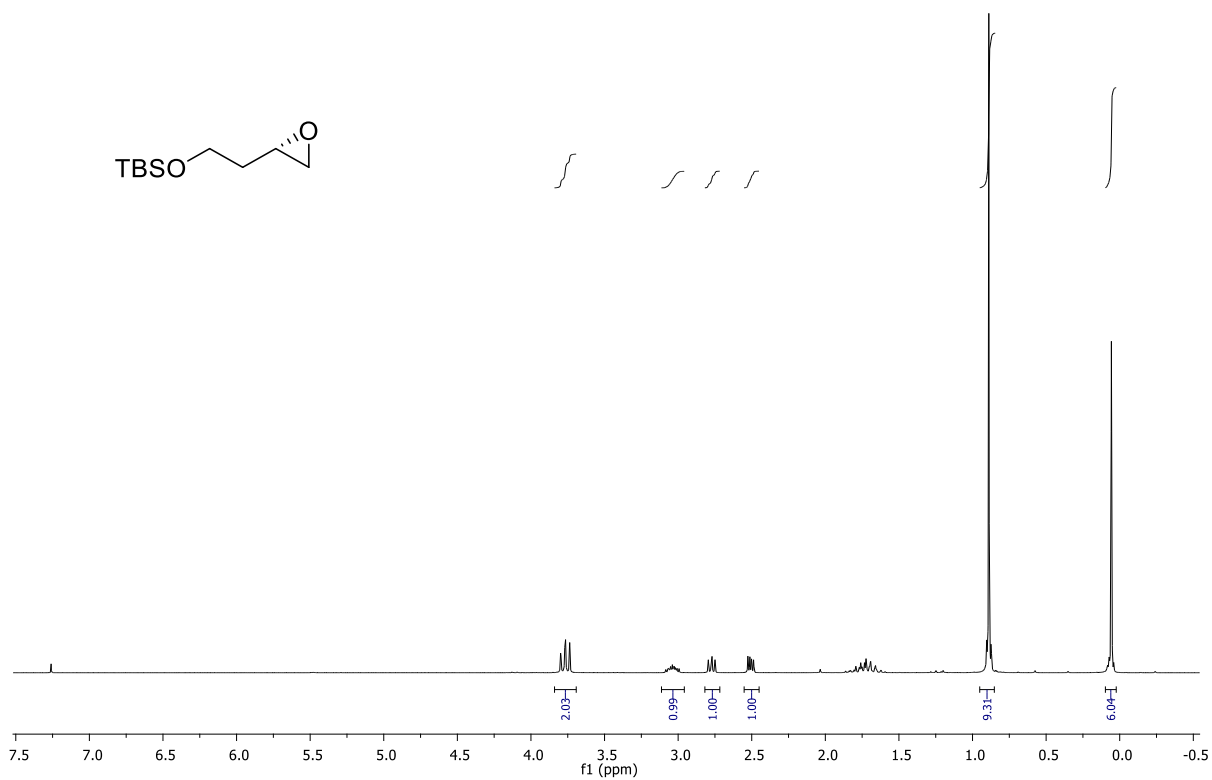
- ¹³⁰ S. Takahashi, Y. Hongo, N. Ogawa, H. Koshino, T. Nakata, *J. Org. Chem.* **2006**, *71*, 6305-6308.
- ¹³¹ P. Albert, *Diplomarbeit*, Leibniz Universität Hannover, **2014**.
- ¹³² J. R. Mohring, P. J. Vreede, S. C. Schultz, C. A. Fierke, *J. Org. Chem.* **1981**, *23*, 4655-4658.
- ¹³³ R. G. Hofstraat, J. Lange, H. W. Scheeren, R. J. F. Nivard, *J. Chem. Soc.* **1988**, 2315-2322.
- ¹³⁴ G. Pattenden, M. A. Gonzalez, P. B. Little, D. S. Millan, A. T. Plowright, J. A. Tornos, T. Ye, *Org. Biomol. Chem.* **2003**, *1*, 4173-4208.
- ¹³⁵ L. C. Diaz, P. R. R. Meira, *J. Org. Chem.* **2005**, *12*, 4762-4773.
- ¹³⁶ A. M. Schelke, V. Rawat, G. Suryavanshi, A. Sudalai, *Tetrahedron: Asymmetry* **2012**, 1534-1541.
- ¹³⁷ D. Ramesh, S. Rajaram, P. Prabhakar, U. Ramulu, D. K. Reddy, Y. Venkateswarlu, *Helvetica Chimica Acta* **2011**, *94*, 7, 1226-1233.
- ¹³⁸ L. Maram, C. G. Kumar, Y. Poornachandra, B. Das, *Tetrahedron Lett.* **2015**, *56*, 31, 4631-4633.
- ¹³⁹ J. Barbier, *Doktorarbeit*, Leibniz Universität Hannover, **2011**

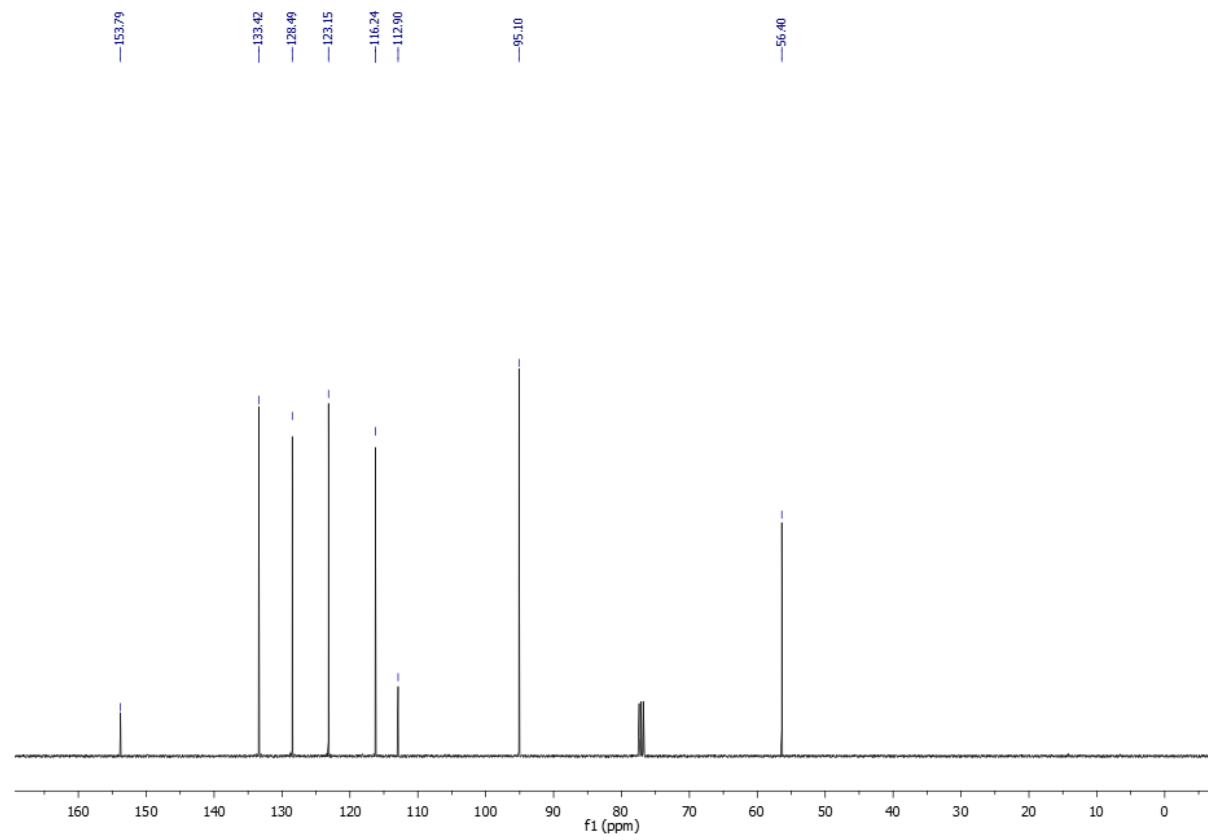
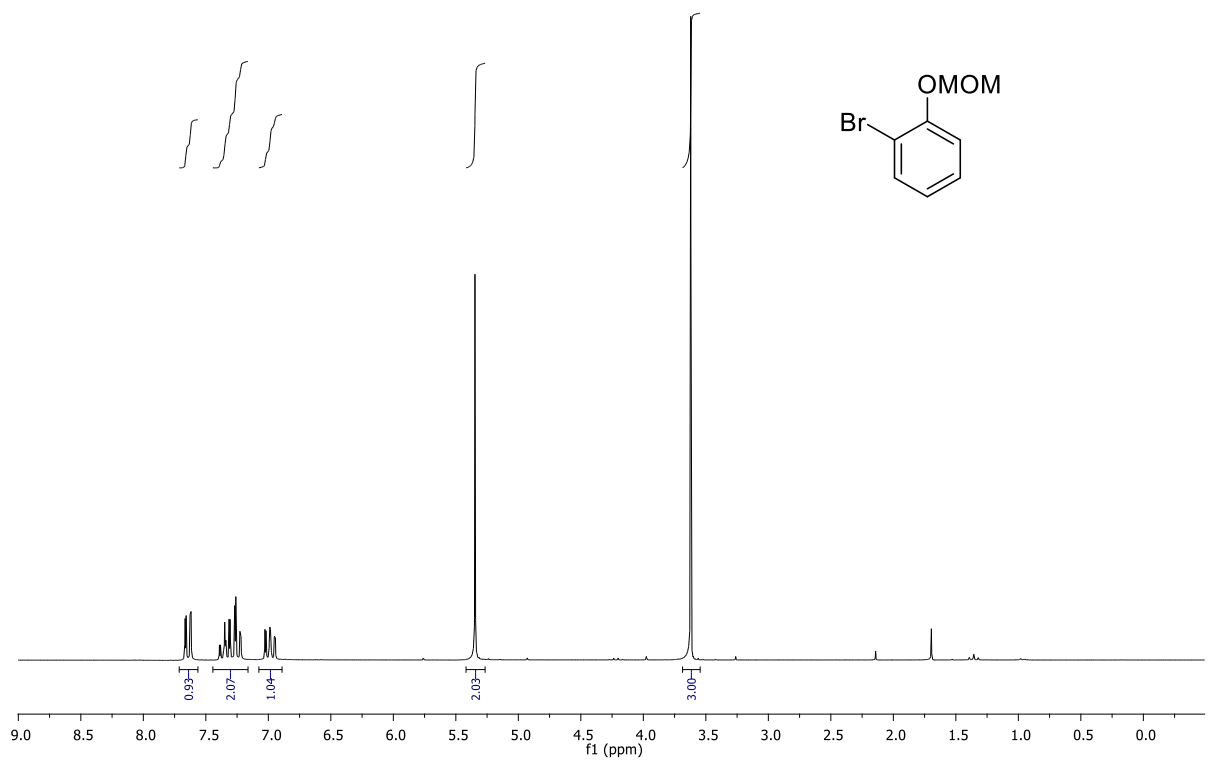
10. Appendix

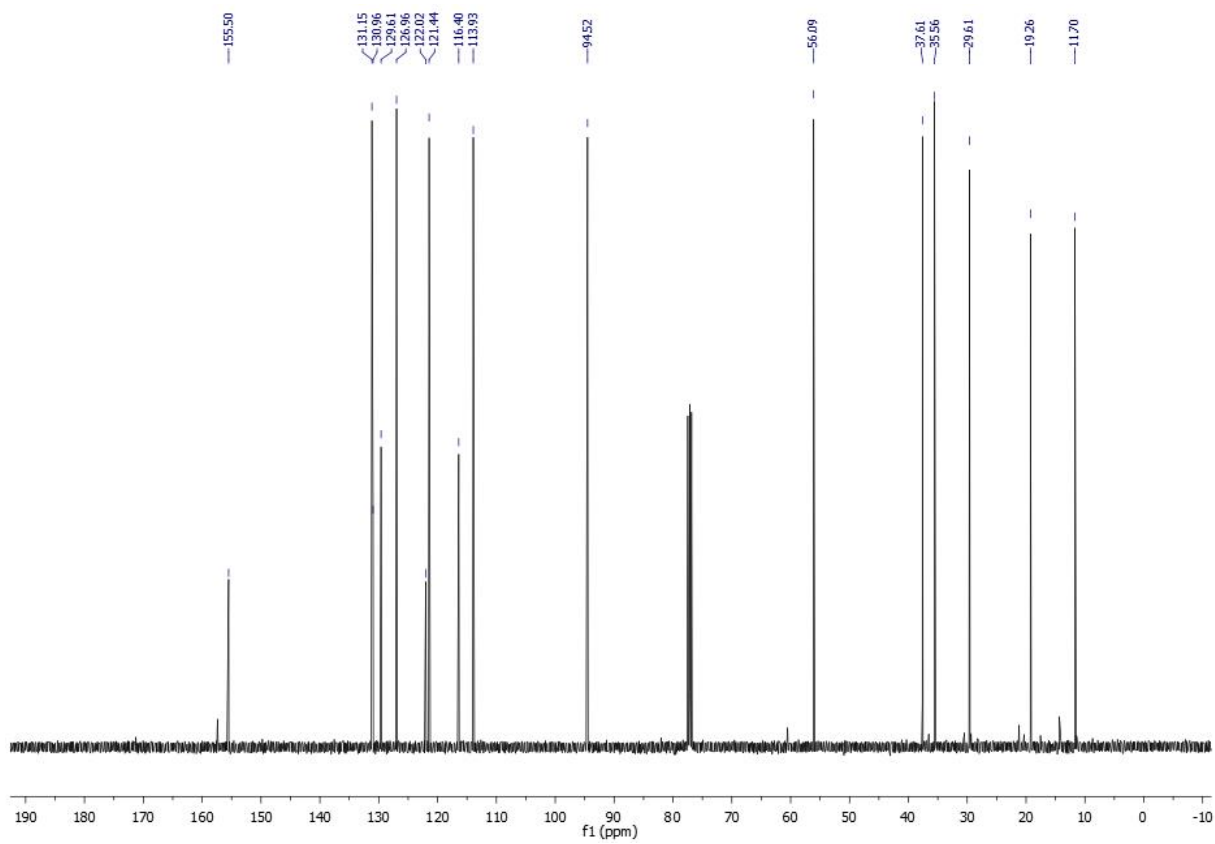
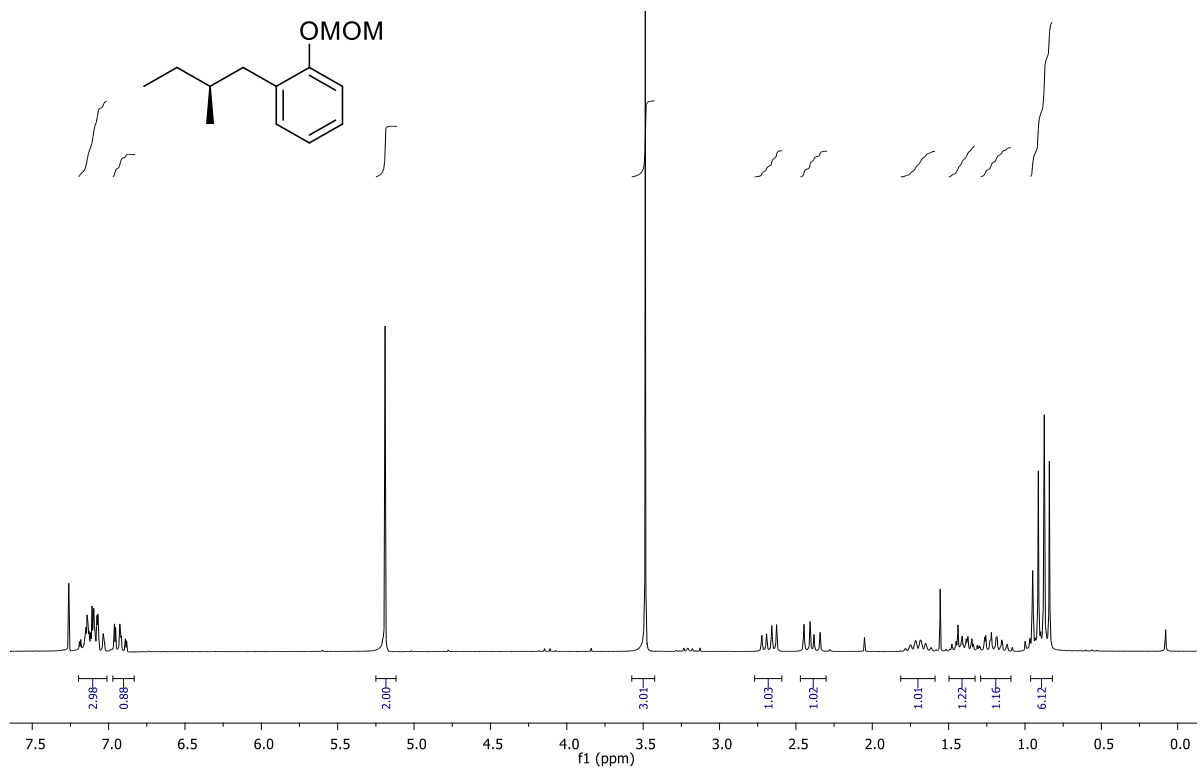


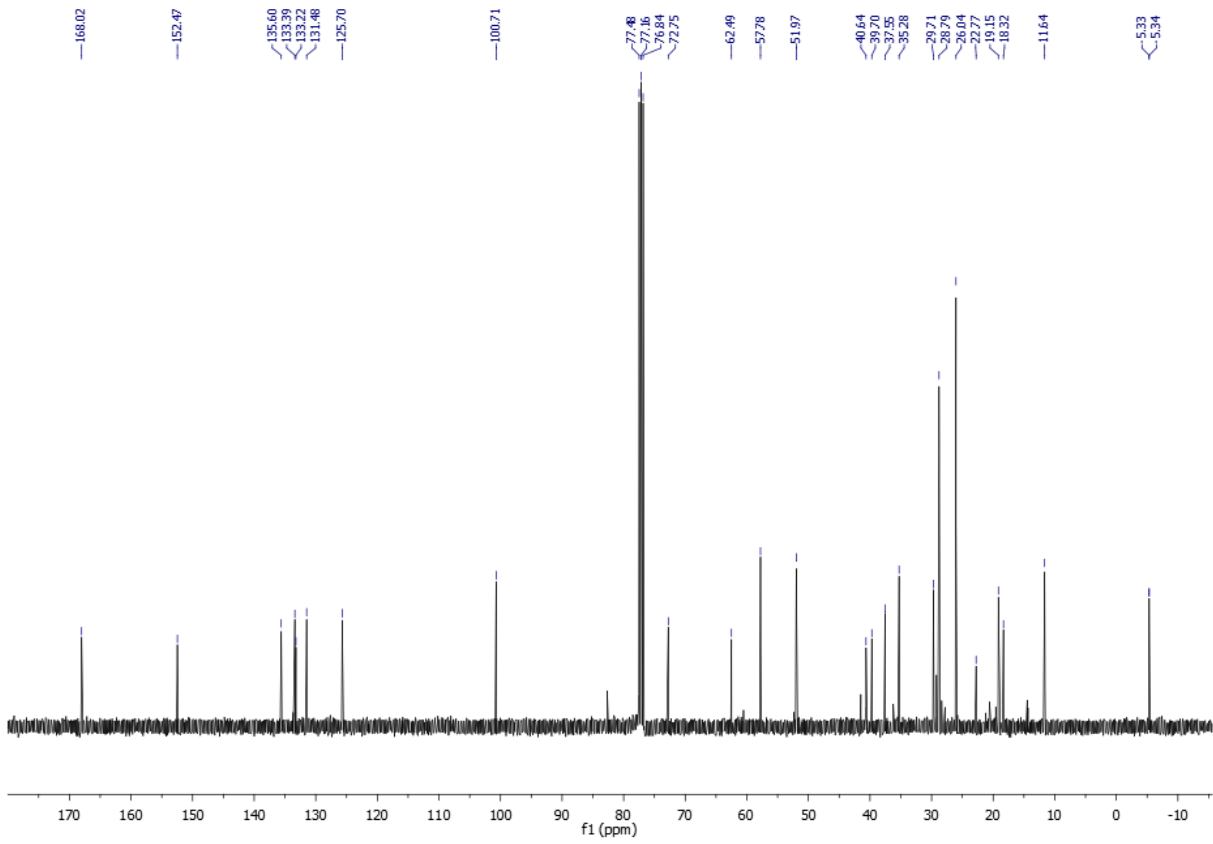
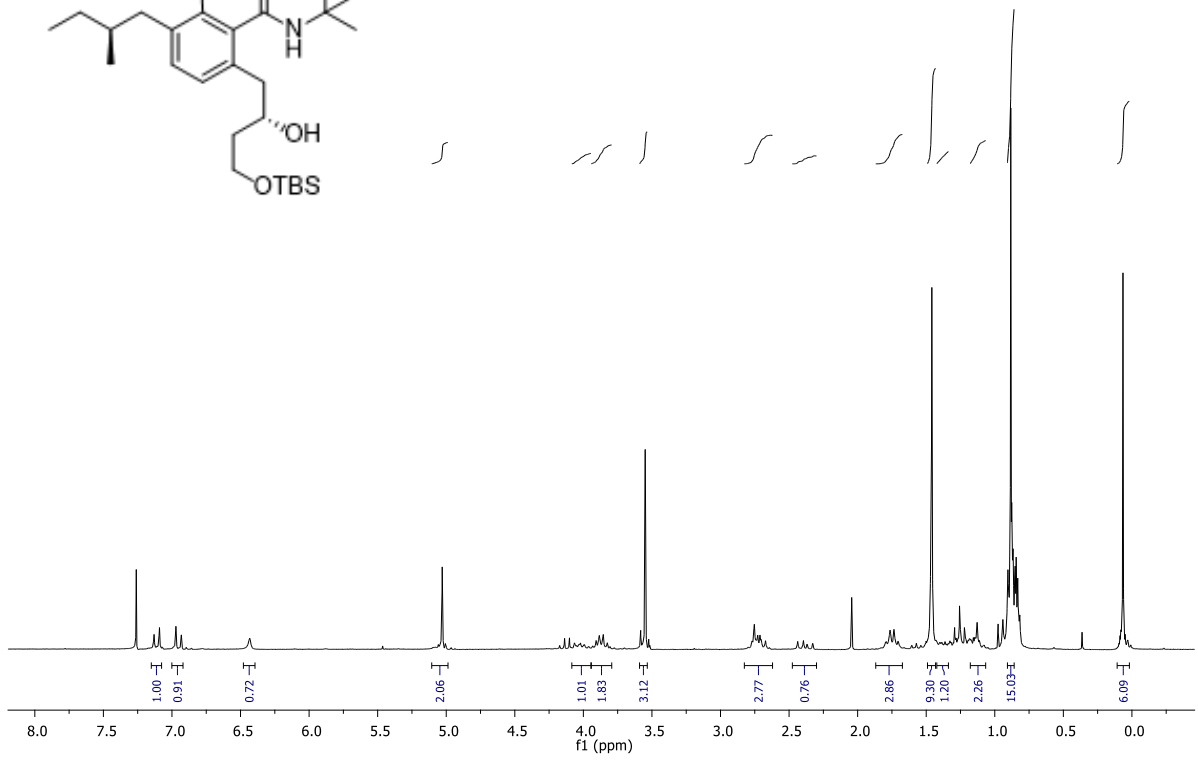
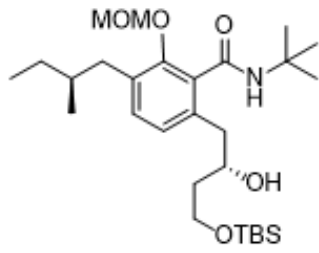


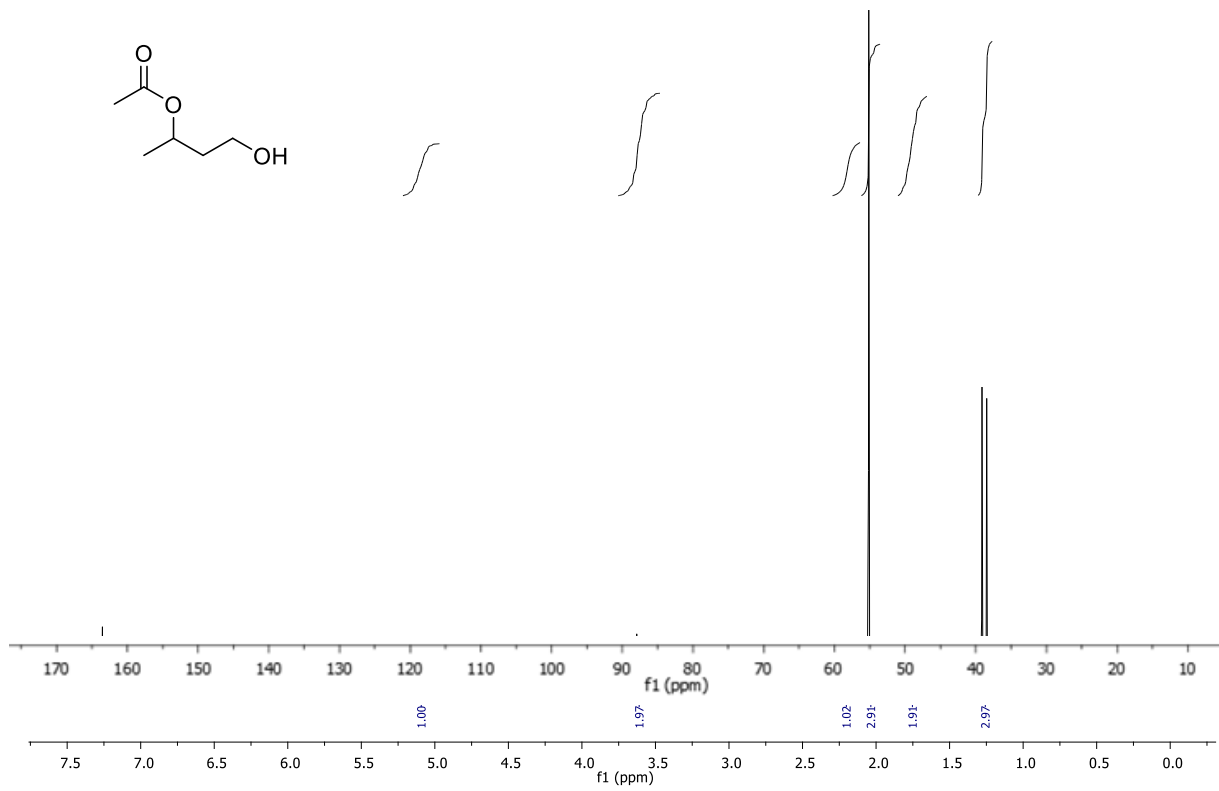
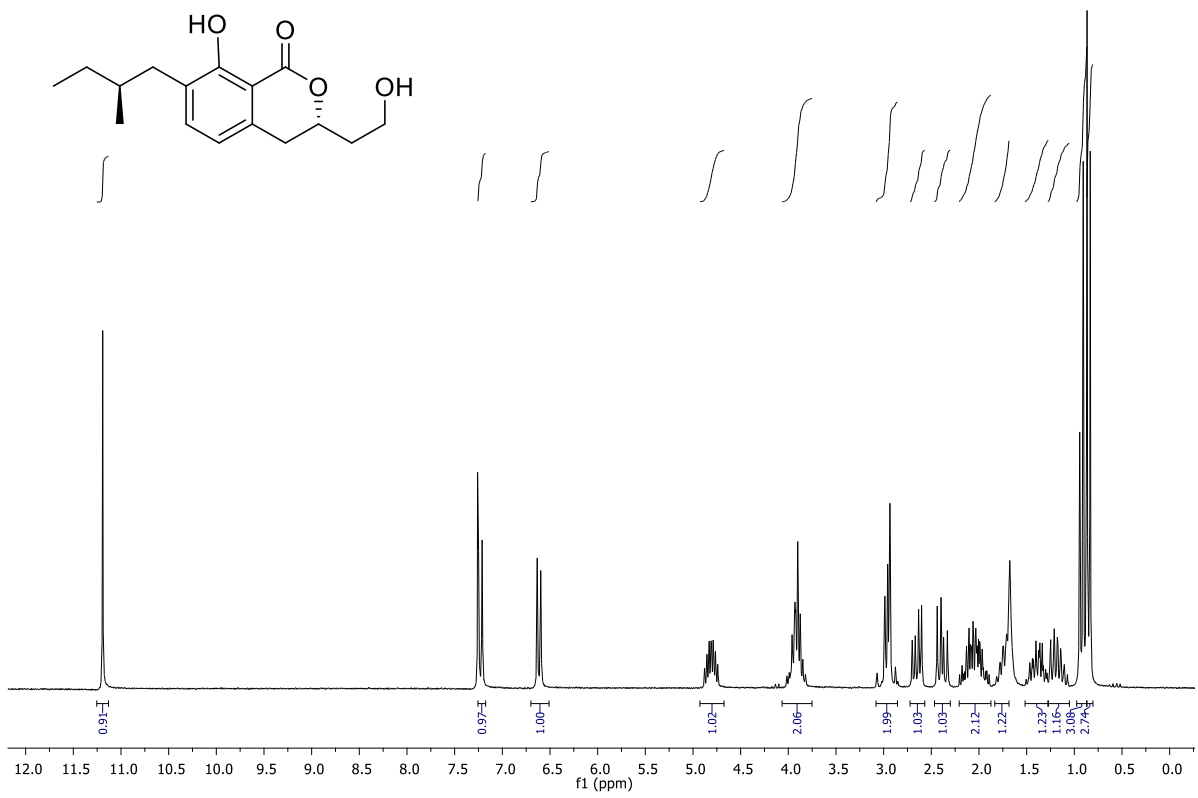


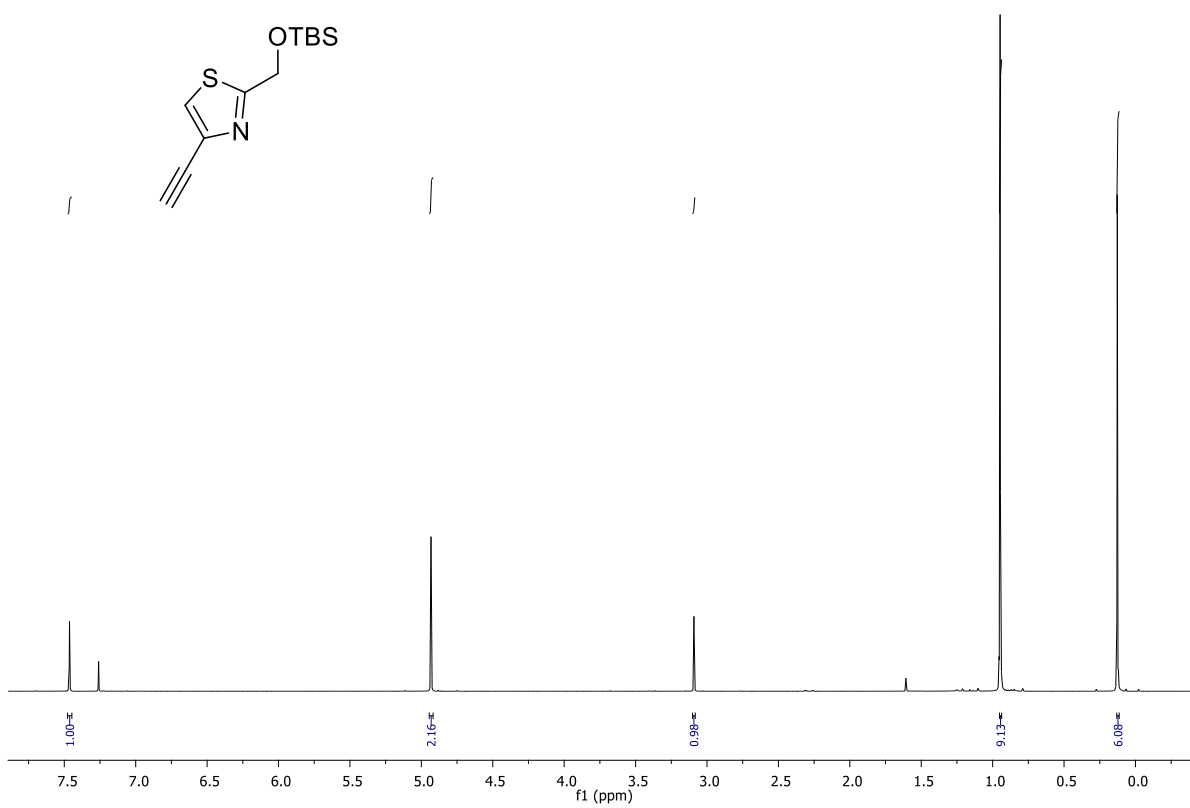
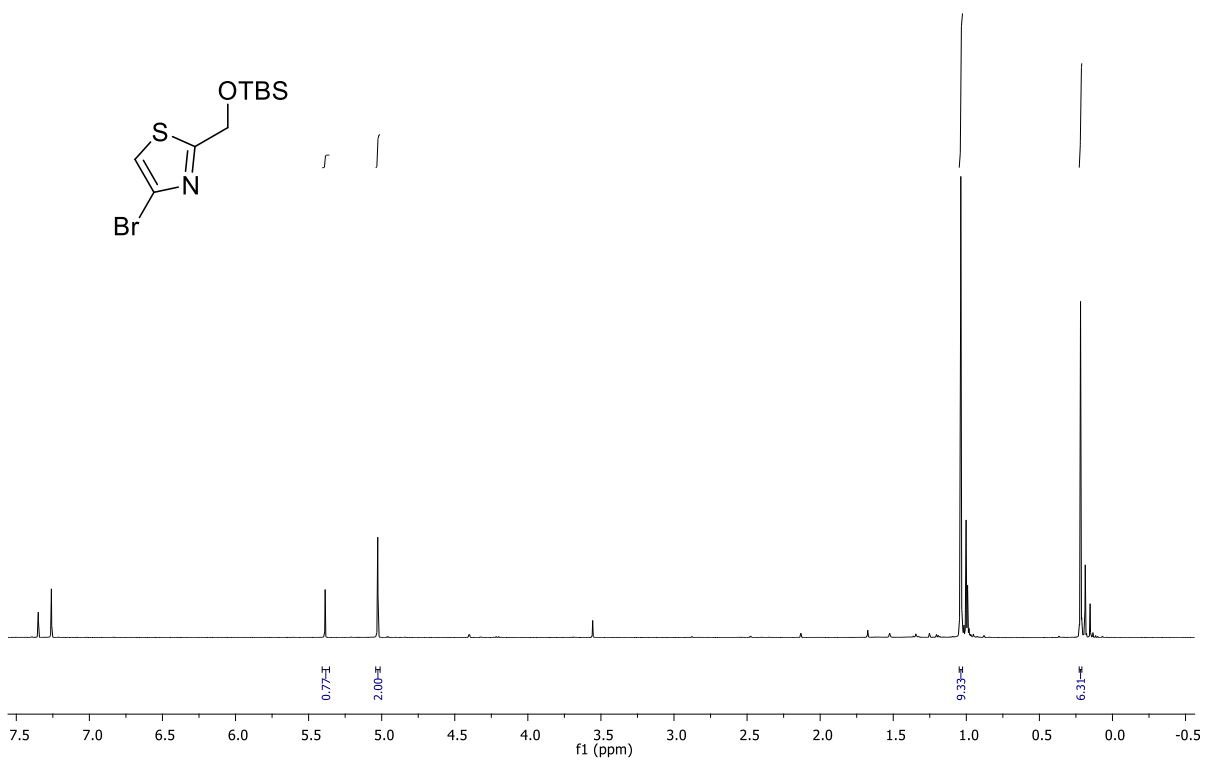


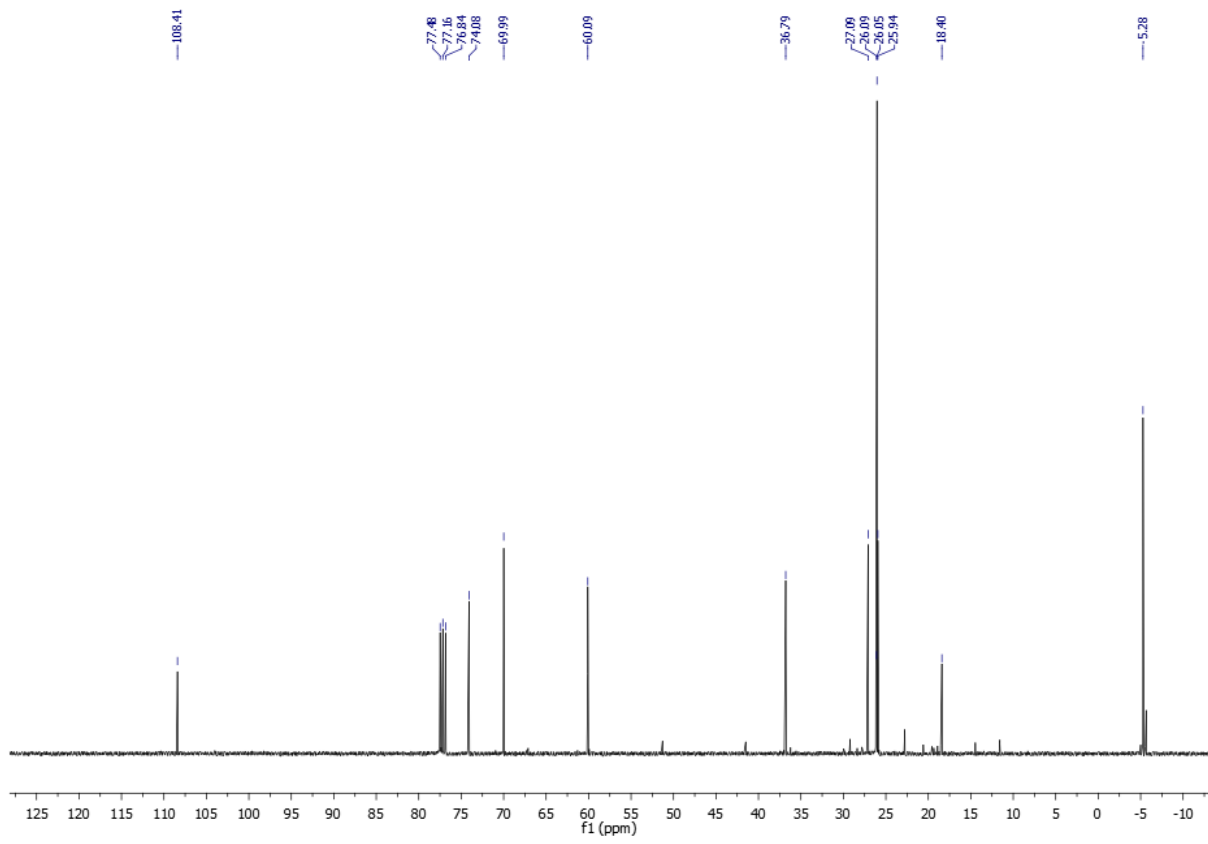
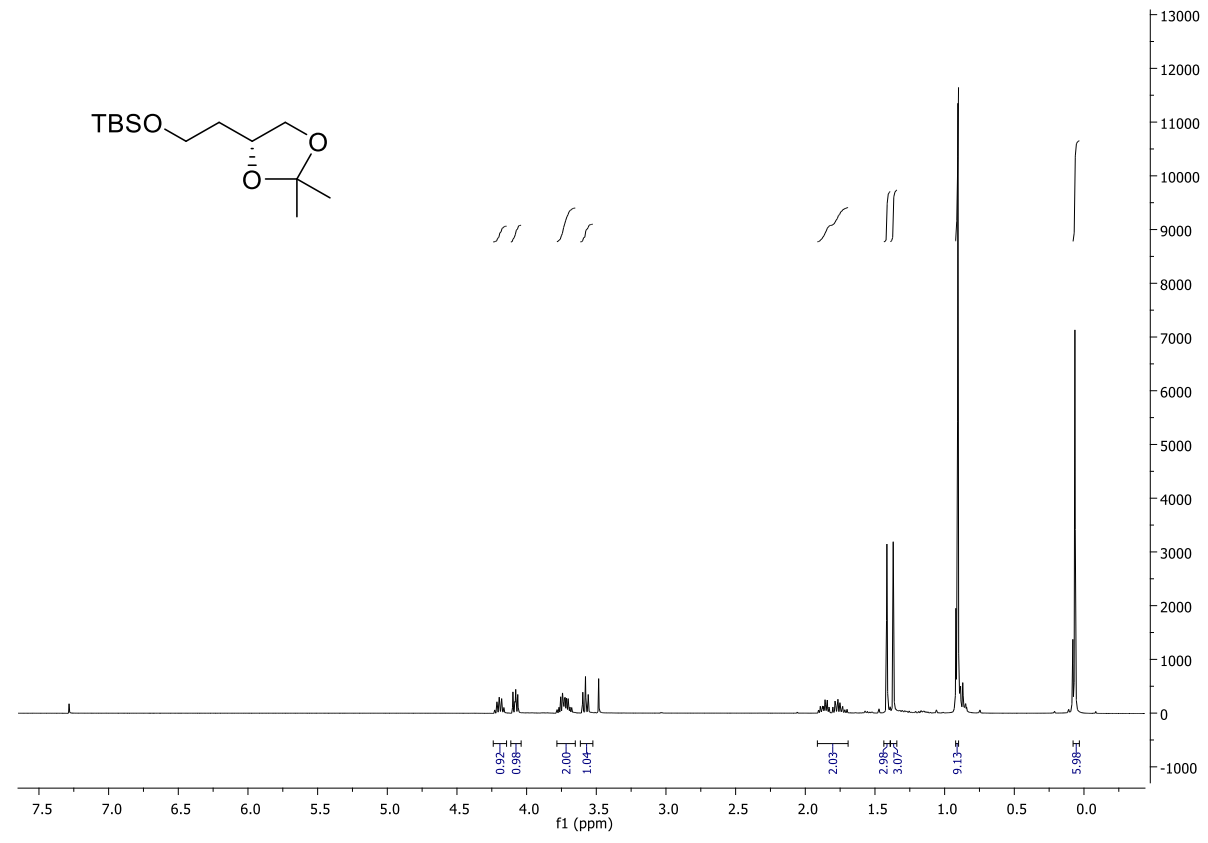


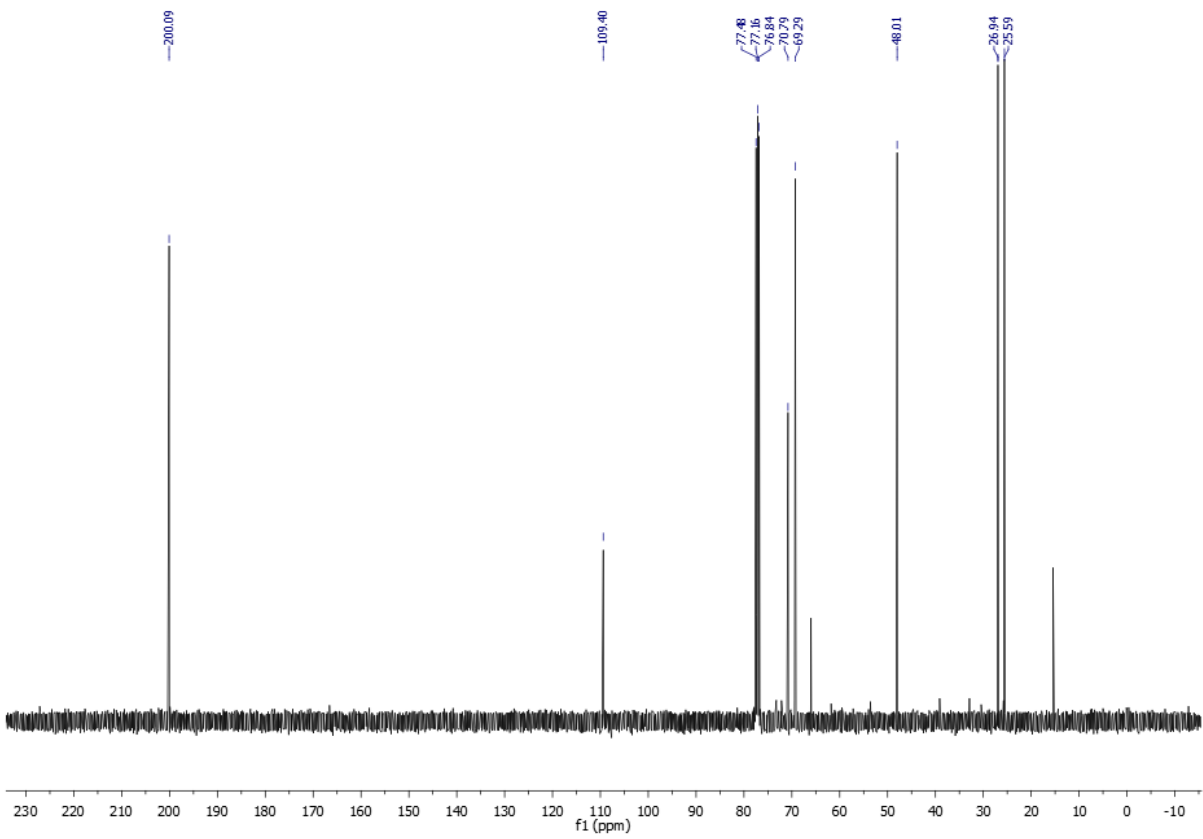
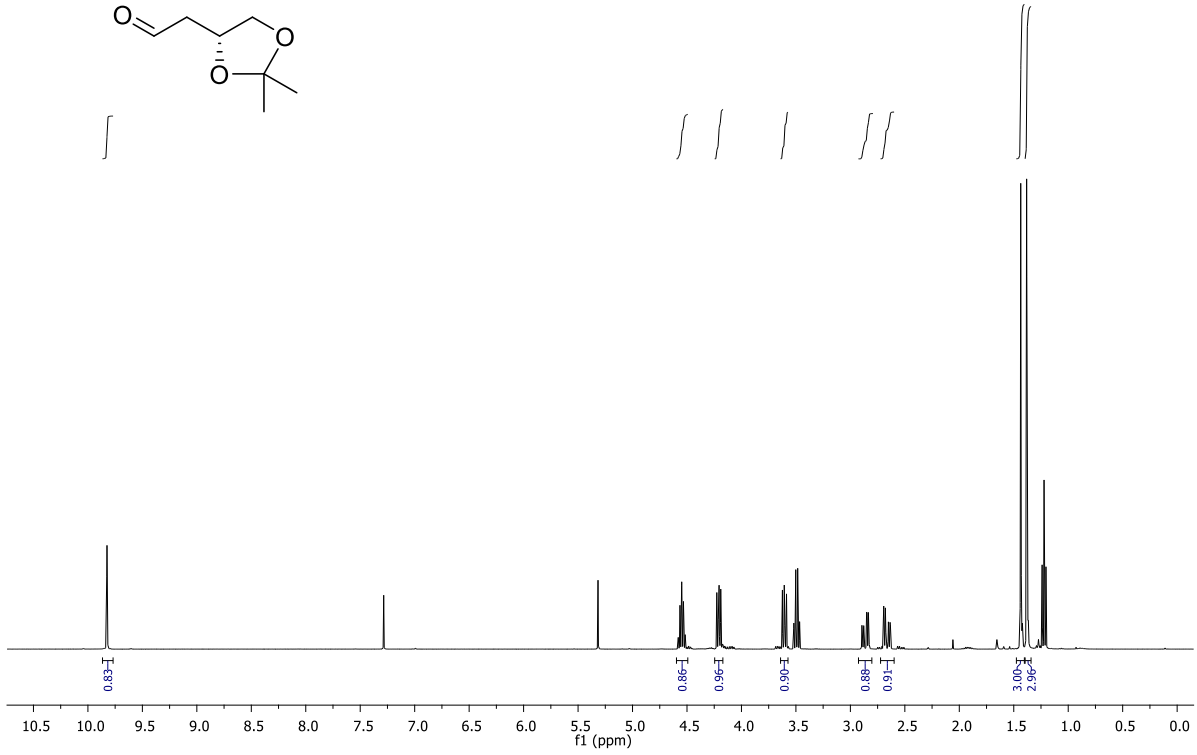
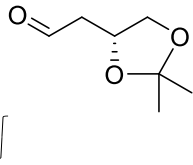


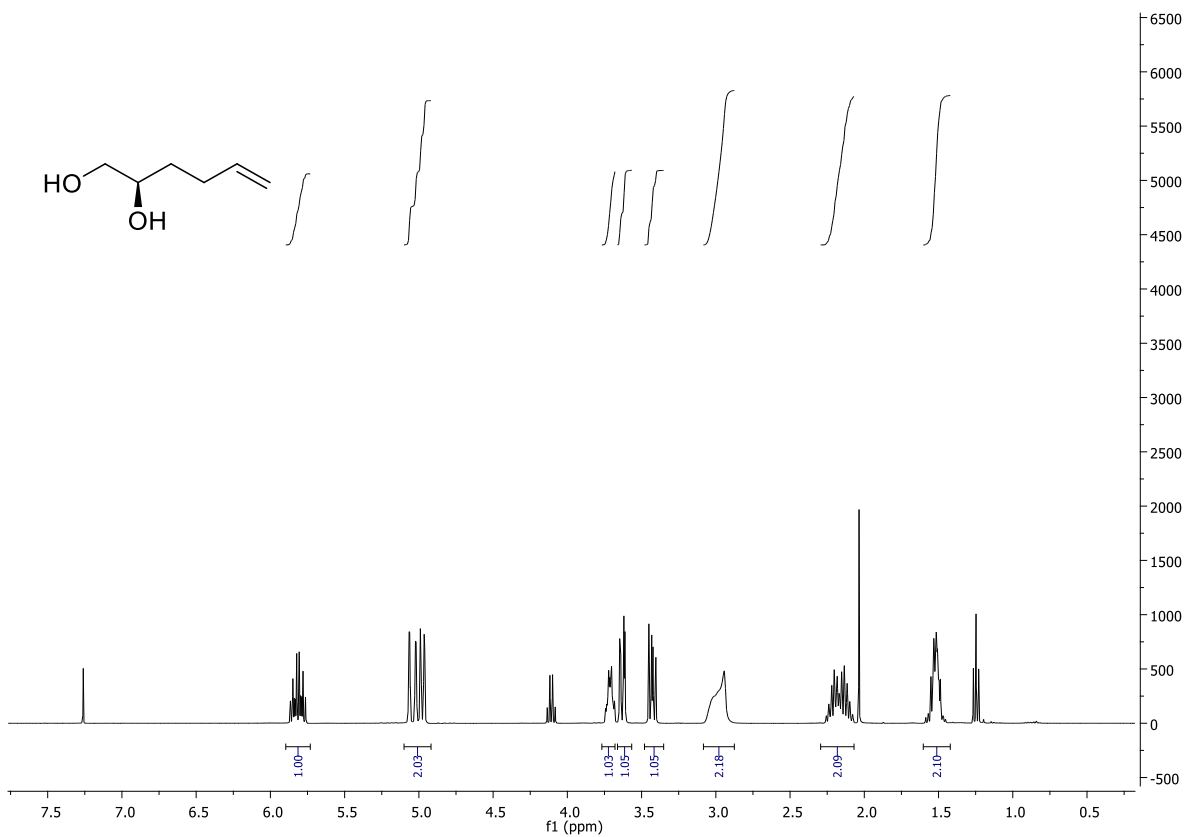
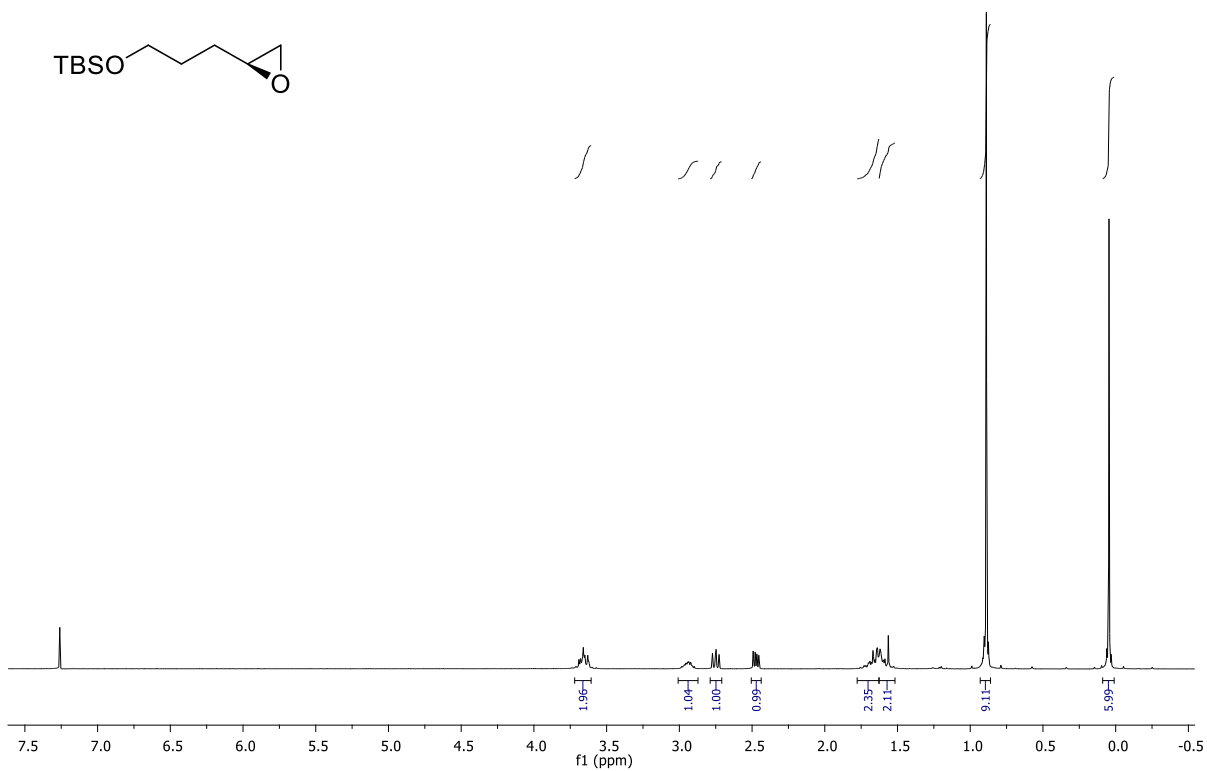


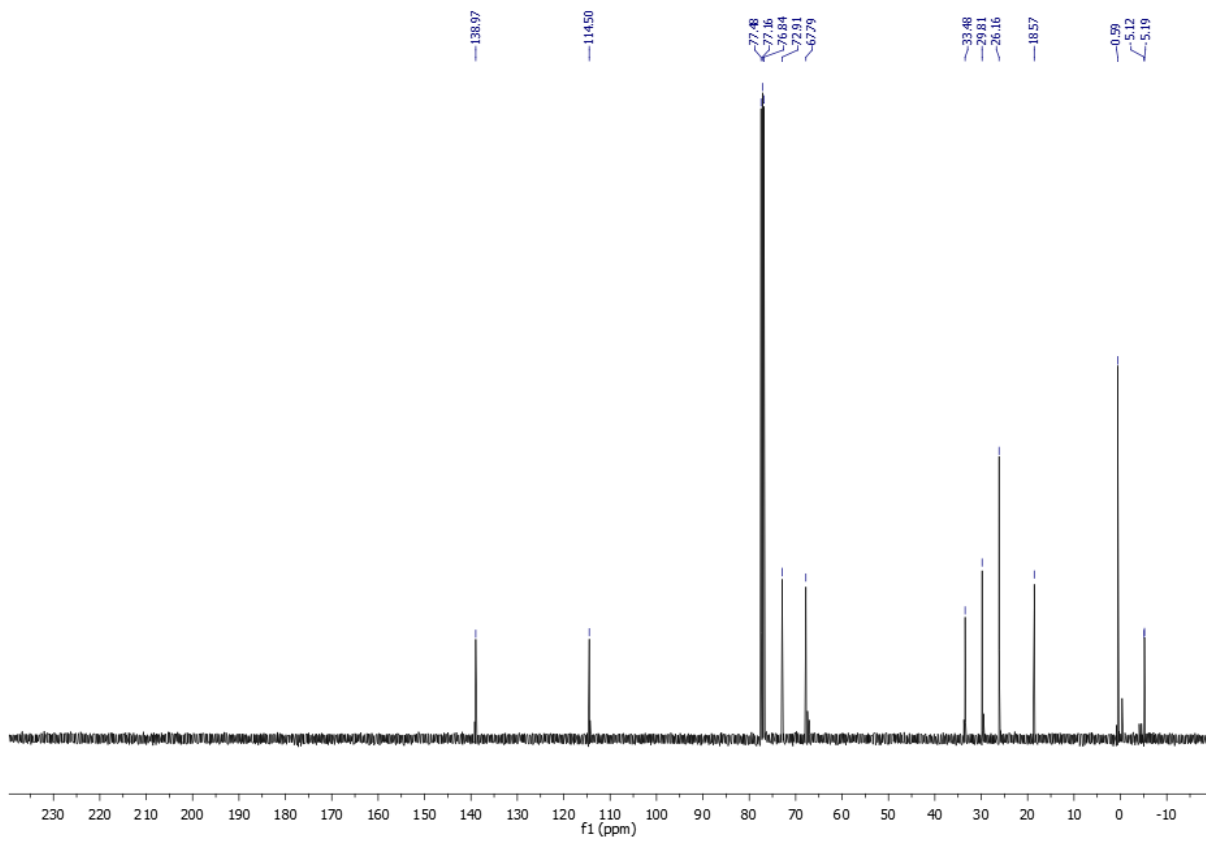
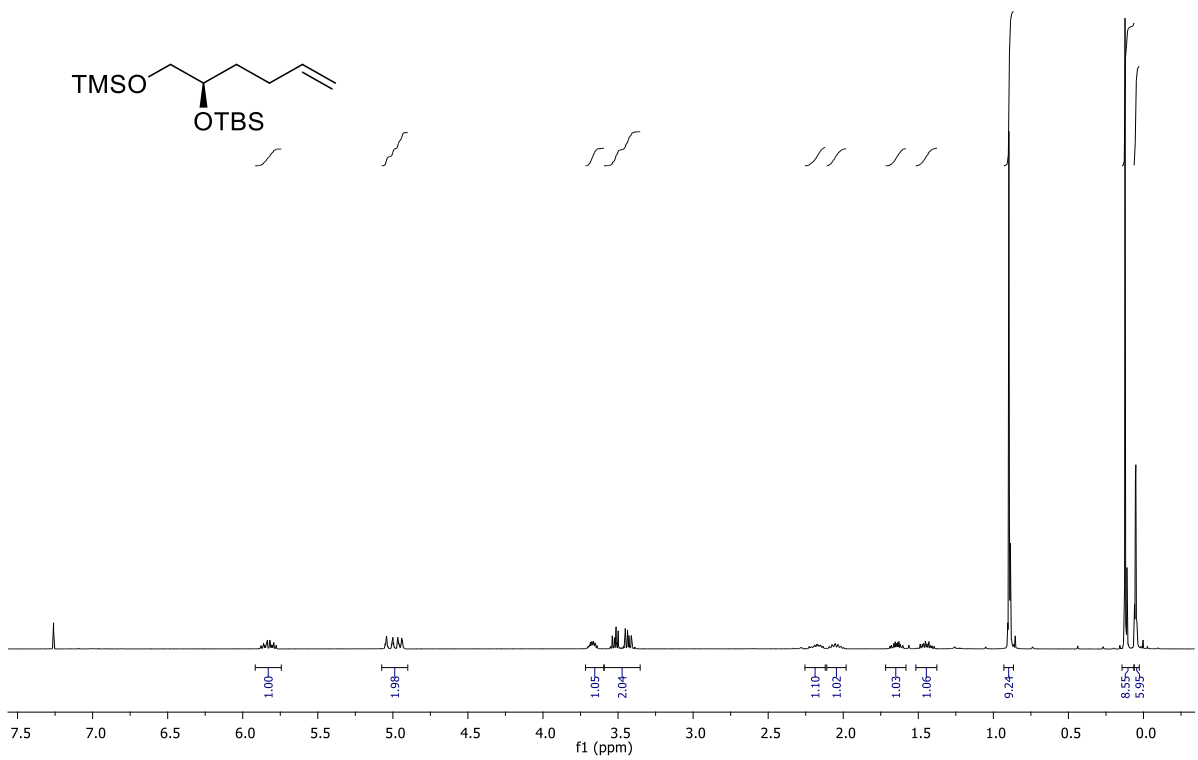
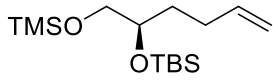


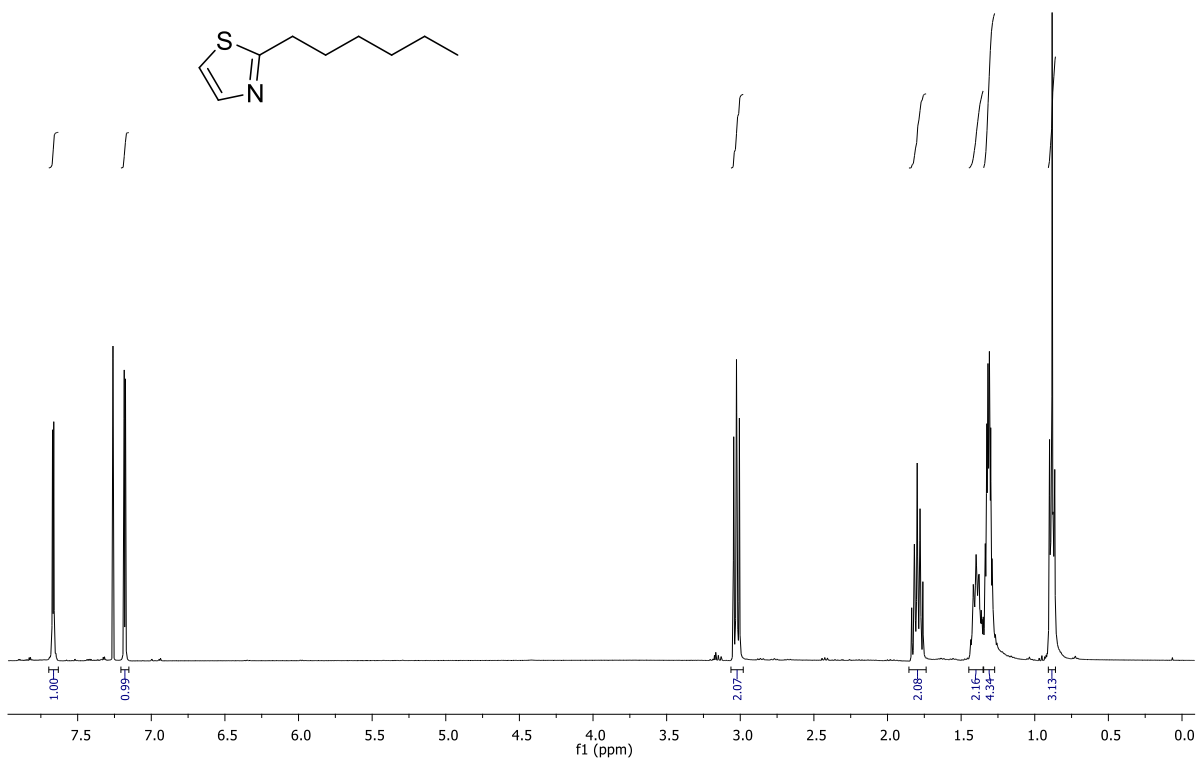
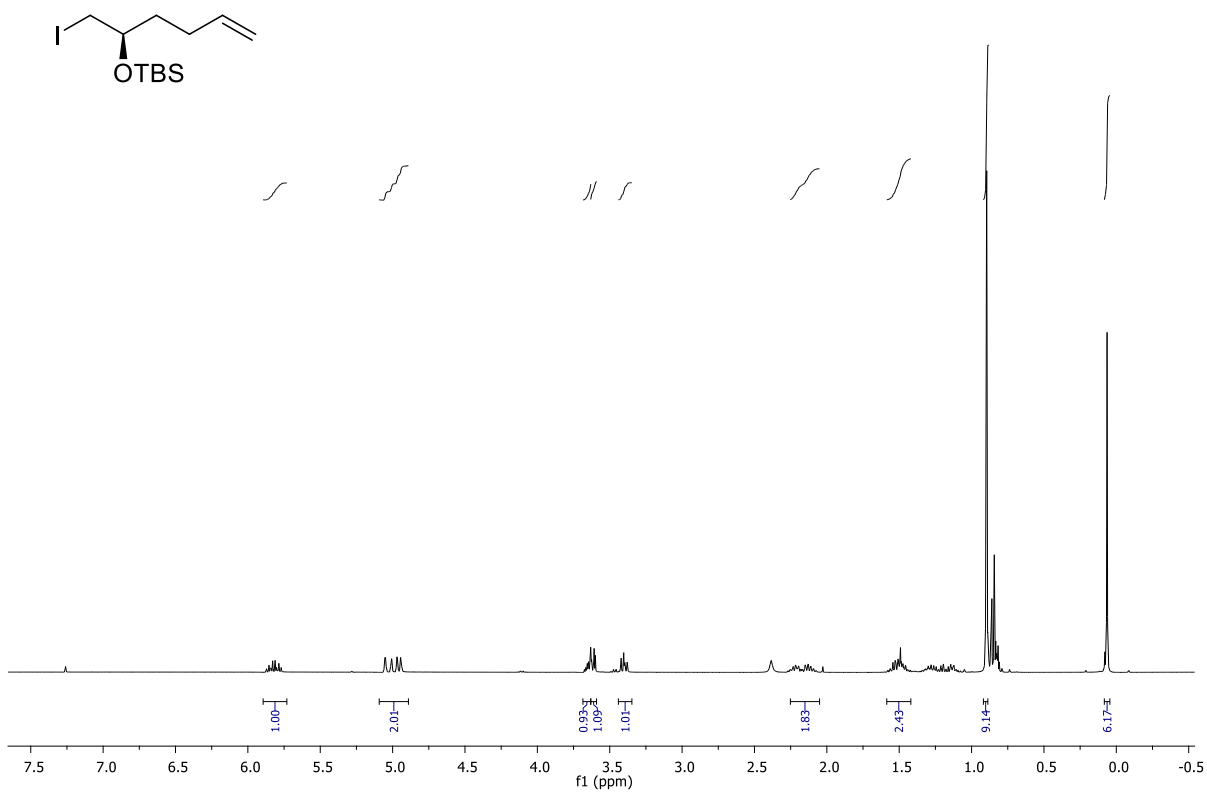


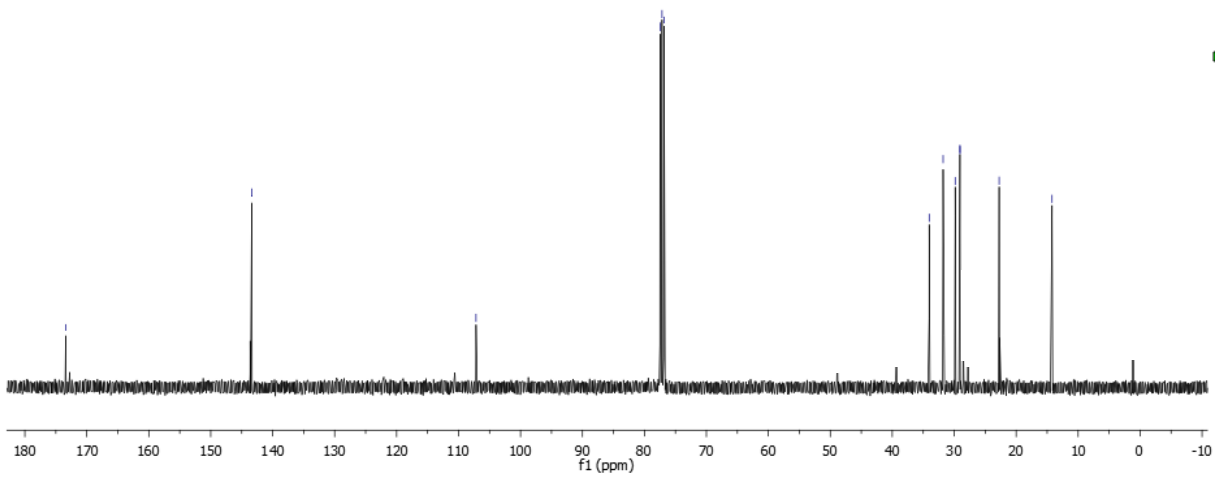
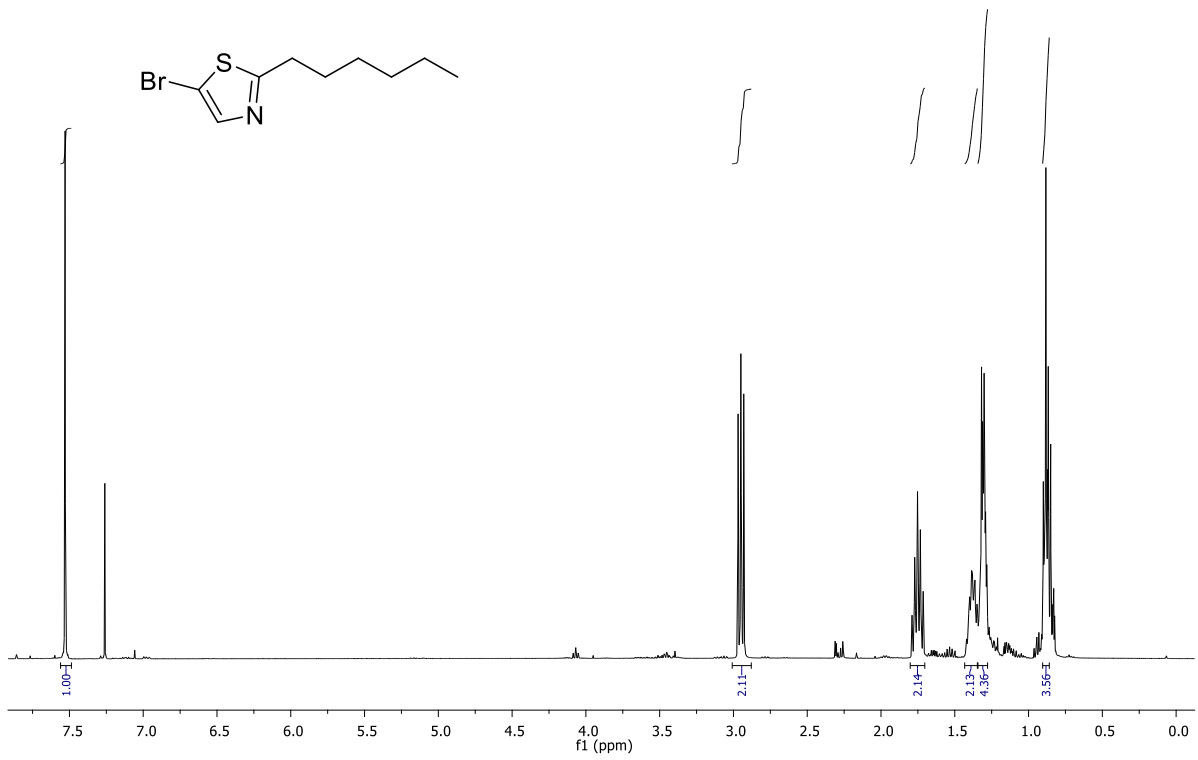
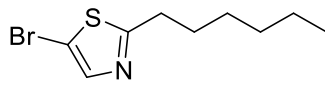


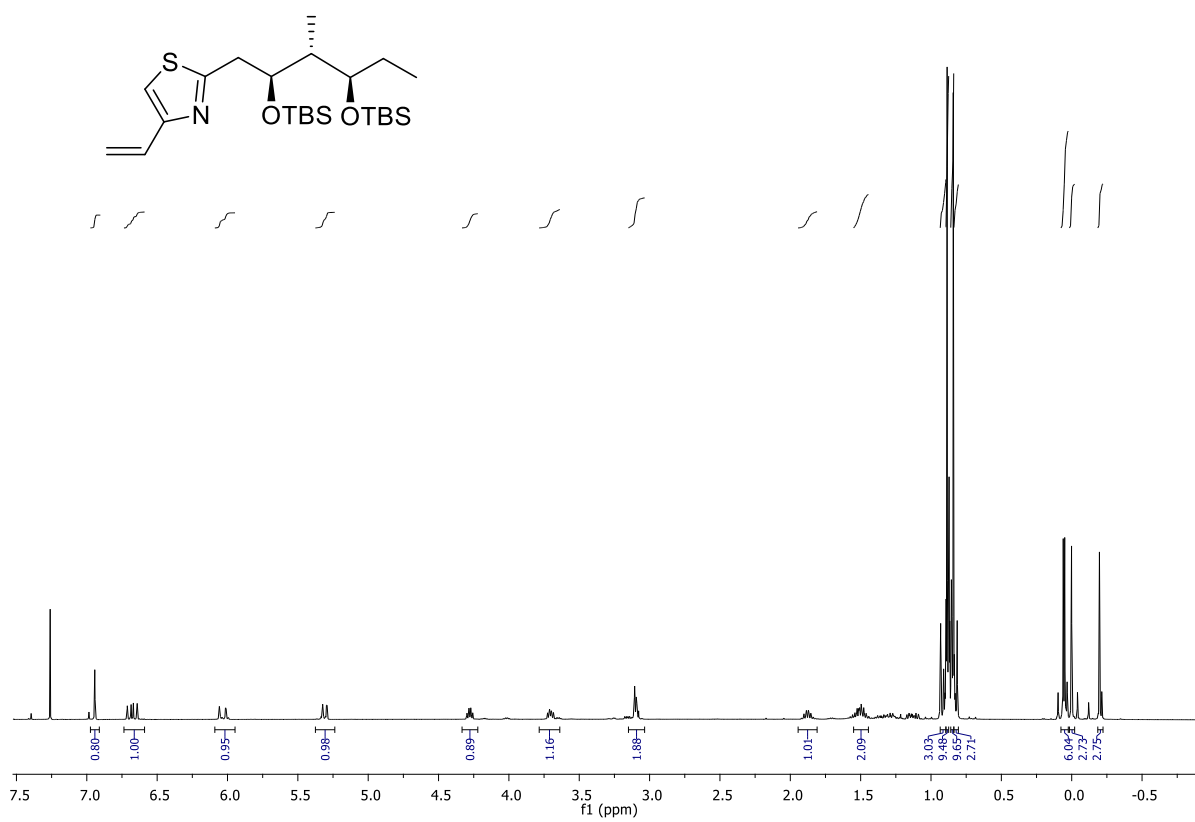
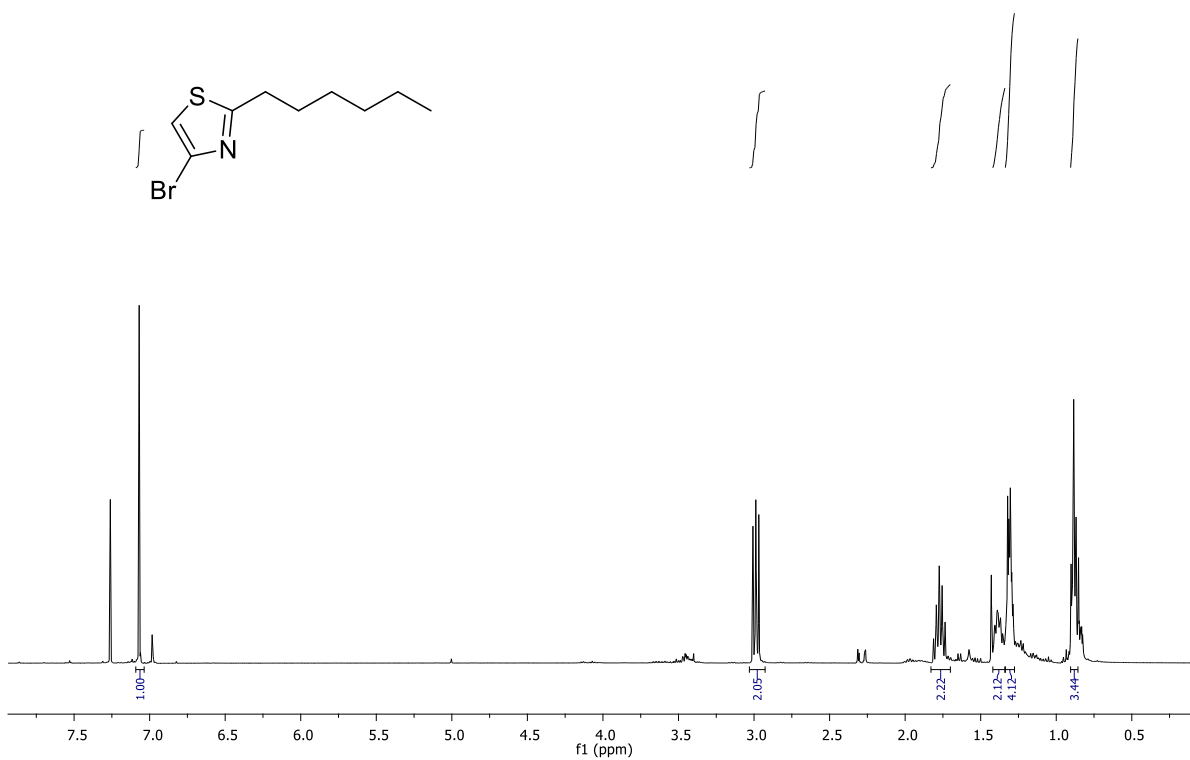


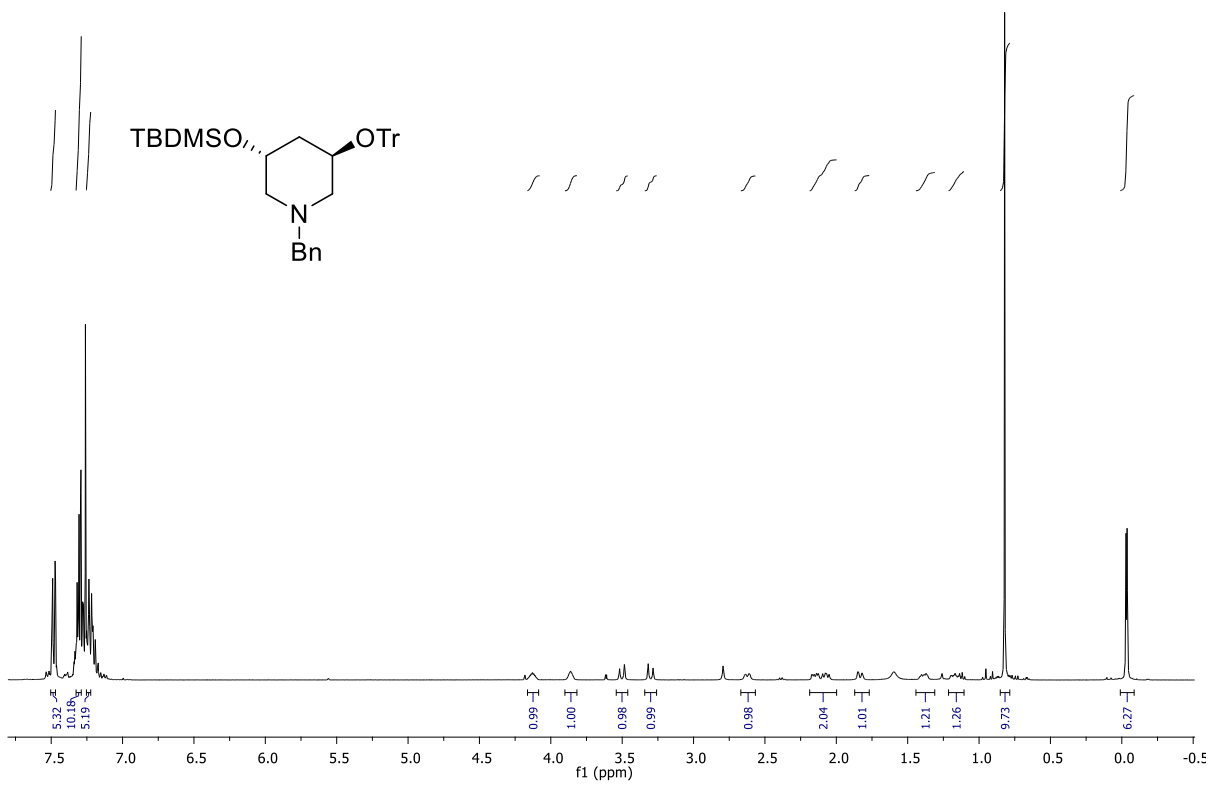


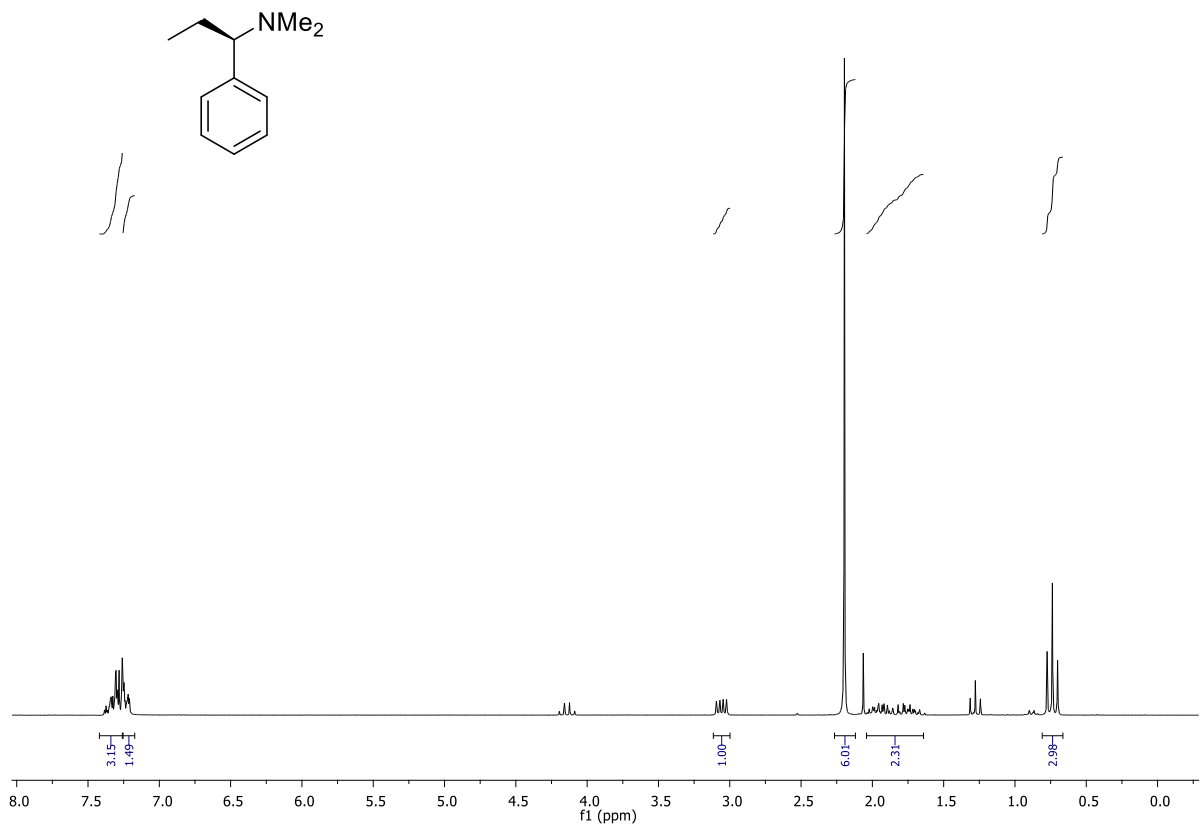
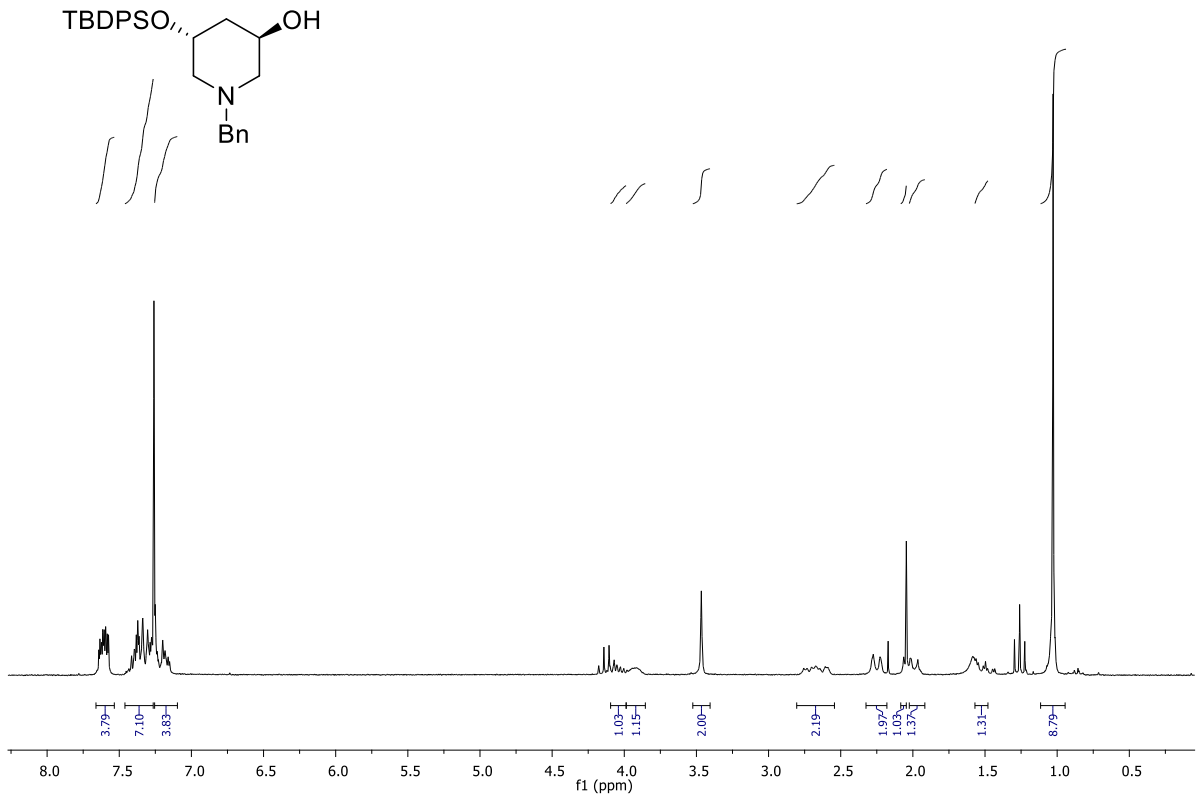


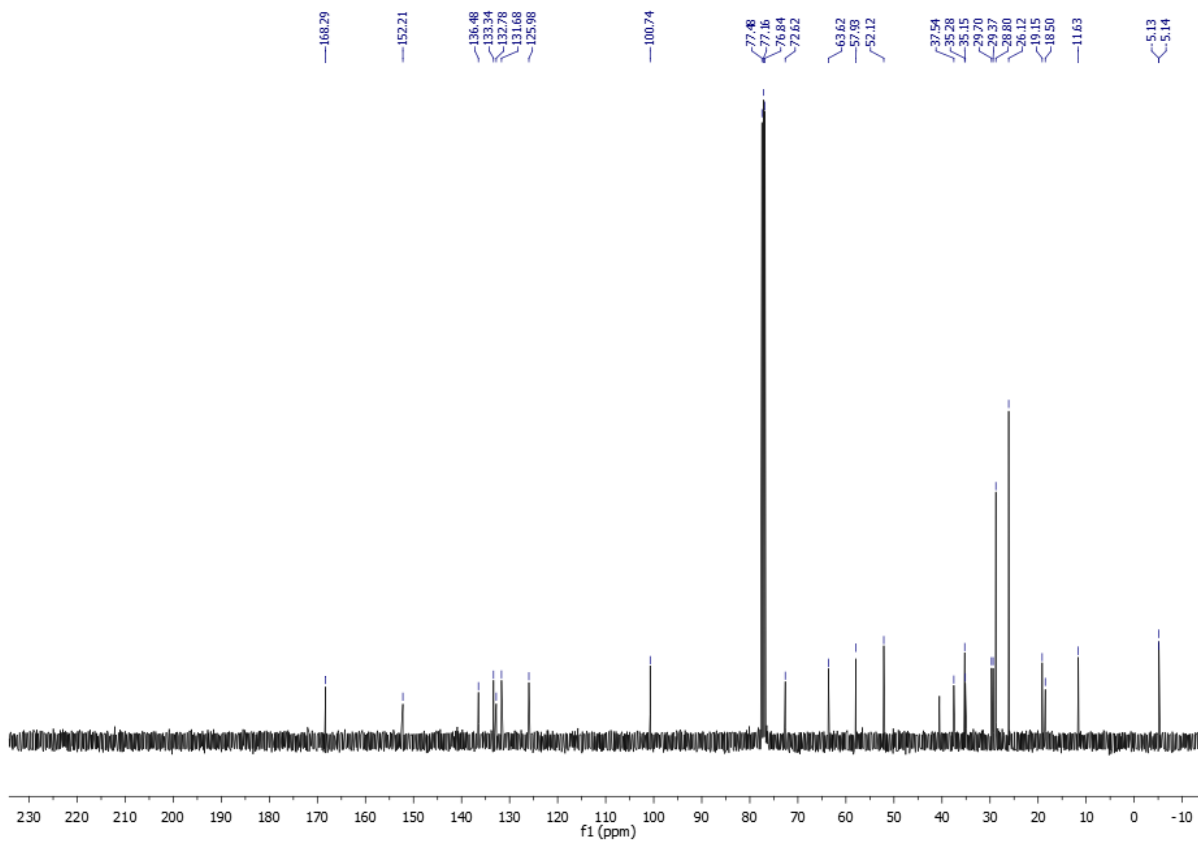
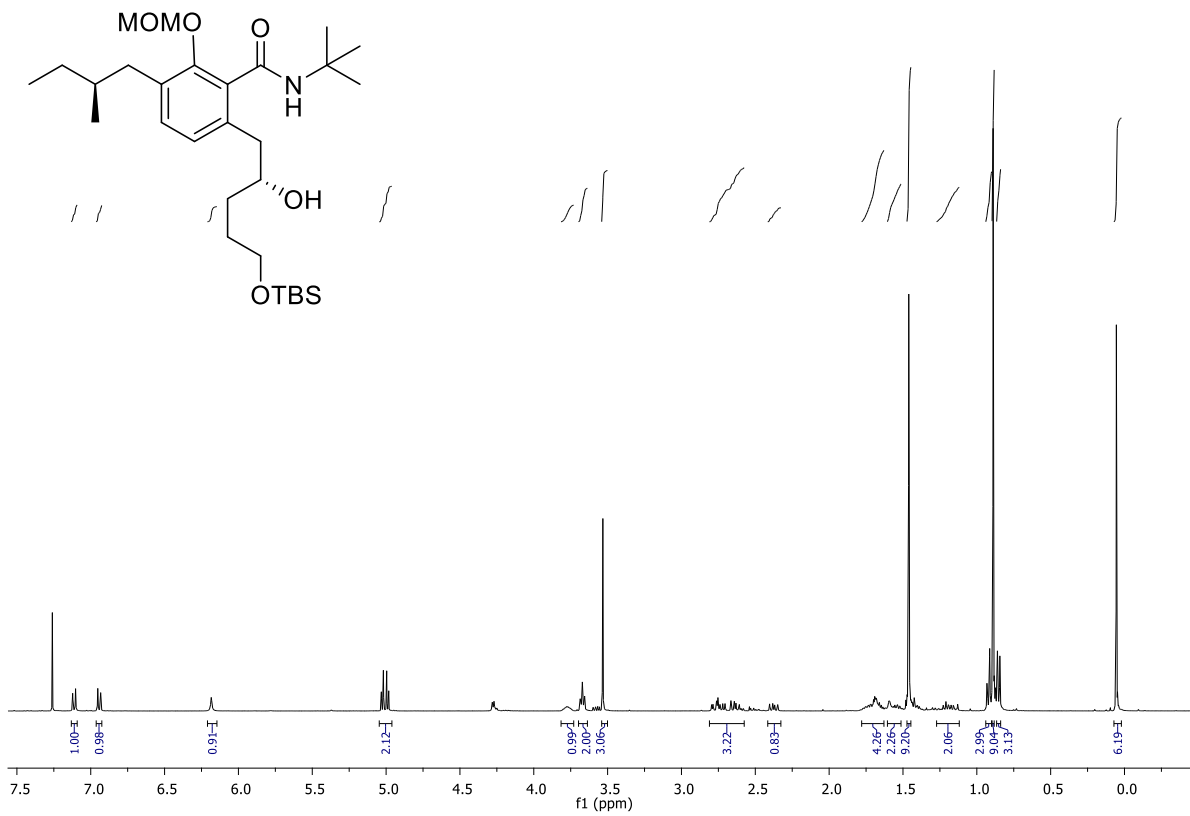


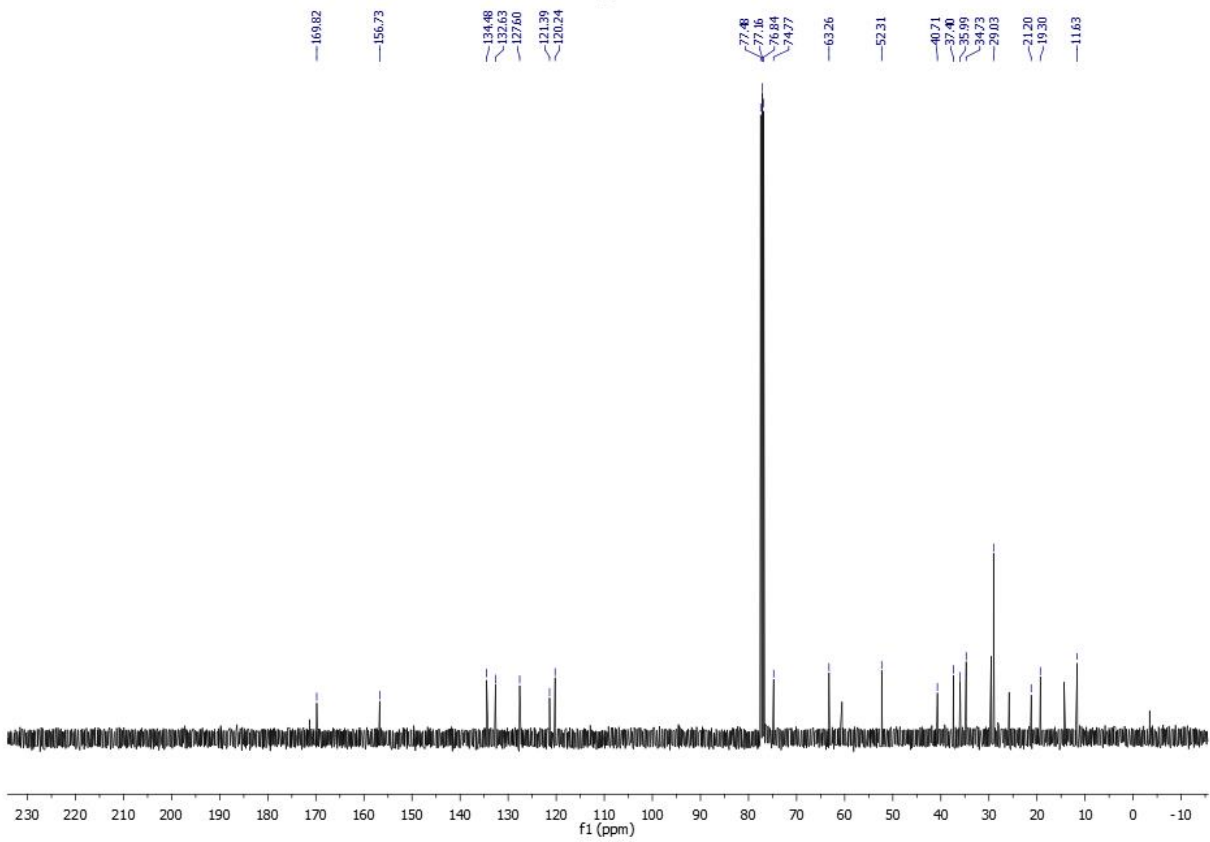
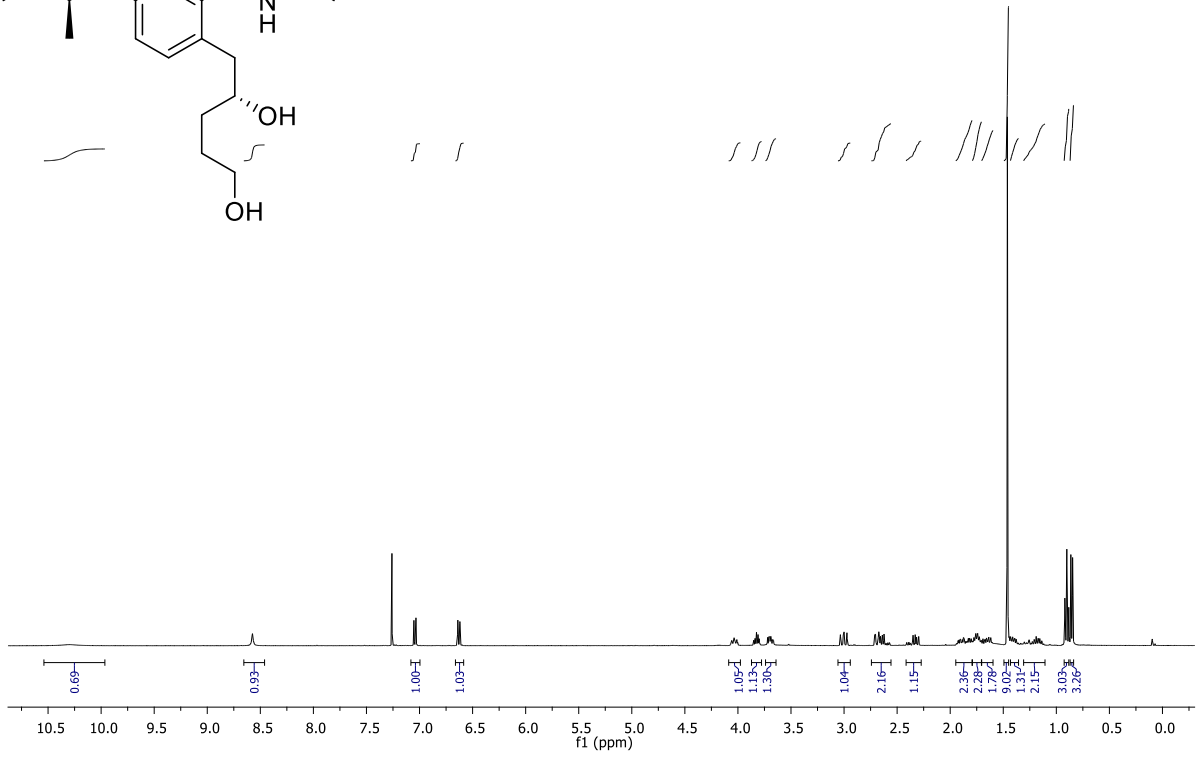
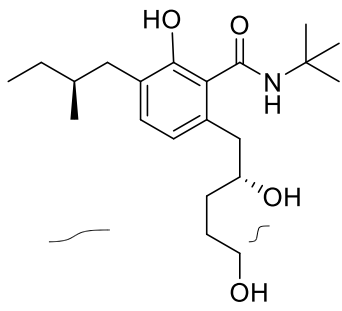


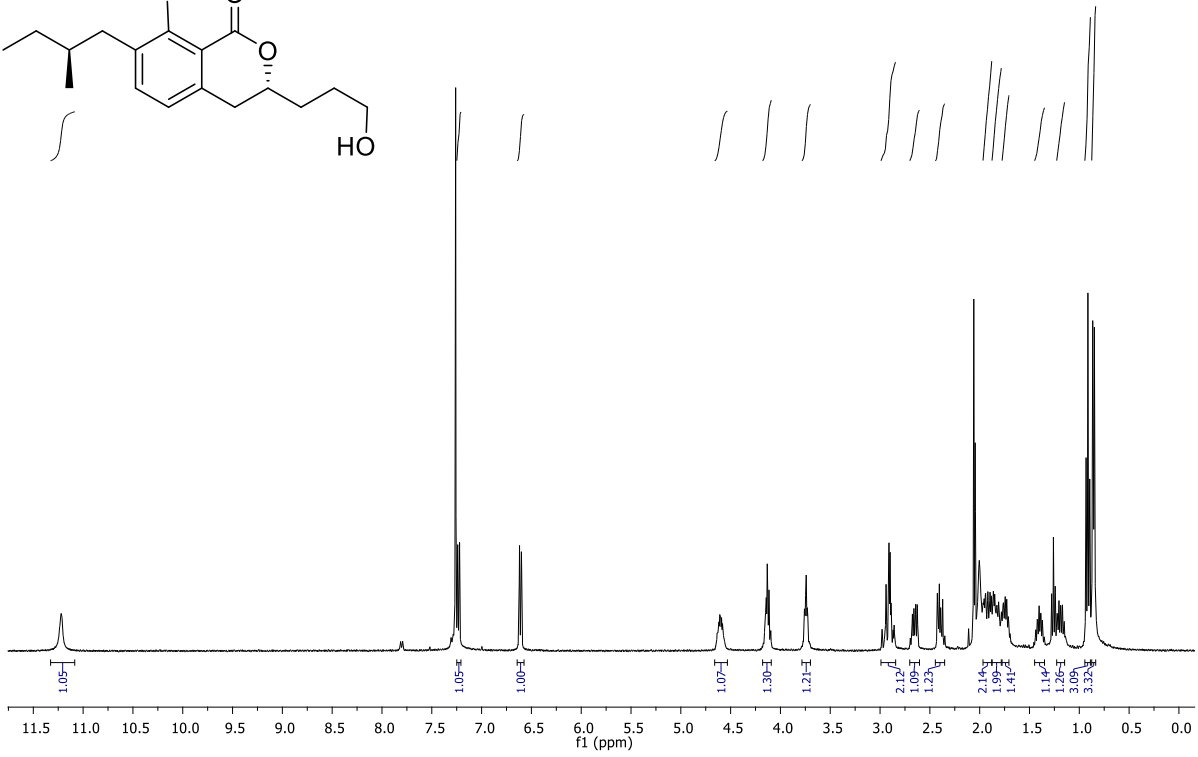
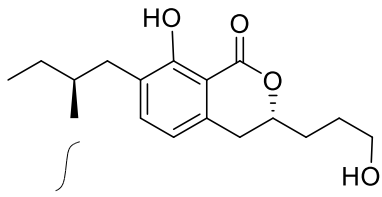




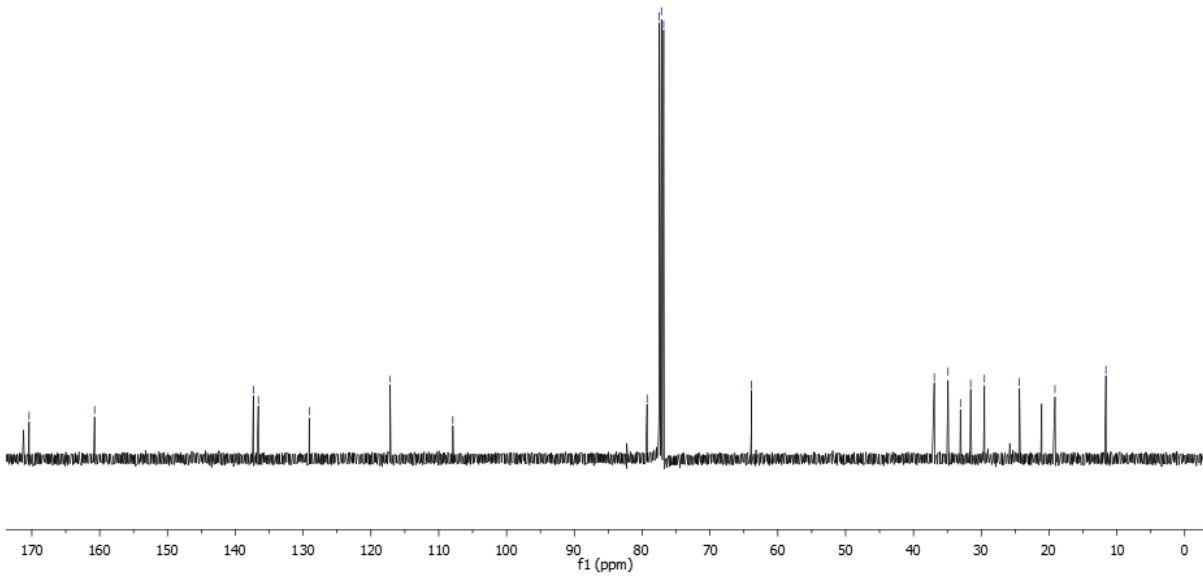








- 170.40
- 160.75
- 137.34
- 136.60
- 129.10
- 117.16
- 107.92
- 79.28
- 77.48
- 77.16
- 76.84
- 63.90
- 36.93
- 34.90
- 33.07
- 31.86
- 29.53
- 24.37
- 19.13
- 11.62



Acknowledgments

First and foremost, I would like to express my deep and sincere gratitude to my advisor Prof. Dr. Andreas Kirschning for giving me the opportunity to work on this PhD project within his group. I am forever grateful for his understanding, guidance and encouragement that have provided a good basis for this thesis.

Furthermore, I would like to express my deep gratitude to Dr. Carsten Zeilinger for his supervision of the biophysical work and for his great enthusiasm and encouragement without which it would have been very difficult to conduct this research.

I would also like to thank Prof. Dr. Markus Kalesse and Prof. Dr. Marie Weinhart for their interest in my thesis and for being part of my graduate committee.

Additionally, I would like to thank the NMR and mass spectrometry departments for their assistance with analytical characterization. A special thank you to Dr. Gerald Dräger for his support with mass analyses, solving technical problems and his support during my graduate studies.

My sincere thanks also to the administrative staff of the OCI for all their help with the paperwork and various organizing matters.

I would like to further thank all the past and present members of the Kirschning group with a special thank you to Dr. Jenny Barbier for her substantial research into the Noricumazole synthesis. I thank my lab-mates Dr. Ilona Bulyszko, Dr. Maria Moreno, Dr. David Candito for the enjoyable times together. Special thank you to my colleagues Dr. Franziska Hemmerling, Dr. Jonas Ammermann and Dr. Jana Franke for the wonderful times and all the fun we had in and out of the lab.

I would like to thank my family and friends for all their support, encouragement, understanding and love over the years. A special thanks also to Benjamin Rogge for all the support and cozy times especially at the beginning of my stay in Hannover.

Finally, I dedicate my thesis to my parents, my brother and my partner.

Curriculum Vitae

Personal information

Name: Dobromira Nedeva Lekova
Date and place of birth: 02.12.1986; Haskovo, Bulgaria
Nationality: Bulgarian

Education

10.2012 – 12.2016
Doctoral Research Program
Leibniz University Hannover
Prof.Dr.Andreas Kirschning working group
Research topic *Studies on Noricumazole A derivatives and their HCV p7 inhibitory activity*

10.2011 – 07.2012
Master of Science: Organic synthesis
University of Chemical Technology and Metallurgy,
Sofia, Bulgaria

01.2012 – 07.2012
Master thesis studies
Otto von Güricke University, Magdeburg, Germany
Prof. Dr. Dieter Schinzer working group
Diploma Thesis *Model testing of Negishi cross-coupling of a series of alkynes and the Z,Z-diene fragment of Sorangicin A*

10.2010 – 07.2012
Master of Science: Industrial management
University of Chemical Technology and Metallurgy,
Sofia, Bulgaria
Diploma Thesis *The patent application process at the European Patent Office*

10.2010 – 10.2011
Postgraduate diploma in education: Chemistry pedagogy
University of Chemical Technology and Metallurgy,
Sofia, Bulgaria
Diploma Thesis *Bologna process, qualification frames and education results*

09.2005 – 05.2010
Bachelor of Science: Organic chemistry engineering
University of Chemical Technology and Metallurgy,
Sofia, Bulgaria
Diploma Thesis *Synthesis of 2-amino-1H-benzimidazole derivatives as compounds with potential biological activities*

09.2000 – 05.2005
Foreign language high school `Prof.Dr.Asen Zlatarov`,
Haskovo, Bulgaria

Science conferences and seminars

- 2015 Anatolian Conference on Synthetic Organic Chemistry (ACSOC), Antalya, Turkey
Poster presentation
- 2014 14th Belgian Organic Synthesis Symposium, Louvain-la-Nueve, Belgium
Poster presentation
- 2011 European summer school and innovation week on `Photovoltaic systems engineering and other renewable energy sources`, Patras, Greece
Presentation
- 2011 4th Spring seminar on `Interdisciplinary Chemistry` for Ph.D. students and young scientists, Bulgarian Academy of Sciences, Sofia, Bulgaria
Presentation

Rewards and Scholarships

- 03.2013 - 08.2016 MINAS graduate school scholarship
Granted by the Ministry for Science and Culture of the State of Lower Saxony /MWK/
- 01.2012 - 07.2012 ERASMUS scholarship for master thesis studies
Granted by European Union student exchange programme fund
- 06.2012 - 07-2012 European summer school and innovation week reward
Granted by University of Chemical Technology and Metallurgy, Sofia, Bulgaria